JOURNAL OF TELECOMMUNICATIONS AND INFORMATION TECHNOLOGY

1,2/2000

JOURNAL OF TELECOMMUNICATIONS AND INFORMATION TECHNOLOGY

The National Institute of Telecommunications in Warsaw, Poland dates its existence since 1934, when a similar Institute was established by Professor Janusz Groszkowski. After the Second World War, the Institute was re-established in its present form in 1951. In its long history, the Institute was the editor of various research periodicals. Before the beginning of the new millennium, the Institute decided to start two new scientific journals: one more technical, edited in Polish and another more fundamental, edited in English. The journal edited in Polish aims at Polish audience and has more technical, informational character, while the journal edited in English, presented here, is more fundamental and aims at European audience. - Both journals, however, respond to the needs of information revolution and the development of information society.

The development of information society is characterised by its three giant megatrends: the social megatrend of changing professions due to the dematerialization of work resulting from information technologies; the technical megatrend of convergence or integration due to the digitalisation of most equipment and systems; finally, the megatrend of intellectual challenges resulting from various cultural, social, economic, legal and ethical problems generated by the development of information society technologies. Both new journals should respond to all these megatrends: both are oriented towards the increasing integration of telecommunications, computer science or informatics and other fields of information technology.

The Journal of Telecommunications and Information Technology aims to become an international research journal with high standards of editorship, serving between others Central and Easter Europe, edited in English. It will be published as a quaterly, in first editions as biquaterly. This journal will be publishing results of scientific research, both fundamental and experimental, broadening the knowledge not only in the field of telecommunications and other fields of information technology – in particular informatics and computer science, photonics, electronics, control sience, telematics etc. – but also in interdisciplinary studies related to information society and technology.

We invite all authors from Europe to contribute to our new journal. All standard forms of publications – regular papers, short papers and letters, invited papers, book reviews, informations about scientific conferences and other events – will be considered for publications. We hope that the readers and contributors will find our new journal interesting.

Andrzej P. Wierzbicki,
Director of the National Institute of Telecommunications,
Member of Advisory Board of Journal of Telecommunications and Information Technology.

Introductory Remarks on European Project „Applications of Nonlinear Optical Phenomena" COST Action P2

In recent years, the importance of photonic technologies has grown substantially in a number of high technology activiti such as telecommunications, information technology, medical diagnostics and treatment, quality control, etc. The ter „Photonics" covers a wide variety of human activities linked with the interaction between light and matter: it is defined the technology of generating and harnessing light and other forms of radiant energy whose quantum unit is the photon. T science includes light emission, transmission, deflection, amplification and detection by optical components and instrument lasers and other light sources, fibre optics, eletro-optical instrumentation, related hardware and electronics. Among the applications for the foreseeable future, those based on the nonlinear optical (NLO) properties will prove especial promising. The importance of NLO phenomena has been known for some time. Since the mid-1980s, however, there h been an explosion of interest in the search for and development of nonlinear optical materials that possess commerci device applications. To date, the systems have been utilised in information processing, optical switching, optical frequen conversion, telecommunications and, with the advancing development of Optoelectronics, ever increasing demands f suitable materials are becoming apparent. Nonlinear optical effects are increasingly used as scientific tools to investiga physical and chemical processes in atoms, molecules, crystals, thin organised films and polymers. Ultrashort laser pulse in the femto-and picosecond range are essential in many technological applications as well as in the characterisation materials. In a world where the rate of exchanges in the communication is growing exponentially, the applications nonlinear optics are certainly meant to play an outstanding role in achieving the goals of exchanging more informati higher speed!

COST is a European framework for scientific and technical cooperation, allowing the coordination of national research a European level. COST Actions consist of basic and precompetitive research as well as activities of public utility. The are 25 COST member countries: the fifteen EU Member States plus Iceland, Norway, Switzerland, the Czech Republ Slovakia, Hungary, Poland, Turkey, Slovenia and Croatia.

The main objective of Action COST P2 is to improve the understanding of the Physics underlying the nonlinear optic phenomena and also to orient the research towards the technological solutions which must be put forward in order implement viable useful devices. Applications of nonlinear optical phenomena are extremely numerous and diverse. It clear that the use of nonlinear optics as a scientific tool to investigate physical and chemical processes in atoms, molecul crystals, thin organised films and polymers are bound to lead to new discoveries which can not be foreseen at the momer however, at the present state of knowledge, it is already possible to state that the characterisation of new materials or of ne molecular structures or arrangements are promising or commercial applications. Another objective is the organisation a truly European research network in this field in collaboration with European commercial firms by sharing the resourc in materials and in manpower already present in each participating laboratory.

Research topics covered included: polymer waveguides, spatial optical solitons, liquid crystal based waveguides and fibre electro-optical devices, photorefractive crystals and polymers, nonlinear processes including degenerate four-wave mixin Z-scan, frequency conversion, stimulated scattering, nonlinear waveguide characterisation, optical switching, nonlin propagation effects, soliton transmission, femtosecond and picosecond source characterisation and development, and nov NLO materials such as quantum wire and quantum dot systems.

The first Workshop of COST P2 was organised on June 12-13, 1998, in Limerick, Ireland.

The second one was organised on October 6-9, 1999, in Amalfi, Italy. The year 2000 Workshop is planned on Octob 26-28, 2000, at the University of Twente, the Netherlands.

More information on this action can be found at web site http://www.phg.ulg.ac.be/COST.

Blau Werner
Physics Department
Trinity College Dublin
Dublin 2, Ireland
Tel: +353 1608 1708
Fax: +353 1671 1759
E-mail: wblau@tcd.ie

Prof. Yves Lion,
COST P2 Action Chairman
Laboratoire de Physique Generale
Universite de Liege
Institut de Physique Bat B5
allee du 6 aout, 17
B-4000 Sart-Tilman, Liege, Belgique
Tel: +32 4 3663626
Fax: +32 4 3664516
E-mail: ylion@ulg.ac.be

The present and future of nonlinear optics applications in photonic telecommunication networks

Marian Marciniak and Marian Kowalewski

Abstract — A state-of-the art of photonic telecommunication technology is reviewed and possible directions of future developments are outlined. In particular, the impact of nonlinear optical phenomena inherent to silica glass on the transmission performance of wavelength-division multiplexed optical signal through fibres is discussed. Also potential applications of nonlinear photonic devices for the purposes of optical signal processing that is foreseen in future all-optical networks are pointed out.

Keywords — optical fibre communications, photonic networks, wavelength-division multiplexing, nonlinear optical phenomena.

Optical technology and infrastructure

Recent years have shown a rapid growth of demand for capacity of telecommunication networks. It has inspired many laboratories to explore new techniques of more efficient utilisation of the huge bandwidth offered by optical fibre links. One of the most promising and cost effective ways to increase optical link throughput is a technique known as Wavelength Division Multiplexing (WDM).

Optical transparent transmission offers almost infinite optical bandwidth. This is especially attractive in view of future information society needs for exchange of enormous information streams, resulting from a general use of multimedia and hypermedia services.

Transparent optical networks that are actually being introduced on the basis of existing silica cable infrastructure offer almost infinite transmission bandwidth [1]. This is of crucial importance in view of future information society needs for exchange of enormous information streams, resulting from a general use of multimedia and hypermedia services.

The transparent network technology is actually in a mature state: a number of elements are already commercially available. Those are: tunable laser diodes and laser arrays as WDM sources based on a ITU 100 GHz optical frequency grid, Arrayed-Waveguide Gratings (AWG) as multiplexers and demultiplexers including optical add-drop (de)multiplexers, fibre Bragg gratings as filters, etc.

Optically transparent technology is actually advancing very fast. Although almost unlimited capacity is available, the future technology has to meet new demands especially in the field of optical signal digital processing, including full 3R (Reamplification, Reshaping, Retiming) regeneration. Moreover, a new concept of 4R regeneration [2] has recently appeared that reclaims also a proper regeneration of the optical spectrum of the aggregate signal in introduced recently commercial transmission systems exploiting WDM technology.

In a WDM system many information channels are transmitted through one fibre using different optical wavelengths modulated by independent data streams. This method is analogous to Frequency Division Multiplexing (FDM) which is widely exploited in other communication systems, especially in radio broadcasting. Using WDM we can easily increase the capacity of already existing fibre links that is particularly significant in the areas where placing new cables is impossible or too expensive. One can also envision the application of WDM in broadcast networks and/or in subscriber loop [3].

The introduction of Erbium-Doped Fibre Amplifiers (EDFA) which have replaced electronic regenerators in fibre based transmission links in early 90 s resulted in optical transparency of the links. This was in contrary with electronic regenerator based links. In those a combination of electronic logic circuit along with electro-optical and opto-electrical conversions of the digital signal transmitted has been used in order to cope with signal distortion. In optical links the distortion results from physical limitations of the transmission of light signals through fibres, namely from fibre attenuation, dispersion, and nonlinear distortion.

An enhancement of optical link exploitation enabled by the EDFAs and WDM technologies have resulted in a dramatic decrease of cost of transmission bandwidth. Moreover, WDM offers an orthogonality between wavelength and time, so they can be processed independently and simultaneously. However, significant research challenges still remain to realize the huge potential offered by optical networking.

WDM transmission is actually being introduced in commercial fibre telecommunication systems. Transmitting several wavelengths (16, 32, 64 or more) and amplifying the aggregate signal in optical amplifiers results in an increase of the total optical power, what causes nonlinear interactions very effective. The transmission performance of the system can be then seriously degenerated, mainly via nonlinear signal distortion and nonlinear crosstalk (power transfer between different wavelength channels). Thus, there exists a great need to minimize the nonlinear distortion and to optimize the transmission parameters. On the other hand there is an urgent necessity to establish new international standards for WDM nonlinear systems.

Nonlinear limitations

Analogous features of a silica fibre: attenuation, dispersion, and nonlinear distortion result in distortion, crosstalk and noise of the transmitted optical signal. Therefore, a digital signal can be transmitted successfully only at certain distance of the fibre link, this distance is called transparent length.

Silica glass exhibits only small value of nonlinear coefficient. However, due to small spot-size of modal beams in the core of the fibre and high power at the output of optical sources and amplifiers, going up to 100 mW, and also extremely long distances of propagation which is of the order of hundreds or thousands of kilometres, nonlinear effects are accumulated along fibre link and can cause a significant change of the optical signal in positive or negative way. Moreover, the fibre nonlinearity is believed to decrease signal distortion caused by Polarisation Mode Dispersion, which is fibre intrinsic defect that is due to lack of ideal symmetry of practical fibres.

At present state of technology nonlinear effects affect the transmission system performance in great scale. This is due to combining high level of optical power at the output of modern lasers and amplifiers with extremely small cross-section of guiding core of the fibres.

In spite of its merits the WDM technique is not free from limitations. The most characteristic and essential problem for multichannel optical systems, beside attenuation and dispersion, is interchannel crosstalk [4]. One can distinguish crosstalk caused by nonlinear interactions between the light in different channels or between the light and the fibre material. In spite of the intrinsically small values of the nonlinearity coefficients in fused silica, the nonlinear effects in optical fibres can be observed at low power levels. This is possible because of important characteristics of single-mode fibres, a very small optical beam spot-size, and extremely low attenuation.

In WDM systems a nonlinear interplay between many different spectral components of the aggregate signal causes interchannel crosstalk. The nonlinear phenomena involved are Self-Phase Modulation (SPM), Cross-Phase Modulation (XPM), Four-Wave Mixing (FWM), Stimulated Raman Scattering (SRS), and Stimulated Brillouin Scattering (SBS).

System requirements

A number of functions in the optical domain can be realized only via nonlinear effects. This is an inherent feature of optics in contrary to electronics: two electrons interact strongly via electrostatic and magnetic forces even in the vacuum, while two photons do not at all. Actually this was the reason successful application of photonic transmission in fibre links. Unfortunately, this is also the reason why it is so difficult to realise processing of light by light. This can be done only via nonlinear interaction between light and matter or between the beams themselves.

Core networks

Core networks represent the backbone of the information superhighway. Optical cable infrastructure is well developed in many countries and no substantial investment is needed to upgrade the transmission capacity. The most promising one is WDM technology, which does not need to install faster electronics.

Broadband access networks

The expected introduction of optical transparency to subscriber loop will allow taking advantage also from WDM technology. A combination of various signals (i.e. analogue or digital television, interactive broadband services) could be transmitted simultaneously. New ways of providing access are emerging based upon the need for interactive broadband services. This means a need for a mass deployment of fibre in access.

ATM networks

Multimedia service networks based on fibre core networks and ATM technology can provide the broadband communications platform needed by business and residential users for integrated services with of voice, data and visual information transmission. This should provide high-quality performance and economic advantages of ATM networks.

The future transparent photonic network

It is generally believed that opticalisation which is a term standing for keeping the signal in optical domain thus avoiding its conversion to electronic domain in the whole transparent network should result in a much more complete exploitation of the combined huge low-loss fibre window and optical amplifier bandwidth, which is actually estimated to be equal to ten terahertz.

All optical networks offer new possibilities for high bandwidth applications. New techniques will be demonstrated for optical switching and network management for complex optical networks. WDM systems allow upgrading of the backbone optical network. This theme explores the current state of research and future developments of optical network technology and applications. End-to-end broadband transparent transmission is an essential condition to provide reliable broadband services. The demand for Internet is a driving force leading rapidly towards WDM. However, WDM is an analogue technology that suffers from analogue distortions of the signal. On the other hand, special kind of optical pulses exploring silica glass nonlinearity called solitons have a digital nature (they exist or do not). Solitons are then more compatible with digital transmission. A combination of both technologies appears as a very promising one. Solitons are better for synchronous (SDH) digital

systems, while a passive WDM network is better suited for ATM.

WDM is a technique compatible with the idea of all-optical networks, where one can create transparent optical paths connecting successive network nodes by switching optical channels organized at the different light wavelengths. Wavelength converters (λC) are developed in order to profit from another degree of freedom of transparent network, which is the signal wavelength. This allows a realisation of wavelength routing functions.

Transparency is very attractive also from user point of view: he/she sends his/her own data streams and the transparent network transmits them regardless of their format, bitrate etc. A functional model of a transparent passive network consists of an optical telecommunication cloud through which clients send and receive their messages of various kinds.

Reduced cost of bandwidth enabled by the optical amplifier and WDM technologies have resulted in a dramatic reduction of cost of transmission bandwidth. Moreover, WDM offers an orthogonality between wavelength and time, so they can be processed independently and simultaneously [5]. However, significant research challenges still remain to realize the huge potential offered by optical networking.

References

[1] M. Marciniak, „Transparency of optical networks: How to manage it?", in *International Conference on Transparent Optical Networks ICTON'99*, Conference Proceedings, Kielce, Poland, June 1999, Invited Paper Th.B.2, pp. 85–88.

[2] L. Thylén, „Some aspects of photonics and electronics in communications and interconnects", in *1st International Conference on Transparent Optical Networks ICTON'99*, Opening Lecture, Kielce, Poland, June 1999.

[3] Y. Namihira, „Relationship between nonlinear effective area and mode field diameter for dispersion shifted fibres", *Electron. Lett.*, vol. 30, no. 3, pp. 262–264, 1994.

[4] G. P. Agrawal, *Fiber-optic communication systems*. New York: Willley-Interscience Publication, 1992.

[5] R. C. Alferness, „Research challenges in optical networking", in *ECOC'98*, Madrid, Spain, Sept. 1998.

Marian Marciniak
National Institute of Telecommunications, 1 Szachowa Str., 04-894 Warsaw, Poland, e-mail: M.Marciniak@itl.waw.pl
Marian Kowalewski
National Institute of Telecommunications, 1 Szachowa Str., 04-894 Warsaw, Poland, e-mail: M.Kowalewski@itl.waw.pl

New pico- and femtosecond laser based sources: from the Infra-Red to the XUV

Guillaume Petite

Abstract — In this paper, we review a number of recent developments concerning laser or laser-based sources generating pico- or subpicosecond pulses of light at wavelengths now ranging from the mid Infra-Red (50 μm) to the XUV (11.9 nm). Those include the new generation of „Chirp Pulse Amplification" laser systems, Free Electron Lasers operating in the IR or visible range, and a number of laser driven sources covering the XUV range, generally based on the high intensity irradiation of solid or gaseous targets. The main perspectives, applications and essential issues concerning such sources are discussed.

Keywords — *lasers, short pulses, ultrafast phenomena.*

Short pulse laser systems: the CPA/KLM revolutions

There has been a constant decrease of the available pulse durations ever since the laser existed. Picosecond lasers have been used for more than twenty years now, and sub-picosecond lasers (very few of them really deserving the current „femtosecond" laser appellation) for more than ten. The essential moves of these past years have been the huge increase of the energy available per pulse, and a no less considerable spreading of the wavelength range over which short light pulses are available, which now spans from the mid Infra Red (IR: about 50 μm with the best IR Free Electron Lasers) to the XUV where subpicosecond pulses are available down to wavelengths in the 50 nm range, and picosecond X-laser pulses down to 11.9 nm.

One major breakthrough occurred in the late 80's with the invention of the „Chirped Pulse Amplification" (CPA) concept. Indeed the task of extracting the maximal possible energy from an amplifier system requires to work as close as possible to the „saturation fluence" which varies considerably with the type of medium used. As shown in Fig. 1, it is of the order of mJ/cm^2 for dyes, tens of mJ/cm^2 for excimers but can reach beyond the J/cm^2 for solid amplifying materials. An essential problem is then that one has also to stay below the „breakdown threshold" for the material used. This precludes the possibility of working at the saturation fluence in solid-state amplifiers in the pico- or subpicosecond regime. However, the saturation fluence can be reached if one works with pulse durations close to one nanosecond, because of the strong pulse duration dependence of the breakdown fluence. Since one is interested in amplifying short laser pulse, those are always associ-
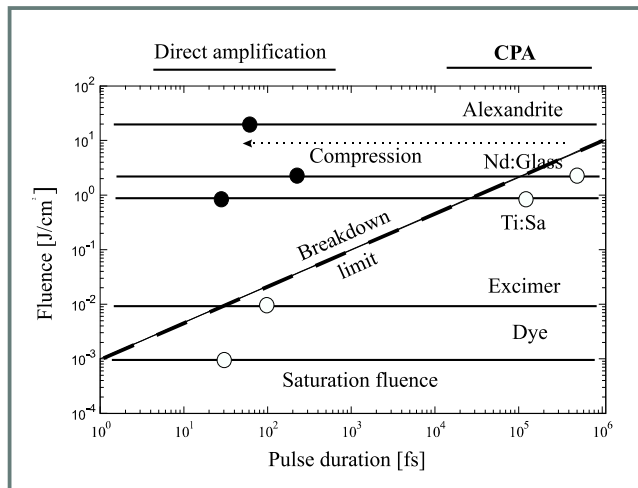

Fig. 1. Saturation fluence and breakdown limit for different materials (*by courtesy of F. Salin*)
An efficient amplification in solid state systems requires to work with pulses of nanosecond duration.

ated with a significant bandwidth (the Fourier transform limitation imposes that $\Delta\omega\tau \geq k$, where $\Delta\omega$ is the bandwidth, τ the pulse duration, k being a parameter whose value depends on the exact pulse shape but is always of the order of 0.5). Any dispersive element, in which the long wavelengths travel generally faster than the short ones, will therefore produce a lengthening of the broadband pulse and result in a so-called „chirped pulse" in which the frequency will vary from „red" to „blue" along the pulse. This dispersive element can be any amount of dispersive material, or more elaborated optical systems (where dispersion is generally provided by sets of prisms or gratings). In the first case, the dispersion is always positive, whereas in the second, depending on the configuration, the dispersion can be either positive of negative, suggesting the idea that a short pulse can be expanded in time and then recompressed : this is the basic idea in CPA [1]. A short pulse (with pico- or subpicosecond duration) is produced in an oscillator, stretched in time up to durations in the nanosecond range, amplified (in conditions where the saturation fluence is reached below the damage threshold) and finally recompressed almost down to its original duration.

CPA was first applied to Nd:Glass systems and already allowed in the late 80's to reach peak powers in the terawatt range with table-top systems operating at 1064 nm with pulse durations close to one picosecond, opening a wide

new field of applications (such peak powers had been so far reserved for giant multibeam laser systems). However the amplifying bandwidth of Nd:Glass was not yet sufficient to obtain „femtosecond" pulses, but using a combination of different glasses in the amplifying system, a number of large size lasers succeeded to produce pulses of duration down to 600 fs, with energies per pulse of the order of tens of joules, and the giant lasers now under construction (NIF in LLL–USA or LMJ in CESTA, Bordeaux, Fr) will most likely be equipped with a „PetaWatt" line allowing to reach laser intensities in excess of 10^{20} W/cm^2. Ultrashort pulses were still the speciality of dye and, to some extent, excimers systems until another revolution completely changed the picture, due to the emergence of a new class of oscillators based on the so called „Kerr Lens Mode-locking". Indeed, Titanium doped sapphire was expected, due to its large fluorescence bandwidth, to be an excellent candidate for the realization of solid-state femtosecond lasers. Moreover, in the process of designing a passively mode-locked oscillator based on this amplifying medium, the researchers discovered a quite unexpected possibility to obtain mode locking without inserting any Q-switching element in the cavity (hence the original appellation of this system: „magic" mode locking). Later on, this was found to be due to nonlinear effects occurring in the amplifying medium [2], hence the final appellation of „Kerr Lens Mode Locking", whose principle is depicted in Fig. 2. The cavity
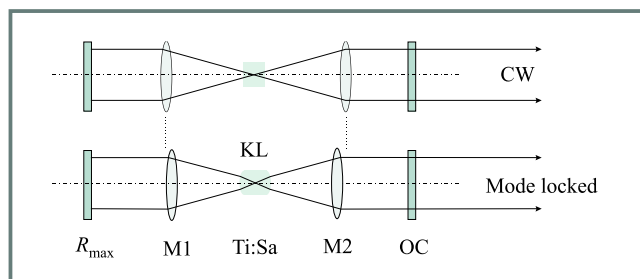

Fig. 2. Principle of the Kerr Lens Mode Locking
The cavity design has been simplified to the elements necessary for the understanding of the mode-locking principle. In the real set-up, lenses M1 and M2 are replaced by spherical mirrors. R_{max}: 100% reflecting mirror, OC : output coupler (3 to 10% transmission), KL : „Kerr Lens", in the mode locked regime only.

design includes two folding mirrors (symbolized by lenses for clarity on the figure), which focus both the pump and laser beam in the amplifying crystal. In the mode locked regime, the intensity is such in the crystal that nonlinear contributions to the refractive index (Kerr effect) turn the amplifying crystal (a plane parallel slab) into a lens, thus modifying the cavity stability, which is restored by a minor correction of the lenses position. The cavity can so be adjusted so that the best stability is obtained for the mode locked operation, conferring excellent stability to this type of lasers.
The real cavity design of course includes an internal negative dispersion line to compensate for Group Velocity Dispersion, mainly in the amplifying crystal. With such a

set-up, pulse durations of the order of 30 fs are routinely achieved with both commercial and home-built systems, with energies per pulse of the order of a few nanojoules, repetition rates in the 80 MHz range, and excellent beam qualities. Because of this, intensities up to 10^{10} W/cm^2 at 800 nm can be obtained at a lens focus, and GW/cm^2 at 400 nm (after frequency doubling). This is more than needed for a number of nonlinear optics applications.
Amplification of such pulses using the CPA method in regenerative amplifiers yield energies per pulse of the order of a few millijoules, and can be obtained at repetition rates now reaching the kHz. Beam characteristics are usually quite good (nearly gaussian beams), allowing a number of very high intensity experiments (up to 10^{16} W/cm^2) with quite reasonable scale equipment. The use of extra multipass amplifiers can boost the energy per pulse to 100 mJ, and the peak intensity in the TW range, at repetition rates of about 10 Hz, a considerable progress compared to the Nd:Glass based CPA systems. The recent progresses in this respect are represented in Fig. 3 and 4. It is clear
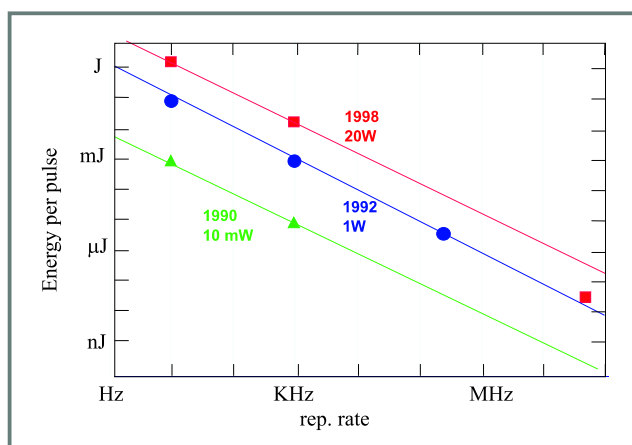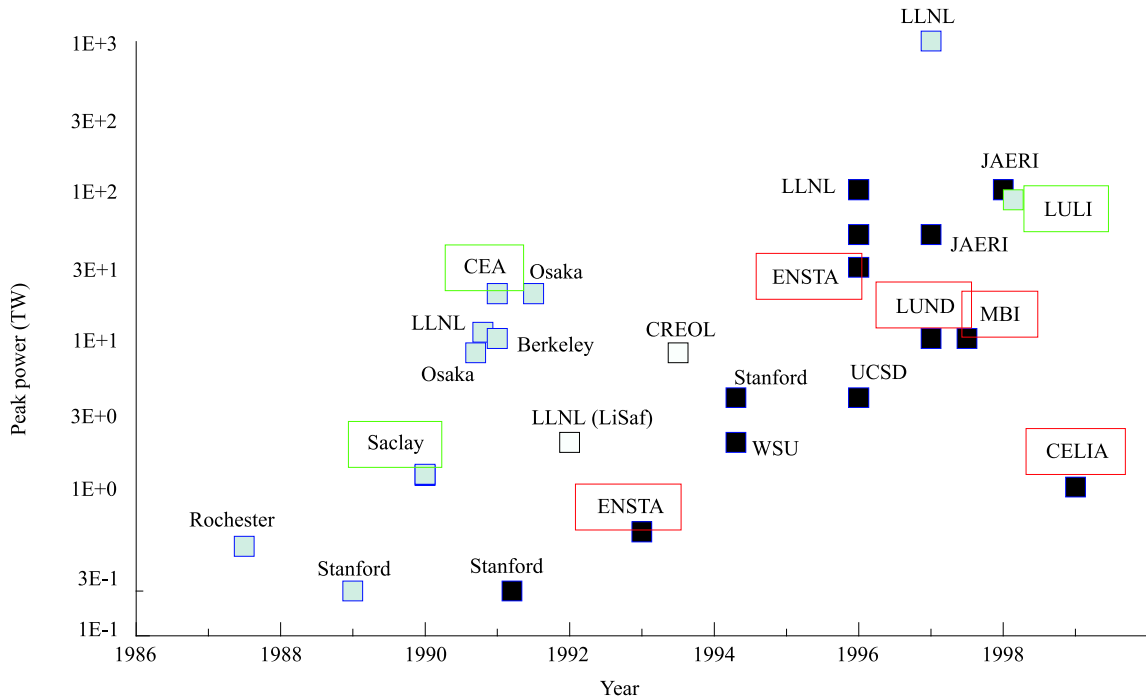

Fig. 3. State of the art concerning amplified Ti:Sa laser systems (*by courtesy of F. Salin*)
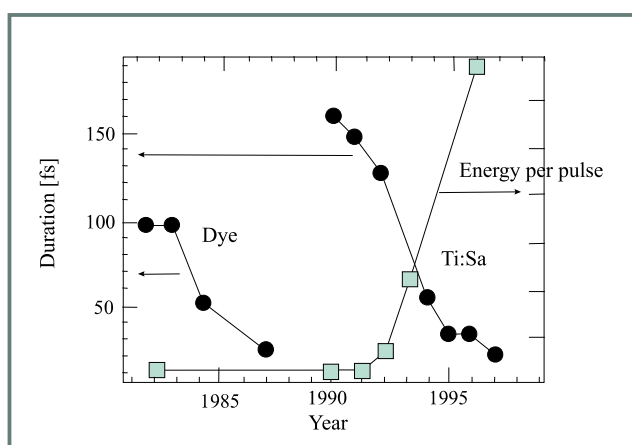
Fig. 4. Passed evolution on pulse duration (circles) and pulse energies (squares) for subpicosecond lasers

that one now disposes of laboratory scale systems allowing to investigate up to very high intensity effects at repeti-

Fig. 5. Past evolution of the peak power of high intensity CPA based laser systems (*by courtesy of C. Leblanc and C. Barty*) In grey: Nd:Glass, Empty: LiSaf, Black: Ti:Sa; European based systems are circled.

tion rates which are orders of magnitudes above those of Nd:Glass based systems (whose rep rate would probably express best in milli or microhertz!). On the other side, Fig. 4 clearly shows the huge impact of both breakthroughs detailed above.

Figure 5 shows a world wide view of the evolution and of the present status in terms of intense lasers.

Note that some world records of a different type are not mentioned in this figure. In particular, concerning the pulse duration, a Ti:Sa cavity design employing „chirped mirrors" (multilayered mirrors reflecting in which different wavelengths have different penetration depths) produced pulses with a 5 fs duration [3], thus setting for such lasers a record that was only reached but very sophisticated dye based systems. Worth mentioning is also the operation of Ti:Sa subpicosecond oscillators using for energy extraction a cavity dumper. This reduces the repetition rate to the 100 kHz - 1 MHz range, but increases the pulse energy by the same amount compared to the classical design (up to μJ per pulse). The stability of such systems is however reduced and they are more complicated to operate.
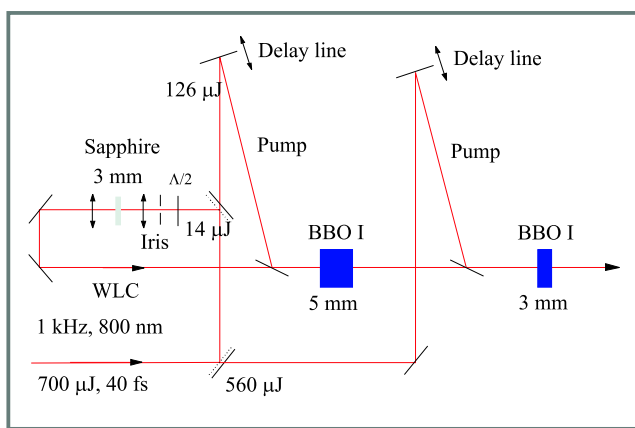
Tunable short pulse optical sources

Both dye lasers and Ti:Sa, who lead the race towards shorter laser pulses are the prototypes of tunable laser sources because, as explained above, a broad emission band is necessary in both cases. However, the actual tunability of the operational short pulse lasers is quite reduced. In the case of Ti:Sa, it is indeed possible to slightly vary the centre wavelength of the laser (e.g. between 770 and 830 nm), but to the expense of a loss of performances. Concerning the dye systems, short pulse generation required (in the CPM design) the use of a couple of complementary dyes, the operation is essentially restricted to 620 nm. Essentially three solutions were found to achieve a broadband tunability: White Light Continuum (WLC) amplification, frequency mixing and, more recently, Optical Parametric Oscillators/Amplifiers (OPO/OPA) WLC amplification is based on the observation that focusing even a very small amount (microjoules) of energy into e.g. water (but any transparent material works to some extent) allows to generate, through a number of nonlinear optical mechanisms, a more or less broad continuum of white light centred around the pump wavelength, whose pulse duration equals that of the pump pulse. A straightforward solution is then to select a band in this WLC and to amplify it in a set of dye amplifiers. This solution has been used for several years to generate subpicosecond pulses almost throughout the whole visible, with pulse energies in the 100 μJ range in the yellow-red part of the spectrum (pumping with Nd:YAG second harmonic) and 10 μJ in the blue part (pumping with Nd:YAG third harmonic). However, in the latter case, the photostability of the dyes used (contrary to that of those used in the red) is not good, which is at the source of many complications. Likewise, on a general basis, use of dye amplification is at the source of many inconveniences (such as the use of poisonous solvents) so that the search for „all solid state" solutions has been active and recently successful.

If one disposes of both a tunable source in the yellow-red part of the visible spectrum, and of a number of fixed-wavelength sources (Ti:Sa and its different harmonics), it is possible to use sum-frequency generation to obtain tunable short pulse optical pulses at shorter wavelengths. Indeed, WLC amplification, sum frequency generation and harmonic generation combined allow to cover practically all the visible and a significant part of the UV (down to approx. 220 nm), with energies per pulse ranging from a few 100 μJ in the red to about 1 μJ in the UV. However, due to the limitations of the available NL crystals in particular, some holes remain in the tunability curve which can be filled using Optical Parametric Generation. Optical Parametric Generation (OPG) is a process which can be viewed as symmetric of sum frequency generation. In the latter case, the energy of two different photons is added in a nonlinear crystal to generate a photon with the sum energy. In OPG, it is on the contrary the energy of the incident photon (pump beam) which is split in two smaller energy photons. The obtained energies (usually referred to as „signal" and „idler", in a quite arbitrary fashion) are imposed by the necessity of conserving in this operation both the total energy and momentum, and are located on either sides of the „degeneracy wavelength" which is equal to twice the pump wavelength. The phase matching condition generally depends on the optical characteristics of the nonlinear crystal and of the geometry of the optical configuration, and tuning is simply obtained by rotation of the nonlinear crystal.

The signal created in the OPG can be further amplified in an Optical Parametric Amplifier based on the same principle. A filtered WLC can also be used as a seed pulse for amplification in OPA, as represented in Fig. 6, which shows the principle of a subpicosecond OPA system at 1.3 μm. Note that the amplifying stages have to be separated. The reason for this is that since the group velocity of the pump, signal and idler waves are different in the amplifying crys-

tal, they slip off-phase as the thickness increases, an it is then necessary to use a new delay setting before starting the amplification again in a new crystal [4].

A number of OPG/OPA pumped either by Nd:YAG lasers (tens of picosecond of pulse duration) or lately by Ti:Sa lasers, and their harmonics, are presently commercially available, covering the whole visible spectrum on one hand, but also a significant part of the Infra-Red. In the visible, they are clearly competitive compared to dye amplified WLC in the blue part of the spectrum where they are generally preferred, which is not quite the case in the red part of the spectrum, where dyes work best. It seems however that solutions employing different frequency mixing, whose tunable part is provided by a dye system in the red offer better efficiency and stability, but they are not commercially available and require the presence of a team with some expertise in nonlinear optics.

One of the main interest of the OPO is that they have a capability of extending the wavelength range in which short pulses are available to the mid IR (up to 7.5 μm at present, up to 12 μm probably possible), a very interesting region because it is that of vibrational spectroscopy. Up to a recent past this range was covered only by Free Electron Lasers (FEL), a quite specific type of source that we now discuss.

Free Electron Lasers

The principle of the Free Electron Laser (FEL) consists in using as the gain mechanism, instead of the stimulated emission, the synchrotron radiation emitted by free electrons bunches inside a specific alternating magnetic configuration known, in the Synchrotron Radiation language as an „undulator". The permanent magnetic field is sinusoidal in space, and the transverse acceleration of the electrons allows them to radiate along their propagation axis a synchrotron radiation at the „resonance" wavelength λ:

$$\lambda = \frac{\lambda_0}{2\gamma}\left(1 + \frac{K^2}{2}\right) \quad \text{with} \quad K = 0.94\,\lambda_0 B_0(\text{T})\,, \quad (1)$$

where γ is the electron (or positron) normalized energy, λ_0 the magnetic field spatial period [cm] and B_0 its magnitude. It is clear from Eq. 1 that this source can be tuned, at a given beam energy by adjusting the magnetic field, and that a large tunability is in principle available also through the choice of the beam energy. The complex description of the field interaction with the particles is outside the scope of this paper (and the author's possibilities as well!), but it is enough to remember that FEL operate just as a standard laser whose gain medium is the relativistic electron beam. The laser gain increases when (i) the interaction length increases, (ii) the beam intensity increases, (iii) the beam energy decreases. Another peculiarity of FEL is that they produce a significant amount of harmonics of the laser.

The need for a relativistic particle beam implies that such lasers are built around particle accelerators, either linear, or as an insertion on a section of a Synchrotron Radiation

Fig. 6. Layout of a subpicosecond OPA system (*by courtesy of C. Leblanc*)
A white light continuum is generated in a Sapphire plate, and then amplified in a pair of BBO I type OPAs. The characteristics of this system are a pulse duration of 20 fs, a pulse energy of 50 μJ, at a wavelength of 1.3 μm.

machine. In all cases they are operated as a Large Scale Facility. However, their interest is such that there are a significant number of machines in operation, most of them as user facilities : about 10 machines in the USA, 5 in Japan and 7 in Europe are either in operation or construction.

For beam energies in the tens of MeV range, laser operation is achieved in the Infra-Red [5]. We have taken as an example the „CLIO" laser facility in Orsay. The laser is built around a „low" energy linear accelerator. It produces pulses with a specific time structure : a series of 1 to 10 μs macropulses with a repetition rate between 1 to 50 Hz, each of such macropulses consisting in a series of a few hundreds of micropulses, whose duration is pico and even subpicosecond (down to 300 fs have been achieved) depending on the cavity settings and of the position in the macropulse (shorter pulses are observed in the build-up of the macropulses). Fig. 7 illustrate the tunability of this
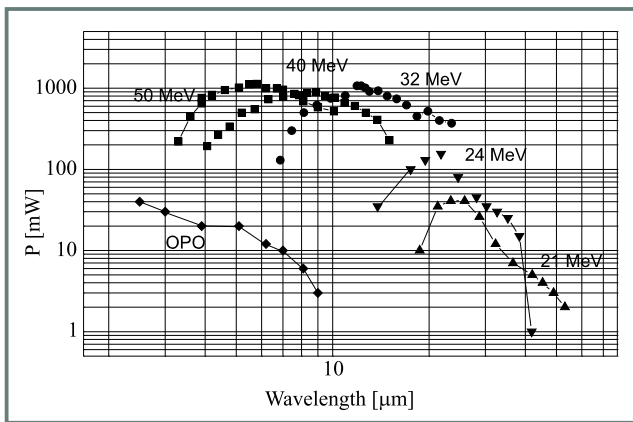

Fig. 7. Tuning curve of the IR-FEL „CLIO" (Orsay, France), as a function of the beam energy (*by courtesy of J. M. Ortega*)
In the lower left corner, the tuning curve of a Nd:YAG pumped OPO is presented for comparison.

laser for different beam energies. It shows that a very large wavelength range (more than one decade) can be obtained with this laser source. Peak powers at the maximum of the tuning curves reaches the 100 MW range, and about 5 MW are still obtained at the extreme wavelengths around 50 μm. On the same plot (in the lower left corner) is included the tuning curve of an IR-OPO pumped by a Nd:YAG laser. It illustrates the point mentioned above concerning the IR capabilities of OPO's. Though not as intense as the IR-FEL, they can still provide intensities in the 10 MW range, and they are by far not so complicated to operate as the LEL, and constitute a very serious alternative for the near IR, and are probably promised to a bright future.

Another exciting feature of FELs is their ability to operate simultaneously on two different wavelengths, as demonstrated in Fig. 8 [6]. This operated mode is obtained using two undulators with different spacing. The only principle restriction is that the two wavelengths must be obtainable with the same beam energy.

FEL can also operate in the visible-UV part of the spectrum [7], for beam energies in the GeV range. Such FEL are usually installed on storage rings. At present, their
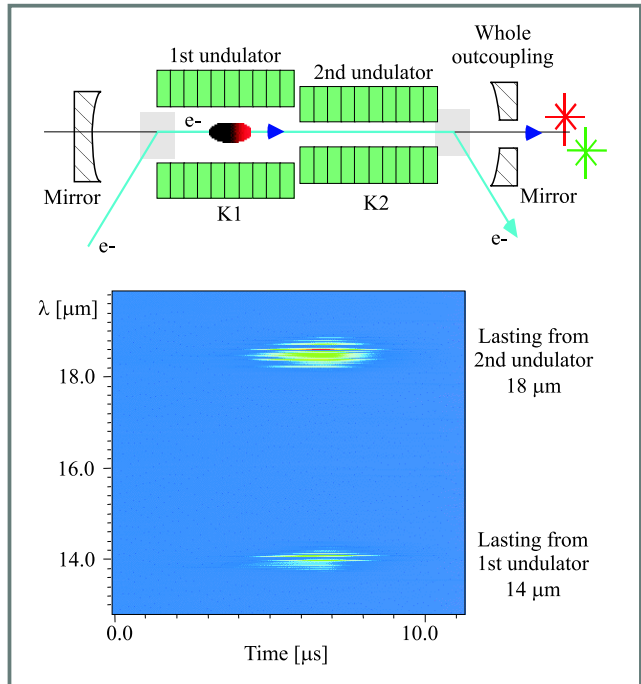
Fig. 8. IR-FEL cavity design, and operation in the „two-colour" mode (*by courtesy of J. M. Ortega*)

cost/performance ratio is not so impressive compared to other systems in the same wavelength range, and their essential interest is that they are synchronized by nature with Synchrotron Radiation which allow to consider a number of innovative pump probe experiments. However, the recent appearance of third generation rings should lead to a dramatic improvement of the UV-FEL characteristics. Pulse durations of the order of a few picoseconds should be available, and the peak power is expected to reach beyond the MW. Intensities of the order of 10 TW/cm^2 can reasonably be expected, at a repetition rate of tens of MHz. Besides, an increased harmonic content is expected, so that using the fifth harmonic of the laser, intensities close to the MW/cm^2 should be obtained for photon energies of 20 to 80 eV so that, given the high repetition rate, it should be possible to observe nonlinear effects in the XUV wavelength range. This has been one of the aims of the recent development of intense XUV sources, that we now comment.

Short–pulse, high–intensity XUV sources

The important progresses discussed above on the lasers gave birth to a number of schemes for producing high intensity, short pulses of XUV light through the interaction of high power laser pulses with matter in its different states. Attempts to obtain population inversion between states of highly ionised atoms, as they can be obtained in the plasmas generated in the interaction of high energy (hundreds of joules) laser pulses with metals have an already long story. A number of schemes have been proposed to realise this

way a „X-ray laser". In particular, several successes were obtained using the „collisional pumping" scheme, particularly in the case of a number of Ni-like and Ne-like metal ions. Among the lasing transitions observed, one finds Ne-like Fe at 21.2 and 25.5 nm [8], Ti at 32.6 [9] and Ge at 19.6 nm [10], and also, more recently, Ni-like Ag at 13.9 nm and Sn at 11.9 nm. Some laser schemes using a half cavity to increase the gain length have been realised, and some of these laser are presently operated as user facility providing pulses for applications. The essential difficulty in achieving such a goal was that the gain medium is essentially very inhomogeneous and nonstationary, since it is composed of an expanding plasma in front of the metallic target, so that it is necessary first to optimise the plasma conditions through the definition of a sequence of pumping pulses in order to control both the density gradient in the plasma and the electron temperature, which requires a significant amount of know-how. Such X-ray lasers are generally pumped by multibeam giant lasers with energies per (nanosecond) pulse in the 10 to 100's of Joules. They deliver pulses with durations of tens of picoseconds, and are presently the most intense X-Ray sources. In a recent past, the possibility of obtaining very high transient gains by pico or subpicosecond heating of a preformed plasma has resulted in the first observations of very short X-ray laser pulses (whose duration, though not yet precisely measured is most likely of the order or below 1 ps).

In the X-ray laser case, as already mentioned, the laser induced plasma which is the emitting medium has been allowed to expand, which means that its density, as well as its temperature have significantly decreased. With the appearance of subpicosecond lasers able to produce intensities in excess of 10^{15} W/cm^2, one obtained also the possibility of creating very hot (temperatures of tens of keV) and dense (solid density) plasmas since the dense matter can be heated in a time much shorter than the „hydrodynamical time constants". This was at the origin of a number of new sources of hard X-ray radiation (keV and more) [11]. The emission spectrum strongly depends on the nature of the metallic target, and can be dominated by the K lines of the used element (in the case of light species, e.g. : Al), but can also contain a significant continuous contribution when heavy (e.g.: Au) elements, in which Bremsstrahlung dominates the emission mechanisms, are used. Let us note that despite a high number of emitted photons per pulse, the emission occurs in 2π steradians, so that it is not easy to obtain high intensities on target with the help of such sources, contrary to the case of X ray lasers whose spatial coherence is much better.

Finally, in this category of laser-driven plasma sources, one should mention an already ancient observation [12] that interaction of moderately intense picosecond laser pulses (in the TW/cm^2 intensity range) with metal surfaces can produce hard X-ray radiation when the surface is placed under high cw polarization (MV/cm) so as to block the electron emission. Despite an only very limited characterisation, its seems that under such conditions, intense emission extend-

ing into the 10's of keV range is observed [13]. There is so far no interpretation of this effect, but it could clearly constitute an easy alternative to the use of very sophisticated laser sources (the necessary conditions can be achieved with a moderate size table top system) to produce high energy X ray.

Besides these laser-driven plasma sources, there is another important class of XUV sources based on high order harmonic generation of intense laser pulses [14]. Their appearance dates from more than ten years ago, at that time using Nd:Glass lasers as a pump source. They have also immensely benefited from the progresses in laser sources, and can now be found in almost every laboratory operating a high intensity Ti:Sa system. They are generally based on high order (up to 150 or more) harmonic generation in high density jets of rare gases. They present a very characteristic spectrum (Fig. 9): after a rapid decrease for the first few orders, the harmonic yield stabilizes through a region known as the „plateau", up to a cut-off frequency. Both the extension of the plateau as well as the yield depend on the type or rare gas used : the lighter elements provide the highest harmonics, but a better yield is obtained using heavier elements. In the general case, because of symmetry reasons, only the odd harmonics are produced. However, by adding fundamental and second harmonic frequencies [15], some even harmonics can be obtained (top of Fig. 9).
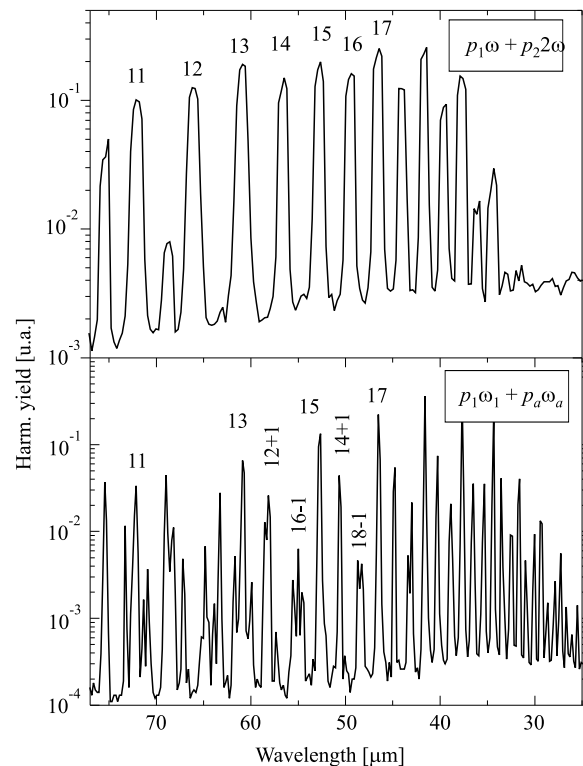
Fig. 9. High order harmonic spectra of the Ti:Sa laser obtained in Argon: top: fundamental and second harmonic of the pump laser are added to obtain even harmonics; bottom: the Ti:Sa fundamental is added to an OPA to obtain fine tunability (*by courtesy of B. Carré and F. Salieres*)

The number of harmonic photons in a given harmonic is of course the result of a combination of the single atom response and of the phase matching conditions in the pumping laser focal region. It is now well established that the important phase slips resulting from ionisation of the gas in the focal region limits the useable intensity range to less than the saturation intensity for a given element. Since the intensity also determines the cut-off frequency (ω_{co}), following a law of the type : $\hbar\omega_{co} = I.P. + nU_p$, where *I.P.* is the element ionisation potential, *n* a model dependent quantity usually between 2 and 3 and U_p the light „ponderomotive potential" (proportional to the intensity), it is easy to understand its increase for lighter element which are harder to ionise. Otherwise, the overall characteristics of the source depend on the focusing conditions, but they are now rather well under control, and high order harmonic sources are now reliable and can be used for applications. let us note in particular that their pulse duration has been measured using cross-correlation experiments with subpicosecond laser pulses, and they were shown to be even shorter in time than the pumping laser pulse (which is expected due to the nonlinear character of the interaction), so that they represent to date the shortest type of XUV pulses (40 fs has already been obtained, and 20 fs is expected for a near future. Their tunability is large and can be quite precise. It is first possible to select a given harmonic either with use of a spectrometer (which still causes an appreciable amount of lengthening of the pulse) or even using a selective multilayer mirror (which conserves the pulse duration, but is not by far as selective). Fine tuning of the harmonic frequency can even be obtained (Fig. 9) by combining in the generation processes photons of fixed frequency (usually a Ti:Sa laser) and tunable ones (from an OPA system) [15]. Any even combination of frequency can be obtained this way. Note in Fig. 9 that despite the fact that the pulse energy in the OPA system was quite small (about 50 µJ only) this does not affect the overall harmonic yield on combined-frequency peaks which are less than one order of magnitude below the pure laser harmonics ones.

It is instructing to compare the characteristics of these different sources, since they operate on a quite broad variety of mechanisms (Fig. 10). It should be noted that the result of the comparison may apparently depend on the quantity used to qualify a source. Here, we use the instantaneous brilliance, since it is the useful characteristics for nonlinear application: a source is efficient if it is energetic, point-like, delivers short pulses and has a low divergence. We note that in this respect, all the sources we have discussed are very competitive, even compared with future third generation undulators. However, if one cares about average power (as in linear applications), the picture would be completely reversed. In this respect, it is clear that FEL on third generation rings, operating at the five harmonics will represent a very competitive solution when it will be available, if they hold their promises, even if their pulse duration is not expected to fall down to what is now obtained with harmonics.

Applications

Nonlinear optics is of course deeply involved in the physics underlying the production of short intense pulses through the whole wavelength range discussed above. This is quite obvious in the case of OPO/OPAs, Kerr Lens Mode Locking or High Order Harmonics. It is also true in the case of plasma based sources since the plasma ionisation and heating mechanisms are in general highly nonlinear (multiphoton ionisation or resonant absorption come into play). We will not discussed here these aspects. Applications both concern the linear and nonlinear domain. We will discuss here three examples pertaining to the infra-red, the visible and the XUV range.

Infrared vibrational spectroscopy is one of the most important tools of physico-chemistry to characterize the chemical bonds in even complicated compounds (polymers for instance). On the other hand, the physico-chemistry of interfaces has become increasingly important with the rapid development of thin layers science, with applications to electrochemistry or catalysis for instance. One therefore needs methods for characterising the interfaces which are frequently buried under some amount of bulk material. In this respect, electronic spectroscopies (such as XPS)
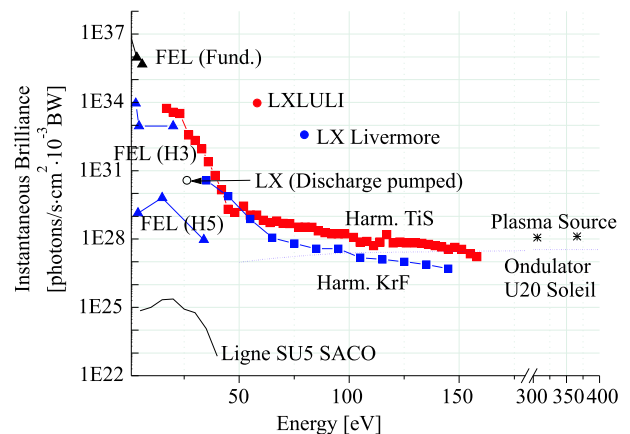
**Fig. 10.** Comparison of the instantaneous brilliance of different XUV sources (*by courtesy of P. D'Oliveira*)
Typical repetition rates for (LX): a few shots per hour Harm.: 10–20 Hz, FEL and Synchrotron radiation operate at MHz rep rates, but represent extrapolation to future third generation rings (except SACO).
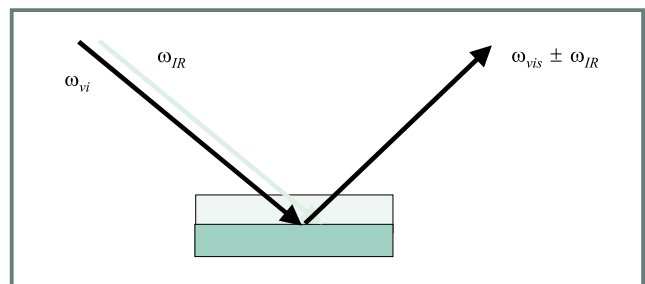
Fig. 11. Principle of the Sum (or Difference) Frequency Generation at interfaces
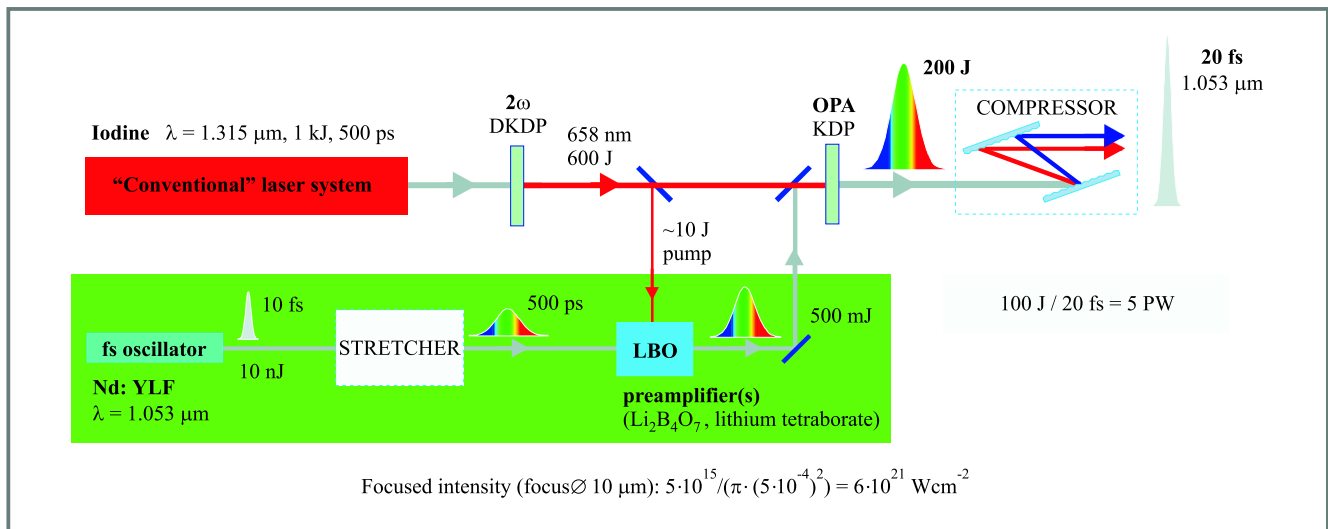
Fig. 12. Proposed scheme „Optical Prarametric Chirped Pulse Amplification" of an iodine laser at PALS (Prague Asterix Laser System) (*by courtesy of Bedrich Rus*)

rapidly reach their limits because the interface shift of a core level can sometimes be very small, and is rapidly masked by the increasing contribution of bulk material. In this respect Sum and Difference Frequency Generation (SFG/DFG)[16], whose principle is shown in Fig. 11, are of paramount importance since they are interface-selective. Indeed sum frequency generation, just as second harmonic generation, is forbidden in the case of centro-symmetric media, which is almost always the case of the overlaying material so that only the interface (where centro-symmetry is broken) contributes to the signal. By tuning the wavelength of the IR radiation, it is then possible to study the Infra Red spectroscopy of the interface. More sophisticated applications can be considered whith ultrashort pulses since this methods gives access to the dynamics of the interface vibrations (measure of the coherence times). An essential advantage of this method, besides its interface selectivity, is the fact that the measurements are made in the visible, where the detectors are much more efficient. SFG/DFG has become one of the most important applications of short intense IR pulse generated by OPOs and FELs.

We have mentioned the important applications of nonlinear optics to parametric generation, it can also be used in combination with CPA to improve the performances of laser systems which do not possess the short pulse capacity because of their limited bandwidth. This is for instance the case of Iodine lasers which can deliver high energies, but have an emission width of less than 2 Å. Figure 12 presents a proposed scheme for producing short pulses with help of an iodine laser, whose implementation is proposed on PALS (for Prague Asterix Laser System, a facility under construction in order to move the MPI-Garching Iodine laser). This scheme combines Optical parametric Amplification and Chirped Pulse Amplification, hence his appellation of OPCPA.

In this scheme, the iodine laser is used to amplify in nonlinear crystals an Nd:Ylf oscillator whose spectral width has been increased through self-phase modulation (another widely used nonlinear mechanism in the production of short laser pulses), so as to be able to produce 10 fs pulses, and then stretched to 500 ps to match the Iodine laser pulse duration. Amplification is then realised in standard OPA with pumping by the iodine second harmonic. The pulse is then recompressed so as to obtain 20 fs pulses of 100 J energy.

Finally, we would like to finish with a linear application in development on XUV sources, that is to say X-Ray Wavefront Division Interferometry applied to surface imaging [17]. In Wavefront Division Interferometry, spatial coherence is of paramount importance since it is different zones of a single input beam which are made to interfere through the use of a Fresnel bi-mirror (instead of the more traditional interferometry where two coherent identical beams are interfering, generated with use of beam splitters which do not exist in the XUV). The principle of this experiment is shown in Fig. 13. impinges on a Nb mirror whose left half is placed in front of an anode biased to an adjustable high voltage (so as to submit the Nb surface to fields in the 10 s of MV/m range). Then the beam is reflected by a Fresnel bi-mirror so as to make the part of the beam reflected on the biased area of the Nb mirror to interfere with the other part (reference wave). The bias voltage is progressively increased between the laser shots until changes in the interferograms, signalling the appearance of a field-induced surface defect are visible. This surface defect will upon further increase of the bias voltage cause a breakdown of the surface. This type of experiments can be of paramount importance to understand the basic effects at the origin of the gain limitation in superconducting cavities for future accelerator. Wavefront division interferometry requires highly spatially coherent intense sources. Originally demonstrated in the XUV range on synchrotron radiation, it has now been implemented on both X ray lasers and high order harmonic sources. One can thus consider high
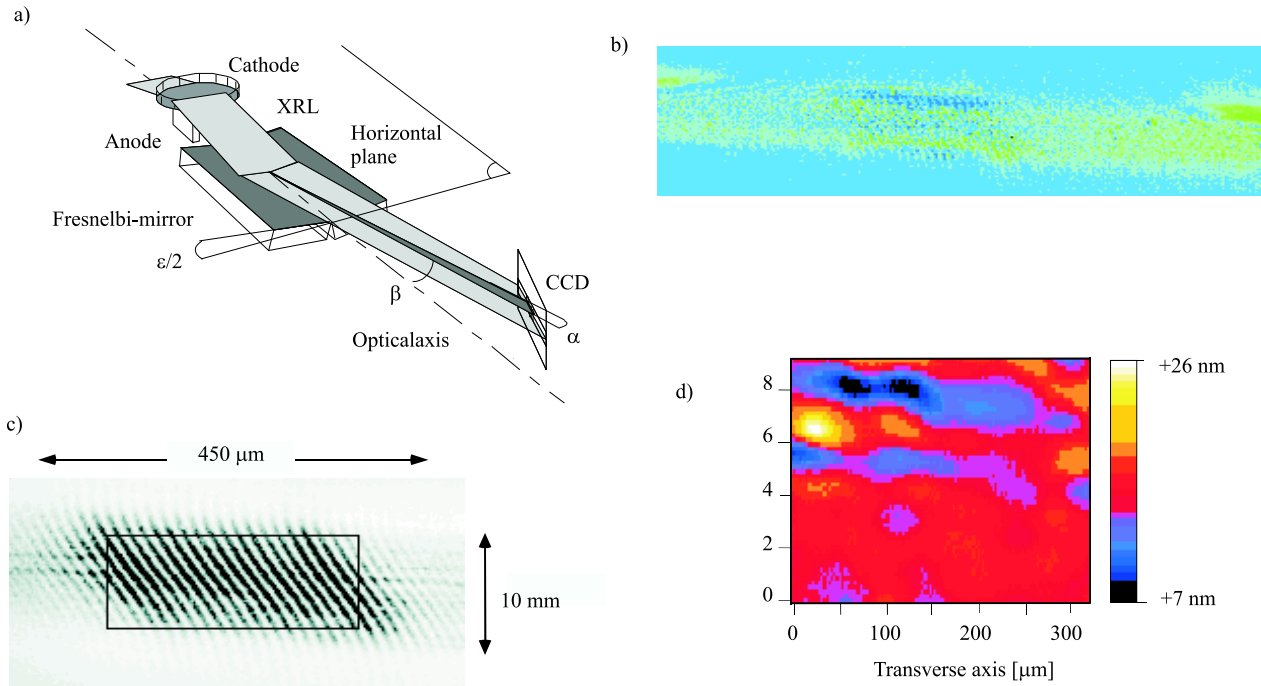
Fig. 13. Wavefront-division interferometric imaging of field-induced surface defects with X-ray lasers (*by courtesy of F. Albert*): a – eksperimental set up; b – interferogram substraction between 14 MV/m and 0 MV/m (reference); c – example of experimental interferogram; d – height variation of the surface between 27 and 37 MV/m obtained by phase reconstruction.

time resolution pump-probe types of experiments using this time-resolved imaging technique, with applications to fast optically driven processes such as laser breakdown for instance.

Other applications of short pulse intense XUV sources include for instance time-resolved photoelectron spectroscopies, and of course X-ray microlithography which can be of extreme importance as a future technology for submicron integrated electronics. Let us also note that mixed nonlinear processes involving one XUV photon and one laser photon have already been observed (laser-assisted Auger decay [18]), but that so far there is no experimental evidence of a purely XUV nonlinear process.

Perspectives and problems to be solved

As explained above, there has been huge progresses in the recent past on all the fronts concerning the production and the use of short and intense optical pulses. However, some progresses can still be expected in the near future, not all of them requiring technological breakthroughs.

Some prospective aspects mentioned above are of course linked to progresses in other domains such as for instance FELs which requires the construction of third generation rings (with some contradictory aspects since the FEL prefers low beam energies, which is generally not the case of other synchrotron radiation users).

Concerning the lasers in the optical and near IR domains, progresses are still ongoing. One should not expect a significant decrease of the available pulse duration (already down to 20 fs for high intensity Ti:Sa systems). Gain narrowing due to the amplification, as well as the extreme precision required in the design and alignment of the compressor (geometrical aberrations already have to be compensated up to the fifth order) seriously precludes such a possibility. Moreover, even keeping the pulse duration at this level through the optical system required by the application is already hard enough, and going further could make the experiment simply intractable. The essential progresses are expected on the repetition rates. Most of today's systems are operated at 10 or 20 Hz, but KHz systems with outputs in the mJ/pulse range are already available. High intensity kHz systems under construction now should deliver energies in the 20 mJ/pulse range. Progresses along this line are essentially expected to stem from progresses in diode pumped Neodymium lasers. Of course, high intensity diodes able to efficiently pump directly the Ti:Sa would be in this respect a major improvement, but they are not in view yet.

Any progress in terms of driving laser readily transpose to progresses in the derived XUV sources. Indeed, the X-ray laser greatly suffers from its low repetition rate (limited to a few shots per hour so far). Improvement can be expected from ongoing projects of diode pumped high energy Neodymium lasers (such as the Mercury project in

LLL), but also from an improvement of the X-ray laser's pumping scheme. In this respect, short pulse operation using transient pumping is obtained at pump level below 10 J per pulse, which is a significant progress. Concerning the X-ray lasers, it is also important to make the new experimental schemes available for application experiments, which is not a simple matter since X-ray lasers are still pumped by „giant" laser systems which are in very small number. Concerning the harmonic generation, reaching the kHz repetition rate is possible, but so far impeded by simple technical problems as the pumping speed in the vacuum system they require. Recent experiments based on guided propagation of the pump laser together with the harmonics in hollow fibres seem to offer an effective alternative to production in gas jets, but the important question of phase matching in such conditions have to be revisited to obtain an optimized efficiency.

An extremely serious bottleneck concerning the wide use of XUV radiation (which is common to all sources of this type) is the limited performances of X-ray optics. Except for a very limited wavelength range (around 14 nm) where a good solution exists (B-Si), multilayer mirrors achieve at best a 25% reflection efficiency, and the limitation of the number of useable layers precludes a good wavelength selectivity. Problems to be solved concern the choice of materials, as well as the roughness of the interfaces. This is an extremely serious problem since applications concerning BECU-size programs (such as microlithography in the USA) may turn out to be useless if it is not solved. Another problem concerns harmonic's selection with use of gratings. As mentioned above, using a single grating stretches the pulse duration to several picosecond, but it should be in principle possible to use a double grating system, in the same way it is used in the optical domain for pulse compression. We are only aware of unsuccessful attempts in this area, for reasons which are not quite clear.

Finally, the nonlinear crystals used for both low order harmonic generation and OPO/OPA have reached a satisfactory level. Their operation in this context is essentially limited by group velocity dispersion which precludes the use of long crystals, and thus limits their overall efficiency. This is especially true in the UV. It is clear that any improvements on this side would greatly benefit to laser systems.

Likewise, OPAs in the IR are already very exciting sources, but broadband tunability is here of paramount importance since the essential application concern vibrational spectroscopy. The 1–10 μm wavelength range achieved with Nd pumped OPAs, with hopes to extend it to more than 12 μm in a near future, if it could be achieved with Ti:Sa pumped systems would represent a major improvement since more than one order of magnitude would be gained in terms of pulse duration.

References

[1] M. Pessot, P. Maine, and G. Mouroux, *Opt. Commun.*, vol. 62, p. 419, 1987; P. Maine, B. Strickland, P. Bado, M. Pessot, and G. Mouroux, *IEEE J. QE*, vol. 24, p. 398, 1988.

[2] D. E. Spece, P. N. Kean, and W. Sibbet, „Digest of Conference on Laser and Electro-optics", in *Optical Society of America*, Washington D.C., 1990, paper CPDP 10/619.

[3] C. Spielman, L. Xu, R. Szipocs, and F. Krausz, *CLEO'96*, vol. 9, p. 28, 1996.

[4] W. Joosen, P. Agostini, G. Petite, J. P. Chambaret, and A. Antonetti, *Opt. Lett.*, vol. 17, p. 133, 1992.

[5] R. Prazeres, J. M. Berset, F. Glotin, D. Jaroszynski, J. M. Ortega, *Nucl. Instr. Meth. Phys. Res. A*, vol. 331, p. 15, 1993.

[6] D. Jaroszynski, R. Prazeres, F. Glotin, O. Marcouille, J. M. Ortega, D. Oepts, A. F. G. Vandermeer, G. M. H. Knippels, and P. W. Vanamersfoort, *Nucl. Instr. Meth. Phys. Res. A*, vol. 375, p. 647, 1996.

[7] M. E. Couprie, D. Garzella, and M. Billardon, *Europhys. Lett.*, vol. 21, p. 909, 1993.

[8] B. Rus, A . Carillon, P. Dhez, P. Jaeglé, G. Jamelot, A. Klisnick, M. Nantel, and P. Zeitoun, *Phys. Rev. A*, vol. 51, p. 1918, 1997.

[9] P. V. Nickles, V. N. Shlyaptsev, M. Kalachnikov, M. Schnürer, I. Will, and W. Sandner, *Phys. Rev. Lett.*, vol. 78, no. 14, p. 2748–51, 1997; M. P. Kalachnikov, P. V. Nickles, M. Schnürer, W. Sandner, V. N. Shlyaptsev, C. Danson, D. Neely, Wolfrum, C. L. S. Lewis, P. J. Warwick, A. Behjat, A. Demir, and G. J. Tallents, *Phys. Rev. A*, Nov. 1997 (submitted for publication).

[10] S. B. Healey, J. A. Ianulewicz, Plowes, and G. Pert, *Opt. Commun.*, vol. 132, p. 442–448, 1996.

[11] A. Rousse, P. Audebert, J. P. Geindre, F. Falliès, J. C. Gauthier, A. Mysyrowicz, G. Grillon, and A. Antonetti, *Phys. Rev. E*, vol. 50, p. 2200, 1994.

[12] Gy. Farkas and Z. Horvath, *Opt. Commun.*, vol. 21, p. 408, 1977.

[13] S. G. Dinev, Ch. I. Radev, K. V. Stamenov, and K. A. Stankov, *Opt. Quant. Electron.*, vol. 12, p. 231, 1980.

[14] A. L'Huillier, T. Auguste, Ph. Balcou, B. Carré, P. Monot, P. Salières, C. Altucci, M. B. Gaarde, J. Larsson, E. Mevel, T. Starczewski, S. Svanberg, C. G. Wahlstrom, R. Zerne, K. S. Budil, T. Ditmire, and M.D. Perry, *J. Nonlinear Opt. Phys. Mat.*, vol. 4, p. 647, 1995.

[15] M. B. Gaarde, P. Antoine, A. Persson, B. Carré, A. L'Huillier, and C. G. Wahlstrom, *J. Phys. B; At. Mol. Opt. Phys.*, vol. 29, p. L163, 1996.

[16] A. Tadjeddine, A. Peremans, and P. Guyot-Sionnest, *Surf. S.*, vol. 335, p. 210, 1995.

[17] F. Albert, D. Joyeux, P. Jaeglé, A. Carillon, J. P. Chauvineau, G. Jamelot, A. Klisnick, J. C. Lagron, D. Phalippou, D. Ros, S. Sebban, and P. Zeitoun, *Opt. Commun.*, vol. 142, p. 184, 1997.

[18] J. M. Schins, P. Breger, P. Agostini, R. C. Constantinescu, H. Muller, G. Grillon, A. Antonetti, and A. Mysyrowicz, *Phys. Rev. Lett.*, vol. 73, p. 2180, 1994.

Guillaume Petite CEA/DSM/DRECAM
Service de Recherches sur les Surfaces et l'Irradiation de la Matière
CEA Saclay, 91191, Gif-sur-Yvette, CEDEX, France

Control of the effects of crystal dispersion at different orders in the mixing of three phase-matched waves on a 5- to 100-fs time scale

Alessandra Andreoni, Maria Bondani, and Marco A.C. Potenza

Abstract — **A number of manners to obtain first-order achromatic phase matching of both type I and type II are presented and the most advantageous ones are identified to generate high-spectral quality 100-fs pulses by either parametric generation or frequency up-conversion. In the case of frequency-doubling high-energy 5-fs Ti:sapphire pulses, a non-collinear phase-matching I geometry in a β-barium borate crystal cut at 44 deg is devised that should allow high conversion efficiency, virtually without pulse lengthening and intra-pulse frequency chirp due to group-velocity dispersion.**

To investigate optical nonlinearities of materials and structures for ultrafast opto-optical and opto-electronic devices, it is becoming more and more necessary to develop table-top solid-state sources of high-power ultrashort pulses, broadly tunable in the near-UV/visible range. Particularly, after refinements of the chirped-pulse amplification (CPA) techniques led to ultra-broadband amplifiers giving multiterawatt pulses, sources based on optical parametric conversion/amplification, capable of sustaining consistently broad bandwidths, received great attention. Nowadays, harmonics of pulses with duration of the order of 100 fs are thus rather extensively used, either as pump pulses for parametric converters/amplifiers or in frequency-mixing schemes. They are typically mixed with the IR-tunable output of parametric generators pumped by the fundamental output of CPA sources such as Ti:sapphire and Nd:glass lasers.

The large chromatic dispersion of all nonlinear crystals available for these parametric interactions, however, makes generation of blue and near-UV wavelengths very critical when the pulse duration is 100 fs or less, in that also the minimal requirement in the frequency domain (first-order achromatic phase matching) becomes difficult to be fulfilled. In fact, only accidentally, the pump wavelengths available from Ti:sapphire and Nd:glass lasers, or from their harmonics, allow phase-matching (PM) with pulses at the wavelengths of interest, collinearly propagating with group velocities (GV's) suitably matched for efficient energy exchange. For type I phase-matching in $\beta - BaBO_4$ (BBO I), this occurs in spectral regions of the signal wave too narrow to be useful when the pump is at short wavelengths. Broad regions in which the GV's are mismatched

by less than 100 fs/mm exist for BBO II collinearly pumped at wavelengths between Nd fundamental and its second harmonic (SH). The case of pump at the Ti:sapphire fundamental represents a particularly fortunate circumstance, in which signal and idler have opposite GV mismatch (GVM) values with respect to the pump, of about 50 fs/mm in magnitude, over a reasonably broad spectral region. Wilson and Yakovlev [1] exploited it with success to amplify a fs near-IR continuum with up to 45% efficiency in 3- and 5-mm long BBO II crystals and obtained broadly tunable high-energy pulses of 30-50 fs duration with frequency-conversion techniques in thin crystals.

The problem of GVM is obviously also relevant to SH generation itself on the 100-fs time scale [2-5]: for instance, when Ti:sapphire high-energy pulses are frequency-doubled to pump parametric converters/amplifiers, there is a trend to circumvent such problem by using thin crystals and high intensities of the fundamental pulses. This attitude should be revised, according to a recent and extended study of the various effects, which affect the SH conversion efficiency in collinear PM I, pulse width and intra-pulse spectral distribution [5]. In fact, the interplay of dispersion and nonlinear interactions leads to crystal lengths and fundamental-pulse intensity values that are optimal for frequency doubling Ti:sapphire pulses of 150 fs. More specifically, the analysis carried out in [5], which includes both second-order-dispersion effects and third-order nonlinearities, shows that, as soon as the crystal depth goes beyond the length of the pathway over which fundamental and SH pulses keep superimposed while travelling, the use of high intensities may turn out to be disadvantageous. All experimental and theoretical results reported in [5] lead to the conclusion that the most critical effect in both BBO and LBO (LiB_3O_5) is that related to first-order dispersion.

A number of groups proposed a more fundamental approach to the problem of GVM and developed interaction schemes that allow GVM compensation [6-12]. These schemes are obviously specific for each nonlinear material and type of PM: while those developed for high-quality SH generation must only couple the GV's of fundamental and SH pulses [3-7, 13], those for optimizing the parametric interactions of pulses at three different wavelengths can ensure the fulfillment of various GV matching conditions that are all of interest. As to sum-frequency generation,

schemes linking the GV's of the pulses at ω_1 and ω_2 either to each other or to $GV_{\omega_1+\omega_2}$ were considered [8]. As to parametric generation/amplification, we demonstrated both theoretically [14] and in a number of experiments [9, 11, 12] that, in noncollinear PM geometries, the excess in the signal and idler GV's with respect to the pump GV can be cancelled, at each wavelength in the tuning range of the crystal adopted, by a proper choice of the pump angles, *i.e.* the angles of pump **k**-vector, $\mathbf{k}_p$, to crystal axis. By using such a GVM-compensated travelling-wave BBO generator to seed a collinear amplifier pumped by 120 μJ pulses at 0.4 μm, we demonstrated a 17% conversion efficiency into nearly transform-limited sub-100 fs pulses [15]. Since a specific noncollinear configuration of the seeder works properly in a tuning range that covers at most 100 nm, this approach, though of rather general applicability [14], is not ideal for obtaining a broadly tunable parametric source, but could be useful for SH generation (*vide infra*). For parametric sources, it is more interesting the collinear PM I configuration described in [16]: here, GV compensation is achieved over the entire tuning range of BBO by suitably tilting the pulse front of the Ti:sapphire SH pulse used as the extra-ordinary pump. In fact, a pump pulse, whose front is tilted by an angle γ on the same side of the walk-off angle ρ, exhibits a GV in the direction of $\mathbf{k}_p$ that is greater than that of an untilted pulse by the amount $\Delta GV = GV \tan\rho \tan\gamma$. We used this effect to match the GV-component parallel to $\mathbf{k}_p$ of the tilted pump pulse with the mean value of the GV's of the signal and idler pulses, this condition granting that they can be amplified while staying locked to the pump pulse, without broadening or gain saturation [17, 18]. By using 100-fs SH Ti:sapphire pump pulses, we thus obtained collinearly generated superfluorescence pulses tunable to wavelengths as short as 456 nm [16]. Recently, we showed that these pulses could be efficiently amplified, in the same BBO I crystal in which they are generated with tilted pulse fronts, by using pump pulses with the fronts tilted by the same γ angle as before. The tilt of the amplified signal pulses could be fully compensated. By characterizing the output of the system as to pulse spectrum and time profile, we found values of the time-bandwidth product close to the Fourier limit for signal-pulse energies of up to 1.5 μJ [19].

A general conclusion concerning three-wave interactions in crystals such as BBO, $LiIO_3$ and KH_2PO_4 (KDP) [14] as well as LBO [5] can be drawn: pulses of duration of the order of 100 fs and at almost any wavelengths in the tuning ranges of the crystals can strongly interact because geometries can be generally devised simultaneously producing phase-matching and GV-matching conditions that ensure suitably broadband interaction. Furthermore, making the pathway over which the three travelling pulses are superimposed greater than the crystal length renders the three-wave interaction unexpectedly insensitive to the effects of dispersion at orders above the first one. All experiments reported in the literature (*e.g.* [5, 9, 11, 12, 15, 16, 19]), in which the interaction is made to occur in such

a situation, show that transform-limited output pulses are observed whenever the intense incident pulse is transform-limited.

In this paper, we report on what we consider a noticeable application of an accurate cancellation of first-order dispersion effects in BBO I and give useful criteria to identify the best operating conditions, as to first- and second-order dispersion effects, for frequency-doubling Ti:sapphire laser pulses, as short as those recently obtained [20, 21]. We find that the GVM arising from first-order dispersion of BBO can be cancelled over such an extended frequency range that efficient conversion to SH, without noticeable pulse lengthening, can be obtained by using relatively long crystals and hence fundamental pulses at non-extreme intensities. This is so true that it becomes worthwhile to control the frequency chirp due to GV dispersion (GVD), which is a second order effect usually overcome by the chirp due to self-phase modulation in travelling-wave up-conversion schemes.

In a noncollinear PM I geometry of SH generation, in which we call θ the $\mathbf{k}_F$-to-$\mathbf{k}_{SH}$ angle inside BBO, the value that ensures

$$GVM_{F,SH} = (GV_F \cos\theta)^{-1} - (GV_{SH})^{-1} = 0 \quad (1)$$

at $\lambda_F = 0.79$ μm is $\theta = 10.25$ deg and the PM angle is $\alpha = 42$ deg (for calculations, see [14]). We first observe that, if the crystal is cut at an angle equal to α, the two fundamental pulses entering the crystal at incidence angles $\theta_{ext} = \pm 17.1$ deg, which corresponds to the desired value for the internal angle, θ, undergo pulse-front tilting by angles smaller than tenths of degree over a spectral range as broad as that of a transform-limited 5-fs pulse. Furthermore, due to the symmetric incidence of the two fundamental beams, the SH pulse is generated untilted. It is worth noting that the lateral spectral components of the Ti:sapphire pulse [20], that we keep undispersed when entering the crystal, by travelling at angles $\theta \neq 10.25$ deg, are likely to form distinct wavepackets, no more exactly GV-matched with their frequency-doubled counterparts. If we call λ_F^* the wavelength corresponding to the pulse central frequency, Ω, and $\alpha^* = \alpha(\lambda_F^*)$ and $\theta^* = \theta(\lambda_F^*)$ the angles that verify Eq. (1) at λ_F^*, the internal angles at which the different components travel are given by:

$$\theta_{int}(\lambda_F) = \arcsin\left[n_F(\lambda_F^*)\sin\theta^*/n_F(\lambda_F)\right]$$
$$= \arcsin\left[\sin\theta_{ext}/n_F(\lambda_F)\right]. \quad (2)$$

This produces a fundamental-to-SH time-drift per millimeter, given by

$$d(\lambda_F) = \left[GV_F(\lambda_F)\cos\theta_{int}(\lambda_F)\right]^{-1} +$$
$$- \left[GV_{SH}(\alpha^*, \lambda_F/2)\right]^{-1}. \quad (3)$$

Since the dispersion of BBO is such that this effect is more pronounced at short than at long λ_F values, to make the effect minimal across the whole spectrum of a 5-fs fundamental pulse, say between 0.7 and 0.85 μm [20], it is convenient to adopt a geometry optimised, for instance, at

$\lambda_F^* = 0.76$ µm, instead of 0.79 µm, which would correspond to Ω. According to our calculations, this amounts to taking $\alpha^* = 44$ deg $(= \theta_{cut})$ and $\theta^* = 10.72$ deg $(\theta_{ext} = 18.0$ deg).
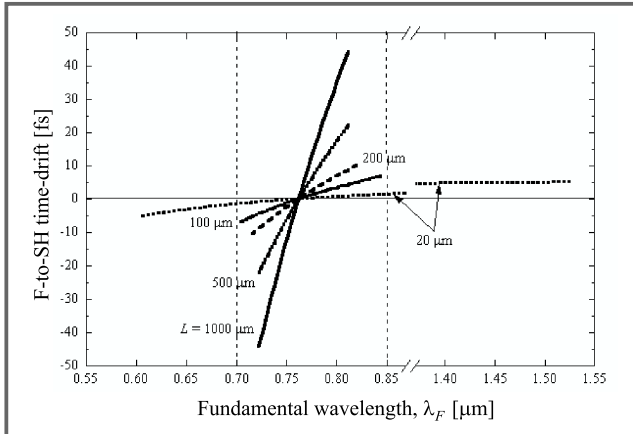
Fig. 1. Fundamental-to-SH time-drift in BBO I, at different crystal depths, L, as a function of λ_F in the spectral range of Ti:sapphire, when SH generation occurs in conditions of ideal GV-matching at $\lambda_F^* = 0.76$ µm. The curves are plotted in the regions where the time-drift due to GVM is below the time broadening due to GVD. The two vertical dashed lines mark the positions of the lateral peaks in the spectrum of the 5 fs pulse of Ref. [20]

The fundamental-to-SH time-drift accumulated across different BBO depths, L, are plotted in Fig. 1 as a function of λ_F, in the range of Ti:sapphire: the drift is obviously zero at 0.76 µm and increases, in magnitude, on going towards the edges of the spectral range. In our opinion, it is reasonable to accept time-drifts smaller than the duration with which an incident pulse of full-width at half-maximum (FWHM) duration $\tau_0 = 5$ fs would leave a BBO crystal of depth L, being affected by pure GVD effects. We thus calculated such duration values, $\tau(L)$, according to [22]:

$$\tau(L) = \tau_0 \sqrt{1 + \left(\left| \frac{\partial^2 k}{\partial \omega^2} \right|_\Omega 4 \ln 2 \frac{L}{\tau_0^2} \right)^2} \qquad (4)$$

in which

$$\left(\frac{\partial^2 k}{\partial \omega^2} \right)_\Omega = GVD_\Omega = -\frac{1}{GV^2} \left(\frac{\partial GV}{\partial \omega} \right)_\Omega \qquad (5)$$

with $GVD_{\Omega(0.79\mu m)} \cong 76$ fs^2/mm [23] and truncated the time-drift plots in Fig. 1 at $\pm\tau(L)$. We observe that these plots extend over spectral regions that broaden on decreasing L. This originates from the fact that, on decreasing L, the time spread due to GVD, *i.e.* $\tau(L) - \tau_0$, decreases less than linearly with L, whereas the fundamental-to-SH time-drift is proportional to L. As a result, a spectrum as broad as that comprised between 0.7 and 0.85 µm [20] becomes achieveable to SH generation with a BBO I crystal of depth between 100 and 200 µm. Note that such depth values, which allow keeping under control both first- and second-order dispersion effects, are greater by one order

of magnitude than the distance over which first-order dispersion effects are negligible in collinear SH generation [5]. Finally, the fact that, in our noncollinear geometry, the fundamental- and SH- pulses are perfectly GV-matched in the direction of $\mathbf{k}_{SH}$ around their central frequencies, ensures that the strongest field-components experience the strongest coupling and hence produces a sort of locking of the interacting pulses [8, 9, 12, 24]. We are also confident that the concomitant absence of pulse-front tilt and negligibility of higher-order nonlinear phase shifts in BBO up to intensities well above 100 GW/cm^2 [5] should limit the effects of first- and second-order dispersion below those shown in Fig. 1 for the SH intrapulse-frequency chirp.

Acknowledgements

References

[1] K. R. Wilson and V. V. Yakovlev, „Ultrafast rainbow: tunable ultrashort pulses from a solid-state kilohertz system", *J. Opt. Soc. Am. B*, vol. 14, pp. 444–448, 1997.

[2] J. Comly and E. Garmire, „Second harmonic generation from short pulses", *Appl. Phys. Lett.*, vol. 12, no. 7-9, 1968.

[3] O. E. Martinez, „Achromatic phase matching for second harmonic generation of femtosecond pulses", *IEEE J. Quant. Electron.*, vol. QE-25, pp. 2464–2468, 1989.

[4] G. Szabo and Z. Bor, „Broadband frequency doubler for femtosecond pulses", *Appl. Phys. B*, vol. 50, pp. 51–54, 1990.

[5] J.-Y. Zhang, J. Y. Huang, H. Wang, K. S. Wong, and G.K. Wong, „Second-harmonic generation from regeneratively amplified femtosecond laser pulses in BBO and LBO crystals", *J. Opt. Soc. Am. B*, vol. 15, pp. 200–209, 1998.

[6] K. Hayata and M. Koshiba, „Group-velocity-matched second-harmonic generation: an efficient scheme for femtosecond ultraviolet pulse generation in periodically domain-inverted β-BaB2O4", *Appl. Phys. Lett.*, vol. 62, pp. 2188–2190, 1993.

[7] G. Y. Wang and E. M. Garmire, „High-efficiency generation of ultrashort second-harmonic pulses based on the Cherenkov geometry", *Opt. Lett.*, vol. 19, pp. 254–256, 1994.

[8] C. Radzewicz, Y. B. Band, G. W. Pearson, and J. S. Krasinski, „Short pulse nonlinear frequency conversion without group-velocity-mismatch broadening", *Opt. Commun.*, vol. 117, pp. 295–303, 1995.

[9] P. Di Trapani, A. Andreoni, G. P. Banfi, C. Solcia, R. Danielius, A. Piskarskas, P. Foggi, M. Monguzzi, and C. Sozzi, „Group-velocity self-matching of femtosecond pulses in noncollinear parametric generation", *Phys. Rev. A*, vol. 51, pp. 3164–3168, 1995.

[10] V. Krylov, A. Kalintsev, A. Rebane, D. Erni, and U. P. Wild, „Noncollinear parametric generation in LiIO3 and β-barium borate by frequency-doubled femtosecond Ti:sapphire laser pulses", *Opt. Lett.*, vol. 20, pp. 151–153, 1995.

[11] P. Di Trapani, A. Andreoni, C. Solcia, P. Foggi, R. Danielius, A. Dubietis, and A. Piskarskas, „Matching of group velocities in three-wave parametric interaction with fs pulses and application to travelling-wave generators", *J. Opt. Soc. Am. B*, vol. 12, pp. 2237–2244, 1995.

[12] P. Di Trapani, A. Andreoni, P. Foggi, C. Solcia, R. Danielius, and A. Piskarskas, „Efficient conversion of femtosecond blue pulses by travelling-wave parametric generation in non-collinear phase matching", *Opt. Commun.*, vol. 119, pp. 327–332, 1995.

[13] T. R. Zhang, H. R. Choo, and M. C. Downer, „Phase and group velocity matching for second harmonic generation of femtosecond pulses", *Appl. Opt.*, vol. 29, pp. 3927–3933, 1990.

[14] A. Andreoni and M. Bondani, „Group-velocity control in the mixing of three non-collinear phase-matched waves", *Appl. Opt.*, vol. 37, pp. 2414–2423, 1998.

[15] P. Di Trapani, A. Andreoni, C. Solcia, G. P. Banfi, R. Danielius, A. Piskarskas, and P. Foggi, „Powerful sub-100-fs pulses broadly tunable in the visible from a blue-pumped parametric ganerator and amplifier", *J. Opt. Soc. Am. B*, vol. 14, pp. 1245–1248, 1997.

[16] R. Danielius, A. Piskarskas, P. Di Trapani, A. Andreoni, C. Solcia, and P. Foggi, „Matching of group velocities by spatial walk-off in collinear three-wave interaction with tilted pulses", *Opt. Lett.*, vol. 21, pp. 973–975, 1996.

[17] R. Danielius, A. Piskarskas, A. Stabinis, G. P. Banfi, P. Di Trapani, and R. Righini, „Travelling-wave parametric generation of widely tunable, highly coherent femtosecond light pulses", *J. Opt. Soc. Am. B*, vol. 10, pp. 2222–2232, 1993.

[18] S. A. Akhmanov, A. S. Chirkin, K. N. Drabovich, A. I. Kovrigin, R. V. Khokhlov, and A. P. Sukhorukov, „Nonstationary nonlinear optical effects and ultrashort light pulse formation", *IEEE J. Quant. Electron.*, vol. QE-4, pp. 598–605, 1968.

[19] R. Danielius, A. Piskarskas, P. Di Trapani, A. Andreoni, C. Solcia, and P. Foggi, „A collinearly phase-matched parametric generator/amplifier of visible femtosecond pulses", *IEEE J. Quant. Electron.*, vol. 34, pp. 459–464, 1998.

[20] S. Sartania, Z. Cheng, M. Lenzner, G. Tempea, Ch. Spielmann, F. Krausz, and K. Ferencz, „Generation of 0.1-TW 5-fs optical pulses at a 1-kHz repetition rate", *Opt. Lett.*, vol. 22, pp. 1562–1564, 1997.

[21] M. Nisoli, S. De Silvestri, O. Svelto, R. Szipoecs, K. Ferencz, Ch. Spielmann, S. Sartania, and F. Krausz, „Compression of high-energy laser pulses below 5 fs", *Opt. Lett.*, vol. 22, pp. 522–524, 1997.

[22] S. A. Akhmanov, V. A. Vysloukh, and A. S. Chirkin, *Optics of femtosecond laser pulses*. New York: American Institute of Physics, 1992.

[23] A. Andreoni, M. Bondani, and M. A. C. Potenza, „Ultra-broadband and chirp-free frequency doubling in β-barium borate", *Opt. Commun.*, vol. 154, pp. 376–382, 1998.

[24] H. Wang, K. S. Wong, D. Deng, Z. Xu, G. K. L. Wong, and J. Zhang, „Kilohertz femtosecond UV-pumped visible β-barium borate and lithium triborate optical parametric generator and amplifier", *Appl. Opt.*, vol. 36, pp. 1889–1893, 1997.

Alessandra Andreoni, Maria Bondani, and Marco A.C. Potenza
Dipartimento di Scienze Chimiche, Fisiche e Matematiche, University of Insubria
Via Lucini, 3 - 22100 Como, Italy
Phone: +39 (31) 326225 Fax: 326230
E-mail: ANDREONI@FIS.UNICO.IT

Nonlinear optics of the thin-film quasiwaveguide amplifier: applications to directional switching in the optical communication systems

Gagik P. Djotyan, Vilik M. Arutunyan, Joseph S. Bakos, and Zsuzsa Sörlei

Abstract — **We examine nonlinear optical effects in the active medium of the thin-film quasiwaveguide amplifier-oscillator with injection of the external signal. The injection locking has been obtained in the case when both the frequency and the direction of propagation of the injected signal differ from those for a free-running thin-film laser which offers a possibility for the frequency and directional switching of the output of the thin-film laser. The effects of four wave mixing and phase conjugation have been discussed in the active medium of the thin-film laser when additional mirrors forming an external resonator have been used.**

Keywords — *thin-film laser, directoral switching, four-wave mixing, optical communication systems.*

Fig. 1. Schematic diagram of the thin-film amplifier-oscillator

Introduction

The injection of an external reference signal into the laser cavity when the injected signal frequency differs from that of the free-running laser is of significant practical interest and is being extensively used as an effective tool for frequency stabilization, increasing the output power and spectral brightness of different types of oscillators, (see for example, [1-3]). As a rule, alone the frequency of the injected signal differs from that of the free-running oscillator in the applications reported earlear. A question arises, what will be the response of a free-running laser on injection of an external signal, which differs not only by the frequency but by the direction of propagation as well from the free-running mode of the laser. The answer on this question is important from the practical point of view for spacially extended laser-active systems, for example, waveguide lasers [4], or surface emitting semiconductor lasers [5].

This paper deals with a thin-film quasiwaveguide (TQ) amplifier-oscillator, which consists of a plane thin film laser-active medium of refractive index n_2 and gain factor α, bounded by two passive dielectric media of refractive indicies n_1 and n_2 under the condition $n_2 < n_1, n_3$, see Fig. 1. Due to this condition, this system has only leaky modes. Because of the large gain factor of the laser-active medium (a dye solutions or polymers with laser pumping are usually used) and the structural peculiarities (the layer thickness is of order of a wavelength), operation of TQ with comparatively large spectral-angular dispersion is possible [6,7].
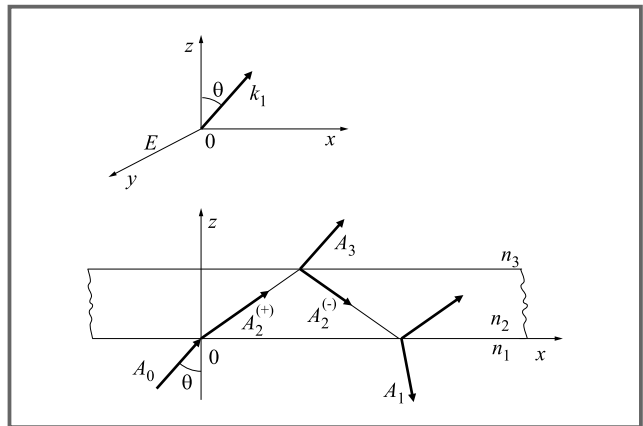
There is a possibility in this system for the injected signal to differ not only by the frequency but also by the direction of propagation from the free-running TQ laser output, in contrast with the ordinary laser systems. We consider the interaction between a plane monochromatic electromagnetic wave and the TQ amplifier taking into account the amplification saturation. We show that the injection locking takes place at sufficiently high intensity of the injected signal. This injection locking differs from the well known ordinary one. Namely, not only the frequency of the free-running TQ is being locked by the injected signal, but the direction of propagation of the TQ's output radiation also coincides with that of the injected signal.

The effects of four-wave mixing and phase conjugation in the active medium of TQ laser with two additional mirrors making an external resonator for the output radiation are briefly discussed as well.

A two-level homogeneously broadened amplifying medium of resonant frequency ω_0 has been assumed in this paper. We have the following equations for the electric field strength in the steady-state interaction regime under consideration (see Fig. 1)

$$\left(\Delta + \frac{\omega^2}{c^2} n_j^2\right) E_j = i\, \frac{\omega}{c}\, \frac{\alpha}{1 + \gamma^2 |E|^2}\, \delta_{j2} E_j, \qquad (1)$$

where Δ is the Laplace operator, ω is the frequency, n_j is the refractive index of the j-th medium and δ_{ij} is the

Kronecker's delta ($i, j = 1, 2, 3$). $\alpha = \frac{8\pi}{ch}\omega|d|^2\frac{\Delta_0}{\Gamma}$ is the gain coefficient describing the amplification properties of the medium, with d being the dipole moment, and Γ being the linewidth of the active transition, Δ_0 is the initial population inversion density, $\gamma = \frac{8T_1|d|^2}{h^2\Gamma}$ is the saturation parameter with T_1 being the longitudinal relaxation time.

The case of a symmetric system, where $n_1 = n_3 = n$, ($n_2 < n$) is discussed in this paper for the sake of simplicity.

We consider here the case of signal amplification with a wave vector lying in the plane $X0Z$ and the electric field strength polarized along the y axis, as in Fig. 1. The electric field strengths in the three media are given by

$$
\begin{aligned}
E_1(x,y,z) &= \frac{1}{2}\left[A_0\exp(ik_1z) + A_1\exp(-ik_1z)\right]\times \\
&\times \exp\left[i(q_1x - \omega t)\right] + c.c. \quad (2)
\end{aligned}
$$

$$
\begin{aligned}
E_2(x,y,z) &= \frac{1}{2}\left[A_2^{(+)}(z)\exp(ik_2z) + A_1\exp(-ik_2z)\right]\times \\
&\times \exp\left[i(q_2x - \omega t)\right] + c.c. \\
E_3(x,y,z) &= \frac{1}{2}A_3\exp\left[i(k_3z + q_3x - \omega t)\right] + c.c., \quad (3)
\end{aligned}
$$

where $k_1 = k_3 = \frac{\omega}{c}n\cos(\Theta)$, and Θ is the incident angle, as in Fig. 1.

The condition of the system homogeneity along the x axis leads to the relation:

$$
q_1 = q_2 = q_3 = \frac{\omega}{c}n\sin(\Theta).
$$

In Eqs (2), A_0 is a given amplitude of the incident wave, A_1 is the amplitude of the wave reflected from the active film, $A_2^{(+)}(z)$ and $A_2^{(-)}(z)$ are the amplitudes of the waves propagating in the active film with positive and negative projections of the wave vector on the z axis, respectively, and A_3 is the amplitude of the transmitted wave.

Our aim here is to obtain and analyse the intensities of the reflected $I_r = |A_1|^2$ and transmitted $I_{tr} = |A_3|^2$ waves as functions of the incident wave intensity $I_0 = |A_0|^2$.

We obtain the following set of equations in the amplifying medium ($j = 2$) for the normalized amplitudes $a^{(+)} = \sqrt{\gamma/2}A_2^{(+)}$ and $a^{(+)} = \sqrt{\gamma/2}A_2^{(+)}$ using the slowly varying envelope approximation:

$$
\frac{d}{dz}a^{(+)} - \exp(-2ik_2z)\frac{d}{dz}a^{(+)} = \frac{\beta}{2}f(z), \quad (4)
$$

where

$$
f(z) = \frac{a^{(+)}(z) + a^{(-)}(z)\exp(-2ik_2z)}{1 + |a^{(+)}(z)|^2 + |a^{(-)}(z)|^2 + a^{(+)*}(z)a^{(-)}(z)\exp(-2ik_2z) + a^{(+)}(z)a^{(-)*}(z)\exp(2ik_2z)},
$$

and

$$
\beta = \frac{\omega}{c}\frac{n_2\alpha}{k_2}.
$$

It is important to note, that $f(z)$ is a periodic function with period π/k_2. It means that we can represent the function $f(z)$ in the form of a Fourier series

$$
f(z) = \sum_{m=-\infty}^{\infty}C_m\exp(-2imk_2z)
$$

with

$$
C_m = \frac{k_2}{\pi}\int_{-p/k_2}^{p/k_2}f(z)\exp(-2imk_2z)dz. \quad (5)
$$

We obtain the following equations for the normalized amplitudes by equating the coefficients of exponentials with equal indicies:

$$
\frac{d}{dz}a^{(+)} = \frac{\beta}{2}C_0,
$$

$$
-\frac{d}{dz}a^{(-)} = \frac{\beta}{2}C_{-1}.
$$

We have the following set of equations from the last one after substitution of the C_0 and C_{-1} calculated from Eq. (4):

$$
\begin{aligned}
\frac{d}{dz}a^{(\pm)} = &\pm\frac{\beta}{2}\frac{1}{a^{(\pm)*}}\cdot \\
&\cdot\frac{|a^{(\pm)}|^2 - \frac{d}{2}\left[1 - (1 - 4|a^{(+)}|^2|a^{(-)}|^2/d^2)^{1/2}\right]}{d(1 - 4|a^{(+)}|^2|a^{(-)}|^2/d^2)^{1/2}},
\end{aligned} \quad (6)
$$

where

$$
d = 1 + |a^{(+)}|^2 + |a^{(-)}|^2.
$$

We have from Eq. (5) for intensities of the counter-propagating waves in the active medium of TQ in the case of week saturation when $\eta = 2|a^{(+)}|^2 + |a^{(-)}|^2/d \ll 1$, keeping terms up to second order of η:

$$
\begin{aligned}
\frac{d}{dz}I^{(+)} &= \beta\frac{I^{(+)}}{1 + I^{(+)} + I^{(-)}} - \left[1 - \frac{I^{(-)}}{1 + I^{(+)} + I^{(-)}}\right]' \\
\frac{d}{dz}I^{(-)} &= \beta\frac{I^{(-)}}{1 + I^{(+)} + I^{(-)}} - \left[1 - \frac{I^{(+)}}{1 + I^{(+)} + I^{(-)}}\right]
\end{aligned} \quad (7)
$$

with $I^{(\pm)} = |a^{(\pm)}|^2$.

These equation have the following motion integral

$$
\begin{aligned}
&\frac{I^{(+)}(z)I^{(-)}(z)}{\left[1 + I^{(+)}(z)\right]\left[1 + I^{(-)}(z)\right]} = \\
&= \frac{I^{(+)}(z=0,L)I^{(-)}(z=0,L)}{\left[1 + I^{(+)}(0,L)\right]\left[1 + I^{(-)}(0,L)\right]} = K = \text{const.}
\end{aligned} \quad (8)
$$

The boundary conditions of the problem under consideration are the continuity conditions of the tangential components of the electric and magnetic vectors of the waves on the interfaces of the laser-active and the passive dielectric media at $z = 0$ and $z = L$.

We integrate the Eqs. (6) by introducing the amplification parameter $\xi = I^{(+)}(L)/I^{(+)}(0) = I^{(-)}(0)/I^{(-)}(L)$ (which describes the wave amplification during one pass through the film) and using the boundary conditions. The equation

for the parameter ξ has the following form

$$\frac{(1-K)^2}{(1+K)^2}\left\{(1+K)I^{(+)}(L)(1-1/\xi)+\right.$$
$$+\frac{K}{K+I^{(+)}(L)(1+K)}\left[1-\frac{K+I^{(+)}(L)(1+K)}{K+(1+K)I^{(+)}(L)/\xi}\right]+$$
$$\left.+(1-K)\ln\left[\frac{K+I^{(+)}(L)(1+K)}{K+(1+K)I^{(+)}\{L\}/\xi}\right]\right\}=\beta L,$$

$$a^{(+)}(L)=a^{(+)}(0)\xi^{\frac{1}{2}};$$

$$a^{(-)}(0)=a^{(-)}(L)\sqrt{\frac{\xi+I^{(+)}(L)}{\left[1+I^{(+)}(L)\right]\left[1+I^{(-)}(L)\right]-I^{(-)}(L)\left[\xi+I^{(+)}(L)\right]}},$$

where $K=\dfrac{I^{(+)}(L)I^{(-)}(L)}{\left[1+I^{(+)}(L)\right]\left[1+I^{(-)}(L)\right]}$.

The intensities $I(L)$ may be expressed through the intensity I_{tr} of the wave transmitted through the TQ using the boundary conditions at the interface $z=L$:

$$I^{(\pm)}(L)=\frac{1}{4}\left(1\pm\frac{k_1}{k_2}\right)^2 I_{tr}.$$

We obtain the following expressions for the normalized intensities of the transmitted $I_{tr}=\frac{\gamma}{2}|A_3|^2$ and the reflected $I_r=\frac{\gamma}{2}|A_1|^2$ waves using boundary conditions on the interface $z=0$ and Eq. 9), and assuming that the parameter $K\ll 1$:

$$I_{tr}=I_0\frac{\xi(1-P)^2}{\xi^2 P^2-2\xi P\cos(2k_2 L)+1},$$

$$I_r=\frac{1}{\xi}I_{tr}\left(\frac{k_2^2-k_1^2}{4k_1 k_2}\right)\left[1+\xi^2-2\xi\cos(2k_2 L)\right], \quad (9)$$

where $I_0=\gamma/2|A_0|^2$ is the normalized intensity of the incident wave, and $P=(k_1-k_2)^2/(k_1+k_2)^2$.

The oscillation regime of the TQ laser corresponds to the zero denominator condition in Eq. (10). Using this condition, we can determine the eigenvalue of the wave vector k_2, the threshold value α_{th} and the amplification parameter ξ_{th} in the oscillating regime:
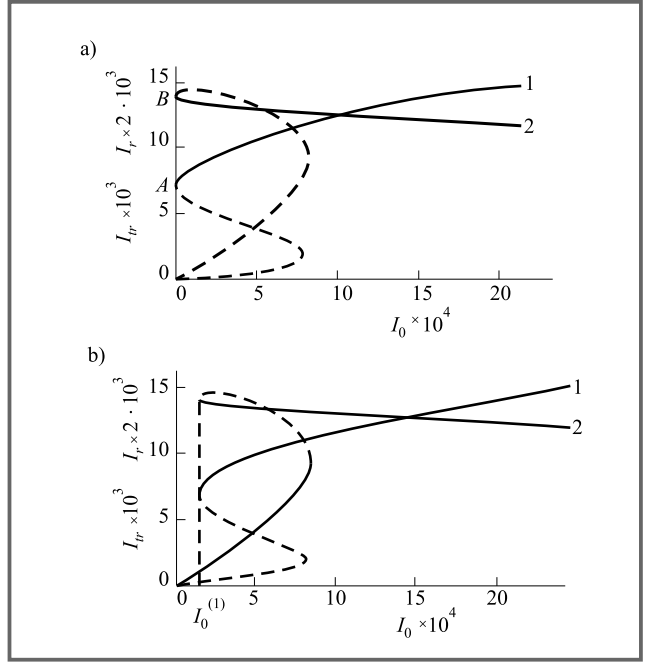
$$k_2 L=m\pi,(m=\pm 1,\pm 2...);\ \xi_{th}=1/P;$$

$$\alpha_{th}=\frac{2}{\beta}\ln(1/\sqrt{P}).$$

The dependencies of I_{th} and I_r on I_0 calculated using Eqs. (8, 10) are plotted in Fig. 2.

It should be noted that the nonsingle-valued dependencies in Fig. 2 are observed only when the gain coefficient exceeds the threshold value $\alpha_{th}:\alpha\geq\alpha_{th}$.

These dependencies are single-valued when $\alpha<\alpha_{th}$, see Fig. 3.

Fig. 2. Dependence of the normalized intensity of the transmitted I_{tr} (curve 1) and reflected I_r (curve 2) waves on the normalized intensity I_0 of the injected signal, at $\alpha=10\,\mathrm{cm}^{-1}$, and $\lambda=2\pi c/\omega=5.7\times 10^{-5}$ cm, and in (a) $k_2 L=\pi$, $A=B=I_G$; and in (b) $k_2 L=(1+5\times 10^{-3})\pi$. The unstable parts of the curves are marked by dashed lines.
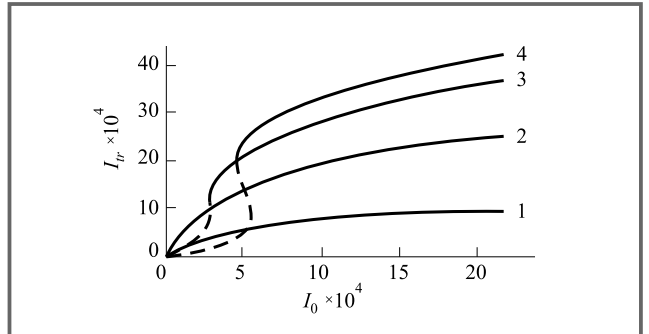
Fig. 3. Dependence of the normalized intensity I_{tr} of the transmitted wave on the normalized intensity I_0 of the injected signal at different values of the gain factor $\alpha:\alpha=4\,\mathrm{cm}^{-1}$ (1), $\alpha=5\,\mathrm{cm}^{-1}$ (2), $\alpha=6\,\mathrm{cm}^{-1}$ (3), $\alpha=6.5\,\mathrm{cm}^{-1}$ (4), at $k_2 L=(1+5\times 10^{-3})\pi$, $L=10^{-3}$ cm, $\lambda=5.7\times 10^{-5}$ cm. The unstable parts of the curves are plotted by dashed lines.

Conclusions

In conclusion, the injection locking effect in the TQ laser has been studied in this paper. The possibility of the frequency and directional switching of the TQ output radiation by means of external signal injection has been shown.

The saturation effects and the nonlinearity of the refractive index of the laser-active medium of TQ may lead to the nonlinear interaction between the eigenmodes of TQ. This interaction is strong in the case when an additional external resonator has been performed by a pair of external mirrors.

The analysis shows that the interference between the eigen-modes of TQ with an external resonator leads to generation of light-induced gratings of the complex refractive index in the laser-active medium. The scattering from these gratings of the modes of TQ which are nonresonant in respect to the external resonator results in four wave parametric mixing and phase conjugation effects in the laser-active medium of TQ.

The features of the TQ laser-amplifyer presented in this paper allow one to propose this system as a promising laser-active element with tunable frequency for directional and frequency switching in the optical communication systems.

References

[1] A. E. Siegman, *Lasers*. CA: Univ. Science Books, 1988.

[2] M. B. Spencer and W. E. Lamb, *Phys. Rev. A*, vol. 5, p. 884, 1972.

[3] ———, „Special issue on optical bistability in semiconductor lasers", *Opt. Quant. Electron.*, vol. 19, 1987.

[4] J. A. Kuecken, *Fiberoptics*. N.Y.: 1980.

[5] G. P. Agrawal, Ed., *Semiconductor lasers: Past, Present and Future*. Woodbury, New York: American Institute of Physics, 1995.

[6] V. M. Arutunyan, G. P. Djotyan, A. P. Karmenyan, A. V. Meliksetyan, and E. M. Sarkissyan, *Opt. Commun.*, vol. 36, p. 227, 1981.

[7] V. M. Arutunyan, G. P. Djotyan, A. P. Karmenyan, A. V. Meliksetyan, and E. M. Sarkissyan, *Opt. Commun.*, vol. 52, p. 114, 1984.

Gagik P. Djotyan, Joseph S. Bakos, Zsuzsa Sörlei
Research Institute for Particle and Nuclear Physics
Budapest, XII. Konkoly Thege ut 29–33,
H-1525, POBox 49 Hungary

Vilik M. Arutunyan
„Laser Technique" Corp., Yerevan State University
Yerevan, Armenia
e-mail: djotjan@kmki.kgki.hu

Optical Josephson effects using phase-conjugating mirrors: an analogy with superconductors

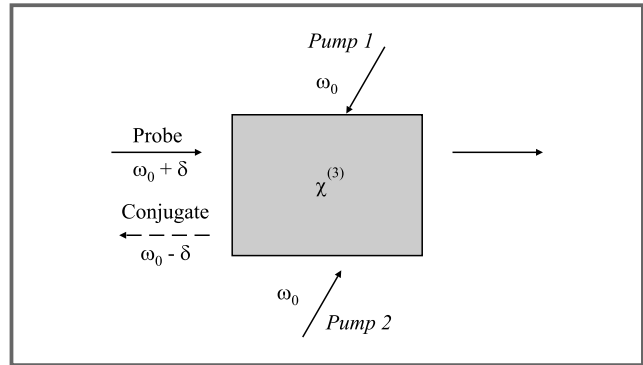Miriam Blaauboer, Daan Lenstra, and Adri Lodder

Abstract — **Motivated by the analogy between a phase-conjugating mirror (PCM) and a superconductor, we search for optical counterparts of the well-known DC and AC Josephson effects. We show that in a system consisting of two PCM's separated by vacuum an „optical supercurrent" arises as a function of an applied phase difference between the PCM's, which is the *optical analogue* of the DC supercurrent flowing in a superconducting weak link. The corresponding AC effect occurs when the two PCM's are pumped by light of a different frequency, causing the phase difference to oscillate in time with the frequency difference.**

Keywords — *Josephson effects, phase-conjugation mirrors, superconductors, four-wave mixing.*

Fig. 1. A phase-conjugating mirror realized through a four-wave mixing process

Introduction

A phase-conjugating mirror (PCM) is a nonlinear optical device capable of reversing both the direction of propagation and the overall phase factor of an incident beam of light [1]. It consists of an optical medium with a large third-order susceptibility $\chi^{(3)}$ and can be realized through a four-wave mixing process, see Fig. 1. The medium is pumped by two intense counterpropagating laser beams of frequency ω_0. When a probe beam of frequency $\omega_0 + \delta$ is incident on the material, a fourth beam will be generated due to the nonlinear polarization of the medium. The latter propagates with frequency $\omega_0 - \delta$ in the opposite direction as the probe beam and is referred to as the conjugate beam [1]. The probe-to-conjugate reflection process at a PCM is the optical analogue of Andreev reflection, the electron-to-hole reflection which occurs at the interface between a normal metal (N) and a superconductor (S) [2]: just as the hole is sometimes called a „time-reversed" electron, the conjugate can be seen as the „time-reversed" of the probe wave. The role of the chemical potential μ in a superconductor is played by the pump frequency ω_0 in a PCM, and the energy gap Δ of the bulk superconductor corresponds to the coupling strength γ between probe and conjugate waves in the nonlinear optical medium, to be defined later (see below Eq. (1)).

This by now well-established analogy between a PCM and a superconductor [3, 4] can be extended to a system consisting of two PCM's separated by vacuum, which is then the analogue of a superconductor–normal-metal–superconductor (SNS) structure or weak link [5]. In these weak links the famous DC and AC Josephson effects oc-

cur, which were originally predicted for tunnel junctions [6]. The DC effect in a tunnel junction is the sinusoidal dependence of the supercurrent I_S on the phase difference $\Delta\phi$ between the pair potentials in the two superconductors, $I_S \sim \sin(\Delta\phi)$. In a point contact, i.e. a weak link consisting of a constriction in between two superconductors, it also occurs, but the current-phase dependence is then found to be $I_S \sim \sin(\Delta\phi/2)$ for $|\Delta\phi| < \pi$ [7, 8, 9]. The nonstationary (AC) Josephson effect arises when a voltage V is applied across a tunnel junction or weak link, causing the phase difference to change with time as $\dot{\Delta\phi} = 2eV/\hbar$.

The carriers of the supercurrent flow in weak links are the quasiparticle bound states [10], or „Andreev levels". These quasiparticle bound states are formed when an electron (or hole) with energy E above (below) the Fermi energy, but with E smaller than the gap energy Δ of the superconductor is present in the normal layer. The electron cannot enter the superconductor without pairing with another electron, which leaves a hole behind in the normal metal: the well-known process of Andreev reflection [2]. Conversely, a hole can break up a Cooper pair and produce an electron in the normal metal. The bound-state spectrum is found by calculating the condition for constructive interference of electron/hole waves in the middle layer after one roundtrip (corresponding to two Andreev reflections, electron-to-hole at one superconductor and hole-to-electron at the other superconductor). Here, we assume clean NS interfaces without any potential barriers, so that normal reflections can be neglected. Since each Andreev reflection is accompanied by a phase-shift which depends on the phase of the superconducting pair potential, these bound states produce

a coupling between the phases of the order parameters of the two superconductors and are the carriers of the super-current.

Returning to the optical configuration of two PCM's separated by a layer of vacuum, it is known that just as bound states are formed in a SNS structure due to Andreev reflections at the NS interfaces, so-called axial modes[1] are formed in the vacuum region due to phase-conjugate reflections at the PCM's [4]. We will show here that like the Andreev bound-state levels are the „channels" for the supercurrent flow, the axial modes form the „channels" for an „optical supercurrent" flow: when the vacuum region is short and the two PCM's are pumped by light of the same frequency, but with a small phase difference $\Delta\phi$, a photonpair(„super")current arises as a function of this phase difference, similar to the supercurrent in a short superconducting weak link. The calculation and analysis of this DC optical Josephson effect forms the topic of section , after a discussion of the axial modes in section . In section the corresponding AC effect is discussed and we conclude in section with a suggestion for a possible experimental realization of these optical Josephson effects.

Axial modes

Consider the double PCM configuration depicted in Fig. 2. Just as the equilibrium state of a superconductor is described by the eigenfunctions of the Bogoliubov-de Gennes equations [11], each PCM-medium is described by the eigenfunctions of the matrix equation [3]

$$
\begin{pmatrix} -\dfrac{c^2}{2\omega_0}\dfrac{\partial^2}{\partial x^2}-\dfrac{\omega_0}{2} & -\gamma \\ \gamma^* & \dfrac{c^2}{2\omega_0}\dfrac{\partial^2}{\partial x^2}+\dfrac{\omega_0}{2} \end{pmatrix} \begin{pmatrix} \mathcal{E}_p(x) \\ \mathcal{E}_c^*(x) \end{pmatrix} =
$$
$$
= i\frac{\partial}{\partial t}\begin{pmatrix} \mathcal{E}_p(x) \\ \mathcal{E}_c^*(x) \end{pmatrix}. \tag{1}
$$

Here $(\mathcal{E}_p(x), \mathcal{E}_c^*(x))$, with $\mathcal{E}_p$ and $\mathcal{E}_c^*$ the electric field amplitude of the probe and conjugate waves respectively, represents an excitation in the pumped medium with a mixed probe/conjugate character: an „optical quasiparticle", in analogy with the mixed electronlike/holelike quasiparticles in a superconductor [11]. The off-diagonal parameter $\gamma = \gamma_0 e^{i\phi} = \frac{3\omega_0}{\varepsilon_0}\chi^{(3)}\mathcal{E}_1\mathcal{E}_2$ is the pumping induced coupling strength between the probe and conjugate wave in the PCM-medium, and ϕ denotes the phase of $\chi^{(3)}\mathcal{E}_1\mathcal{E}_2$, with $\mathcal{E}_1$, $\mathcal{E}_2$ the electric field amplitudes of the two pump beams. The PCM's in Fig. 2 are both pumped by two counterpropagating laser beams with the same frequency ω_0 but with a different phase, say ϕ_1 on the left and ϕ_2 on the right.

[1]By „axial" modes we mean longitudinal modes, to distinguish them from transverse modes. The latter are formed due to finite dimensions of the whole system in the transverse direction(s), e.g., when it is embedded in a waveguide. Here we consider a quasi-1D configuration, in which only one transverse mode is present.
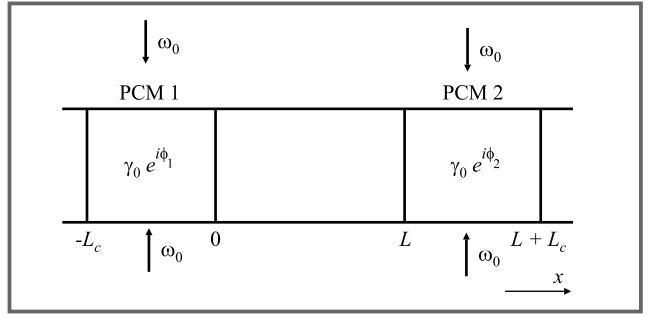
Fig. 2. Two PCM's of equal length L_c separated by a layer of vacuum of length L. The PCM's are each pumped with two laser beams of the same frequency ω_0, but such that the phases on the left and right are different, which leads to different phases of their coupling constants γ.

In the region between the PCM's, a probe beam incident on either mirror will be reflected as a conjugate beam, which again emerges as a probe beam after reflection at the other PCM. The condition for the formation of an axial mode is that the acquired phase shift on one round trip equals an integer multiple of 2π, and is given by [4]

$$
2\frac{\delta}{c}L + 2\arctan\left(\frac{\delta}{\sqrt{\delta^2+\gamma_0^2}}\tan(\beta L_c)\right) \pm \Delta\phi = 2\pi n. \tag{2}
$$

Here $\Delta\phi = \phi_1 - \phi_2$, $\beta = \frac{1}{c}\sqrt{\delta^2+\gamma_0^2}$ and the $\pm$-sign corresponds to a probe wave travelling with frequency $\omega_0 \pm \delta$ to the right and being reflected as a conjugate wave with frequency $\omega_0 \mp \delta$. Eq. (2) is the analogue of the bound-state spectrum (Andreev levels) of a SNS junction[2] [10]

$$
k_F \frac{E}{E_F}L - 2\arccos(E/\Delta_0) \pm \Delta\phi = 2\pi n, \tag{3}
$$

where k_F and E_F are the Fermi wavevector and energy respectively and $\Delta_0 = |\Delta|$. For a short weak link, in which the distance between the superconductors is much less than the superconducting coherence length $\xi_S = \frac{\hbar v_F}{\pi\Delta_0}$, the first term in (3) may be neglected, so that the mode spectrum simplifies to $E = \Delta_0\cos(\Delta\phi/2)$ [8, 9]. By analogy, we restrict ourselves here to the situation in which the vacuum region that separates the two PCM's is short compared to the „optical coherence length"[3] $\xi_0 = c/\gamma_0$. The axial mode spectrum (2) then reduces to

$$
\frac{\delta}{\sqrt{\delta^2+\gamma_0^2}}\tan(\beta L_c) = -\tan\left(\frac{\Delta\phi}{2}\right), \tag{4}
$$

[2]The first term on the left-hand side of Eq. (3) does not have a factor „2" as Eq. (2) has; this is due to the different (parabolic) dispersion relation of an electron in a normal metal compared with the linear dispersion relation of light in vacuum.

[3]ξ_0 is a a measure of the minimum spatial extent of the transition layer between a PCM and vacuum, just as the superconducting coherence length ξ_S is a measure of the minimum spatial extent of the transition layer between a normal metal and a superconductor, see e.g. [12].

independent of the mode-index n. For frequencies $\delta \ll \gamma_0$, Eq. (4) takes the simple form

$$\delta = -\gamma_0 \frac{1}{\tan\left(\dfrac{\gamma_0 L_c}{c}\right)} \tan\left(\frac{\Delta\phi}{2}\right)$$

for

$$\left| \frac{\tan\left(\dfrac{\Delta\phi}{2}\right)}{\tan\left(\dfrac{\gamma_0 L_c}{c}\right)} \right| \ll 1. \tag{5}$$

Now there is a *single* axial mode. This axial mode spectrum can support a stationary photon-current, which we now proceed to derive.

The stationary (DC) optical Josephson effect

The starting point of our search for a phase-dependent Josephsonlike photon-current in the double-PCM configuration is the fact that due to spontaneous emission and quantum fluctuations, photons with a range of frequencies are generated in each PCM, part of which are emitted into the region between the PCM's. Out of these, only the frequencies that satisfy the condition (4) will lead to the formation of axial modes, which can be the carriers of a phase-dependent current. Before analyzing this any further, we now first mention an important difference between Andreev reflection at a superconductor and phase-conjugate reflections at a PCM. Whereas the former always occurs with probability 1 at an ideal NS interface [13], i.e. one electron is reflected as one hole and particle conservation applies, the reflected conjugate beam at a PCM can be stronger than the incoming probe beam. Because the two pump beams continuously add energy to the medium, the PCM can act as a phase-conjugate amplifier. In fact, the probability for phase-conjugate reflection is given by [1]

$$R_c = \frac{\sin^2(\beta L_c)}{\cos^2(\beta L_c) + \left(\dfrac{\delta}{\gamma_0}\right)^2}, \tag{6}$$

$$R_c \approx \tan^2\left(\frac{\gamma_0 L_c}{c}\right) \text{ for } \delta \ll \gamma_0. \tag{7}$$

It can easily be seen from Eq. (6) that for frequencies $\delta \gg \gamma_0$ the phase-conjugate reflectance $R_c < 1$, so that the reflected beam is weaker than the incoming beam. In the opposite limit of $\delta \ll \gamma_0$, Eq. (7) applies, and then $R_c \geq 1$ for $|\gamma_0 L_c/c| \geq \pi/4$, in which case the reflected beam is stronger than the incoming one. According to (7) it may even become infinitely strong, for when $\gamma_0 L_c/c \to \pi/2$, $\tan(\gamma_0 L_c/c) \to \infty$. However, in reality the intensity of the reflected beam is limited by the intensity of the pump beams: if the former approaches the latter, pump depletion will set in and the expression (6) for R_c is no longer valid, since it was derived under the condition of undepleted pump beams [1].

The magnitude of R_c plays an important role in the formation of an equilibrium current in our double-PCM configuration. For if the phase-conjugate reflection is less than 100%, any current will decrease in time and eventually die. If, on the other hand, the phase-conjugate reflection is more than 100%, the wave is amplified at the expense of the pump beams upon each reflection at the PCM's. Then after a while pump depletion will set in, causing the reflected intensity and the current to decrease again, until a stable situation is reached in which there is neither gain nor loss. If the probability of phase-conjugate reflection is exactly 100%, the current in the region between the PCM's is „automatically" stable. This situation forms the closest analogy with the superconducting case.

Before calculating anything explicitly, we now thus already know that an equilibrium photon-current in the region between the PCM's can only form for frequencies which: (a) satisfy the axial-mode condition (4) and (b) are neither weakened nor amplified upon phase-conjugate reflection, i.e. for which a steady state exists or is established in the region between the PCM's. The important question is thus for which frequencies satisfying (4) a steady state is formed. The answer to this question requires a nonlinear analysis of the phase-conjugate reflection process which takes pump depletion into account. This is the topic of a separate paper *M. Blaauboer (to be published)*, and the main result is that a steady state is established for all frequencies δ that satisfy the condition $R_c \geq 1$, provided the PCM operates such that $|\tan(\gamma_0 L_c/c)| \geq 1$.

Here, we restrict ourselves to the case of $|\tan(\gamma_0 L_c/c)| = 1$, corresponding to $R_c = 1$ for $\delta \ll \gamma_0$, which most closely brings out the analogy with the superconductor (see for the general case *M. Blaauboer, submitted to Phys. Rev. Lett.*). The equilibrium current density in the region between the PCM's is obtained from the (normalized) eigenfunctions of Eq. (1) and given by

$$j = \frac{c^2}{\omega_0} \sum_\delta \mathrm{Re}\left(\bar{\mathscr{E}}_p^* i\nabla\bar{\mathscr{E}}_p + \bar{\mathscr{E}}_c^* i\nabla\bar{\mathscr{E}}_c\right), \tag{8}$$

where the sum is over all frequencies δ satisfying the axial-mode condition and $(\bar{\mathscr{E}}_p, \bar{\mathscr{E}}_c^*)$ is the eigenfunction corresponding to δ. The latter has been calculated (*M. Blaauboer*) for a short ($L \ll \xi_0$) PCM-vacuum-PCM junction, by adopting a WKB model for the propagation of each mode in the PCM-vacuum-PCM junction[4]. In essence, the WKB model requires that the length of the vacuum region $L \gg \lambda_0$ [with λ_0 the wavelength of the pump beams] and that the width of this region varies smoothly over L, leading to an x-dependent coupling constant $\gamma_0(x)$, phase $\phi(x)$ and wavevector $k_0(x)$ between $x = 0$ and $x = L$. The axial-mode eigenfunction is then given by

$$\begin{pmatrix} \bar{\mathscr{E}}_p(x) \\ \bar{\mathscr{E}}_c^*(x) \end{pmatrix} = \sqrt{\frac{\gamma_0}{2c}} \begin{pmatrix} e^{i\bar{\phi}/2} \\ e^{-i\bar{\phi}/2} \end{pmatrix} e^{\pm i \int_0^x dx'\, k(x')} \tag{9}$$

$$\delta \ll \gamma_0,$$

[4]This model has also been used in Ref. [9] for a superconducting weak link.
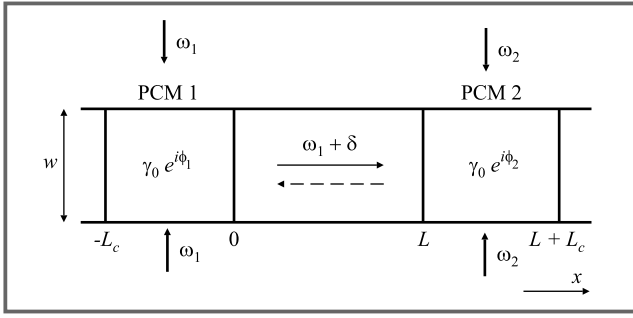
Fig. 3. Two PCM's separated by a distance L

for

with

$$\bar{\phi} = \phi(x) + i\,\text{arcsinh}\,(\tan(\Delta\phi/2)) \qquad (10)$$

$$k(x) = k_0\left(1 + \frac{\gamma_0(x)}{\omega_0}\cos(\phi(x) - \bar{\phi})\right). \qquad (11)$$

Here, we have used the axial-mode condition (5); the approximation $\delta \ll \gamma_0$ is justified because in our case of $R_c = 1$ only for these frequencies a steady state is established (*M. Blaauboer*)[5]. Substituting (9) into (8) yields

$$I = \gamma_0 \tan\left(\frac{\Delta\phi}{2}\right) \quad \text{for} \quad \tan(\Delta\phi/2) \ll 1. \qquad (12)$$

This is the *optical analogue* of the DC supercurrent $I_S = \frac{e\Delta_0}{\hbar}\sin\left(\frac{\Delta\phi}{2}\right)$ for $|\Delta\phi| < \pi$ flowing through a quasi-1D superconducting weak link. Note, however, that Eq. (12) is only valid for small angles $\Delta\phi$, in order to be consistent with the condition $\delta \ll \gamma_0$. For larger phase-differences no steady-state, and hence no equilibrium current exists. If there were N propagating modes in the intermirror region, Eq. (12) would be multiplied by N and so for a given $\Delta\phi$ each mode would contribute γ_0 to the resulting current *(M. Blaauboer)*.

The nonstationary (AC) optical Josephson effect

When a voltage V is applied across a superconducting tunnel junction, or weak link, the phase difference between the pair potentials changes in time as $\mathrm{d}(\Delta\phi)/\mathrm{d}t = 2eV/\hbar$. The Josephson current is then an oscillating function in time, $I_S(t) \sim \sin(\Delta\phi) = \sin(\frac{2eV}{\hbar}t + (\Delta\phi)_{t=0})$, and this is called the nonstationary (AC) Josephson effect.

The optical analogue of the Fermi energy in a superconductor is the pump frequency of a PCM. The analogue of a voltage difference V across the two superconductors,

which is in fact a difference in Fermi energies, is then a frequency difference between the two pump beams on the left and right. In view of this analogy one might wonder whether such a frequency difference gives rise to an optical AC Josephson effect. It is straightforward to show that this is indeed the case.

First we examine the axial modes for the situation depicted in Fig. 3. The only difference with the PCM-system considered before (Fig. 2) is that the nonlinear media on the left and right are now pumped with different frequencies, ω_1 and ω_2 respectively. As a result of this frequency difference a probe (or conjugate) wave propagating in the region between the two PCM's will have a different frequency after each round-trip. Consider e.g. a probe beam of frequency $\omega_1 + \delta$ travelling to the right (see Fig. 3). The detuning of this beam with respect to ω_2 is $\omega_1 - \omega_2 + \delta$, so after phase-conjugate reflection at the PCM on the right a conjugate beam will travel to the left with frequency $2\omega_2 - \omega_1 - \delta$. Reflection at PCM 1 leads to a probe beam with frequency $3\omega_1 - 2\omega_2 + \delta$. The frequency change is thus $2(\omega_1 - \omega_2)$ per round-trip, or, equivalently, $\omega_1 - \omega_2$ per unit of time L/c. In the same time, during propagation from 0 to L, the phase ϕ of the coupling constant γ changes from ϕ_1 to ϕ_2. Stable axial modes then only occur if the frequency change causes a change in time of the phase difference

$$\frac{\mathrm{d}(\Delta\phi)}{\mathrm{d}t} = \pm(\omega_2 - \omega_1). \qquad (13)$$

This is the optical analogue of the AC Josephson effect. If the frequency difference $\omega_2 - \omega_1$ is much smaller than the inverse response time of the PCM's (for Kerr-type materials typically GHz to THz) the system will adiabatically follow and produce an alternating optical current with the pump-frequency difference as its fundamental frequency.

Summary and experimental outlook

In conclusion, we predict a new analogy between optics and micro-electronics [14], which exploits the known analogy between quasiparticle excitations in a superconductor and optical phase conjugation by four-wave mixing in a nonlinear optical Kerr-type material, and consists of the optical analogue of the DC and AC Josephson effects that occur in superconducting weak links.

A PCM is typically pumped with frequency $\omega_0 \approx 10^{15}$ rad s^{-1}, has length L_c usually several millimeters and coupling strength $\gamma_0 \approx 10^9 \div 10^{10}$ s^{-1} [15]. One can thus arrange $\gamma_0 L_c/c \approx \pi/4$, so phase-conjugate reflection at the PCM occurs with probablity 1. Since $\lambda_0 = c/\omega_0 (\approx 10^{-7}$ m$)$ and the coherence length $\xi_0 \approx 10^{-2} \div 10^{-1}$ m, an intermirror distance $L \approx 10^{-3}$ m satisfies the condition $\lambda_0 \ll L \ll \xi_0$, corresponding to a short PCM-vacuum-PCM junction. The optical Josephson current which can then be observed by varying the phase of the coupling constants in the two PCM's with the respective pump beams, through e.g. letting the path lengths of the pump beams differ on the left

---

[5]Strictly speaking, in the case of $R_c = 1$ a steady state is established only for $\delta = 0$. As $|\delta| > 0$, we have $R_c < 1$ and the resulting current wil slowly decay. For frequencies $\delta \ll \gamma_0$, however, this occurs on a timescale of $\geq \mu$s (corresponding to a decay to a value 1/e of the original amplitude), long enough to be observable.

and right, and has frequency $\gamma_0 \approx$ GHz-THz. The AC optical Josephson effect would be observable for a frequency-difference between the pump waves on the left and right of $10^9 \div 10^{12}$ rad s^{-1}. The alternating current will then oscillate on a nano- to picosecond time scale.

References

[1] R. A. Fisher, Ed., *Optical Phase Conjugation*. New York: Academic Press, 1983.

[2] A. F. Andreev, *Zh. Eksp. Teor. Fiz.*, vol. 46, p. 1823, 1964 (*Sov. Phys. JETP*, vol. 19, p. 1228, 1964; vol. 51, p. 1510, 1966; vol. 24, p. 1019, 1967).

[3] D. Lenstra, in: *Huygens Principle 1690-1990; Theory and Applications*, H. Blok, H. A. Ferwerda, and H. K. Kuiken, Eds. Amsterdam: North-Holland, 1990.

[4] H. van Houten and C. W. J. Beenakker, *Phys. B*, vol. 175, p. 187, 1991.

[5] K. K. Likharev, *Rev. Mod. Phys.*, vol. 51, p. 101, 1979.

[6] B. D. Josephson, *Phys. Lett.*, vol. 1, p. 251, 1962; *ibid., Adv. Phys.*, vol. 14, p. 419, 1965.

[7] I. O. Kulik and A. N. Omel'yanchuk, *Fiz. Nisk. Temp.*, vol. 3, p. 945, 1977; vol. 4, p. 296, 1978 (*Sov. J. Low Temp. Phys.*, vol. 3, p. 459, 1977; vol. 4, p. 142, 1978).

[8] C. W. J. Beenakker and H. van Houten, in: *Proceedings of the International Symposium on Nanostructures and Mesoscopic Systems*, W. P. Kirk, Ed. Santa Fe: 1991.

[9] C. W. J. Beenakker and H. van Houten, *Phys. Rev. Lett.*, vol. 66, p. 3056, 1991.

[10] I. O. Kulik, *Zh. Eksp. Teor. Fiz.*, vol. 57, p. 1745, 1969 (*Sov. Phys. JETP*, vol. 30, p. 944, 1970).

[11] P. G. de Gennes, *Superconductivity of Metals and Alloys*. New York: Benjamin, 1966.

[12] C. Kittel, *Introduction to Solid State Physics*. New York: Wiley, 1986.

[13] G. E. Blonder, M. Tinkham, and T. M. Klapwijk, *Phys. Rev. B*, vol. 25, p. 4515, 1982.

[14] W. van Haeringen and D. Lenstra, Eds. *Analogies in Optics and Micro-Electronics*. Dordrecht: Kluwer, 1990; *ibid.*, Amsterdam: North-Holland, 1991.

[15] M. Y. Lanzerotti, R. W. Schirmer, and A. L. Gaeta, *Appl. Phys. Lett.*, vol. 69, p. 1199, 1996.

Miriam Blaauboer, Daan Lenstra, and Adri Lodder
Faculteit Natuurkunde en Sterrenkunde,
Vrije Universiteit, De Boelelaan 1081,
1081 HV Amsterdam, The Netherlands
e-mail: miriam@nat.vu.nl

Linear and nonlinear optical spectroscopy of CdS nanoparticles in Nafion membranes

Emmanuel Bourdin, Fryod Z. Henari, Werner J. Blau, and John M. Kelly

Abstract — CdS nanoparticles embedded in Nafion membranes were studied by a variety of optical spectroscopic methods. Quantum confinement was achieved (particle mean diameter of 40 Å) and the growth was found to follow a linear temporal kinetic law. Discrete energy levels were observable, even at room temperature. They could be attributed to light hole and heavy hole 1S and 2S transitions. The experimental results are in good agreement with theoretical calculations of light hole and heavy hole masses in the cases of cubic CdS. An enhancement of the nonlinear susceptibility $\chi^{(3)}$ at the quantized exciton energy levels was observed. The clusters were found to be photo-unstable, with a diffusion-limited growth rate due to Ostwald ripening.

Keywords — optical spectroscopy, Nafion membranes, CdS nanoparticles.

Introduction

In the past decade, carrier confinement in semiconductors has attracted substantial interest, because of its technological importance and the interesting new phenomena and devices observable in such low dimensional structures. In this paper, we shall deal with materials confined in three dimensions, commonly referred to as quantum dots [1]. In that case, the energy levels are quantized and their optical response appears in the form of excitonic delta functions, with an enhanced oscillator strength. The semiconductor used is CdS. Confinement was achieved by embedding the material into an ionic exchange membrane with exceptionally well defined pore size, Nafion. Confinement effects were observed at room temperature in both linear absorption and luminescence spectroscopy. The nonlinear optical susceptibility $\chi^{(3)}$, is particularly sensitive to carrier confinement. Hence, its values were measured and showed a behaviour characteristic of a band-filling effect. The clusters, of different diameters, but still well confined after their formation, were found to aggregate following an Ostwald ripening processing over a period of days/weeks.

General background

Electronic structure

Simple quantum mechanics may be applied to determine the basic electronic structure of a quantum dot. We suppose that the particle radius, R, is much smaller than the

exciton Bohr radius ($a_B = 28$ Å for CdS). The wave function is zero outside the particle, corresponding to an infinitely large potential barrier. Neglecting the Coulombic interaction of created electron-hole pairs, the wave function is of the following form [1, 2]:

$$\Psi_{n,l,m} = \Psi_{l,m}(\Theta,\phi)\frac{1}{R}\left\{\frac{2}{r}\right\}^{\frac{1}{2}}\frac{J_{l+\frac{1}{2}}(k_{nl}r)}{J_{l+\frac{3}{2}}(k_{nl}R)}, \qquad (1)$$

where $\Psi_{l,m}$ are the normalized spherical functions; n is the principal quantum number, l is the momentum and J_x is a Bessel function. The quantities k_{nl} are defined by

$$J_{l+\frac{1}{2}}(k_{nl}R) = 0 \qquad (2)$$

the roots of the Bessel function. Hence, k_{nl} may be written

$$k_{nl} = \Phi_{nl}/R. \qquad (3)$$

For $l = 0$ we get from Eq.(2) that

$$k_{n0} = n\pi/R, \qquad (4)$$

where $n = 1, 2, 3, \dots$. For $l > 0$ the solutions are not simple, the first few being $\Phi_{0,1} = 3.14, \Phi_{1,1} = 4.49, \Phi_{2,1} = 5.76$ [3]. Using this wave function, Eq. (1) gives energy levels

$$E_{n,l} = E_g + \frac{\hbar^2 k_{nl}^2}{8m_e\pi^2}. \qquad (5)$$

This result leads to a series of discrete energy levels. For simplicity, the above treatment is formulated in terms of the conduction band states, but applies equally to the valence band. In considering transitions between conduction and valence states, the above equations will apply where m_e is replaced by the reduced mass $\mu = m_e m_h/(m_e + m_h)$, m_h being the hole effective mass. Because of the orthogonality of the wave functions, transitions are only allowed between states of the same quantum number; this condition, however, would be relaxed under more realistic conditions. The above treatment takes the most simplistic approach. The Coulomb interaction of a created electron-hole pair and polarization effects due to created charges should be included. As a first approximation, the 1S ($n = 0$, $l = 1$) wave function of the electron and hole can be used. Substituting into Schrödinger equation gives the energy for the lowest excited state as

$$E_{1S} = \frac{\hbar^2}{8R^2}\left(\frac{1}{m_e} + \frac{1}{m_h}\right) - \frac{1.8\,e^2}{\varepsilon R} + polarization\ term. \qquad (6)$$

Emmanuel Bourdin, Fryod Z. Henari, Werner J. Blau, and John M. Kelly

The second term has to be replaced by $\frac{1.7e^2}{\varepsilon R}$ for the levels 1P and 1D [4]. If we can neglect the polarization term since it includes high order terms in $\frac{1}{R}$, then the Coulomb interaction (which actually corresponds to the exciton binding energy) can cancel the confinement term. In practice, the Coulombic term can be neglected for materials with a low band gap and a high dielectric constant, such as GaAs. But, higher band gap materials with large effective masses and smaller dielectric constant will show a cancellation of the electrostatic and quantum terms for one specific radius R_0. In the case of CdS, R_0 takes the value of 80 Å [4]. One more feature to consider is the fact that the valence energy levels are degenerate, leading to the well-known notions of light-hole and heavy-hole.

Nonlinear optical properties

Optical nonlinearity in the band gap region of the semiconductors has attracted much attention due to large nonlinearities observed in this region [7]. Such nonlinearities are attractive, both from the point of view of the basic physics and for practical device applications in optical switching and signal processing. They mean that only low intensities and short device length are required, making an integrated miniaturized device technology possible.

Unlike in the bulk, where they are broad bands within which excitations could occur, now there are only single transitions separated by large gaps. Screening effects, whereby interactions are modified due to the presence of other charge carriers will be suppressed. A particular level may only be occupied by electrons of opposite spin, and so the exchange interaction is identically zero. The only mechanism which may operate in a true quantum dot is state filling and so for each spin the behaviour can be modelled as a simple two level saturable absorber. This implies that saturation will be achieved for one electron-hole pair per dot and that total saturation of the transition should be possible.

When semiconductors are confined, the stability of the excitons increases (the Coulombic interaction energy is much less than the separation between the quantum confined levels), and, as a consequence, its resonances are strongly enhanced and well resolved at room temperature.

It is possible to estimate the third-order nonlinear susceptibilityb $\chi^{(3)}$ from induced absorption changes $\Delta\alpha$ and refractive index Δn [5], we obtain then in a simple two level system:

$$\frac{\Delta\alpha}{I} = K_1 \left(\frac{a_B}{R}\right)^3 \mathrm{Im}\,\chi^{(3)} \text{ and } \frac{\Delta n}{I} = K_2 \left(\frac{a_B}{R}\right)^3 \mathrm{Re}\,\chi^{(3)}, \tag{7}$$

where I is the intensity inside the quantum dot and K_1 and K_2 are prefactors scaling the absorption and dispersion changes.

One can see immediately that large nonlinearities are expected when the confinement is such that the particles radius R is smaller than a_B. ·

There are several theories that have been proposed to predict the nonlinear optical behaviour of nanoparticles in the band gap region. Band-filling is the most likely effect and has been suggested by Roussignol et al. [6]. It arises from relaxation of free carriers to the band extrema before recombination. An analysis of this effect [7] predicts that

$$\chi^{(3)} \approx \frac{\alpha(\omega)}{\omega_o - \omega}, \tag{8}$$

where $\alpha(\omega)$ is the absorption at the wavelength corresponding to the frequency ω and $\frac{\hbar\omega_0}{2\pi}$ is the first excitation energy. A characteristic detuning factor will then appear at the resonance at an exciton energy level.

Others analyse the finite-size effects on the excitons in semiconductor microcrystallites [8]. The enhancement of the nonlinear polarizability originates from two conflicting concepts. One is due to the size quantization of excitons, this results in an enhancement factor of L^6 for $\chi^{(3)}$ per microcrystallites, i.e., an enhancement factor of L^3 for $\chi^{(3)}$ per unit volume. The other enhancement comes from deviation of the electronic excitation from an ideal harmonic oscillator. When the size of the microcrystallite is reduced, the latter effect increases while the former decreases.

The nonlinear optical polarizability is greatly modified for an assembly of semiconductor microcrystallites if the excitons in a single microcrystallite intereact strongly enough. It has been demonstrated [7] that $\chi^{(3)}$ vanishes when the interaction energy of two excitons is negligible in comparison with the off-resonance energy $(\omega - \omega_0)$. Under such conditions, excitons behave as harmonic oscillators, which do not show any nonlinear response. But under the opposite condition, we have an enhanced optical nonlinearity, and calculations give

$$\chi^{(3)} = K \frac{|p_{cv}|^4}{(\omega - \omega_0)^3}, \tag{9}$$

where K is constant depending on the geometry and size of the particles and p_{cv} is the transition dipole moment for the lowest excited states. Hence, from the wavelength dependence of the resonance behaviour, one can obtain in indication whichever effect may be dominant.

Fabrication of CdS in Nafion

Chemical preparation

The idealized pore/channel structure of Nafion is depicted in Fig. 1. Nafion 117 membranes (0.8 cm large, 3 cm long and 0.4 cm thick, furnished by Du Pont) were purified according to the following procedure. They were first stirred in boiling 0.2 M NaOH for two hours, then washed in Millipore water and ultrasonically treated with a 50% ethanol/50% water (in mass) mixture for 2.5 hours. Then, the membranes were treated with a 1M H_2SO_4 for one hour, finally the ultimate stage was a further ultrasonic treatment in Millipore water for 30 min. The incorporation of cadmium ions was achieved by soaking the membrane in an
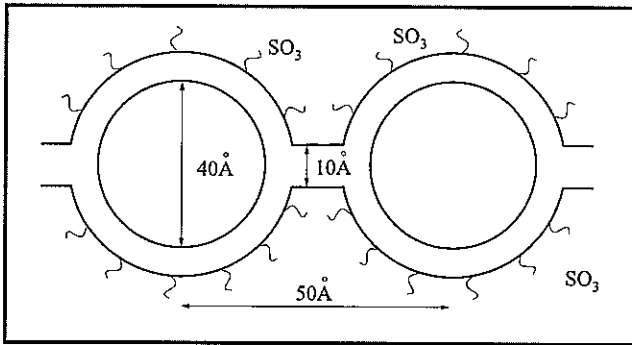
Fig. 1. Pore structure of Nafion membrane

appropriate volume of a 0.01 M cadmium sulphate solution for one hour. Two different exchange ratios (Cd^{2+} : Nafion) were used experimentally, namely 1:10 and 1:100. The samples were then dried at room atmosphere. The membranes were then mounted in a 1 ml quartz cell and exposed to dried hydrogen sulphide (atmospheric pressure) to convert them into the sulphide.

Transmission electronic microscopy

The microscopic morphology of the Nafion membranes will obviously dictate the cluster size and shape. Transmission electron microscopy shows a large number of particles, the largest having a diameter of around 800 Å. We do not observe a largely dispersed range of diameter from 40 to 800 Å, but two families of clusters. A small clusters family ($\emptyset \approx 40$ Å) and a mature and large clusters family ($\emptyset \approx 800$ Å), with some fluctuation ($\pm 20\%$) around those mean diameters. After 2 months of ageing, evidence of diffusion growth is clear. It can be noticed that clear regions, corresponding to a smaller density of clusters, are present around and beside the largest clusters, which suggests a diffusion of the small clusters that migrate towards the largest as described in the Ostwald ripening process: due to the moisture contained into the film, the smaller particles tend to dissolve in time, the solvated ions can then recrystallize on the larger semiconductor particles where they have a greater thermodynamic stability.

Optical spectroscopy

Linear absorption

Samples of Cd^{2+} membranes with different exchange ratios (1:10 and 1:100) were exposed to H_2S gas (atmospheric pressure) in a 5 ml quartz cell. The cell was mounted into the sample holder of a spectrophotometer (Phillips PYE UNICAM 8800). Their absorption spectra were recorded at different times of the CdS particles formation in the gas, this was carried at room temperature.

Figures 2 and 3 show the evolution of the absorption spectrum of the 1:100 and 1:10 exchange ratio samples, respectively. As can be seen, we have the formation of a shoulder in the bandtail of the absorption. This corresponds to the
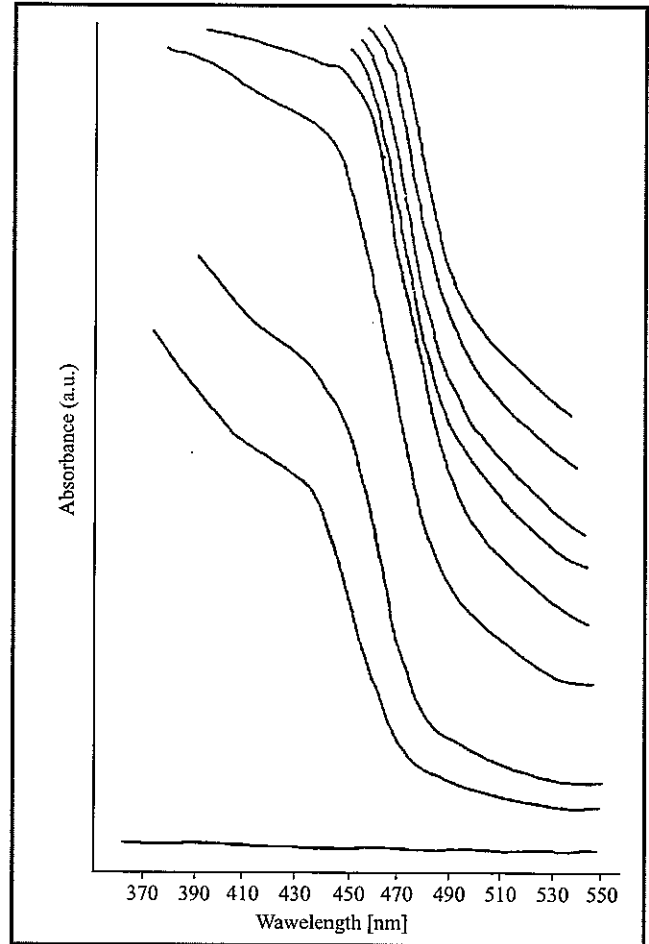

Fig. 2. Evolution of the absorption spectrum with time of exposure of a 1:10 exchange ratio Cd membrane exposed to dried hydrogen sulphide
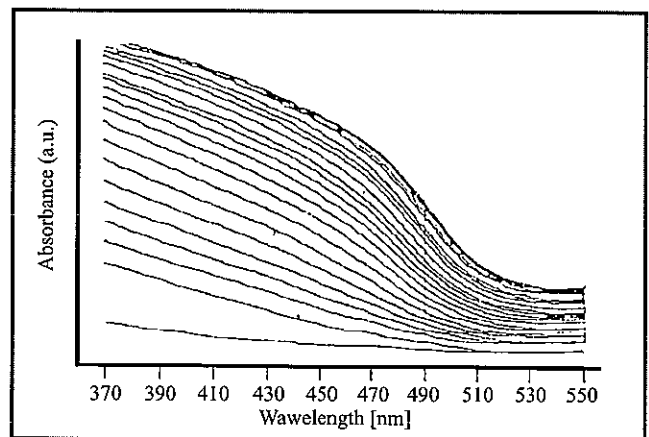
Fig. 3. Evolution of the absorption spectrum with time of exposure of a 1:100 exchange ratio Cd membrane exposed to dried hydrogen sulphide

The bottom curve corresponds to the absorption of the exchanged membrane just before exposure. The following curves, from bottom to top, correspond to different time of exposure with a 1 minute step up to 15 minutes of exposure, then the absorption was recorded every ten minutes until a final exposure of 50 minutes.

first transition 1S denoted before. As the growth of the particles goes on, the band edge of the absorption is found to be red-shifted, which corresponds to the decrease of the confinement factor. The 1S transition energy was calculated at the tip of the shoulder. Using the Eq. (6) we can calculate the radius of the particle.

Figure 4 shows the plot of diameter versus reaction time. For both samples, we obtain a linear kinetic growth law. As expected, the 1:10 sample shows larger particles (mean
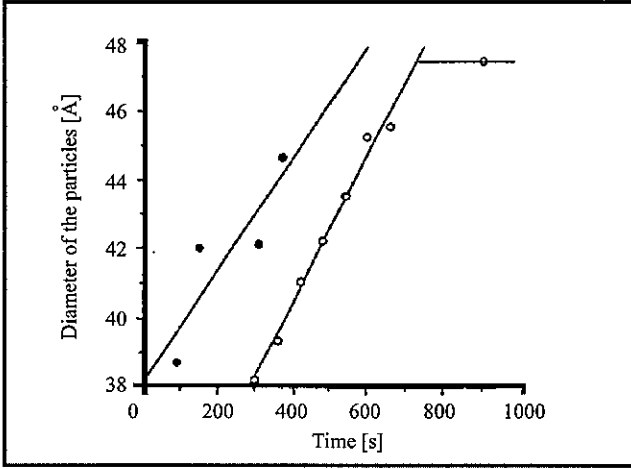

Fig. 4. A linear kinetic law is obtained for the growth of the nanoparticles
The black circles stand for the 1:10 exchange ratio sample and the white circles for the 1:100 exchange ratio sample.

initial diameter = 39 Å) than the 1:100 sample (mean initial diameter = 32 Å), but they both have approximately the same growth rate, which is around 1 Å/45 s. A saturation state is reached after 15 minutes for the case of the 1:100 sample. We attribute this to the fact that there are no more Cd^{2+} sites available for the reaction. The stabilization of the band gap is associated with the saturation of the absorption coefficient, indicating clearly that the growth has stopped for a mean diameter of approx. 50 Å.

Those values are very much in agreement with previous measurements made with ferric ions clusters in Nafion membranes [9]. It was found that the ions are present under two species: clusters of variable sizes or monomeric /dimeric species bridged by oxygen or hydroxyl ions. In this case, the mean diameter of the clusters was also ≈ 40 Å. A large proportion of dimers could also be observed, the concentration depending on the solution and the drying procedure.

If all the Cd^{2+} ions were in the clusters, then we should have ratio of $\left(\frac{1:10\ \mathrm{mean\ radius}}{1:100\ \mathrm{mean\ radius}}\right)^3 = \frac{1:10}{1:100} = 10$. In fact, we found a value of 1.8. This reflects the importance of the dimeric form of the ions in the membrane. Those smaller units are present in the channels in between the clusters, and have been reported to be responsible for the ion transport through the membrane [9]. In that case, it is obvious that the fraction of such dimers is more important in the 1:10 sample than in the 1:100 sample. We shall discuss their importance later on.

Luminescence excitation

The luminescence spectra were recorded with a PERKIN-ELMER MPF-44 B fluorescence spectrophotometer at room temperature. The excitation wavelength was chosen to be 450 nm, 2.76 eV, i.e. well above the band gap. The results obtained for a 1:10 exchange ratio are shown in Fig. 5. At the early stage of the reaction, we can distin-
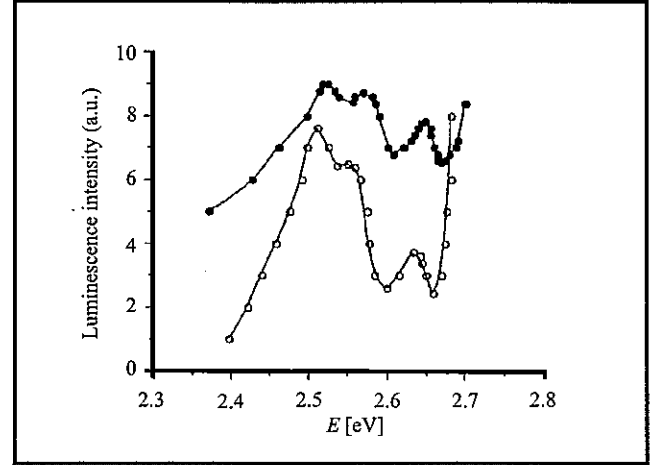

Fig. 5. Luminescence spectrum of a 1:10 exchange ratio membrane
White circles curve after 2 minutes and black circles curve after 5 minutes of exposure to dried hydrogen sulphide. The excitation wavelength is 450 nm (2.76 eV).

guish 3 sharp peaks at 2.52 eV, 2.57 eV and 2.65 eV. The fact that there are not equidistant shows that we cannot attribute them to phonons interaction. They can, however, be assigned to the confinement of the energy levels, since the mean diameter measured in the former section is 40 Å. We attribute the peaks at 2.52 eV, 2.57 eV and 2.65 eV respectively to the transitions $E_{1S,HH}$, $E_{1S,LH}$ and $E_{1P,HH}$. We have:

$$E_{1S,HH} = E_g + \frac{\hbar^2}{8R^2}\left(\frac{1}{m_e} + \frac{1}{m_{HH}}\right) - E_{b.exc.} \qquad (10)$$

$$E_{1S,LH} = E_g + \frac{\hbar^2}{8R^2}\left(\frac{1}{m_e} + \frac{1}{m_{LH}}\right) - E_{b.exc.}, \qquad (11)$$

$$E_{1P,HH} = E_g + \frac{\hbar^2}{8R^2}\left(\frac{4.49}{\pi}\right)^2\left(\frac{1}{m_e} + \frac{1}{m_{HH}}\right) - E_{b.exc.} \qquad (12)$$

Two facts support the attribution of the peaks. First of all, we can calculate the values of the m_{HH} and m_{LH}. The effective mass of the electron m_e has been reported to be in between 0.16 m_0 in CdS bulk samples [10,11]. The masses of the heavy hole and the light hole are given by [12]

$$m_{HH} = \frac{m_0}{\gamma_1 - 2\gamma_2}, \qquad (13)$$

$$m_{LH} = \frac{m_0}{\gamma_1 + 2\gamma_2},$$ (14)

where γ_1 and γ_2 are the Luttinger parameters of the valence band. In the case of cubic CdS, the literature values give [10]

$$m_{HH} = 0.94\, m_0 \quad \text{and} \quad m_{LH} = 0.16\, m_0.$$

First, let us assume that the exciton binding energy is not too important. Then, using the data of $m_{HH} = 0.94\, m_0$ and $m_e = (0.18 \pm 0.02)\, m_0$, and the experimental data shown in Table 1 for the peaks values, we find $m_{LH} = 0.1\, m_0$.

Table 1
Evolution of the energy levels as the particles grow

Time after the begining of the reaction	$E_{1S,HH}$ [eV]	$E_{1S,LH}$ [eV]	$E_{1P,HH}$ [eV]	α	
				$E_{exc} = 0$	E_{exc} for the cancellation at 80Å
2 min	2.52	2.57	2.65	0.43	0.47
5 min	2.51	2.55	2.63	0.43	0.5
5 hours	2.46				
1 day	2.42				

In order to take into account the exciton binding energy, we use the fact that the value of the radius for which we see a cancellation of the electrostatic and quantum terms is 80 Å and we can take a value of 40 Å for the diameter of the particles after 2 minutes. We then arrive to the following results $m_{LH} = (0.15 \pm 0.01)\, m_0$. Those results are very much in agreement with the theory thus supporting the attribution of the peaks made before. Secondly, assuming that the binding energy of the exciton is the same in both states 1S and 1P and can be neglected, compared to the confinement term, then it follows that the ratio α

$$\alpha = \frac{E_{1S,HH-E_g+E_{exc.}}}{E_{1P,HH-E_g+E_{exc.}}} = \left(\frac{4.49}{\pi}\right)^{-2} = 0.49.$$ (15)

Experimental data of that ratio are given in Table 1. We find a value of 0.43 which is slightly lower than 0.49. It is obvious that this discrepancy comes from the assumptions made earlier. As before, in order to take into account the exciton binding energy, we use the fact that the value of the radius for which we see a cancellation of the electrostatic and quantum terms is 80 Å and we take a value of 40 Å for the diameter of the particles after 2 minutes and 5 minutes. We then arrive to a value of 0.47 (after 2 min) and 0.5 (after 5 min). Once again, those values support the attribution given to the peaks.

The attribution of the peaks is strongly supported by the values of the ratio α definited in Eq. (15).

As the growth goes on, the small sharp peaks shift towards lower energies and the fine and discrete structure disappears, this is due to the growth of the particles and the decrease of the confinement term, associated with a hybrid molecular-semiconductor structure of the clusters.

Another aspect to consider is the relative importance of the different intensity of the peaks. At the early stages of the reaction, they all have approximately the same intensity, indicating well separated energy levels, i.e. each band is quickly filled up and one has a carrier recombination at every levels. However, as the growth proceeds, it becomes clear that the 1S,HH transition becomes predominant. This is expected, since as the particles grows, we tend more towards a quasi-bulk structure which is characterized with only one recombination peak occurring at the bottom of the conduction band.

Figure 6 shows the ageing effect on the particles. A general remark on the data is that after five hours in room atmosphere, the excitation peak value is still larger than 2.42 eV, indicating then that the confinement term is dominating the Coulombic term, which means that the mean radius of the cluster is less than 80 Å.
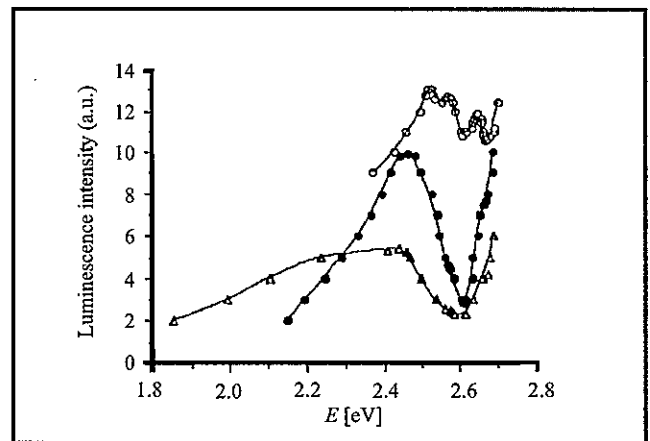

*Fig. 6.* Ageing effect on the luminescence spectrum of a 1:10 exchange ratio membrane
White circles curve after 2 min of exposure to dried hydrogen sulphide, black circles curve after 5 hours of storage at room atmosphere, and triangle curve after 1 day of storage at room atmosphere. The excitation wavelength is 450 nm (2.76 eV).

Several further features were observed in the luminescence spectra. A small peak at 825 nm (1.51 eV) is present in every case. This is explain by the following reaction where oxygen acts as a donor:

$$1/2\, O_2 \Longleftrightarrow CdO + V_{Cd^{2-}} + 2h^+$$
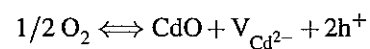
which predicts a peak at 820 nm.
After storage at room atmosphere a large excitation peak is found to appear at 700 nm (1.78 eV) which was attributed to Sulphur vacancies

$$h^+ + V_S \longrightarrow V_{S+} + h\nu$$
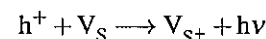
and ionised vacancies are subsequently refilled by conduction band electrons produced concomitantly with h^+ by band gap excitation.
Finally, the effect of ageing on the samples was to, firstly shift the peak value to lower energy, and subsequently, decrease its intensity. The first point is reflecting the fact

that the particles keep on growing, even in the absence of H_2S gas. This is due to the presence of moisture in the membranes, which contains dilute form of the H_2S, and which helps the migration of the cadmium ions within the channels. These ions then react at the surface of the clusters, causing then an enlargement of them according to the following reaction:

$$(CdS)_n + Cd^{2+}_{solv} + S^{2-}_{solv} \Longleftrightarrow (CdS)_{n+1}$$
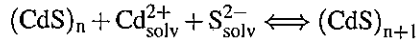
The fact that the intensity decreases is analysed as showing the quenching by surface defects, appearing during that diffusion-limited growth phase.

Nonlinear optical properties

Two methods are used to investigate the nonlinear response of these systems. As discussed in section *Nonlinear optical properties*, semiconductor quantum dots should show saturable absorption. Therefore, the intensity dependence of the transmission must be investigated. A laser induced grating, i.e. degenerate four-wave mixing set-up was used to measure the magnitude and dispersion of $\chi^{(3)}$ [13]. Maximal nonlinear response is expected when the excitation wavelength is in resonance with the quantized transitions. Since this depends on the particle dimensions, a tunable laser source is required. In all experiments described below, a Molectron DL-100 dye laser, pumped by a low pressure Molectron UV-300 N_2 laser, was employed giving pulses of 5 ns duration and typically 30 μJ energy.

Nonlinear absorption

Two types of samples with different emission spectra but the same 1:10 exchange ratio were studied. One had an maximal emission peak at 500 nm and the second one had an emission maximum at 700 nm. Although the signal was found to slightly decrease along the experiment (a couple of percent in 2–3 hours), some general trends can be deduced. The experimental set-up was as follows: The output of the dye laser was focused onto the samples. The input and transmitted energy were measured using calibrated silicon photodiodes, a fraction of the input being split-off with a beamsplitter. The input intensity could be varied using neutral density filters to attenuate the energy per pulse. The beam waist at the sample was measured with calibrated pinhole apertures to determine the intensity.

For small initial absorption ($T_0 > 0.1$), the transmission versus the input intensity will the follow equation

$$T = T_0 \quad 1 \Big/ \left(1 + \frac{I}{I_{sat}}\right). \tag{16}$$

Here, I_{sat} is the saturation intensity and, for a two-level system, is given by

$$I_{sat} = \frac{h\nu}{2\sigma_0 \tau}, \tag{17}$$

where σ_0 is the carrier absorption cross-section (10-17 cm^2 for CdS) and τ is the excited state lifetime of the carriers. Figure 7 shows the results obtained for the 700 nm emission peak sample. No major difference was found between both samples, they both had a saturation intensity of (2.5 ± 0.5) 10^{11} W/cm^2 and an extremely short, calculated lifetime of 1 ps (at a wavelength of 446 nm). Saturation ($T_{(I \to \infty)} \to 1$)
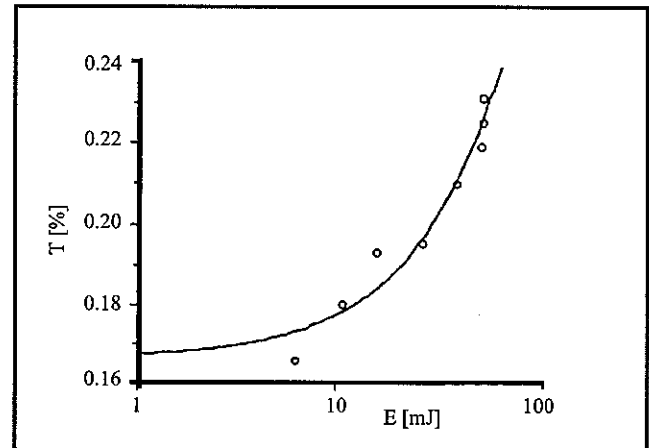

Fig. 7. Pulse energy dependent bleaching of the sample transmission $T = \exp(-\alpha l)$, and hence absorption saturation for a CdS Nafion membrane (exchange ratio of 1:10) with an emission peak at 700 nm
The solid line represents a fit to Eq. (13).

did not occur completely which demonstrates a sizeable non-saturable absorption which may be either due to excited free carrier absorption and/or non-saturable background absorption due to extremely fast relaxing species.
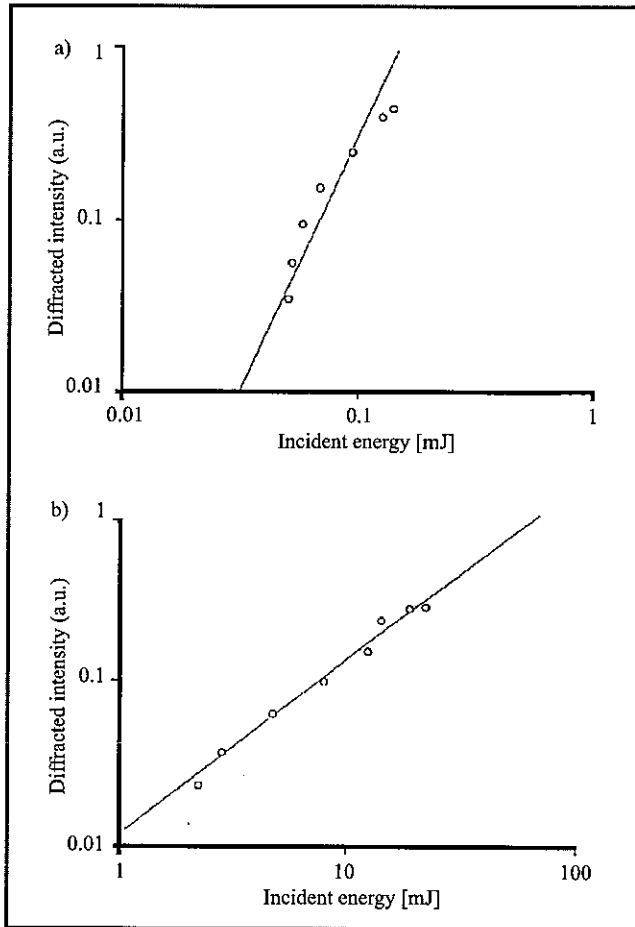
Degenerate four-wave mixing

To produce a laser induced grating, two coherent beams must be made to interfere. The output from the dye laser was collimated and brought around the table into a 50/50 cubic beam splitter. To achieve temporal overlap of the pulses a delay line was introduced on one arm; this proved especially necessary because of the very short coherence length of the pulses. The two collinear beams were brought to a focus and overlap by either a 30 or 50 cm focal length lens. When a material with a suitable nonlinear response was introduced into the overlap region, self-diffraction will occur. This may be observed by monitoring the beams on the opposite side of the sample. Two bright spots will be seen, corresponding to the straight through beams. To either side, fainter spots appear corresponding to the diffracted beams. For highly nonlinear materials, several diffracted orders may be observed. When measuring the magnitude of the diffracted beam, the signal obtained with the nearer pump beam blocked was also measured, and subtracted from the diffracted signal. This removes the component due to background scatter and it also ensures that only a transient grating is measured. Permanent gratings may also be written by physical damage to a material, or by other photochemical effects.

Degenerate four-wave mixing theory was used to calculate the magnitude of the effective third-order susceptibility, $|\chi^{(3)}|$. The self diffraction effect may be viewed as forward four-wave mixing where the probe beam is equal to and collinear with one of the pump beams. For this geometry $|\chi^{(3)}|$ can be calculated [14]:

$$|\chi^{(3)}| = \frac{8c^2 n^2 \varepsilon_0 \alpha \sqrt{\eta}}{3\omega I_1 (1-T)} , \qquad (18)$$

where c is the speed of light, n-the linear refractive index, α-the linear absorption, ω-the frequency, I_1-the pump intensity, and T-the transmission at I_1. It should be noted that the diffraction intensity depends quadratically, and thus the diffracted signal cubically, on the incident intensity I_1, as expected for a third-order nonlinear process.

The results of the intensity dependence of $|\chi^{(3)}|$ are shown in Fig. 8. They show within experimental accuracy ($\pm 20\%$

Fig. 8. Dependence of the diffracted intensity in the degenerate four-wave mixing experiment on incident pulse energy (proportional to intensity) for a CdS Nafion sample: a) exchange ratio of 1:10 - emission peak at 500 nm; the straight line corresponds to a slope of 3; b) exchange ratio of 1:10 - emission peak at 700 nm. The straight line corresponds to a slope of 1.

of intensity) that a third-order process occurs in the first sample, whereas we obtain a perfectly linear behaviour in the case of the second sample. This corresponds to

a quenching of the third-order process which is identical to the effect observed as 'photo-darkening' in doped glasses [1, 6], and is due to the presence of traps in the middle of the band gap, attributes to the 700 nm emission peak.

As discussed above in section *Nonlinear optical properties*, the wavelength dependence of the third-nonlinear susceptibility $\chi^{(3)}$ should give an indication of the process going on in each of both samples. It is expected that this should get enhanced at wavelengths in resonance with an exciton energy level.

Such a detuning effects can be seen in Fig. 9. Enhancement occurs when the exciton interaction is larger than off-resonance energy. If the band-filling theory applies [7]:

$$|\chi^{(3)}| = \frac{M \alpha(\omega)}{\omega_{g1} - \omega} + \frac{N \alpha(\omega)}{\omega - \omega_{g2}} , \qquad (19)$$

which yields $\omega_{g1} = 2.89$ eV and $\omega_{g2} = 2.72$ eV, M and N being two fitting constants. None of the other effects outlined in section *Nonlinear optical properties* give a satisfactory alternative fit. We believe that band filling depicts the physical reality quite well since we have a hybrid band structure, i.e. we have indeed a discrete repartition of quite broad bands. From the experiments presented, it is not
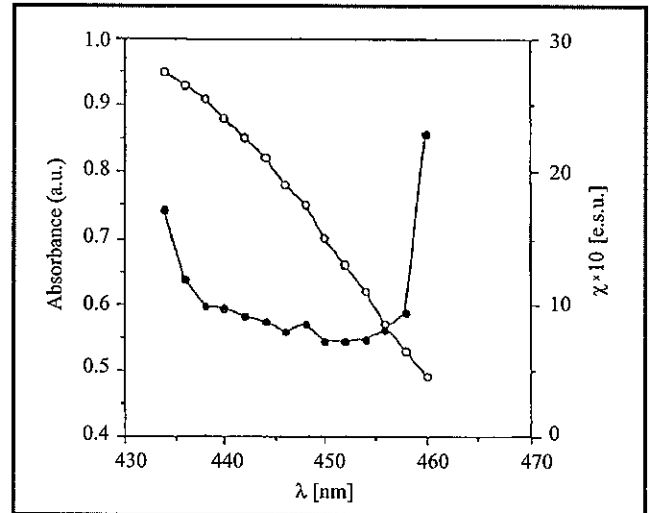
Fig. 9. The third nonlinear susceptibility $\chi^{(3)}$ (full circles) and absorption spectra (open circles) of a CdS Nafion sample (exchange ratio of 1:10 - emission peak at 500 nm).

possible to conclude what energy levels exactly correspond to the two observed resonances. 2.89 eV and 2.72 eV might correspond to two different diameter particles (one in Nafion cluster of 40 Å, and one located in the channel with diameter of 10 Å), or alternatively two consecutive exciton energy levels.

The magnitude of $|\chi^{(3)}|$ measured was very sizeable with an off-resonance value is $6 \cdot 10^{-9}$ esu and a resonance enhancing factor of at least 10. Those results are well in accordance with previous results reported by Hayashi et al. [16]. In their case, CdS particles embedded in acrylonitrile - styrene copolymer films with diameter ranging from 3 to 5 nm were studied. The ratio of nonlinearity to absorption

coefficient, which represents some kind of 'figure-of-merit' of the nonlinear material, was found to be $9 \cdot 10^{-10}$ esu/cm. This is comparable to a value of 8-10-10 esu/cm observed in the experiments reported here. An enhancement of the ratio $\frac{\chi^{(3)}}{\alpha}$ by one order of magnitude was observed near the exciton shoulder in the absorption spectrum, similar to our results.

Time resolved measurements were made by delaying one of the excitation beams with respect. The temporal resolution gives information about the speed of the nonlinear response of the samples and with incoherent pulses such as the ones applied here, in particular, about the dephasing time [17]. The temporal width (FWHM) of the peak was 3 ps which corresponds to the coherence time rather than to the width of the laser pulse. This indicates that the dephasing time is considerably faster than ≈ 1 ps. The excited state lifetime of 1 ps derived from the saturation measurements presented in section *Nonlinear absorption* also agree well with a reported relaxation time of 1.3 ps in similar samples [18].

Conclusions

Small clusers of CdS have been prepared in Nafion and their optical properties have been characterized. The kinetics of particle growth in H_2S gas was found to be linear in time. The diameter of the clusters was found to increase with time, and this is linked to the presence of moisture within the film. Exciton peaks were observed at room temperature in absorption and emission, and their attribution fits well with available data. Nonlinear measurements are very encouraging and clearly show an enhancement of the discrete energies of the excitons. The results show clusters with a mean diameter of approx. 40 Å and a hybrid band like structure.

Acknowledgements

References

[1] P. Horan and W. Blau, *Phase Trans.*, vol. 24–26, p. 605, 1990.

[2] Al. Efros and A. L. Efros, *Sov. Phys. Semicond.*, vol. 16, p. 775, 1982.

[3] S. Flügge, *Practical Quantum Mechanics*. Berlin: Springer-Verlag, 1971.

[4] L. Brus, *IEEE J. Quant. Electron.*, vol. QE-22, no. 9, p. 1909, 1986.

[5] G. A. Ozin, S. Kirby, M. Meszaros, S. Ozkar, A. Stein, and G. D. Stucky, in *Materials for Nonlinear Optics: Chemical Perspectives* (ACS Symposium Ser. 455, Boston, Massachussetts, April 1990), p. 554.

[6] P. Roussignol, D. Ricard, J. Lukasik, and C. Flytzanis, *J. Opt. Soc. Am. B*, vol. 4, no. 5, 1987.

[7] B. S. Wherrett and N. A. Higgins, *Proc. Roy. Soc. London Ser. A*, vol. 379, p. 67, 1982.

[8] E. Hanamura, *Phys. Rev. B*, vol. 37, no. 3, p. 1273, 1988.

[9] C. Heitner-Wirguin, E. R. Bauminger, F. Labensky de Kanter, and S. Ofer, *Polymer*, vol. 21, p. 1327, 1980.

[10] S. V. Nair, L. M. Ramaniah, and K. C. Rustagi, *Phys. Rev. Lett.*, vol. 68, no. 6, p. 893, 1992.

[11] K. I. Kang, B. P. McGinnis, Sandalphon, Y. Z. Hu, S. W. Koch, N. Peyghambarian, A. Mysyrowicz, L. C. Liu, and S. H. Risbud, *Phys. Rev. B*, vol. 45, no. 7, p. 3465, 1992.

[12] C. Weisbush and B. Vinter, *Quantum Semiconductor Structure*. New York: Academic Press, 1991.

[13] H. E. Eichler, P. Günter, and D. W. Pohl, *Laser Induced Dynamic Gratings*. Berlin: Springer Verlag, 1986.

[14] R. C. Caro and M. C. Gower, *IEEE J. Quant. Electron.*, vol. QE-18, p. 1376, 1982.

[15] A. I. Ekimov and A. A. Onushchenko, *J. Opt. Soc. Am. B*, vol. 10, no. 1, p. 100, 1993.

[16] T. Hayashi *et al.*, in *Organic Materials for Non-linear Optics III* (Royal Society of Chemistry, Oxford, 1992), p. 197.

[17] K. Misawa, T. Hattori, T. Kobayashi, Y. Ohashi, and H. Itoh, *Springer Proc. Phys.*, vol. 36, p. 66, 1989.

[18] T. Kobayashi, S. Nomura, and K. Misawa, *Proc. SPIE*, vol. 1216, p. 105, 1990.

Emmanuel Bourdin, Fryod Z. Henari, Werner J. Blau,
Department of Physics,
John M. Kelly,
Department of Chemistry
Trinity College Dublin, Dublin 2, Ireland

Growth and study of nonlinear optical crystals at the Hungarian Academy of Sciences

Istvan Földvári, Katalin Polgár, Ágnes Péter, Elena Beregi, and Zsuzsanna Szaller

Abstract — **The former Research Laboratory for Crystal Physics continues the growth and defect structure investigation of nonlinear optical single crystals in a new organization, as a part of the Research Institute for Solid State Physics and Optics, Hungarian Academy of Sciences. The aim of the activity is to prepare specific crystals for basic and applied research as well as for applications. We improve the quality or modify the properties of well known nonlinear oxide and borate crystals and develop new materials. The principle nonlinear optical crystals in our profile are the followings: Paratellurite (TeO_2), congruent, Mg-doped and stoichiometric lithium niobate ($LiNbO_3$), a variety of sillenite structured crystals ($Bi_{12}MeO_{20}$, Me=Si, Ge, Ti, etc.), bismuth tellurite (Bi_2TeO_5) and nonlinear borates (BBO–β-BaB_2O_4, LBO–LiB_3O_5, LTB–$Li_2B_4O_7$, CLBO–$CsLiB_6O_{10}$ and YAB–$YAl_3(BO_3)_4$). Details of the crystal preparation and the major achievements are discussed in the paper.**

Keywords — *crystal growth, nonlinear optical materials.*

Introduction

The Research Laboratory for Crystal Physics (RLCP) was established in 1976 for continuing the Hungarian tradition in crystal growth and characterization. During the years, the RLCP has earned reputation in growth and investigation of various insulator crystals, first alkali chlorides and fluorides then oxides and borates. The Hungarian Academy of Sciences has recently reorganized its institute network and the RLCP became a part of the Research Institute for Solid State Physics and Optics (RISSPO). The new institute keeps the entire crystal growth profile. The recent program of the Crystal Technology Department covers two sorts of optical materials; nonlinear optical crystals and scintillators. We use here the extended meaning of „nonlinear properties" including electro-optical, acousto-optic and photorefractive properties too. In this paper we want to summarize the state of the art of and the recent achievements on nonlinear optical crystals at RISSPO.

Experimental techniques

Synthesis of the starting materials

Quality requirements and the price of commercial chemicals motivated us to use own raw materials for crystal growth. In addition, some of the binary oxides in our profile, like Bi_2TeO_5 are not available commercially. Table 1 shows a review for the raw materials applied for crystal growth and their preparation methods.

Optical applications require the use of high purity materials (at least 5N). TeO_2, Bi_2O_3 and GeO_2 are prepared from the respective metals by chemical digestion which means a complex acidic oxidation of the metals, often including a purification step too. The other constituents are optical grade commercial materials. The starting material for crystal growth are prepared by multi step solid phase reaction that consists of a few hours treatment of the mixed oxide constituents at a previously determined optimum temperature, grinding of the transition composite, then a second (and further) anneal at higher temperature. The final composition of the synthesized materials was tested by X-ray phase analysis. Some examples for the preparation of starting materials for the individual crystals are presented in [1-2].

Chemical analysis

The chemical analysis directs to determine the actual crystal compositions and the impurity and dopant concentrations. Because of the relative accuracy required, the ratio of the major constituencies in the crystal are followed by wet chemical methods. The impurity and dopant concentrations are determined by atomic absorption spectroscopy (AAS). Appropriate solvents from the crystals are prepared by a chemical digestion specific to the individual crystals. The matrix effect of the host components are taken into account and, occasionally, solvent stabilizer is applied, e.g. [3-4]. The detection limit of the various impurities in the presence of host crystal components is around 1 ppm.

Crystal growth

The standard method applied for crystal growth is the diameter controlled Czochralski technique. The growth instruments consists of precision commercial pulling mechanisms, furnaces with resistance heating elements and specific diameter controlling units developed in the RLCP [5]. The open air growth systems use protection for the harmful vapor from the high temperature melts. Among the nonlinear optical crystals, the congruent and Mg-doped $LiNbO_3$, TeO_2, sillenites, Bi_2TeO_5, $CsLiB_6O_{10}$ and $Li_2B_4O_7$ are grown with the Czochralski technique. For the crystals

Istvan Földvári, Katalin Polgár, Ágnes Péter, Elena Beregi, and Zsuzsanna Szaller

Table 1
Raw materials and preparation techniques of starting compounds for crystal growth

Crystal	Raw materials	Preparation technique
Paratellurite – TeO_2	Te metal	chemical digestion
Lithium niobate – $LiNbO_3$	$Li_2CO_3 + Nb_2O_5$	two step solid phase reaction
Bismuth tellurite – Bi_2TeO_5	$TeO_2 + Bi_2O_3$	two step solid phase reaction
Sillenites – $Bi_{12}MeO_{20}$ (Me = Ge, Si, Ti)	$Bi_2O_3 + MeO_2$	two step solid phase reaction
β barium metaborate – BaB_2O_4 (BBO)	$B_2O_3 + BaCO_3$	multi step solid phase reaction
Lithium triborate – LiB_3O_5 (LBO)	$Li_2B_4O_7 + B_2O_3$	multi step solid phase reaction
Lithium tetraborate – $Li_2B_4O_7$ (LTB)	commercial	
Cesium-lithium borate – $CsLiB_6O_{10}$ (CLBO)	$Li_2CO_3 + Cs_2CO_3 + B_2O_3$	multi step solid phase reaction
Yttrium-aluminum-borate – $YAl_3(BO_3)_4$	$Y_2O_3 + Al_2O_3 + K_2CO_3 + MoO_3$	two step solid phase reaction

having non-congruent melting or phase transition between the melt temperature and room temperature, top seeded flux (TSSG) method and, occasionally, spontaneous nucleation are applied. The flux method is also used for stoichiometric $LiNbO_3$. The actual flux compositions are discussed at the description of the individual crystals.

Orientation, processing and characterization of the crystal samples

The sample preparation from the crystal boules includes an X-ray orientation by a specific single crystal diffractometer (Secasi), cutting by diamond blade and polishing. The orientation and processing technique makes it possible to keep the orientation accuracy of the sample within a few arc minutes that required for some applications like as the acoustic propagation direction for acousto-optic crystals. The crystal processing methods has recently been completed in the RISSPO by the possibility of surface coating.

The single crystal samples are characterized by conventional optical methods and microscopic techniques including chemical etching for developing the characteristic defects like as dislocations, grain boundaries, twinning, etc. Selective etching agents and etching technique have been developed for the specific crystals and surface orientations. Another test method applied is the absorption spectroscopy in the UV-visible and infrared spectral range. If needed, additional investigations were performed in an extended international cooperation.

Materials and achievements

Paratellurite – TeO_2

Single crystals of paratellurite have excellent acousto-optical properties due to their low ultrasound velocity, high refractive indices and large piezo-optic constants [6,7]. The M_2 acousto-optic figure of merit for one of the shear modes in TeO_2 is the highest known value for materials transparent in the visible range [8]. The chemical and mechanical stability of paratellurite promotes also its applications in different acousto-optic devices. Deflectors, modulators and tunable filters are just a few from the realized possibilities.

The TeO_2 crystals are colorless. Impurities are harmful for the crystal growth but not for the coloration since the incorporation of various dopants are extremely, e.g. [1,9]. This is related to the characteristic asymmetric covalent bonding of Te to O that is hard to replace by any impurity of ionic character. Consequently, the absorption edge of the TeO_2 crystal is sharp and it obeys the Urbach rule [10]. The crucial question in the crystal performance is the acoustic attenuation that is closely related with the dislocation density. After a systematic improvement of the growth conditions, the lowest known dislocation density was published for TeO_2 (in specific samples 3000–4000 cm^{-2} on (110) face [11]). Also, it resulted in the lowest observed acoustic attenuation (2.2 db/cm for the slow shear mode in the [110] direction at 100 MHz [12]). The recent progress in the growth of paratellurite is the increased crystal diameter to 5 cm.

Lithium niobate – $LiNbO_3$

Lithium niobate is one of the most widely used nonlinear optical materials. Besides its nonlinear optical applications, the outstanding electro-optical and electro-acoustic properties are also employed (e.g. electro-acoustic transducers, acoustic surface wave filters, integrated optical elements). The achievements in study and application of LiNbO3 have been published in more than 8000 papers and dozens of reviews. Some recent books cover the major results [13,14]. LiNbO3 is a typical nonstoichiometric material. Homogeneous single crystals can only be grown from the congruent melt composition (48.6 mole% Li_2O and 51.4 mole% Nb_2O_5), e.g. [15,16]. The quality of the undoped congruent crystals is excellent. One exception is the limited resistance to visible laser light („laser hardness"). A major breakthrough in the laser hardness problem was the application of Mg dopant [17,18]. Mg doping pushes away the „antisite„ Nb ions from the lithium position and shifts the absorption edge of $LiNbO_3$ toward the shorter wavelengths. This enhanced absorption range looks to be the major reason of the increased laser resistance [19]. There were several attempts to get stoichiometric $LiNbO_3$ in which there are no antisite Nb ions without using dopants. Growth from Li reach melt did not produce homogeneous crystal composition. Remarkable progress was only achieved

by the double crucible method (with abs.edge position at 308 nm [20]). The annealing of the congruent crystals in Li rich vapor resulted in only a surface layer of stoichiometric $LiNbO_3$. It was shown that the composition of the $LiNbO_3$ crystals grown from melt with a large K_2O content approached the stoichiometric composition [21]. We have improved this technique and pointed out that the heavy K_2O containing melt was actually a flux that reduced the growth temperature [22]. By the developed flux technique we published the growth of the $LiNbO_3$ crystals that was closest to the stoichiometric composition [22]. We introduced also a simple, non-destructive test method for determine the crystal composition based on the absorption edge position of the crystal [23]. This method has recently been improved [24]. The state of art of our stoichiometric crystal is represented by the 303 nm abs. edge position (at 20 cm-1 abs. coeff.). The technical conditions were the followings: top seeded flux with K_2O. The Li/Nb ratio was 1 and the K_2O content corresponded to the K/Nb ratio of 0.38 in the melt. The actual growth temperature was in the 1030–1075ºC range.

Sillenites – $Bi_{12}MeO_{20}$ (Me = Si, Ge, Ti)

The first use of sillenites related to the acoustic surface wave applications. Their outstanding photorefractive properties were first reported in [25]. The subsequent comprehensive studies of the photorefractive effects are summarized in topical books and reviews e.g. [26,27]. The single crystals grown from the melt exhibit yellow-brown coloration that was studied by several authors and reviewed in [28,29]. The color is related to an absorption shoulder near the intrinsic absorption edge and there are still debate on the origin of the coloration. It was recently pointed out that photochromic effect contribute to the color through generation of color centers stabile at room temperature [31]. The color of the sillenites grown from heavily doped melt with Al or Ga are pale and the absorption shoulder is missing [30,31]. Growth of undoped, colorless sillenite crystals has recently been reported by hydrothermal method [32].

We optimized the solid phase reaction and crystal growth of various sillenite crystals. The $Bi_{12}GeO_{20}$ and $Bi_{12}SiO_{20}$ crystals are grown by the Czochralski technique while the $Bi_{12}TiO_{20}$ by flux method. Ge–Si mixed sillenites and exotic sillenite structured crystals were also grown [33].

It was pointed out that various impurities modify physical parameters that play role in the photorefractive properties of sillenites [34,35]. Fast photorefractive response of Al-doped sillenites was predicted [35].

Bismuth tellurite Bi_2TeO_5

Bismuth tellurite is a new nonlinear optical material that became interesting when its unique photorefractive properties were discovered [36,37]. The crystal exhibits a long-living photorefractive signal component that develops in the four-wave mixing write process and lasts for years without any fixing [38]. Thus Bi_2TeO_5 is a good candidate for holographic memory substrate. The technical details for growth of Bi_2TeO_5 single crystals were first described in our laboratory [2]. There is only one other known source for bismuth tellurite so far (Dniepropetrovsk University, Ukraine). After developing the growth technique, several physical properties of the crystals were determined in the RLCP like the absorption and reflectivity spectra [39], refractive indices and their temperature dependence [40,41] and the nonlinear absorption [42]. The photorefractive investigations were extended to the short pulse (ps) excitation [43,44]. A recent review summarizes the photochromic and photorefractive properties of Bi_2TeO_5 [45]. Another interesting observation was that various dopants build in the crystal with segregation coefficients close to unity [4,46]. This allows to use Bi_2TeO_5 as a host for dopants like rare earth ions and Cr.

Nonlinear borates

Borates applied in nonlinear optics (e.g. BBO–β-BaB_2O_4, LBO–LiB_3O_5, CLBO–$CsLiB_6O_{10}$, LTB–$Li_2B_4O_7$), exhibit broad optical transparency range (160–3500 nm), excellent laser damage threshold and adequate birefringence for phase matching in a wide range of visible and UV wavelengths. The huntite type double borates, $(RM_3(BO_3)_4$ where R^{3+} = Sc, Y, La, Ln, In, Bi and M^{3+} = Al, Cr, Ga, Fe, Sc), can easily be doped with rare earth and transition metals.

BBO is used for generation of higher harmonics of the laser frequency, including the fifth harmonic of the Nd:YAG, for frequency mixing and optical parametric oscillation. This crystal is grown in our laboratory by high temperature top seeded solution growth (HTTSSG) from BaB_2O_4–Na_2O FLUX [47]. The maximum dimensions of the BBO crystal was successfully increased to about 60 mm in diameter and 130 g in weight. A chemical etching technique was developed to test the quality of the crystals [48]. The FLUX method resulted in good optical quality but, occasionally, the crystal contained inclusion.

LBO is used for the generation of non-critical phase matching second and third harmonics of Nd:YAG and frequency mixing down to the far UV range [49]. It is an excellent material for parametric generation of ultrashort pulses. Due to its incongruent melting, LBO is grown also by HTTSSG from LiB_3O_5+B_2O_3 flux [50]. The maximal dimension of the LBO crystals grown in our laboratory was 60 mm ϕ. The main problem in the preparation of LBO is the frequent cracking of the crystal during cooling.

CLBO can be grown by both Czochralski and TSSG methods [51,52]. Its advantage is the high yield in forth and fifth harmonic generation of Nd:YAG laser emission [53]. The major drawback in the application of CLBO is its hygroscopic nature. We grow CLBO by the Czochralski method. The maximal dimension achieved was 40 mm ϕ and 40 mm long.

LTB is applied as temperature independent SAW-filter and as soft-tissue-equivalent thermoluminescent (TL) dosime-

Istvan Földvári, Katalin Polgár, Ágnes Péter, Elena Beregi, and Zsuzsanna Szaller

ter. The effective generation of fourth and fifth harmonic of Nd:YAG laser light is recently reported [54]. The congruently melting material can be grown by the Czochralski or Bridgman technique. We used the Czochralski method and crystals of 25 mm ϕ and 40 mm long were grown. The crystal is hard to dope by simply adding dopants to the melt. The low incorporation of Cu, however, was enough to generate detectable thermoluminescence in LTB:Cu [55]. Planar waveguides were prepared by He$^+$ ion implantation and the properties of the waveguide was presented in [56].

Huntite type double borates

Among the huntite borates, prospective results have been published for rare-earth doped yttrium-aluminum borate (YAB)–YAl$_3$(BO$_3$)$_4$ single crystals [57, 58]. The Nd-doped crystals (Nd:YAB or NYAB) show good laser efficiency with broad excitation range. The optical arrangement for self-frequency doubling (SFD) laser was shown to be free from quenching effects. Note that YAB is transparent to the far UV (down to 165 nm). Laser effects were also shown in Er, Cr and Cr + Ga doped crystals [59]. Microchip lasers made from huntite borates have recently been reported [60-62]. Because of the incongruent melting, YAB and related crystals can be grown from high temperature solution. We grow YAB and Nd$_x$Y$_{1-x}$Al$_3$(BO$_3$)$_4$ (NYAB) crystals with spontaneous nucleation and top seeded methods. The FLUX used is: K$_2$MoO$_4$+B$_2$O$_3$ (80%), YAB or NYAB (20%). The Nd content of the melt for NYAB was 3-12 mole%. The maximum dimension for the HTTSSG grown crystals was $17 \times 15 \times 15$ mm^3. We have preliminary results in the growth of Er$_x$Y$_{1-x}$Al$_3$(BO$_3$)$_4$ and Y$_1$Al$_{3-y}$Cr$_y$(BO$_3$)$_4$ crystals too.

Conclusion

The Research Institute for Solid State Physics and Optics conducts an extended program for growth and characterization of nonlinear optical crystals. These crystals have been studied in a broad international cooperation involving institutes from USA, France, Germany, Italy, Spain, Great Britain, Portugal, Mexico, Poland, Ukraine, Russia and Armenia. We are open for further, mutually interesting joint programs in basic and applied research. Upon request we can provide specific crystals and characterized samples from our profile.

Acknowledgment

References

[1] I. Földvári, K. Raksányi, R. Voszka, E. Hartmann, and Á. Péter, *J. Cryst. Growth*, vol. 52, p. 561, 1981.

[2] I. Földvári, Á. Péter, R. Voszka, and L. A. Kappers, *J. Cryst. Growth*, vol. 100, p. 75, 1990.

[3] L. F. Bencs, O. Szakács, *Spectrochim. Acta B*, vol. 52, p. 1483, 1997.

[4] Á. Péter, O. Szakács, I. Földvári, L. Bencs, and A. Munoz F, *Mater. Res. Bull.* vol. 31, p. 1067, 1996.

[5] F. Schimdt and R. Voszka, *Cryst. Res. Technol.*, vol. 16, p. K-127, 1981.

[6] G. Arlt and M. Schweppe, *Solid State Commun.*, vol. 6, p. 783, 1968.

[7] N. Uchida and Y. Omachi, *J. Appl. Phys.*, vol. 41, p. 2307, 1970.

[8] T. Yano and A. Watanabe, *Appl. Phys. Lett.*, vol. 24, p. 256, 1974.

[9] I. Földvári, R. Voszka, L. A. Kappers, D. S. Hamilton, and R. H. Bartram, *Phys. Lett. A*, vol. 109, p. 303, 1985.

[10] A. Mecseki, I. Földvári, and R. Voszka, *Acta Phys. Hung.*, vol. 53, p. 15, 1982.

[11] J. Janszky, Á. Péter, A. Mecseki, R. Voszka, I. Tarján, I. Földvári, I. M. Silvestrova, and Yu. V. Pisarevskii, *Sov. Phys. Crystallogr.*, vol. 27, p. 90, 1982.

[12] I. M. Silvestrova, Yu. V. Pisarevskii, I. Földvári, Á. Péter, R. Voszka, and J. Janszky, *Phys. Stat. Sol. A*, vol. 66, p. K-55, 1981.

[13] *Properties of Lithium Niobate, EMIS Datareviews Series No. 5*. London: INSPEC Publ., 1989.

[14] A. M. Prokhorov and Yu. S. Kuzminov, *Physics and Chemistry of Crystalline Lithium Niobate*. New York: Hilger, 1990.

[15] P. Lerner, C. Legras, and J. P. Dumas, *J. Cryst. Growth*, vol. 3, p. 231, 1968.

[16] J. R. Carruthers, G. E. Peterson, M. Grasso, and P. M. Bridenbaugh, *J. Appl. Phys.*, vol. 42, p. 1846, 1971.

[17] D. A. Bryan, R. Gerson, and H. E. Tomaschke, *Appl. Phys. Lett.*, vol. 44, p. 847, 1984.

[18] K. L. Sweeney, L. E. Halliburton, D. A. Brysan, R. R. Rice, R. Gerson, and H. E. Tomaschke, *Appl. Phys. Lett.*, vol. 45, p. 805, 1984.

[19] K. Polgár, L. Kovács, I. Földvári, and I. Cravero, *Solid State Commun.*, vol. 59, p. 375, 1986.

[20] K. Kitamura, J. K. Yamamoto, N. Iyi, and S. Kimura, *J. Cryst. Growth*, vol. 116, p. 327, 1992.

[21] G. Malovichko, V. G. Grachev, L. P. Yurchenko, V. Ya. Proshko, E. P. Kokanyan, and V. T. Gabrielian, *Phys. Stat. Sol. A*, vol. 133, p. K-29, 1992.

[22] K. Polgár, Á. Péter, L. Kovács, G. Corradi, and Zs. Szaller, *J. Cryst. Growth*, vol. 177, p. 211, 1997.

[23] I. Földvári, K. Polgár, R. Voszka, and R. N. Balasanyan, *Cryst. Res. Technol.*, vol. 19, p. 1659, 1984.

[24] L. Kovács, G. Russchhaupt, K. Polgár, G. Corradi, and M. Wöhlecke, *Appl. Phys. Lett.*, vol. 70, p. 2801, 1997.

[25] J. P. Huignard and F. Micheron, *Appl. Phys. Lett.*, vol. 29, p. 591, 1976.

[26] P. Günter, *Phys. Rep.*, vol. 93, p. 199, 1982.

[27] P. Günter and J. P. Huignard, Eds. *Photorefractive Materials and their applications*. Vols I and II. Berlin: Springer Verlag, 1988 and 1989.

[28] B. C. Grabmayer and R. Oberschmidt, *Phys. Stat. Sol. A*, vol. 96, p. 199, 1986.

[29] L. Arizmendi, J. M. Cabrera, and F. Agullo-Lopez, *Intern. J. Optoelectr.*, vol. 7, p. 149, 1992.

[30] J. J. Martin, I. Földvári, and C. A. Hunt, *J. Appl. Phys.*, vol. 70, p. 7554, 1991.

[31] S. L. Hou, R. B. Lauer, and R. E. Aldrich, *J. Appl. Phys.*, vol. 44, p. 2652, 1973.

[32] M. T. Harris, J. J. Larkin, and J. J. Martin, *Appl. Phys. Lett.*, vol. 60, p. 2162, 1992.

[33] C. Zaldo, C. Moya, J. L. G. Fierro, K. Polgár, L. Kovács, Zs. Szaller, *J. Phys. Chem. Solids*, vol. 57, p. 1667, 1996.

[34] I. Földvári, J. J. Martin, C. A. Hunt, R. C. Powell, R. J. Reeves, and S. A. Holmstrom, *Opt. Mater.*, vol. 2, p. 25, 1993.

[35] I. Földvári, L. E. Halliburton, G. J. Edwards, and L. Ötsi, *Solid State Commun.*, vol. 77, p. 181, 1991.

[36] I. Földvári, M. P. Scripsick, L. E. Halliburton, and Á. Péter, *Phys. Lett. A*, vol. 154, p. 84, 1991.

[37] I. Földvári, H. Liu, R. C. Powell, and Á. Péter, *J. Appl. Phys.*, vol. 71, p. 5465, 1992.

[38] I. Földvári, H. Liu, and R. C. Powell, *SPIE Proc.*, vol. 162, p. 9, 1992.

[39] I. Földvári, Á. Péter, L. A. Kappers, O. R. Gilliam, and R. Capelletti, *J. Mat. Sci.*, vol. 27, p. 750, 1992.

[40] G. Mandula, L. Kovács, Á. Péter, and E. Hartmann, *Opt. Mat.*, vol. 1, p. 161, 1992.

[41] G. Mandula, Á. Péter, and E. Hartmann, *Pure and Appl. Opt.*, vol. 3, p. 839, 1994.

[42] I. Földvári, B. Taheri, R. J. Reeves, and R. C. Powell, *Opt. Commun.*, vol. 99, p. 245, 1993.

[43] I. Földvári, R. C. Powell, H. Liu, and Á. Péter, *Opt. Mat.*, vol. 2, p. 175, 1993.

[44] I. Földvári, Á. Péter, R. C. Powell, and B. Taheri, *Opt. Mat.*, vol. 4, p. 299, 1995.

[45] I. Földvári, L. A. Kappers, and R. C. Powell, *Mat. Sci. Forum*, vol. 239–241, p. 315, 1997.

[46] I. Földvári, Á. Péter, L. A. Kappers, R. H. Bartram, and R. Capelletti, *Mat. Sci. Forum*, vol. 239–241, p. 231, 1997.

[47] K. Polgár, Á. Péter, and F. Schmidt, *Cryst. Properties and Preparation*, vol. 36–38, p. 209, 1991.

[48] K. Polgár and Á. Péter, *J. Cryst. Growth*, vol. 134, p. 219, 1993.

[49] C. T. Chen, Y. Wu, A. Jiang, B. Wu, G. You, and S. Liu, *J. Opt. Soc. Am. B*, vol. 6, p. 616, 1989.

[50] S. Zhao, Ch. Huang, and H. Zhang, *J. Cryst. Growth*, vol. 99, p. 805, 1990.

[51] Y. Mori, I. Kuroda, S. Nakigama, A. Taguchi, T. Sasaki, and S. Nakai, *J. Cryst. Growth*, vol. 156, p. 307, 1995.

[52] Y. Mori, I. Kuroda, S. Nakigama, T. Sasaki, and S. Nakai, *Appl. Phys. Lett.*, vol. 67, p. 25, 1995.

[53] Y. K. Yap, M. Inagaki, D. Nakijama, Y. Mori, and T. Sasaki, *Opt. Lett.*, vol. 21, 1996.

[54] R. Komatsu, T. Sugawara, K. Sassa, N. Sarukura, Z. Liu, S. Izumida, Y. Segawa, S. Uda, T. Fukada, and K. Yamanouchi, *Appl. Phys. Lett.*, vol. 70, p. 3492, 1997.

[55] M. Martini, F. Meinardi, L. Kovács, and K. Polgár, *Rad. Prot. Dosimetry*, vol. 65, p. 343, 1348, 1996.

[56] A. Boudriona, P. Moretti, J. C. Loulerque, and K. Polgár, *Phys. Stat. Sol. A*, vol. 153, p. 553, 1996.

[57] J. T. Lin, *Lasers and Opt.*, p. 34, December 1990.

[58] S. T. Jung, D. Y. Choi, J. K. Kang, and S. J. Chung, *J. Cryst. Growth*, vol. 148, p. 207, 1995.

[59] M. Iwai, Y. Mori, T. Sasaki, S. Nakai, N. Sarukura, Z. Liu, and Y. Segawa, *Jap. J. Appl. Phys.*, vol. 34, p. 2338, 1995.

[60] B. Braun, F. X. Kartner, U. Keller, J. P. Meyn, and G. Huber, *Opt. Lett.*, vol. 21, p. 405, 1996.

[61] T. Omatsu, Y. Kato, M. Shimosegawa, A. Hasegawa, and I. Ogura, *Opt. Commun.*, vol. 118, p. 302, 1995.

[62] Y. F. Chen, S. C. Wang, C. F. Kao, and T. M. Huang, *IEEE Phot. Technol. Lett.*, vol. 8, p. 1313, 1996.

Istvan Földvári, Katalin Polgár, Ágnes Péter, Elena Beregi, and Zsuzsanna Szaller

Research Institute for Solid State Physics and Optics, Hungarian Academy of Sciences, Konkoly-Thege u. 29–33, 1525 Budpaest, P.O. Box 49, Hungary

Foundations of the theory of open waveguides

Alexander I. Nosich

Abstract — The theory of electromagnetic wave eigenmodes propagating on open dielectric and metallic waveguides has been reviewed. The main steps of different theoretical approaches to the problem are outlined and discussed. The unsolved problems and also directions of future development are pointed out.

Keywords — *open waveguide theory, eigenvalue problems*

The theory of natural waves (also known as normal waves, travelling waves, eigenmodes) able to propagate on open dielectric and metallic waveguides is far from a complete development. Commonly it is supposed that the field components of such a wave depend on the longitudinal coordinate z and time t as $e^{ihz-ikt/c}$, where h is the propagation constant (or modal wavenumber), k is the free-space wavenumber, and c is the free-space propagation velocity. Only in several simple cases, such as dielectric slab and coaxially-layered circular dielectric fiber, it is possible to study the waves in explicit form. Such a study has brought into consideration a variety of waves: surface-wave or guided modes, leaky waves, complex surface modes of lossless fiber, etc., differing by the field behavior as a function of coordinates. However, if the fiber cross-section is arbitrary, or if additional metal elements are present, as in the microstrip or slot lines, the theory meets great problems. There are many questions to be answered even for a mathematical formulation of the problem of natural waves. Clearly it should be a sort of eigenvalue problem for modal wavenumber h. However, what should be the domain of the variation of the eigenvalue parameter? In what class should one seek the modal field components as a function of coordinates in cross-section and along the waveguide? There have been several approaches to these problems; all of them appear to be not complete and should be re-examined.

The following is a summary of the results related to the theory of propagation of the time-harmonic waves on arbitrary-shaped electromagnetic open waveguides [1–14]. The main points of this study are as follows:

Start from the excitation problem

It is impossible to come to a reasonably general formulation of the modal eigenvalue problem from any other starting point than the problem of time-harmonic excitation $\left(\sim e^{ikt/c}, k = \text{Re}\,k > 0 \right)$ of an open waveguide by elementary electric and magnetic current sources. This is the same as determining the open waveguide Green functions. Here, a necessary assumption should be made that any field can be presented as a convolution with the Green functions.

Fourier transform

By virtue of infinite length of a regular waveguide along the z-axis, the Fourier transformation with the kernel e^{ihz} is a natural instrument of bringing the problem consideration to the two-dimesional (2D) space, for the field transforms as a function of cross-section r and integration parameter h. Here, another necessary assumption appears that the fields are no more than the slow-growth functions of z; hence, the Fourier integrals should be interpreted in terms of distributions. It is necessary to distinguish between the open waveguides, whose elements have a compact cross-section (embedded in free space) and those of non-compact cross-section, for example, compact open waveguides embedded into a flat-layered medium, whose cross-section has infinite boundaries. Although two cases have much in common, the latter one is more complicated. In the former case, Fourier transform enables one to reduce the excitation problem to a „conventional" one, for the Helmholtz operator $\Delta_t + k^2 \varepsilon(r)\mu(r) - h^2$ in 2D open domain with the boundary and transmission conditions given at bounded curves. Further results relate only to this case.

Analytic continuation

Fourier transform approach naturally brings the analysis to a necessity of analytic continuation of the field transforms, from the real values of parameter h to the complex domain. This complex domain is uniquely determined and is common to all the open waveguides of compact cross-section: it is the infinite-sheet Riemann surface L of the function $\ln(k-h)(k+h)$.

Reichardt condition

On this Riemann surface, it is the Reichardt condition that serves as analytic continuation of the 2D Sommerfeld radiation condition (for $|h| < k$) and the exponential-decay condition (for $|h| > k$) from the real axis of the „physical" sheet. Due to this condition, but also due to the transmission-type conditions at the material boundaries - if they are present, these 2D problems for the analytic continuations of the field transforms are non-selfadjoint ones. Note that this condition permits the field transforms to grow exponentially with $r \to \infty$ if h is located at the sheets other than the „physical" sheet of L. Nevertheless, Reichardt condition guarantees the uniqueness of solution provided that h is not an eigenvalue.

Analytical regularization

For a wide class of open waveguides, 2D boundary-value problems for the Fourier transforms can be converted to the canonical Fredholm operator equations, $(I+A)X = B$, in some Hilbert space. Here, operators A are the meromorphic functions of $h \in L, k$, and all the geometrical and material parameters of the waveguide. Such a conversion is based commonly on the analytical regularization of the singular integral equations equivalent to original boundary-value problem. Here, Reichardt condition guarantees that arbitrary-source field can be represented as a convolution with the transforms of the Green functions for any complex $h \in L$.

Fredholm-Steinberg theorems

Once a regularization has been done, one can use the theory of Fredholm in the form generalized by Steinberg for the operators depending on parameter. The results are as follows: it is possible to prove the existence of the bounded resolvent, and hence, the existence of the Fourier transforms, as no more than meromorphic functions of $h \in L$. They have no finite accumulation points of the poles on L. The poles can be of only finite multiplicity. They are piece-wise-continuos functions of the geometry and piece-wise-analytic functions of k and material parameters. The continuity or analiticity can be lost only at such a value of parameter that two or more poles coalesce. The poles can appear or disappear only at the boundary of the domain of meromorphicity: at infinity and in the branch points $h = \pm k$. The residues of the poles of the Fourier transforms satisfy certain 2D source-free eigenproblem for the Helmholtz equation, in terms of the spectral parameter h located on L.

Generalized modal eigenvalue problems

The latter circumstance leads to a conclusion that the eigenproblems about the natural waves of an open waveguide can be studied independently of the excitation problem. However, in view of the above chain of considerations, it should be formulated in a generalized sense. Namely, it should include the Reichardt condition at the infinity in cross-section. In so doing one gets a universal framework to study all the types of known natural waves: both surface waves, and leaky, and complex surface ones, etc., and hence trace the transitions of each mode from one type to another with variation of non-spectral parameters.

Symmetry of spectrum

Some properties of the modal spectrum can be deduced directly from the formulation of generalized eigenproblem. It is shown that in any open waveguide the eigenwavenumbers h form symmetric pairs on L. Moreover, in lossles waveguides, they form conjugate quartets on L. Hence, it is enough to study them only in one quadrant of each Riemann sheet.

Free of spectrum domain

By using the vector Green formula, it is shown that on L there exists a non-empty domain, which is free of the spectrum of natural waves. This domain depends on the type of the waveguide. If the latter does not contain material (dielectric or magnetic) elements, this domain includes the whole „physical" sheet of L; in a lossless dielectric waveguide, it includes the intervals $|h| < k$ and $|h| \geq \sup \varepsilon^{1/2}$ of the real axis of the „physical" sheet; in the lossy case this whole real axis is free of spectrum, etc.

Discreteness of modal spectrum

For a wide class of virtually all the practical models of open waveguides, such generalized eigenproblems admit analytical regularization and are equivalently reducible to a homogeneous Fredholm operator equation $[I+A(h)]X = 0$. The set of eigenvalues of h on L forms the spectrum of the operator A and coinsides with the spectrum of generalized natural waves of the waveguide. As one can see, the latter is purely discrete on L. In particular, this enables one to conclude that surface-wave modes, whose wavenumbers are located on the finite interval $k < |h| < k \sup \varepsilon^{1/2}$ of the real axis of the „physical" sheet, can be only of finite number.

Existence of natural waves

Non-emptiness of the spectrum of generalized natural modes is the most hard point of the analysis. It can be proved „locally" based on the operator generalization of the Rusche theorem and explicit existence of eigenvalues of certain canonic open waveguides, as the zeros of well-known special functions. This once again needs a regularized form of the eigenvalue operator equation. However, to complete this proof to a „global" existence, one needs some guaranty that a finite change of nonspectral parameter cannot kick all the eigenvalues off to infinity or annihilate them in the branch-point. This proof needs additional work.

Orthogonality and power flux

Vector Green formula, applied to the eigenmode field, enables one to prove the orthogonality of the surface waves and the complex surface waves, in the power sense. If the modal wavenumber is not located on the „physical" sheet of L, this proof fails. The Green formula is also an instrument to study the properties of the power flux associated with a generalized natural mode. For example, it shows that any complex surface wave in a lossless open waveguide can be only hybrid (i.e., has all the six components of electromagnetic field) and does not carry power, as its total flux in cross-section in identical zero. Another important conclusion is that, in open waveguides, there is no necessity for a surface wave to carry the power strictly in the direction of its propagation; the opposite direction is allowed, although only for the hybrid modes. The analyticity of spectrum points as a function of k enables one to validate the concept of the group velocity.

Multiple poles and „associated" natural waves

Unlike hollow closed waveguides, for the open waveguides it is not possible to prove the simple character of the poles, and hence the eigenvalues. (This is also known for the impedance-wall and multilayer closed waveguides). Hence, multiple poles, of finite multiplicity M, can exist. If so, besides of the „parent" natural wave propagating as e^{ihz}, a finite chain of the „associated" natural waves appears that propagate as $z^m e^{ihz}, m = 1, 2, \ldots M - 1$. This consideration validates the initial assumption, at the early stage of analysis of the excitation problem, that the field functions should be considered in the class of slow-growth functions of z.

Radiation condition

Strictly speaking, in the original 3D problem of the elementary-source excitation of open waveguide, the classical Sommerfeld condition of radiation is not valid for the extraction of unique solution. The reason is the presence of infinite along z boundaries, and hence possible presence of waves able to carry the power to infinity along the waveguide without attenuation. In view of the mentioned above results of study of the 2D problem for the field Fourier transforms, one can formulate an adequate condition of radiation, in the form of asymptotic request to the far-field behavior, that explicitly involves radiation, in the form of asymptotic request to the far-field behavior, that explicitly involves the surface waves. This condition guarantees uniqueness of the 3D problem solution and validates the early assumption that arbitrary-source field can be represented by a convolution with the Green functions. Here, one comes to a necessity of taking account of the direction of the power flux (or, equivalently, the sign of the group velocity) associated with each surface mode. The modified radiation condition enables one to formulate the Principle of Radiation as: *„No waves bringing power from infinity, in the scattered field"*. It is only if the losses are introduced in the waveguide elements that the modified radiation condition is reduced to the Sommerfeld one, as then no surface waves exist. The Principle of Radiation is then reduced to conventional form: *„No waves propagating from infinity, in the scattered field"*.

Defect of the model

A close view at the radiation condition reveals one intrincic defect of the original model of the time-harmonic excitation of a lossless infinite open waveguide. If the parameters of the lossless waveguide and k are such that „associated" surface-wave natural modes exist, then it appears not possible to apply even the modified condition of radiation. The reason is that in this simulation both the „parent" surface wave and the „associated" waves have zero total power flux, hence it is impossible to select proper sign of the modal wavenumber that ensures solution uniqueness.

Similarity between h and k as eigenparameters

From the formulation of the generalized eigenproblem, one can notice that the parameters h and k enter it in a very similar manner. Indeed, one can study this problem for k-eigenvalues, with $h = \text{Re} h > 0$. Much of the above theory is valid in this case as well. E.g., the domain of analytic continuation in k is the same Riemann surface L. The same Reichardt condition and the same analytical regularization approach bring us to the conclusions about the discreteness of the k-spectrum on L and about the properties of eigenvalues as a function of h. However, the mentioned similarity is not total, hence the other properties of the spectrum of generalized natural oscillations are to be studied in more detail. Analysis of such a „dual" eigenproblem appears to be a natural stage of studying a more general problem of the excitation of open waveguide by a δ-pulse or time-dependent source having a fixed distribution along z as e^{ihz}, with $h = const$.

Extentions and unsolved problems

There are several possible directions of the extention of the developed theory, each of them being associated with a separate class of problems. The results obtained for the regular open waveguides can be generalized to the regular-periodic open waveguides. This calls for a generalization of the Fourier transform approach by using the Floquet-expansions in z, in transform domain. Then it is possible to see that the domain of analytic continuation in h is the Riemann surface of the function $\sum_{m=-\infty}^{\infty} \ln(k - h - 2\pi m/l)(k + h + 2\pi m/l)$, where l is the period along z. The other direction of work is the theory of open waveguides with non-compact cross-section, such as microstripline on infinitely wide dielectric substrate. Here, the approach of the double Fourier transform should be used. The study of the Green functions and radiation condition should apparently bring into consideration the surface waves of two types: those which stick to the strip and decay exponentially both in the air and in the substrate, and those which attenuate in the air but propagate in the substrate as cylindrical surface waves. Another interesting direction is the theory of the open waveguide bends and branchings. Here, the key problem is the one of a terminated (semi-infinite) open waveguide in free space.

References

[1] V. V. Kryzhanovsky, A. I. Nosich, A. Y. Svezhentsev, and V. P. Shestopalov, „Theoretical and experimental investigation of cylindrical microstrip line modes", *Doklady Akademii Nauk Ukrainskoi SSR, Ser. A*, no. 10, pp. 43–46, 1986.

[2] A. I. Nosich, „Radiation conditions for open waveguides", *Sov. Phys. Doklady* (Engl. Transl.), vol. 32, no. 9, pp. 720–722, 1987.

[3] A. I. Nosich, „Radiation conditions, limiting absorption principle, and general relations in open waveguides scattering", *J. Electromagn. Waves Applicat.*, vol. 8, no. 3, pp. 329–353, 1994.

[4] A. I. Nosich, A. Y. Poedinchuk, and V. P. Shestopalov, „Discreteness of spectrum of the characteristic waves in open partially screened

dielectric core", *Sov. Phys. Doklady* (Engl. Transl.), vol. 30, no. 8, pp. 669–671, 1985.

[5] A. I. Nosich, A. Y. Poedinchuk, and V. P. Shestopalov, „Existence of discrete spectrum and singular types of waves in an open waveguide", *Sov. Phys. Doklady* (Engl. Transl.), vol. 32, no. 3, pp. 216–218, 1987.

[6] A. I. Nosich and V. P. Shestopalov, „Waveguiding properties of open metallized dielectric transmission lines of the cylindrical type", *Radio Engn. Electron. Phys.* (Engl. Transl.), vol. 24, pp. 1–9, 1979.

[7] A. I. Nosich and V. P. Shestopalov, „Excitation of a partially shielded dielectric rod by lumped sources", *Sov. Phys. - Tech. Phys.* (Engl. Transl.), vol. 28, no. 12, pp. 1421–1426, 1983.

[8] A. I. Nosich, A. Y. Svezhentsev, and V. P. Shestopalov, „Spectrum of quasi -TEM waves in a partially screened dielectric core", *Sov. Phys. Doklady* (Engl. Transl.), vol. 31, no. 7, pp. 559–561, 1986.

[9] A. I. Nosich, A. Y. Svezhentsev, and V. P. Shestopalov, „Electrodynamic analysis of the discrete spectrum of characteristic modes a partially screened dielectric rod", *Sov. J. Commun. Technol. Electron.* (Engl. Transl.), vol. 33, no. 3, pp. 18–26, 1988.

[10] A. I. Nosich and A. Y. Svezhentsev, „Physical features of wave propagation in cylindrical slot and strip lines", *Sov. J. Commun. Technol. Electron.* (Engl. Transl.), vol. 35, no. 1, pp. 51–59, 1990.

[11] A. I. Nosich and A. Y. Svezhentsev, „Accurate computation of mode characteristics for open-layered circular cylindrical microstrip and slot lines", *Microw. Opt. Technol. Lett.*, vol. 4, no. 7, pp. 274–277, 1991.

[12] A. I. Nosich and A. Y. Svezhentsev, „Principal and higher order modes of microstrip and slot lines on a cylindrical substrate", *Electromagn.*, vol. 13, no. 1, pp. 85–94, 1993.

[13] E. I. Veliev, A. I. Nosich, and V. P. Shestopalov, „On the theory of the slot mode", *Doklady Akademii Nauk Ukrainskoi SSR, Ser. A*, no. 10, pp. 928–931, 1976.

[14] E. I. Veliev, A. I. Nosich, and V. P. Shestopalov, „Propagation of electromagnetic waves in a cylindrical waveguide with a longitudinal slit", *Radio Engn. Electron. Phys.* (Engl. Transl.), vol. 22, pp. 29–35, 1977.

———————

Alexander I. Nosich,
Institute of Radiophysics and Electronics,
National Academy of Science,
Kharkov 310085, Ukraine

The possible mechanism for a frequency shift by a time-varying of medium features

Aleksander G. Nerukh, Igor V. Scherbatko, and Marian Marciniak

Abstract — The optical frequency shift of an electromagnetic wave reflecting from a boundary of a medium is studies for two cases: for temporal variations of medium permittivity, and for a moving plasma boundary. It has been shown that a simultaneous occurrence of both cases leads to an enhanced frequency shift.

Keywords — frequency shift, moving plasma boundary.

Introduction

As it's known, temporal variations of medium parameters cause alterations in the frequency and amplitude of the electromagnetic wave propagating in the medium. The wave reflection from a moving medium boundary results in the same effect. A combination of these two phenomena may produce a qualitatively new effect that consists of an enhanced frequency shift.

Frequency transformation by time altering of medium permittivity

It is well known [1-4] that a plane wave $E_0(t,r) = E_0 e^{i\omega t} e^{-i\omega s r}$, as an initial field, maintains a wave number $s = \omega/v$ with a jump changing of a medium permittivity but exhibits a transformation of a frequency and an amplitude. Wave splitting into direct and inverse waves comes about also. For example, for a dissipative dielectric, when a medium goes to a state with a permittivity ε_1 and a conductivity σ_1 at some moment of time, $\varepsilon \to \varepsilon_1, \sigma_1$, the initial field transforms to the form $E_1(t,r) = A(t)e^{-isr}$, where

$$A(t) = \frac{\varepsilon}{2\varepsilon_1} \left[\left(1 + \frac{\omega + i\frac{\overline{\sigma}_1}{2\varepsilon_1}}{\overline{\omega}_1} \right) e^{\left(-\frac{\overline{\sigma}_1}{2\varepsilon_1} + i\overline{\omega}_1 \right)t} + \right.$$
$$\left. + \left(1 - \frac{\omega + i\frac{\overline{\sigma}_1}{2\varepsilon_1}}{\overline{\omega}_1} \right) e^{\left(-\frac{\overline{\sigma}_1}{2\varepsilon_1} - i\overline{\omega}_1 \right)t} \right] \quad (1)$$

and $\overline{\omega}_1 = \sqrt{\omega_1^2 - \left(\frac{\overline{\sigma}_1}{2\varepsilon_1} \right)^2}$, $\omega_1 = \frac{v_1}{v}\omega$, $\overline{\sigma}(t) = \sigma(t)/\varepsilon_0$, $v_1 = c/\sqrt{\varepsilon_1}$, ε_0 is the electric permittivity of vacuum.

For abrupt ionisation of a medium, when a cold plasma is created and the permittivity becomes equal to $\varepsilon = = 1 - \omega_{e1}^2/\omega^2$, where a plasma frequency takes a value ω_{e1}

the transformation has an analogues form

$$A(t) = \frac{1}{2} \left[\left(1 + \frac{\omega}{\sqrt{\omega^2 + \omega_{e1}^2}} \right) e^{i\sqrt{\omega^2 + \omega_{e1}^2}t} + \right.$$
$$\left. + \left(1 - \frac{\omega}{\sqrt{\omega^2 + \omega_{e1}^2}} \right) e^{-i\sqrt{\omega^2 + \omega_{e1}^2}t} \right] . \quad (2)$$

Wave splitting is connected with time variation of a medium parameter and occurs not only with an abrupt change of parameter but with continuous changing of ones [5] as well as for an electromagnetic impulse [6].

When parameters change continuously exact solutions can be derived only in unique cases [5]. But it can be made numerically by virtue of the recursion method [7, 8] that based on the evolutionary approach [9]. The field is determined by means of the equations that for the n-th time step have the form

$$E_n(t,x) =$$
$$= F_n(t,x) - \frac{1}{2v_n} \left\{ \frac{\varepsilon_n - \varepsilon}{\varepsilon_n} \frac{\partial^2}{\partial t^2} + \frac{\overline{\sigma}_n}{\varepsilon_n} \frac{\partial}{\partial t} \right\} \times$$
$$\times \int_{t_{n-1}}^{\infty} dt' \int_{-\infty}^{\infty} e^{-\frac{\overline{\sigma}_n}{2\varepsilon_n}(t-t')} \times \theta \left(t - t' - \frac{|x - x'|}{v_n} \right) \times$$
$$\times I_0 \left(\frac{\overline{\sigma}_n}{2\varepsilon_n} \sqrt{(t-t')^2 - \frac{(x-x')^2}{v_n^2}} \right) F_n(t',x')dx', \quad (3)$$

$$F_n(t,x) =$$
$$= E_0(t,x) - \frac{1}{2v} \sum_{k=1}^{n-1} \int_{t_{k-1}}^{t_k} dt' \int_{-\infty}^{\infty} dx' \left(\overline{\sigma}_0(t') + \right.$$
$$\left. + \frac{\varepsilon(t') - \varepsilon}{\varepsilon} \frac{\partial}{\partial t} \right) \delta \left(t - t' - \frac{|x - x'|}{v} \right) E_k(t',x'). \quad (4)$$

Here, I_0 is the modified Bessel Function, δ is the Dirac function. It is convenient to calculate not electric field but an electric flux density which remains continuous with time jumps of medium parameters: $D_n(\tau,\xi) = \varepsilon_0\varepsilon_n E_n(t,x)$, $L_n(\tau,\xi) = \varepsilon_0\varepsilon F_n(t,x)$, where $\tau = tv\kappa$, $\xi = x\kappa$ are dimensionless variables, and κ is the factor with a wave number dimension.

For example, a transformation of the harmonic primary field $L_0(\tau,\xi) = \cos(\tau - \xi)$ for various time dependencies

46
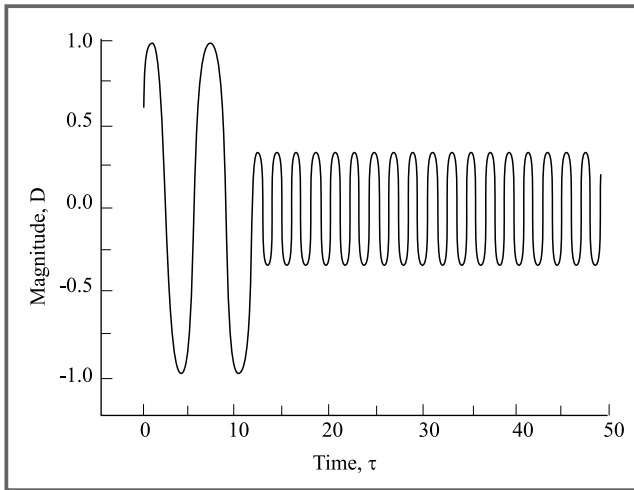
Fig. 1. The frequency shift with time jump of permittivity at $\tau_0 = 12$ when $\varepsilon_1/\varepsilon = 9$

of the permittivity is given below. The coefficients for this calculation are chosen from the data refraction index $n = n' + in''$ for semiconductor of kind InGaAsP [10] that has magnitudes $n' \approx 3.6$, $n'' \approx 0.01$. For an abrupt change
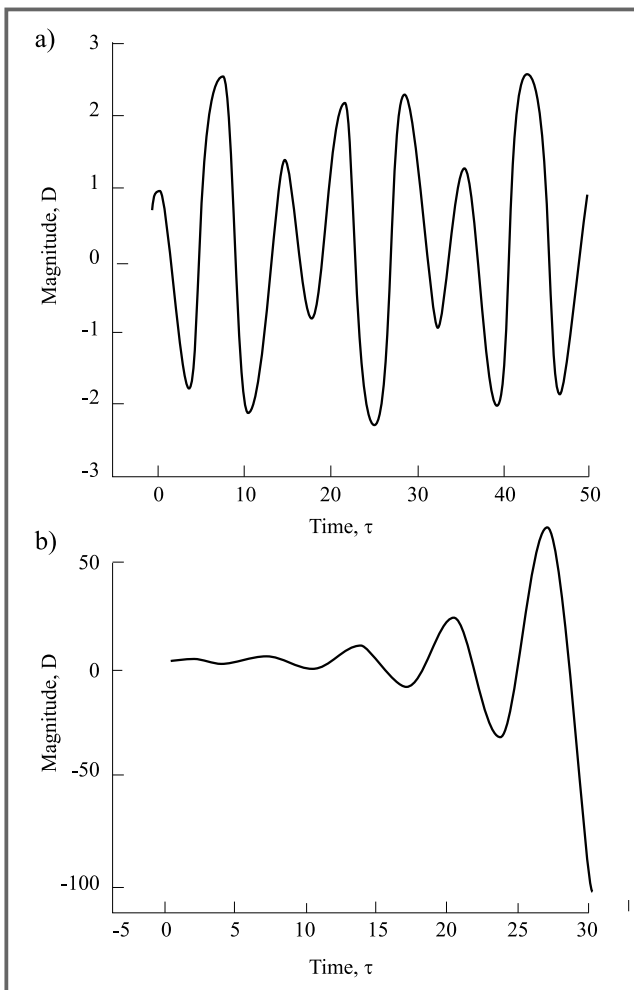
Fig. 2. The field transformation for small modulation depth of the permittivity: (a) $g = \sqrt{2}, b = 0.15$, (b) $g = 1.9, b = 0.2$

of permittivity $\varepsilon(\tau) = \frac{\varepsilon_1}{\varepsilon}\,\theta\,(\tau - \tau_0)$, the result is shown in Fig. 1.

For periodic modulation of the permittivity $\varepsilon(\tau) = [1 + b\sin(g\tau)]^{-1}$ a transformed field is shown in Fig. 2 and 3.
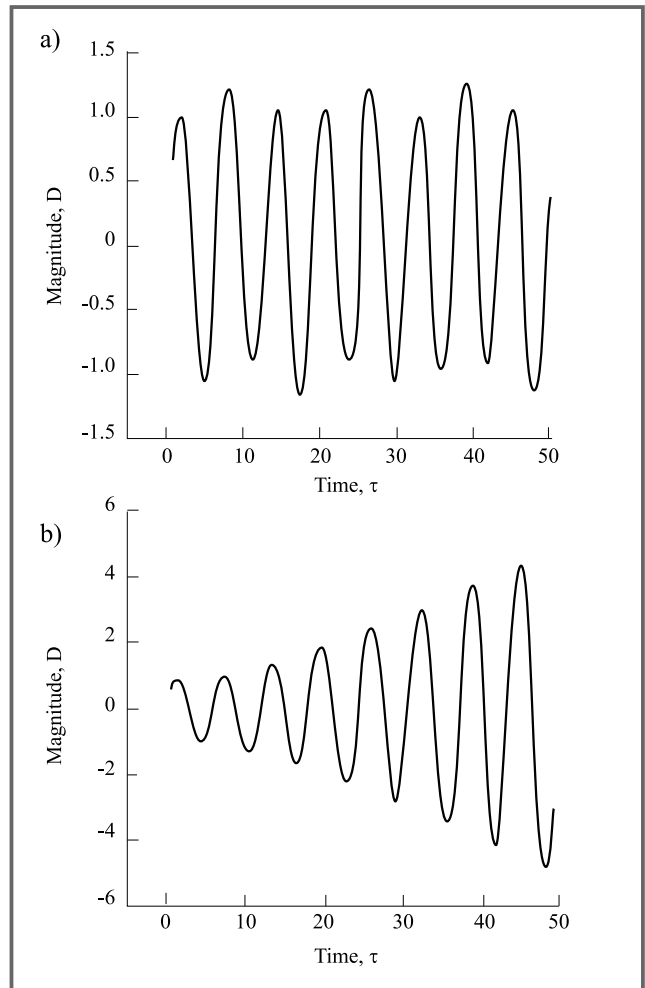
Fig. 3. The field transformation for great modulation depth of the permittivity: (a) $g = \sqrt{2}, b = 0.9$, (b) $g = 1.9, b = 0.7$

Enhanced reflection of electromagnetic wave from a plasma moving in a waveguide structure

Another way to shift a wave frequency and to amplify its amplitude is a double Doppler effect when an electromagnetic wave reflects from a moving medium boundary [11-18].

It is a common practice to characterise the efficiency of such a wave reflection by the ratio of a boundary velocity to a wave phase velocity. However, in a dispersive structure the ratio of a boundary velocity to a wave group velocity is of prime importance [19, 20]. It appears most clearly in a waveguide structure when a double dispersion mechanism is in existence.
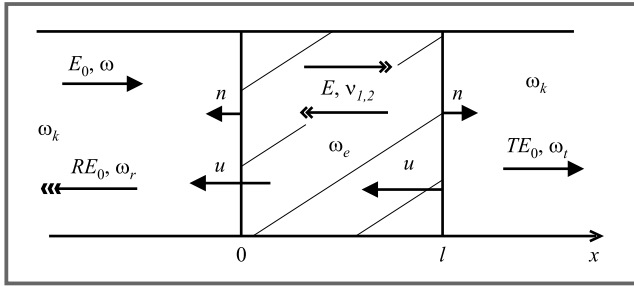
Fig. 4. A wave reflection from a plasma cluster moving in a waveguide

Simulation of such an interaction is a cluster of a homogeneous cold plasma that moves along the waveguide with velocity u (Fig. 4). Let us ω_e is the Lorentz-covariant plasma frequency, $\delta = \omega_e/\omega$ is the plasma factor, $\gamma^2 = (1-\beta^2)^{-1}$ is the relativistic factor, $\beta = u/c$.

The incident electromagnetic wave is of the TE type

$$E_0(t,x) = b_\perp E_0 \exp\left(i(\omega t - k_0 x)\right), k_0(\omega) = \frac{1}{c}\sqrt{\omega^2 - \omega_k^2}$$

is the wave number in an empty waveguide, ω_k - the waveguide frequency, $\Lambda^{-1} = \left(\sqrt{1-(\omega_k/\omega)^2}\right)^{-1}$ is a waveguide factor for the considered mode.

The frequencies and the wavenumbers of the interior waves are

$$\nu_{1,2} = \gamma^2\left(\Omega \pm \beta\sqrt{\Omega^2 - \omega_{ke}^2\gamma^{-2}}\right),$$

$$k_{1,2} = \frac{1}{c}\gamma^2\left(\pm\beta\Omega + \sqrt{\Omega^2 - \omega_{ke}^2\gamma^{-2}}\right),$$

(5)

where $\Omega = \omega - uk_0(\omega)$ and $\omega_{ke}^2 = \omega_k^2 + \omega_e^2$.

For the plasma velocity $\beta > \beta_1$, where β_1 defined by

$$\beta_1 = \left(\Lambda - \delta\sqrt{\delta^2 - \Lambda^2 + 1}\right)\left(\delta^2 + 1\right)^{-1}$$

(6)

depends strongly on waveguide and plasma factors (what is illustrated in Table 1, the interior field consists of the damped waves as the expressions under the roots are negative.

The frequency multiplication coefficient for the reflected wave is determined by the movement velocity and the waveguide factor by virtue of the formula

$$P = \omega_r/\omega = \left(1 - 2\beta\Lambda + \beta^2\right)/\left(1 - \beta^2\right),$$

(7)

and does not depend on the interior parameters of the cluster (length and plasma frequency).

Table 1
The β_1 values

Λ^{-1}	$\delta = 0.5$	$\delta = 1.0$	$\delta = 1.5$
10	0.365	0.665	0.800
2.5	-0.097	-0.472	-0.688
1.25	0.327	-0.183	-0.499
1.001	0.584	-0.090	-0.390

Reflectance and external transmittance are given by the formula

$$R = \frac{Pf2i\sin\alpha}{(1-f^2)\cos\alpha + i(1+f^2)\sin\alpha},$$

$$T = \frac{(1-f^2)\exp(i\gamma\delta\omega c^{-1}gl)}{(1-f^2)\cos\alpha + i(1+f^2)\sin\alpha},$$

(8)

where $q = \gamma\left(\Lambda - \beta\right)/\delta$, $f = \left(q - \sqrt{q^2-1}\right)^2$ and $\alpha = \gamma\delta\omega c^{-1}l\sqrt{q^2-1}$.

When the plasma cluster length tends to infinity one has a reflectance of a half-infinite plasma cluster

$$R_0 = Pf = P\left(q - \sqrt{q^2-1}\right)^2.$$

(9)

This reflectance peaks at $\beta \approx \beta_1$.

Reflectivity and transmittancy of a cluster are determined by the known equations

$$\overline{R} = S_R/S_O = RR^*\nu_{gR}/\nu_{gO}, \quad \overline{T} = S_T/S_O = TT^*,$$ (10)

where S_O, S_R, S_T are the energy fluxes of incident, reflected and passed waves, respectively.

For $\beta_1 \leq \beta$

$$\overline{R} = \frac{\overline{R}_0 sh^2\alpha^*}{4q^2\left(1-q^2\right) + sh^2\alpha^*},$$

$$\overline{T} = \frac{4q^2\left(1-q^2\right)}{4q^2\left(1-q^2\right) + sh^2\alpha^*},$$

(11)

$$\overline{R}_0 = \frac{(1+\beta^2)\Lambda - 2\beta}{\Lambda(1-2\beta\Lambda+\beta^2)}P^2.$$

(12)

For $-1 < \beta < \beta_1$

$$\overline{R} = \frac{\overline{R}_0 4\sin^2\alpha}{\left[1-\left(q-\sqrt{q^2-1}\right)^4\right]^2 + 4\left(q-\sqrt{q^2-1}\right)^4\sin^2\alpha},$$

(13)

$$\overline{T} = \frac{\left[1-\left(q-\sqrt{q^2-1}\right)^4\right]^2}{\left[1-\left(q-\sqrt{q^2-1}\right)^4\right]^2 + 4\left(q-\sqrt{q^2-1}\right)^4\sin^2\alpha},$$

$$\overline{R}_0 = \frac{(1+\beta^2)\Lambda - 2\beta}{\Lambda(1-2\beta\Lambda+\beta^2)}P^2\left(q-\sqrt{q^2-1}\right)^4.$$

(14)

The maximal reflectivity of the electromagnetic wave in the waveguide can take very great magnitudes and is observed not for relativistic values of the cluster velocity but for smaller values as it is noticed in Table 2. The value of this plasma cluster velocity depends on the parameters of the plasma and the waveguide and can be done very small. A strong influence of the waveguide is explained by the fact that the group velocity of the incident wave tends to zero when $\Lambda^{-1} \to \infty$ but the group velocity of the reflected wave $\nu_{gR} = c\left(2\beta - (1+\beta^2)\Lambda\right)\left(1-2\beta\Lambda+\beta^2\right)^{-1}$ does not tend to zero.

Table 2
The reflectivity of the half-infinite cluster

Freq. multipl. coeff. P	The relativistic factor γ	The waveguide factor Λ^{-1}	The plasma factor δ	Reflectiv. of the half-inf. clust. $\overline{R}_0$
2	1.05	1.25	1.25	4.5
2	1.12	2.5	1.1	7.2
2	1.21	20	0.073	70.0
10	1.84	1.25	3.0	125.0
10	1.96	2.5	2.55	225.0
10	2.3	20	2.18	2000.0

The shift of the reflectivity maximum to smaller values of the cluster velocity owes to the existence of a double dispersion mechanism, a plasma dispersion and a waveguide dispersion.

Combination of two mechanisms for a frequency shift

Combination of an effect of electromagnetic wave frequency changing caused by time variation of permittivity and a similar one caused by reflection from a moving boundary gives a new effect. It is shown at an example of a flat dielectric slab whose boundaries move beginning from zero moment of time and meet through any time interval (Fig. 5).
The equation for electromagnetic field inside the slab as well as outside one is analogues to Eq. (5)

$$
E = E_0 - \frac{1}{2\varepsilon v} \times
$$
$$
\times \frac{\partial^2}{\partial t^2} \int_{-\infty}^{\infty} dt' \int_{-\infty}^{\infty} dx' \left[\varepsilon_1 - \varepsilon + (\varepsilon_2 - \varepsilon_1)\theta(t') \right] \times \quad (15)
$$
$$
\times \chi \theta \left(t - t' - \frac{|x - x'|}{v} \right) E .
$$

Here, ε is the permittivity outside a slab; ε_1 and ε_2 are the permittivity inside a slab before zero time moment and after it, respectively; $\chi(t,x)$ - characteristic function that equals to one inside a slab and zero outside of it; $\theta(t)$ - the Heaviside unit function.
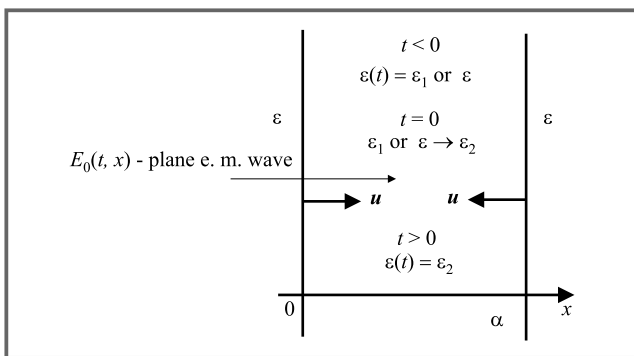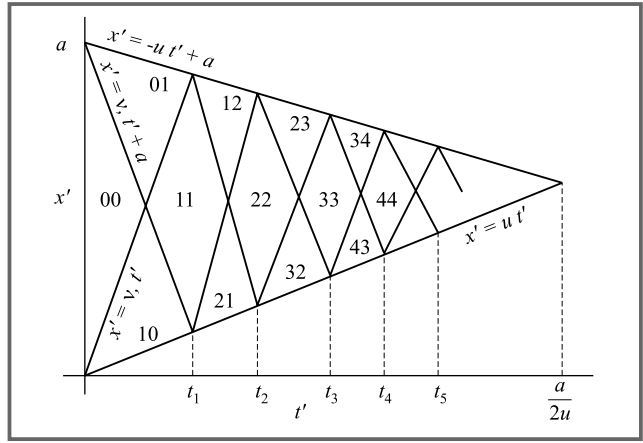
Fig. 5. The geometry of the problem

Fig. 6. Formation of time-spatial zones a slab that is collapsing

Collapsing slab is created after zero moment of time when slab boundaries begin to move with a velocity u and meet at a moment $t_c = a/2u$. The electromagnetic field has qualitatively dissimilar forms in the different zones on the time-spatial diagram, Fig. 6.

A distance between zones decreases by the law (for the case $u < v_2$)

$$
t_n - t_{n-1} = p^{1-n} \frac{a}{v_2 + u} , \quad (16)
$$

so that infinitely many zones are packing up in a finite interval. Here, $p = \frac{v_2 + u}{v_2 - u}$.

If $u > v_2$ the slab boundaries do not influence on a field. The field in the 00 zone consists of two splitting waves [21]

$$
E = C_1 e^{i\omega_2(t - x/v_2)} + C_2 e^{-i\omega_2(t + x/v_2)},
$$
$$
C_{1,2} = \frac{v_2}{v} \frac{v_2 \pm v}{2v}, \quad \omega_2 = \omega \frac{v_2}{v} . \quad (17)
$$

The field in the *mm* zone has more complicated structure

$$
E_{mm} = \frac{\omega^{(+)}}{\omega} C_0 \left\{ e^{i\omega^{(+)}(t - x/v_2)} + \sum_{k=1}^{m-1} R_1^k \exp \left[i\omega^{(+)} \times \right. \right.
$$
$$
\left. \times p^k \left(t - (-1)^k x/v_2 \right) - i \frac{1 - p^{\frac{k+i_k}{2}}}{1 - p^2} q \frac{\omega^{(+)}}{v_2} a \right] \right\} +
$$
$$
+ R_1^m C_1 \exp \left[i\omega_2 p^m \left(t - (-1)^m x/v_2 \right) + \right.
$$
$$
\left. - i \frac{1 - p^{\frac{m+i_m}{2}}}{1 - p^2} q \frac{\omega_2}{v_2} a \right] + R_1^m C_2 \exp \left[-i\omega_2 p^m \left(t + \right. \right.
$$
$$
\left. + (-1)^m x/v_2 \right) + i \frac{1 - p^{\frac{m+i_m}{2}}}{1 - p^2} pq \frac{\omega_2}{v_2} a \right] +
$$
$$
+ R^m C_1 e^{i\omega_2(t - (-1)^m x/v_2)} \Phi^{\frac{m+i_m}{2} \frac{v_2}{v}} +
$$
$$
+ R^m C_2 e^{-i\omega_2(t + (-1)^m x/v_2)} \Phi^{-\frac{m-i_m}{2} \frac{v_2}{v}} , \quad (18)
$$

49

where

$$C_0 = \frac{2v_2}{v + v_2}, \quad q = \frac{2v_2}{v_2 - u},$$

$$\omega^{(\pm)} = \omega \frac{v_2}{v} \frac{v - u}{v_2 \pm (-1)u}, \quad R_1 = pR, \quad R = \frac{v - v_2}{v + v_2},$$

$$\Phi = e^{-i\omega \frac{2a}{v_2}}, \quad i_m = \frac{1}{2}\left(1 - (-1)^m\right). \tag{19}$$

Inside the slab there are two waves caused by splitting waves C_1 and C_2 owing to a permittivity jump, but frequencies of these waves rise with a zone number. The set of the waves that are proportional to C_0 and raised by a field that incidences upon a slab after zero moment of time has a descrete frequency spectrum. Frequencies of all waves grows up with a zone number and with time consequently. A frequency multiplication coefficient equals $p = \frac{v_2 + u}{v_2 - u}$ and grows with $u \to v_2$.

Behavior of the secondary waves amplitudes is determined by a relation between wave phase velocity and a boundary velocity. If $R_1 > 0$, that is $vu - v_2^2 > 0$, the amplitudes grow infinitely during a finite time interval. The region with such a relation between velocities is shown in Fig. 7 as a single crosshatched region.
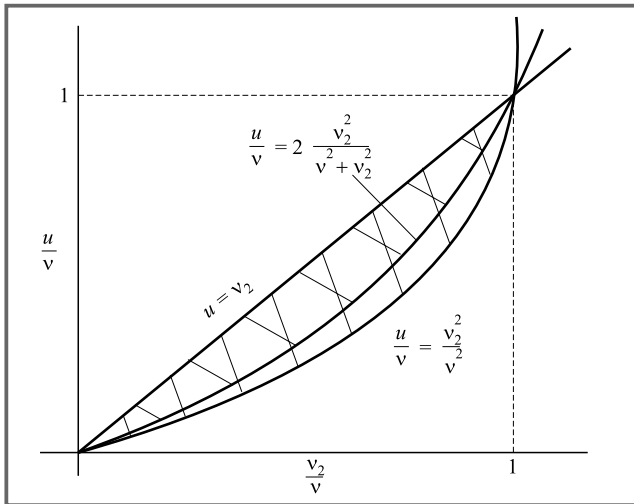
Fig. 7. Regions where amplitudes grow and field energy accumulates

The energy balance for waves raised by the waves C_1 and C_2 in the slab in the time interval $[t_{m-1}, t_m]$ is determined by

$$\frac{dW}{dt} = \varepsilon_2 \left(v_2 - u\right) \left(R_1^2 - p\right) R_1^{2(m-1)} \times \tag{20}$$

$$\times \left\{ C_1^2 \cos^2\left(\omega_m t - \phi_1\right) + C_2^2 \cos^2\left(\omega_m t - \phi_2\right) \right\},$$

where $\omega_m = p^{m-1} \frac{v_2 + u}{v} \omega$.

When a movement is absent $u = 0$ then $dW/dt < 0$. The waves with the frequency ω_2 are shone out.

When boundaries move and $R_1^2 - p > 0$ or

$$\frac{u}{v} > \frac{2v_2^2}{v^2 + v_2^2} \tag{21}$$

then $dW/dt > 0$.

A region where a field energy accumulates is shown in Fig. 7 as a double crosshatched region.

Outside the slab the field represents a sequence of waves packages that are devided by fronts $x_m = vt_m$. The field in such a package within planes vt_{m+1} and vt_m has the form

$$E_m = \frac{2v^2}{v_2(v + v_2)} \frac{v_2 + u}{v + u} C_1^{i_m} C_2^{1-i_m} \times \tag{22}$$

$$\times R_1^m e^{-i\omega p^m \frac{v_2 + u}{v + u}(t + x/v) + (-1)^m i\omega \eta_m \frac{a}{v}},$$

where $\eta_m = -\frac{v_2 - u}{2u} p^{1-i_m} \left(1 - p^{m + i_m}\right)$. This wave frequency rises by a factor p^m. A field energy within the package is proportional to

$$W_{ex} \approx \left[\left(\frac{v - v_2}{v + v_2}\right)^2 p \right]^m. \tag{23}$$

If $\frac{u}{v} > \frac{2v_2^2}{v^2 + v_2^2}$ a field energy within the package outside the slab grows infinitely when $m \to \infty$, that corresponds to approaching to a collapse moment.

References

[1] F. R. Morgenthaler, „Velocity modulation of electromagnetic waves", *IRE Trans. Microw. Theory Technol.*, vol. MTT-6, no. 4, pp. 167–172, 1958.

[2] L. B. Felsen and G. M. Whitman, „Wave propagation in time-varying media", *IEEE Trans. Anten. Propag.*, vol. AP-18, no. 2, pp. 242–253, 1970.

[3] R. L. Fante, „Transmission of electromagnetic waves into time-varying media", *IEEE Trans. Anten. Propag.*, vol. AP-19, no. 3, pp. 417–424, 1971.

[4] L. A. Ostrovsky and N. S. Stepanov, „Nonresonant parametric phenomena in distributed system", *Radiophys. Quant. Electron.* (Eng. transl.), vol. 14, no. 4, pp. 489–529 (in Russian pagination), 1971.

[5] S. I. Averkov and V. P. Boldin, „Waves in nondispersive nonstationary inhomogeneous media", *Radiophys. Quant. Electron.* (Eng. transl.), vol. 23, no. 9, pp. 1060–1066 (in Russian pagination), 1980.

[6] A. G. Nerukh and I. Yu. Shavorikina, „Splitting of electromagnetic impulse under a conductivity jump of restricted medium", *J. Technich. Fis.*, vol. 62, no. 5, pp. 108–118 (in Russian), 1992.

[7] A. G. Nerukh, I. V. Scherbatko, and D. A. Nerukh, „Using the evolutionary recursion for solving electromagnetic problem with time-varying parameter", *Microw. Opt. Technol. Lett.*, vol. 14, no. 1, pp. 31–36, 1997.

[8] A. G. Nerukh, I. V. Scherbatko, and O. N. Rybin, „The direct numerical calculation of an integral Volterra equation for an electromagnetic signal in time-varying dissipative medium", *J. Electromagn. Wav. Appl.*, vol. 12, pp. 163–176, 1998.

[9] A. G. Nerukh and N. A. Khizhnjak, *Modern problems of transient macroscopic electrodynamics*. Kharkov: Test-radio Publ., 1991.

[10] T. D.Visser, H. Block, and D. Lenstra, „Modal analysis of a planar waveguide with gain and losses", *IEEE J. Quant. Electron.*, vol. 31, no. 10, pp. 1803–1810, 1995.

[11] K. Landecker, „Possibility of frequency multiplication and wave amplification by means of some relativistic effects", *Phys. Rev.*, vol. 86, no. 6, pp. 852–855, 1952.

[12] M. A. Lampert, „Reflection of electromagnetic waves by Cerenkov electron gas", *Phys. Rev.*, vol. 102, no. 2, pp. 299-304, 1956.

[13] J. B. Fainberg and V. S. Tkalich, „Electromagnetic wave reflection from a plasma moving through dielectric medium in a constant magnetic field", *Sov. Phys.-Tech. Phys.* (Eng. transl.), vol. 4, no. 4, 1959.

[14] O. G. Zagorodnov, J. B. Fainberg, A. M. Egorov, and B. M. Bolotovsky, „Frequency multiplication by means of a plasma «collapse»”, *Sov. Phys.-Tech. Phys.* (Eng. transl.), vol. 6, no. 3, 1961.

[15] V. I. Kurilko and V. I. Miroshnichenko, „Electromagnetic wave reflection by a moving plasma”, *Sov. Phys.-Tech. Phys.* (Eng. transl.), vol. 7, no. 7, 1962.

[16] C. Yeh, „Reflection and transmission of electromagnetic by waves by a moving plasma medium”, *J. Appl. Phys.*, vol. 37, no. 8, pp. 3079–3084, 1966.

[17] S. N. Stoljarov, *Selected papers by A. Einstein.* Moscow: 1975–1976; „*Nauka*”, pp. 152–215 (in Russian), 1978.

[18] W. B. Mori, „Generation of tunable radiation using an underdense ionization front”, *Phys. Rev. A.*, vol. 44, no. 8, 1991.

[19] A. G. Nerukh and N. A. Khizhnjak, „Energy relations for the interaction of an electromagnetic wave with a plasma cluster moving in a waveguide”, *Radiophys. Quant. Electron.* (Eng. transl.), vol. 26, no. 12, 1983.

[20] A. G. Nerukh, N. A. Khizhnjak, and P. E. Minko, „Electromagnetic wave reflection from stratified plasma cluster moving in a waveguide”, *Radiophys. Quant. Electron.* (Eng. transl.), vol. 33, no. 5, 1990.

[21] A. G. Nerukh, „Electromagnetic waves in the dielectric layer with time-dependent parameters”, *Zhurn. Tekhnich. Fiz.*, vol. 57, no. 11, pp. 2078–2087, 1987.

Aleksander G. Nerukh, Igor V. Scherbatko
Techn. Univ. of Radio Electronics,
Lenin Av. 14, 310726, Kharkov, Ukraine,

Marian Marciniak
Technical University of Kielce
Al. 1000-lecia P.P. 7, 25-314 Kielce, Poland;
National Institute of Telecommunications,
1 Szachowa Str., 04-894 Warsaw, Poland,
e-mail: M.Marciniak@itl.waw.pl

Power penalty caused by Stimulated Raman Scattering in WDM Systems

Sławomir Pietrzyk, Waldemar Szczęsny, and Marian Marciniak

Abstract — In this paper we present results of an investigation into the power penalty introduced by Stimulated Raman Scattering (SRS) in WDM systems with concentration on application of dispersion-shifted single-mode optical fibres (G.653) and unequal channel allocation schemes. System parameters based on ITU-T Recommendation G.692 and analytic formulas were used in calculations. It is shown that SRS does present a practical limitation to the multichannel systems. We also indicate limitations of the G.692 Recommendation and we point at directions of study in the area of nonlinear phenomena and multichannel systems.

Keywords — optical communications, WDM systems, Stimulated Raman Scattering.

Introduction to WDM systems

Recent years have shown a rapid growth of demand for capacity of telecommunication networks. It has inspired many laboratories to explore new techniques of more efficient utilization of the huge bandwidth offered by optical fibre links. One of the most promising and cost effective ways to increase optical link throughput is a technique known as Wavelength Division Multiplexing (WDM).

In a WDM system we transmit many information channels through one fibre using different optical wavelengths modulated by independent data streams. This method is analogous to Frequency Division Multiplexing (FDM) which is widely exploited in other communication systems, especially in radio broadcasting. Using WDM we can easily increase the capacity of already existing fibre links that is particularly significant in the areas where placing new cables is impossible or too expensive. WDM is a technique compatible with the idea of all-optical networks, where we can create the transparent optical paths connecting successive network nodes by switching optical channels organised at the different light wavelengths. One can also envision the application of WDM in broadcast networks and/or in subscriber loop [2].

These and other advantages of WDM have prompted the beginning of standardization work [8]. Nevertheless the job is not yet completed and further research and estimations are required [10].

Nonlinear limitations

In spite of its merits the WDM technique is not free from limitations. The most characteristic and essential problem for multichannel optical systems, beside attenuation and dispersion, is interchannel crosstalk [1]. One can distinguish crosstalk caused by nonlinear interactions between the light and the fibre material, such as: Stimulated Raman Scattering (SRS), Stimulated Brillouin Scattering (SBS), Cross-Phase Modulation (XPM) and Four-Wave Mixing (FWM). This paper is devoted to the influence of SRS on WDM transmission.

Stimulated Raman Scattering is an interaction between the light and molecular vibrations of SiO_2. It results itself as a frequency conversion of the light wave that is put into the fibre. Two new spectral lines appear around the main one. The lower frequency wave is called the Stokes wave and is usually much stronger than the higher frequency wave called the anti-Stokes wave. This causes power depletion of the light injected into the fibre. Generally, this is not a problem for single channel systems, because of relatively high power threshold at which the degradation introduced by SRS is noticeable. But if we inject two optical waves separated by the Stokes frequency into the fibre where Raman interactions take place, the power of the lower frequency wave (called the probe) will increase at the expense of the higher frequency wave (called the pump). Such an energy transfer from one channel to another is called interchannel crosstalk. It is important to underline that SRS appears when the light is present in both channels, i.e. "1" bits are transmitted simultaneously. The Stokes frequency is also called a bandwidth of the Raman gain. In more complex case of higher number of channels, the lower frequency channels are amplified at the expense of the higher frequency channels if only the frequency difference between them lies in the bandwidth of the Raman gain. This phenomenon requires much lower optical power levels than in the case of single channel systems.

Power penalty calculus

In multichannel systems, the channel that is most severely affected by SRS is the highest frequency channel (called the 0-th channel). The power loss that is present at the 0-th channel may be calculated as the sum of power fractions transmitted from this channel to each of the other channels located at lower frequencies. The total fractional power lost by the 0-th channel is given by [1, 3]

$$D = \sum_{i=1}^{N-1} \frac{f_0 P_i g_i L_{eff}}{f_i A_{eff}}, \qquad (1)$$

where: i – channel index, f_0 – frequency of the 0-th channel, f_i – frequency of the i-th channel, N – number of channels, P_i – power injected in the i-th channel, L_{eff} – effective fibre length, A_{eff} – effective core area, g_i – Raman gain coefficient coupling the i-th channel with the 0-th channel.

Effective fibre length L_{eff} can be expressed by

$$L_{eff} = \frac{1 - e^{-\alpha L}}{\alpha} \, , \qquad (2)$$

where α denotes the fibre loss coefficient and L is the actual fibre length.

Raman gain coefficient g_i depends on the frequency difference between the channels that exchange power. Assuming a triangular approximation of the Raman gain profile in silica fibres [3] and full polarization scrambling occurring inside the fibre, we obtain

$$g_i = \frac{G \Delta f_i}{2 \Delta F} \, , \qquad (3)$$

where G is the peak Raman gain coefficient, ΔF is the Raman gain bandwidth, $\Delta f_i = f_0 - f_i$.

The fraction of the power that remains at the 0-th channel (expressed in dB) is:

$$P\_rem1 = -10 \lg(1 - D) \, . \qquad (4)$$

Applying the analysis proposed by [10] we obtain the following equation determining the fraction of the power that remains at the 0-th channel (expressed in dB):

$$P\_rem2 = -10 \lg \left[1 - \sum_{i=1}^{N-1} \left(1 - \exp \left(\frac{P_i f_0 L_{eff} g_i}{f_i A_{eff}} \right) \right) \right] . \qquad (5)$$

Results of theoretical approach

Using the above relations we calculated power penalties introduced by SRS in point to point unidirectional WDM system without in-line amplifiers, employing unequal channel spacing [8] and the dispersion-shifted single-mode optical fibre [6].

The transmission on G.653 fibres is strongly limited by Four-Wave Mixing (FWM) if channels are equispaced. One way to avoid crosstalk introduced by FWM is to apply unequal channel allocation scheme. According to [8] all the channels should be placed on a frequency grid anchored at the reference frequency of 193.1 THz (λ = 1552.52 nm) with interchannel spacings equal to integer multiplies of 100 GHz. The set of the integers is determined by choosing channel allocation scheme. In our work we considered 8-channel system with the following unequal channel allocation plans: A - {1, 3, 5, 6, 7, 10, 2} times 100 GHz, counting from the highest frequency channel (the 0-th channel is assumed to be at 196.1 THz); B - {2, 4, 10, 3, 8, 7, 5} times 100 GHz; C - 3, 7, 12, 2, 6, 5, 4 times 100 GHz;

D - {6, 7, 8, 9, 10, 12, 11} times 100 GHz. These values are suggested by [8]. We also calculated power depletion for the similar system but with equal channel separation (100 GHz), referring to it as the scheme E. Table 1 shows channel frequencies for each of the above allocation schemes.

In our calculations we also assumed the following system parameters:

- fibre loss coefficient for the G.653 fibre: $\alpha = 0.2$ dB/km,

- mode field diameter for the G.653 fibre: MFD = 7 μm; this gives the effective core area [5]: $A_{eff} = 36.33$ μm^2,

- fibre span length: L = 120 km,

- frequency of the 0-th channel: $f_0 = 196.1$ THz,

- Raman gain bandwidth $\Delta F = 15$ THz,

- peak Raman gain coefficient G = $7 \cdot 10^{-14}$ m/W,

- range of power injected in each of the channels: $1 \div 17$ mW.

The analysis concerns the 'worst case', i.e. the case of the 0-th channel and the simultaneous presence of "1" bits in all the channels. Power in the other channels (different than the 0-th one) is assumed not to be affected by the nonlinearities. Beside SRS, influence from other nonlinear phenomena as well as from the dispersion is neglected. The results of calculations are presented in Fig. 1.
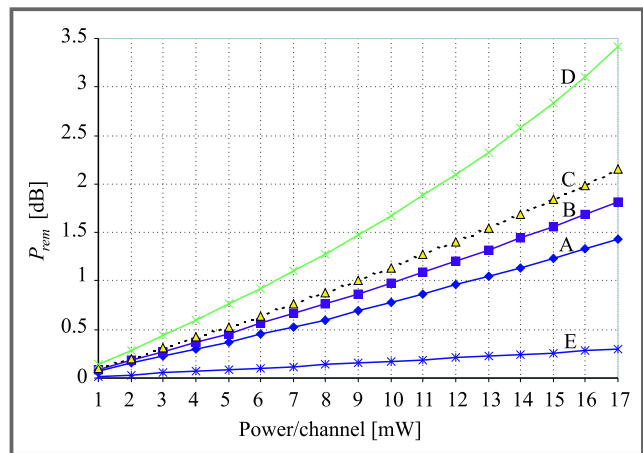
Fig. 1. Worst case power penalty introduced by SRS
The fraction of the power P_rem1 as a function of the power levels injected in each of the channels for various channel allocation schemes (A, B, C, D, E) calculated using formula (4).

Using formula (5) we got the curves very similar to the above ones. The biggest difference between the results obtained by (4) and (5) was 0.3 dB.

In [8] the Class 3A laser limit (17 dBm @ 1550 nm) is suggested as the maximum total optical power. Let us assume

Sławomir Pietrzyk, Waldemar Szczęsny, and Marian Marciniak

Table 1
Channel frequency choices (in THz) for 8-channel system working on G.653 fibre and different channel allocation schemes (A, B, C, D, E)

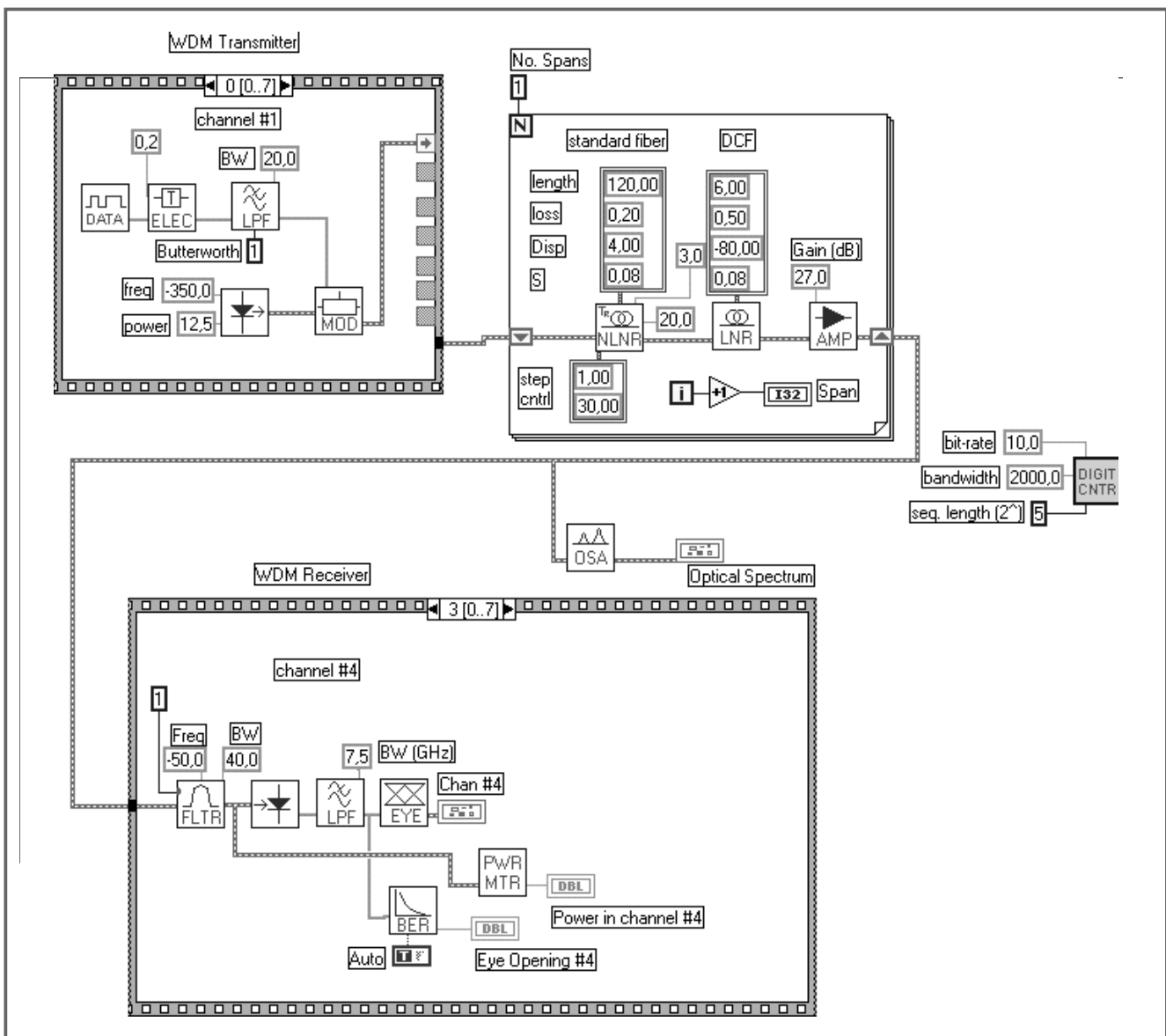| Scheme	Channel index							
	0	1	2	3	4	5	6	7
A	196.1	196.0	195.7	195.2	194.6	193.9	192.9	192.7
B	196.1	195.9	195.5	194.5	194.2	193.4	192.7	192.2
C	196.1	195.8	195.1	193.9	193.7	193.1	192.6	192.2
D	196.1	195.5	194.8	194.0	193.1	192.1	190.9	189.8
E	196.1	196.0	195.9	195.8	195.7	195.6	195.5	195,4

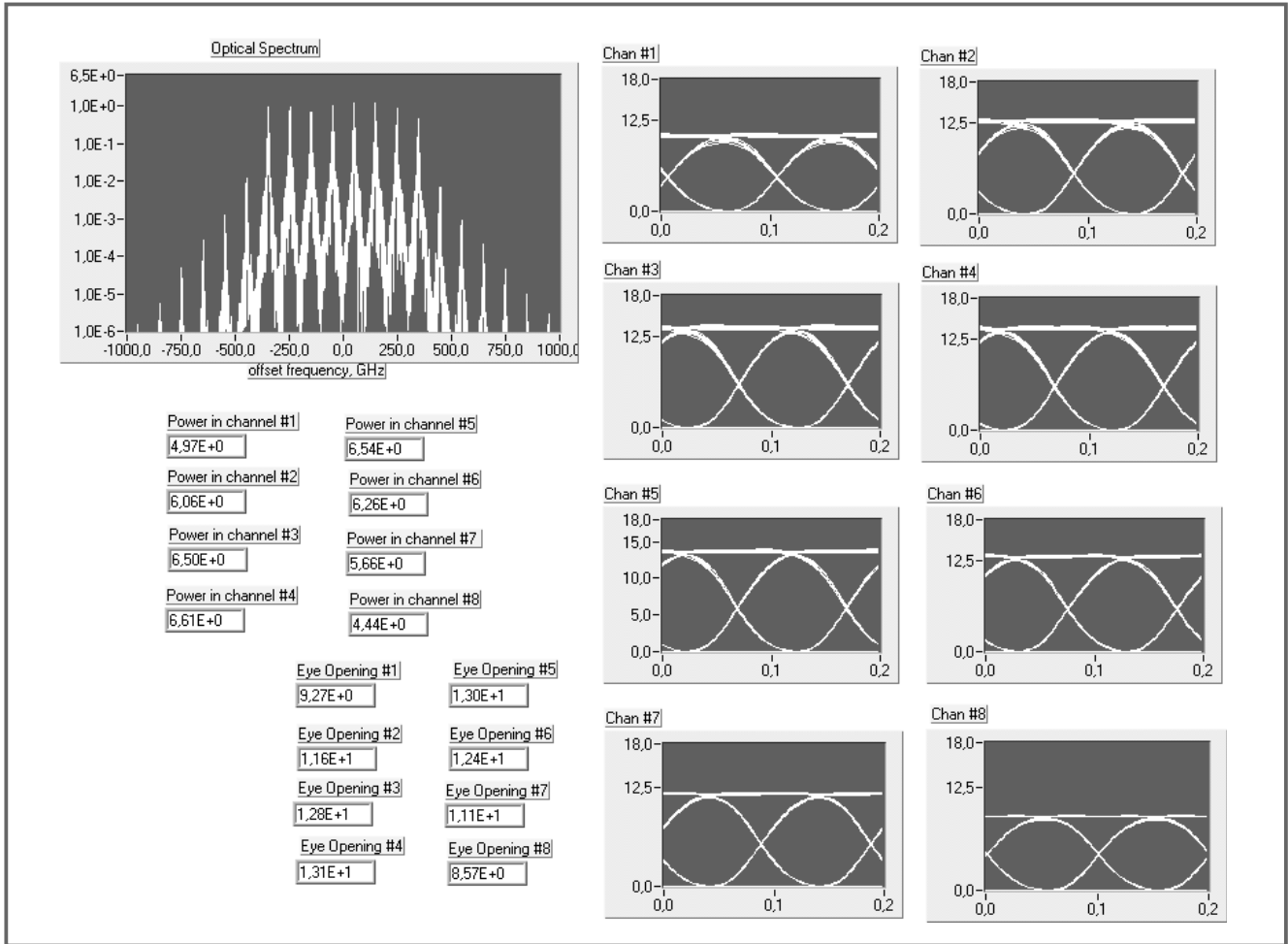**Fig. 2.** Simulation model of the 8-channel WDM system

Fig. 3. Simulation of Raman scattering in a nonlinear fibre transmission of identical binary data streams in all WDM channels - referred as *Case 1*

the scheme A of frequency plan for simplification. An important issue is whether we should use peak or average per channel power [4]. If we consider the average power of the channels in our calculations then for 17 dBm limit the per channel power will be equal to 6.25 mW (for 8-channel system, scheme A) and we will obtain power penalty at 0.47 dB. This corresponds to 90% of the power that remains at the 0-th channel. But if instead of the average per channel power we use the peak per channel power, what is recommended in [10] for G.653 fibres, then for 17 dBm limit we will obtain power penalty at 1 dB. This gives 79% of the power that remains at the highest frequency channel. It is for this reason that the line coding is binary non-return to zero (NRZ) [7], scrambled according to [9] and the probabilities of 1 and 0 bits are equal. Hence the peak per channel power is double the average per channel power (12.5 mW). As seen in Fig. 1, much worse situation occurs for other channel allocation schemes. For example, for scheme D the power penalty is 2.22 dB at 12.5 mW of input peak per channel power and it corresponds to only 60% of the power remaining at the 0-th channel.

Simulation of the WDM system

In order to evaluate the exactness of the theoretical approach we have done extensive computer simulations of the 8 STM-64 channel WDM transmission system reported in the previous section. The highest value of total-mean optical power level of 17 dBm has been investigated. A GOLD^{TM} simulation software has been applied. The architecture of the analysed WDM system is shown in Fig. 2. A 100 GHz frequency grid has been chosen for eight DFB laser sources. The lasers are externally modulated with 10 GHz pseudo-random data sequences. Since the theoretical approach does not include fibre dispersion effects, a 6-km long dispersion compensating fibre is added at the end of the link in order to eliminate totally the pulse dispersion in the link. Propagation of the field in the X-polarization state in a nonlinear fibre is modelled using the following nonlinear partial differential equation [11]:

$$\frac{\partial A_x}{\partial z} - \frac{i}{2}\beta_2\frac{\partial^2 A_x}{\partial T^2} - \frac{1}{6}\beta_3\frac{\partial^2 A_x}{\partial T^2} + \frac{\alpha}{2}A_x =$$
$$-i\gamma\left[|A_x|^2 A_x - T_R A_x\frac{\partial^2 |A_x|^2}{\partial T^2}\right], \tag{6}$$
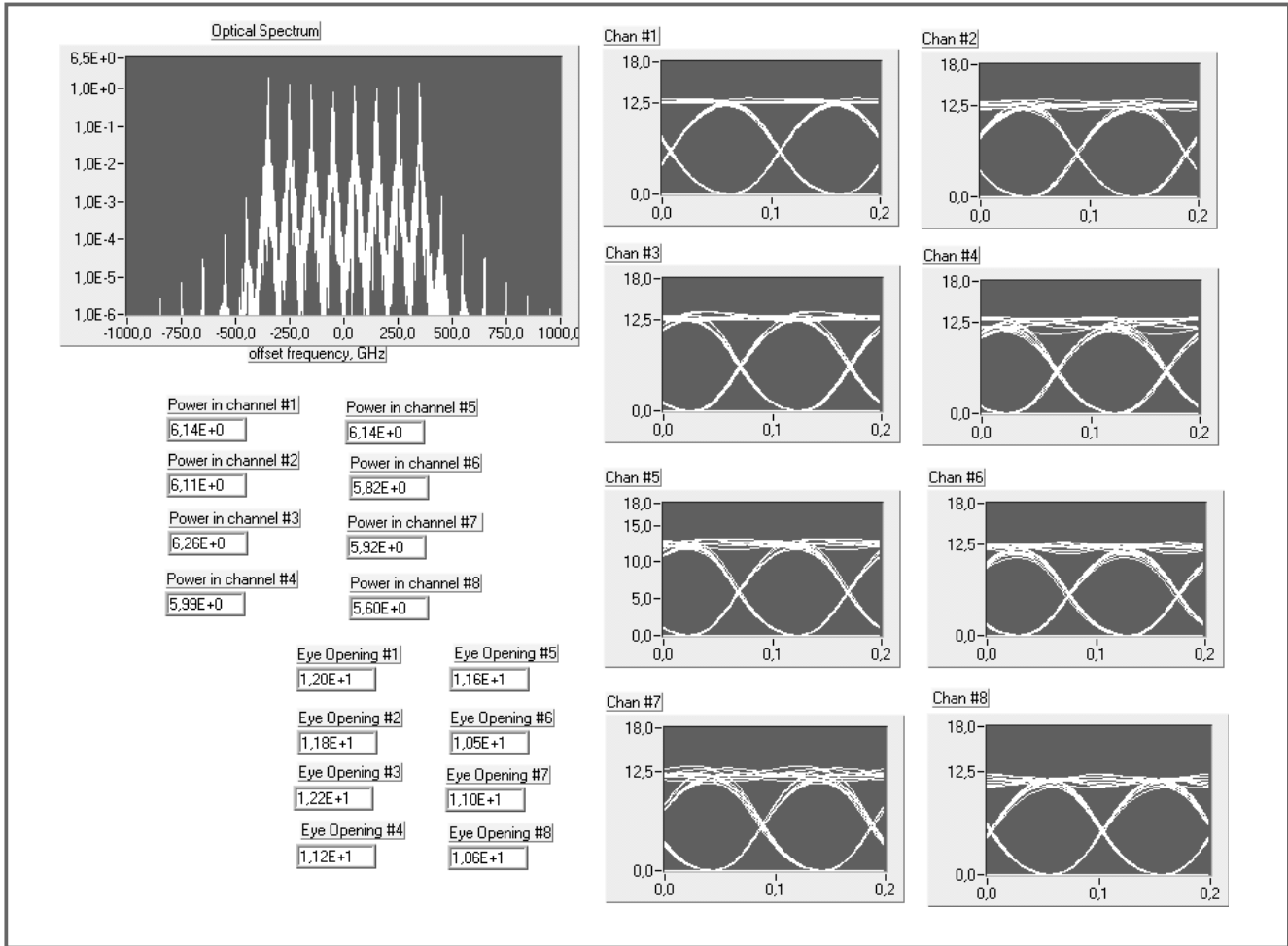
Fig. 4. Simulation of Raman scattering in a nonlinear fibre transmission of non-correlated data streams in different WDM channels referred as *Case 2*

where $A_x(z, T)$ is the slowly varying field envelope and β_2, β_3, α and γ are related to the dispersion, dispersion slope, loss and nonlinearity of the fibre. Equation (6) is solved using the split step Fourier method [11]. The algorithm uses an adaptive step-size [14].

The nonlinear coefficient γ for the fibre is defined as [11]:
$\gamma = \frac{n_2 \omega}{c A_{eff}}$.

Here, n_2 is the Kerr nonlinear index coefficient, ω is the angular optical frequency, A_{eff} is the effective core area, and c is vacuum speed of the light. The coefficient γ accounts for the effects of SPM [12], XPM [13] and FWM [14].

The parameter T_R is related to the slope of the Raman gain and is assumed to vary linearly with frequency in the vicinity of the carrier frequency [11]. The parameter T_R is estimated to be ~ 5 fs [11]. Raman gain is polarization dependent, and consequently the value of T_R has to be halved from its value for identical states of polarization if one wants to account for the effective SRS effect between WDM channels that will have their states of polarization randomly scrambled at long distances.

In order to verify the accuracy of theoretical calculations,

simulations for three different cases have been carried out: *Case 1*: Raman scattering in a nonlinear fibre transmission of identical binary data streams in all WDM channels (worst case), *Case 2*: Raman scattering in a nonlinear fibre transmission of non-correlated data streams in different WDM channels, *Case 3*: the same as in *Case 2* but with absence of SRS.

A comparison of plots in Fig. 3 for *Case 1* (correlated data with Raman scattering) and in Fig. 5 for *Case 3* (non-correlated data without Raman scattering) reveals that additional loss increase resulting from SRS is c.a. 1.2 dB (from 5.84 mW in Fig. 5 to 4.44 mW in Fig. 3) for the highest frequency channel (here marked as the 8-th channel).

A comparison of plots for non-correlated data in Fig. 4 for *Case 2* (with Raman scattering) and in Fig. 5 for *Case 3* (without Raman scattering) gives a small influence of Raman scattering in the absence of data correlation in the channels. The SRS in *Case 2* gives only a small increase of eye closure and decrease of power in the highest frequency channel (from 5.84 mW in Fig. 5 to 5.60 mW in Fig. 4).

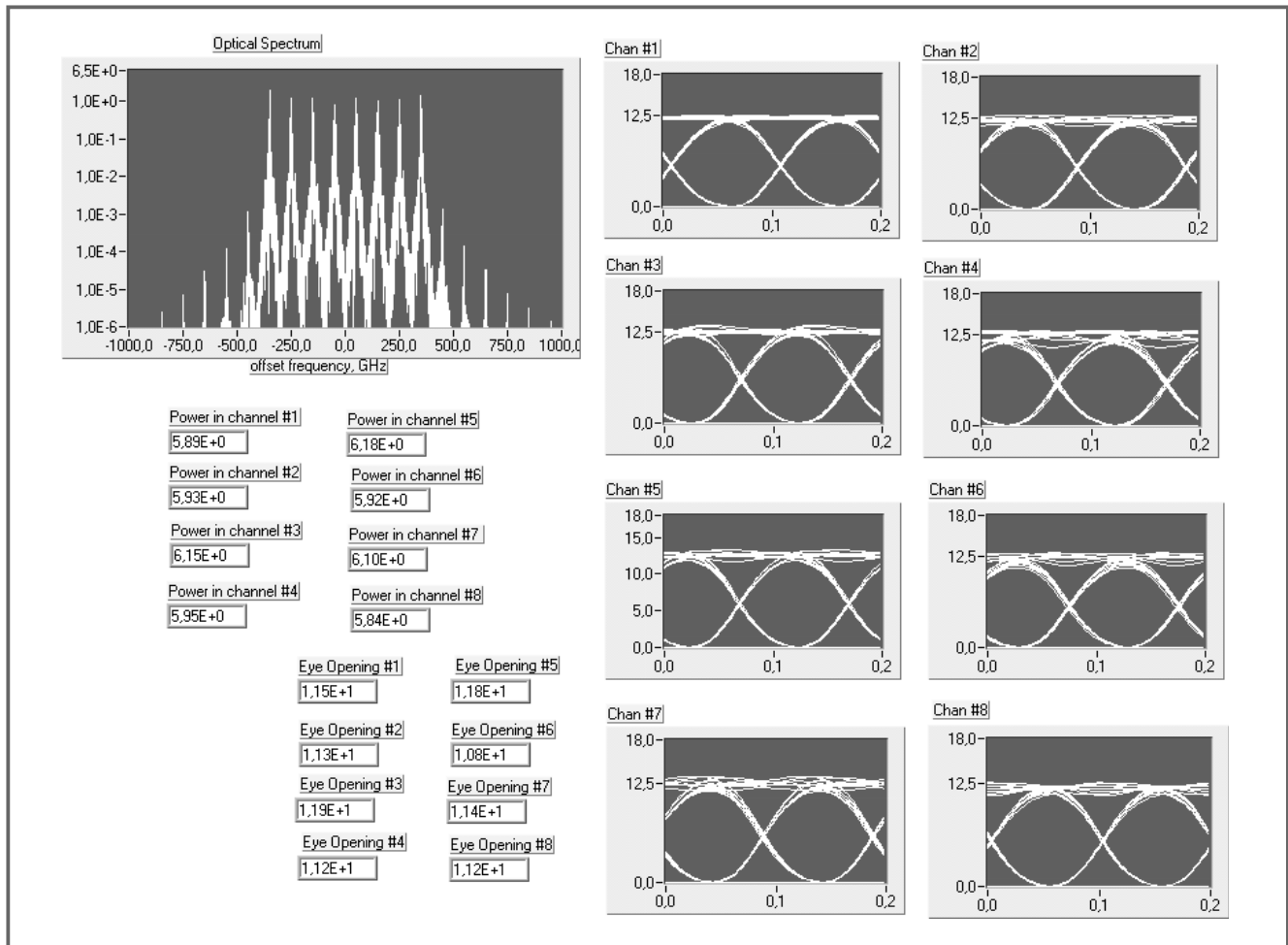Therefore, we conclude that the theoretical approach is valuable for real multichannel optical systems.

Fig. 5. Simulation of Raman scattering in a nonlinear fibre transmission of non-correlated data streams in different WDM channels without Raman scattering – referred as *Case 3*

Conclusions

Our results indicate that the proper choice of channel allocation plan is significant for WDM transmission with application of G.653 fibres. Contrary to what is stated in [8], SRS does present a practical limitation to the multichannel systems.

Moreover, some of the schemes proposed in [8] are contradictory with what can be found in other parts of [8], for example: (1) once 100 GHz is recommended as a minimal frequency spacing (as it is in scheme A) then it is stated that 200 GHz is more suitable because of the EDFA gain dip, (2) in the case of some schemes (like scheme D), the total occupied bandwidth falls out of the EDFA bandwidth, (3) there is no indication in [8] where the channel allocation plan must begin (i.e. the 0-th channel frequency is not determined).

The problems with SRS can be overcome either by employing other channel allocation plans or by reducing the power level injected into the fibre and at the same time lowering the receiver threshold. There are also other important issues that require further study: (1) the impact from SRS on repeated systems with in-line amplifiers [10] which is expected to be more severe than for unrepeated systems, (2) the influence from dispersion that should decrease nonlinear effects, (3) the case of bi-directional WDM transmission, etc.

A standardization procedure of the G.692 Recommendation is not yet closed and we should believe that the future version of this recommendation will be more complete.

References

[1] G. P. Agrawal, *Fiber-Optic Communication Systems*. John Wiley & Sons, 1992.

[2] N. Kashima, *Optical Transmission for the Subscriber Loop*. Artech House, 1993.

[3] A. R. Chraplyvy, „Optical power limits in multichannel wavelength-division-multiplexed systems due to Stimulated Raman Scattering", *Electron. Lett.*, vol. 20, no. 2, pp. 58–59, 1984.

[4] R. H. Stolen, „Nonlinearity in Fiber Transmission", *Proc. IEEE*, vol. 68, no. 10, pp. 1232–1236, 1980.

[5] Y. Namihira, „Relationship between nonlinear effective area and modefield diameter for dispersion shifted fibres", *Electron. Lett.*, vol. 30, no. 3, pp. 262–264, 1994.

[6] ITU-T Rec. G.653, „Characteristics of a dispersion-shifted single-mode optical fibre cable", 1993.

Sławomir Pietrzyk, Waldemar Szczęsny, and Marian Marciniak

[7] ITU-T Rec. G.957, „Optical interfaces for equipments and systems relating to the synchronous digital hierarchy", 1995.

[8] ITU-T Rec. G.692, „Optical interfaces for multichannel systems with optical amplifiers", 1997.

[9] ITU-T Rec. G.709, „Synchronous Multiplexing Structure", 1993.

[10] ITU-T Study Group 15, Delayed Contribution D.170, Geneva, Feb. 9-20, 1998.

[11] G. P. Agrawal, *Nonlinear fiber optics*. Academic Press, 1989.

[12] D. Marcuse *et al.*, „Effect of fiber nonlinearity on long-distance transmission", *J. Lightw. Technol.*, vol. 9, 1991.

[13] D. Marcuse *et al.*, „Dependence of cross-phase modulation on channel number in fiber WDM system", *J. Lightw. Technol.*, vol. 12, 1994.

[14] R. W. Tkach *et al.*, „Four-photon mixing and high speed WDM system", *J. Lightw. Technol.*, vol. 13, 1995.

Sławomir Pietrzyk
Technical University of Kielce, Al. 1000-lecia P. P. 7, 25-314 Kielce, Poland, e-mail: slav@srv1.tu.kielce.pl

Waldemar Szczęsny
National Institute of Telecommunications, 1 Szachowa Str., 04-894 Warsaw, Poland, e-mail: W.Szczesny@itl.waw.pl

Marian Marciniak
Technical University of Kielce, Al. 1000-lecia P. P. 7, 25-314 Kielce, Poland; National Institute of Telecommunications, 1 Szachowa Str., 04-894 Warsaw, Poland, e-mail: M.Marciniak@itl.waw.pl

Ultra-short optical pulses having initial chirp

Tomasz Kaczmarek

Abstract — Arbitrary shape optical pulses in nonlinear guides are discussed. The Nonlinear Schrödinger Equation for complex initial conditions is solved numerically using Split-Step Fourier Method and some selected results for solitons are presented. The computations confirm physical expectations of an influence of the chirp magnitude on pulse propagation in nonlinear guide.

Keywords — solitons, optical fibers.

Introduction

Propagation of ultra-short optical pulses in lossless guides is analysed using Nonlinear Schrödinger Equation (NLSE)

$$j\frac{\partial A}{\partial z} - \frac{1}{2}\beta_2 \frac{\partial^2 A}{\partial T^2} + \gamma |A|^2 A = 0, \qquad (1)$$

where A represents the envelope function, γ – nonlinearity, β_2 – dispersion of the fiber, z and T are, respectively, the spatial and time co-ordinates [1].

This equation is valid when duration of the pulse is greater than 100 fs and it can be solved analytically using the Inverse Scattering Method [2], if the input pulse is of hyperbolic secant shape. Otherwise, numerical methods should be used.

Then, fundamental solution is a secant hyperbolic function, what means that the pulse does not change its shape during propagation. So, it is stable, called soliton.

The soliton occurs due to mutual compensation of the dispersion and the nonlinearity of the fiber. So, if any initial chirp exists, the compensation is not full and the pulse is distorted.

The chirp phenomenon can be taken into consideration in the NLSE assuming complex initial condition of the form

$$u(0,\tau) = N \sec h(\tau) \exp\left\{ \frac{-jC\tau^2}{2} \right\}, \qquad (2)$$

where C represents the magnitude of the chirp.

To include Eq. (2) in NLSE one of numerical methods must be applied: Split-Step Fourier Method (SSFM) or Beam Propagation Method (BPM).

Method description

Split-Step Fourier Method has physical grounds. The idea is based on separate consideration of consequences of nonlinearity and dispersion on the pulse propagation in a short segment of the guide.

It can be represented schematically when Eq. (1) is expressed in the operator form [3–5]

$$\frac{\partial A}{\partial z} = (D+N)A. \qquad (3)$$

Here D and N is the dispersion and nonlinearity operator, respectively.

After some calculations, the optical field can be expressed as follows

$$A(z+h,T) = \exp(hD)\exp(hN)A(z,T), \qquad (4)$$

where h denotes the length of the step.

Results

Making use of the formulas above, computations were carried out for soliton of the first order when $\beta_2 = -1.6 \frac{\text{ps}^2}{\text{km}}$ and $\gamma = 1.6 \, \text{W}^{-1} \, \text{km}^{-1}$ for selected values of C and initial duration of the initial pulse $T_{in} = 1.5$ ps.

The dispersion and nonlinearity parameters have been chosen so, that the effective fibre core section would be $A_{eff} = 80 \, \mu\text{m}^2$, and the threshold power of the pulse $P_{th} = 443$ mW.

As, it is seen the initial chirp throws out of balance the dispersion and nonlinearity, which determine a formation of the soliton in optical fibre. The positive chirp narrows the pulse at the beginning of the propagation (Fig. 1).
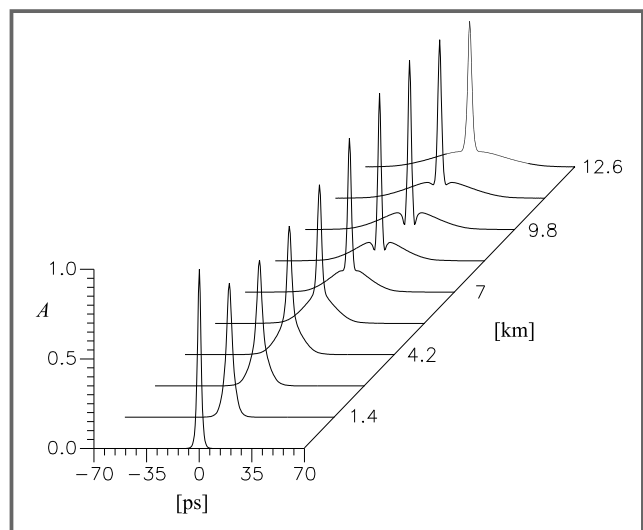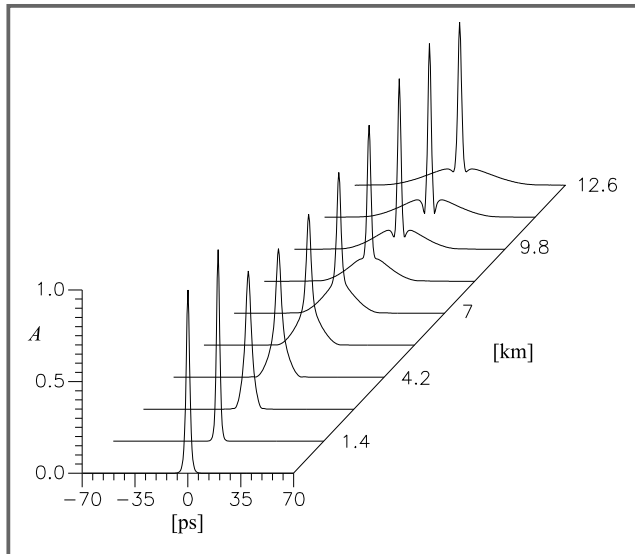

Fig. 1. Evolution of the fundamental soliton when $C = 0.5$

This is an effect of the predominance of the phase modulation over the dispersion. The negative chirp increases the predominance of the dispersion effect (Fig. 2).

Fig. 2. Evolution of the fundamental soliton when $C = -0.5$

Conclusion

The numerical results are physically substantiated. They confirm proper selection of the method.

Generally, initial chirp is undesirable phenomenon especially positive one, besides that, negative effects of it are more observable in a case of long distances.

Prepared software can serve the analysis of the propagation of the pulses not only of hyperbolic secant shape.

References

[1] A. Majewski, *Nieliniowa optyka światłowodowa. Zagadnienia wybrane*. Warszawa: WPW, 1993.

[2] V. E. Zakharov and A. B. Shabat, *Sov. Phys. JETP*, vol. 34, no. 62, 1972.

[3] A. Karczewski, *Solitony optyczne: Analiza właściwości widmową metodą dwukrokową*. Podręcznik akademicki, 1993/94.

[4] A. Hasegawa and F. Tappert, „Transmission of stationary nonlinear optical pulses in dispersive dielectric fibers. I. Anomalous dispersion", *Appl. Phys. Lett.*, vol. 23, no. 142, 1973.

[5] G. P. Agrawal, *Nonlinear Fiber Optics*. Academic Press, 1989.

Tomasz Kaczmarek
Technical University of Kielce
Al. 1000-lecia P.P. 7, 25-314 Kielce, Poland

Impact of nonlinear optical phenomena on dense wavelength division multiplexed transmission in fibre telecommunication systems

Waldemar Szczęsny and Marian Marciniak

Abstract — In the paper results of analysis of nonlinear phenomena in optical fibres: Self-Phase Modulation, Cross-Phase Modulation, Four-Wave Mixing and Stimulated Raman Scattering and their influence on Dense-Wavelength Division Multiplexed system performance are reported. Different non-uniform optical channel allocation schemes based on ITU Recommendation G.692 100 GHz frequency grid are compared with uniform channel distribution. The level of nonlinear cross-talk is determined for different levels of the total optical power. As an example a 10 Gbit/s D-WDM dispersion-shifted single mode fibre link with dispersion-compensating fibres is envisaged. The directions for optimization of the system design in view of actual international standardization trends are pointed out.

Keywords — optical communications, WDM systems, nonlinear transmission.

Introduction

Dispersion-shifted fibres G.653 allow for better transmission parameters in single-channel transmission links due to very small dispersion value in third telecommunications window corresponding to 1.55 μm optical wavelength. However, in Wavelength Division Multiplexed (WDM) systems very small value of dispersion may cause a significant degradation of the systems due to nonlinear optical effects resulting from optical nonlinearity of silica glass. A high optical power level available with modern laser sources causes nonlinear interaction in fibres strongly efficient.

In WDM systems a nonlinear interplay between many different spectral components of the aggregate signal cases interchannel cross-talk. The nonlinear phenomena involved are: Self-Phase Modulation (SPM), Cross-Phase Modulation (XPM), Four-Wave Mixing (FWM) and Stimulated Raman Scattering (SRS).

In dispersion-shifted fibres the interchange of optical power between different propagating optical frequencies corresponding to the third telecommunication window is much stronger than in standard single mode fibres (G.652). The main causes of that are:

1. The effective area [2] of G.653 fibres are smaller then in G.652 fibres, a given power level results in a higher intensity in G.653 fibres than in G.652 fibres.

2. The low dispersion in G.653 fibres can results in low walk-off between bits in the different channels of WDM systems, also known as a phase matching condition. This means that a single 1 in the lowest wavelength channel will have a fair chance for seeing 1 bits in all the other channels throughout the part of the fibre, where the nonlinear interaction takes place.

Signal degradation caused by Stimulated Raman Scattering (SRS)

In the WDM systems SRS manifests itself as a depletion of the "1" level in the lower wavelength channel, which depends on the signal in the higher wavelength, and a gain in the higher wavelength channel, that depends on the signal in lower wavelength channel.

The depletion introduced by SRS has unfortunate characteristic:

The depletion of a given "1" is dependent on the signals that are other channels. This means that „drops" caused by SRS can occur on the timescale of an individual bit, which is much faster than the response time of the threshold setting in the receiver. The depth and the frequency of this drops will dictate the BER for the WDM system that is limited by SRS [1].

Phase modulation

Self-phase modulation (SPM) is the effect whereby the modulated optical signal induces a modulation in the fibres refractive index. SPM leads to considerable spectral broadening of propagating pulses. In a WDM system also a Cross-Phase Modulation (XPM) occurs. The total phase shift depends on the power in all channels and varies from bit to bit depending on the bit pattern of the neighbouring channels.

Four-Wave Mixing (FWM)

FWM generated a new wave at the frequency $f_{ijk} = f_i + f_j - f_k$, whenever three waves at frequencies f_i, f_j, and f_k co-propagate inside the fibre. For N channel system i, j and k can vary from 1 to N. In the case of equally spaced channels the new frequencies coincide with the existing frequencies.
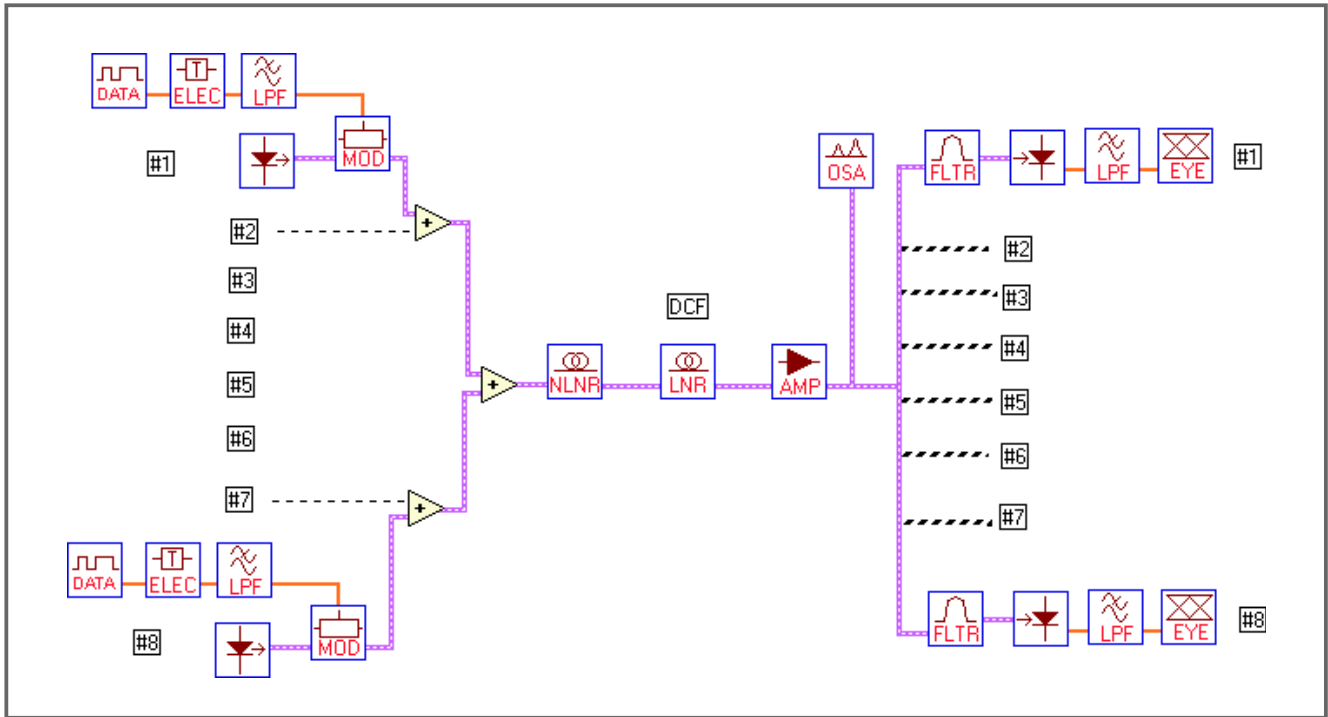
Waldemar Szczęsny and Marian Marciniak

Fig. 1. Architecture of the 8-channel WDM system analysed
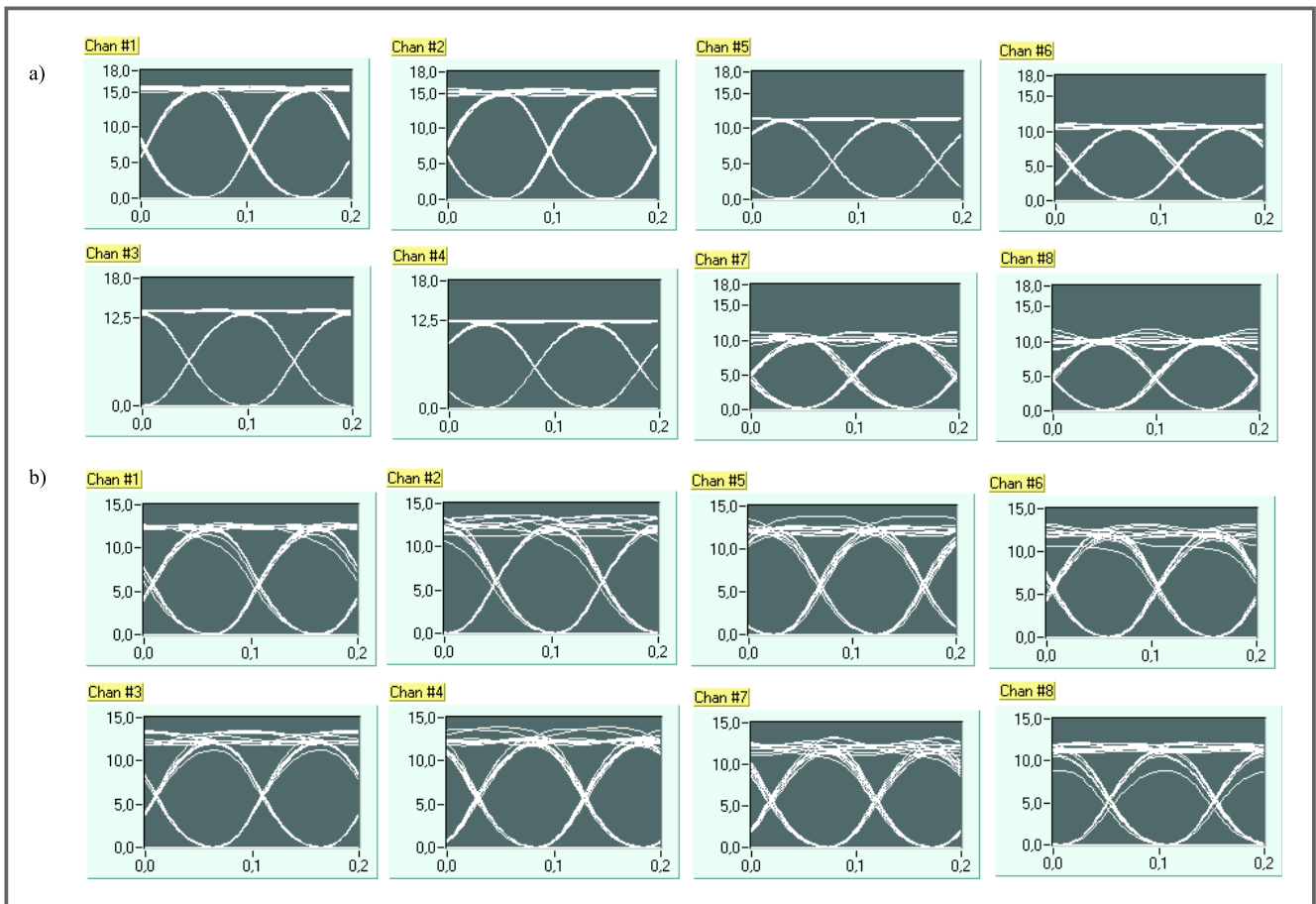

Fig. 2. The eye diagrams of the detected signal for equidistant channel spacing (a) and non-equidistant channel spacing (b)

Table 1
Non-equidistant frequency allocation schemes used in the calculations

Scheme	Channel index							
	0	1	2	3	4	5	6	7
A	196.1	196.0	195.7	195.2	194.6	193.9	192.9	192.7
B	196.1	195.9	195.5	194.5	194.2	193.4	192.7	192.2
C	196.1	195.8	195.1	193.9	193.7	193.1	192.6	192.2
D	196.1	195.5	194.8	194.0	193.1	192.1	190.9	189.8
E	196.1	196.0	195.9	195.8	195.7	195.6	195.5	195,4

Description of the analysed system

Propagation of the field in the X-polarization state in a nonlinear fibre is modelled using the following nonlinear partial differential equation [8]

$$
\frac{\partial A_x}{\partial z} - \frac{i}{2}\beta_2 \frac{\partial^2 A_x}{\partial T^2} - \frac{1}{6}\beta_3 \frac{\partial^2 A_x}{\partial T^2} + \frac{\alpha}{2}A_x =
$$
$$
-i\gamma \left[|A_x|^2 A_x - T_R A_x \frac{\partial^2 |A_x|^2}{\partial T^2} \right], \tag{1}
$$

where $A_x(z,T)$ is the slowly varying field envelope and β_2, β_3, α and γ are related to the dispersion, dispersion slope, loss and nonlinearity of the fibre. Equation (1) is solved using the split step Fourier method [8]. The algorithm uses an adaptive step-size [11].

The nonlinear coefficient γ for the fibre is defined as [8]

$$
\gamma = \frac{n_2 \omega}{c A_{eff}} \ .
$$

Here, n_2 is the Kerr nonlinear index coefficient, ω is the angular optical frequency, A_{eff} is the effective core area, and c is the light velocity in vacuum. The coefficient γ accounts for the effects of SPM [9], XPM [10] and FWM [11] effects. The simulations have been carried out for an 8-channel STM-64 transmission system, with 10 Gbit/s single channel data flow, what means an 80 Gbit/s aggregate transmission speed. The system is shown in Fig. 1 and corresponds to Synchronous Digital Hierarchy (SDH) standards. The inter-channel data synchronization has been obtained as identical 32-bit pseudo-random sequence in each of WDM channels. A de-correlation of the data has been achieved by imposing time delays for varying from channel to channel. At the detector side of the system optical band-pass filters with FWHM 40 GHz bandwidth and different transmission characteristics have been used in order to de-multiplex optical channels. The dispersion-shifted fibre is compatible with ITU-T G.653 standard. The transmission span is 120 km. A dispersion-compensating fibre with negative dispersion value is introduced at the end of the transmission span. The optical gain in Erbium-Doped Fibre Amplifiers has been chosen in a way to compensate for total attenuation of the link. The optical frequency distribution has been based on the 100 GHz ($\sim$0.8 nm) ITU-T G.692 Recommendation grid. The reference frequency for the first WDM channel is 196.1 THz (1552.52 nm). The calculations have been performed for a non-equidistant frequency allocation schemes A, B, C defined in Table 1 that

allow for elimination of FWM generated frequencies, according to G.692 Recommendation. A scheme E has been added which corresponds to 8-channel WDM system with a 100 GHz equidistant grid. A total 8-channel optical power at the transmitter side is 17 dBm, this corresponds to laser peak-power of 12.5 mW and 6.25 mW mean-power for an NRZ code [12].

Results

Table 2 shows optical powers in transmitted channels.

The scheme A experiences minimum power losses caused by nonlinear interaction and this scheme has been analysed in detail. The results are shown in Table 3. The results indicate that Stimulated Raman Scattering causes the largest amount of inter-channel power transfer. Figure 2 shows the eye diagrams of the detected signal for equidistant channel spacing (Fig. 2a) and non-equidistant channel spacing (Fig. 2b). The eye opening is determined by inter-channel frequency gap and it is wider for non-equidistant channel spacing. However, the cross-talk level is as low as -28 dB. Figure 3 shows 8-channel optical spectrum for all channels transmitting (Fig. 3a) and with channel number 7 turned off (Fig. 3b). The absence of optical power in channel 7 results in an increase of optical power in neighbouring channels 6 and 8 what is a result of XPM, and a decrease of FWM
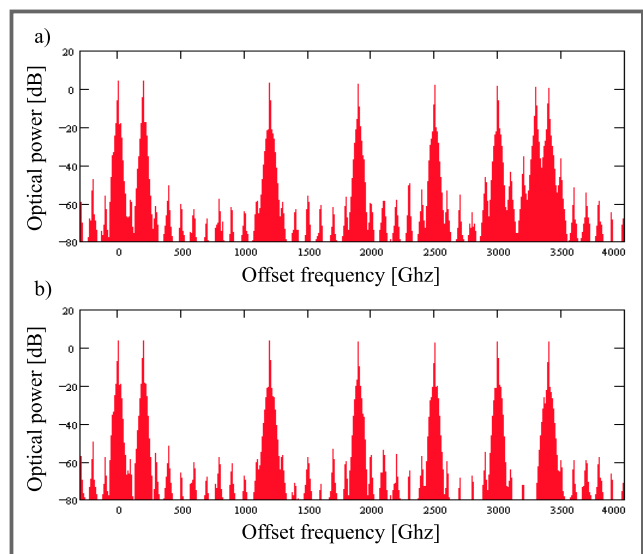

Fig. 3. 8-channel optical spectrum for all channels transmitting (a) and with channel number 7 turned off (b)

Table 2

Optical power in transmitted channels for different frequency allocation schemes

Scheme	Total optical bandwidth [mm]	Mean optical power per channel [mV]								Total optical losses in 8-th channel [dB]
		1	2	3	4	5	6	7	8	
A	28.2	7.56	7.38	6.54	5.99	5.56	5.22	5.01	4.96	1.00
B	31.2	7.71	7.26	6.67	6.03	5.81	5.13	4.88	4.77	1.17
C	31.2	7.48	7.12	6.71	6.21	6.07	5.24	4.79	4.63	1.31

Table 3

Optical power in transmitted channels for allocation scheme A

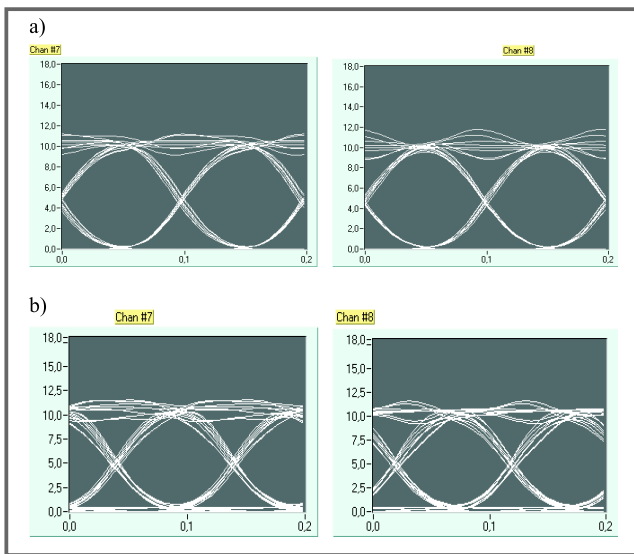| Nonlinear phenomena taken into account	Mean optical power per channel [mV]								Maximum power losses in 8-th channel [dB]
	1	2	3	4	5	6	7	8	
SRS, FWM, SPM, XPM	7.56	7.38	6.54	5.99	5.56	5.22	5.01	4.96	1.00
Without SRS	6.03	6.03	6.04	6.03	6.03	6.02	6.00	6.01	0.17
SRS only									0.83
Without losses	6.25								

Fig. 4. The eye diagrams of the received signal A distortion of the signal depends on data correlation between channels

Fig. 5. The XPM optical spectrum degradation for two channels: with minimal (a) and maximal (b) distortion

components. Figure 4 shows eye diagrams of the received signal. A distortion of the signal depends on data correlation between channels, resulting mainly from XPM. Figure 5 shows the XPM optical spectrum degradation for two channels: with minimal and maximal distortion. Figure 6 shows optical spectra for Gaussian optical filter (Fig. 6a) and Lorentzian optical filter (Fig. 6b).

Conclusion

An 8-channel WDM 120 km dispersion shifted fibre transmission system based on ITU G.692 Recommendation frequency grid has been investigated for different frequency allocation schemes in view of inter-channel nonlinear interactions. The results indicate that:

• The largest amount of optical cross-talk is caused by XPM. The cross-talk can be decreased when using an op-
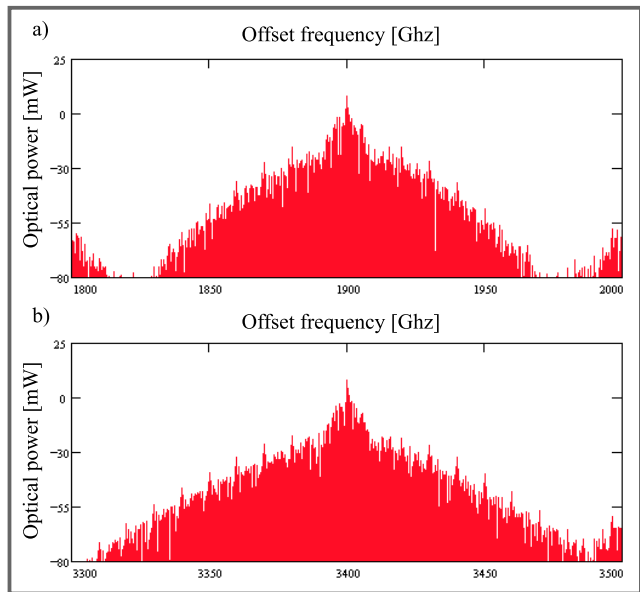
tical fibre with larger dispersion value (standard fibre or non-zero dispersion shifted fibre).

• Non-equidistant frequency allocation in the system results in large value of transmitted bandwidth, exceeding EDFA gain bandwidth.

• Systems with standard fibre and dispersion compensation are the most promising for WDM applications.

References

[1] G. P. Agrawal, *Fiber-optic communication systems*. New York: Wiley-Interscience Publication, 1992.

[2] Y. Namihira, „Relationship between nonlinear effective area and modefield diameter for dispersion shifted fibres", *Electron. Lett.*, vol. 30, no. 3, pp. 262–264, 1994.

[3] ITU-T Rec. G.653, „Characteristics of a dispersion-shifted single-mode optical fibre cable", 1993.
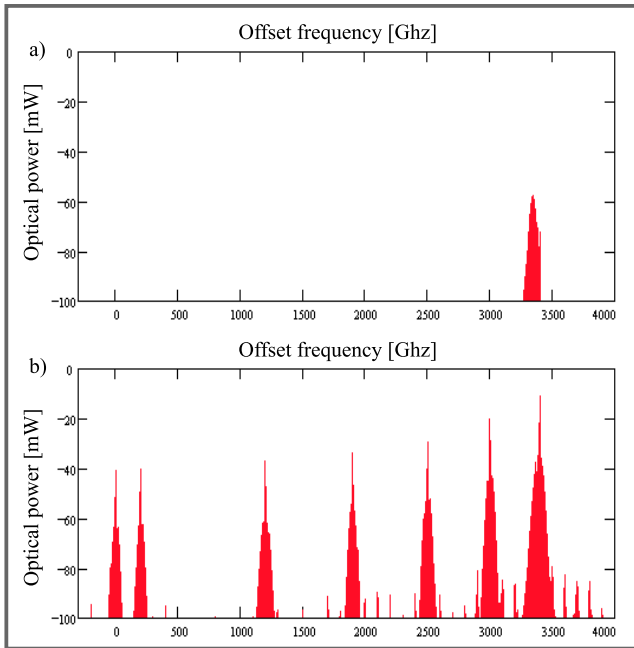
Fig. 6. The optical spectra for Gaussian optical filter (a) and Lorentzian optical filter (b)

[4] ITU-T Rec. G.957, „Optical interfaces for equipment and systems relating to the synchronous digital hierarchy", 1995.

[5] ITU-T Rec. G.692, „Optical interfaces for multichannel systems with optical amplifiers", 1997.

[6] ITU-T Rec. G.709, „Synchronous Multiplexing Structure", 1993.

[7] ITU-T Study Group 15, Delayed Contribution D.170, Geneva, Feb. 9–20, 1998.

[8] G. P. Agrawal, *Nonlinear fiber optic*. Academic Press, 1989.

[9] D. Marcuse *et al.*, „Effect of fiber nonlinearity on long-distance transmission", *J. Lightw. Technol.*, vol. 9, 1991.

[10] D. Marcuse *et al.*, „Dependence of cross-phase modulation on channel number in fiber WDM system", *J. Lightw. Technol.*, vol. 12, 1994.

[11] R. W. Tkach *et al.*, „Four-photon mixing and high speed WDM system", *J. Lightw. Technol.*, vol. 13, 1995.

[12] S. Pietrzyk *et al.*, „Power penalty caused by Stimulated Raman Scattering in WDM systems", in *COST P2 Workshop on „Applications of Nonlinear Optical Phenomena"*, Limerick, Ireland, June 12–13, 1998.

Marian Marciniak,
National Institute of Telecommunications,
1 Szachowa Str., 04-894 Warsaw, Poland,
e-mail: M.Marciniak@itl.waw.pl

Waldemar Szczęsny,
National Institute of Telecommunications,
1 Szachowa Str., 04-894 Warsaw, Poland,
e-mail: W.Szczesny@itl.waw.pl

Optical pulse splitting under temporal variations of reflecting medium

Irena Yu. Vorgul and Marian Marciniak

Abstract — **A possibility of light pulse transformation by transient reflecting medium is investigated theoretically. After solving 1D problem of such a reflection one estimates such a transformation in a plane optical waveguide with time-dependent conductivity of one of the reflected media. Three types of the conductivity time-dependences are considered: harmonic, Bessel-like and splash-like ones. Obtained results show a possibility of pulse splitting under an influence of time-harmonic conductivity and pulse collapse vy the other considered nonstationarities.**

Keywords — *optical pulse splitting, time dependent conductivity, reflecting boundary.*

Motivation and common formulation of the problem

In optics a transformation of electromagnetic field of light has two reasons to be one of the basic problem. The first one is that light sources could not radiate all types of required fields, laser sources radiate fields of a finite number of frequencies. The second one is, as in radio range electromagnetics, a necessity to modulate field for information transmission. Optical waverange field modulation is usually made based on electro-optical Pokker's effect, magneto-optical Faradey's or Kerr's effects and on acousto-optical effect. In all these methods the field is modulated during the transmission through the correspondent modulating media, which is connected with additional losses and additional element of transmission tract. For information transmission it is not convenient to use frequency or phase light modulation, because in the existing light sources for optical communication there is not enough coherence. Besides, such a modulation techniques are well-developed only for harmonic initial fields.

The present work has a goal to find a possibility to transform light pulses by transient reflecting medium and to estimate such a transformation in a plane optical waveguide where one of the reflecting media has time-dependent conductivity.

One has chosen the conductivity as a transient parameter because it can be more easily changed than permittivity whose change besides can leads to destructuring of the full reflection in optical waveguide.

To estimate pulse transformation in a plane optical waveguide with time-dependent conductivity of one of the reflecting media (Fig. 1) one firstly solves rigorously one-space
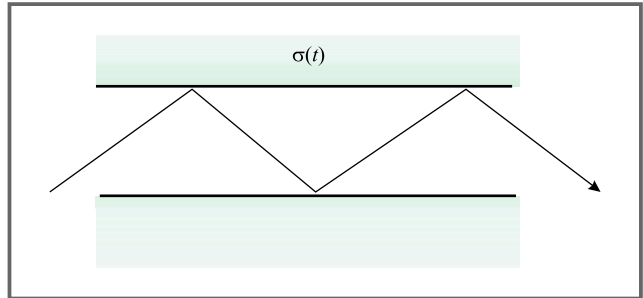

Fig. 1. Plane waveguide with nonstationary reflecting medium

dimensional problem of pulses reflection from a transient conductive half-space for an initial pulse propagating normally to the reflection boarder (Fig. 2).
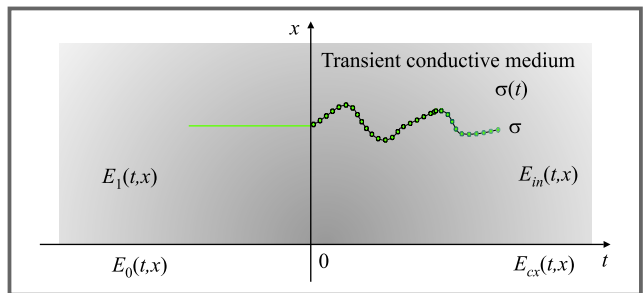

Fig. 2. Formulation of 1D problem

For the conductivity time-dependences considered in 1D case two-space-dimensional problem is investigated. It is solved approximately for the initial pulse falling angle providing a full reflection, in assumption of constant polarisation of the initial and scattered fields (Fig. 9). Then one estimates multiply re-reflection of the transformed pulse from the transient and stationary media forming a plane light waveguide.

One-space-dimensional problem

Problem formulation

The formulation of one-space-dimensional problem is in determination of the reflected field by the reflected field and the initial one and by time-dependence of the relected medium conductivity.

It is considered that the conductivity change starts after the moment $t = 0$ (Fig. 2). Before and after this moment the

fields are called the initial and scattered fields, correspondingly. The fields are assumed to have only those components, which are normal to the x-axis and independent on the y- and z-coordinates.

Mathematically, the problem is formulated in terms of the Volterra integral equation for the electrical component of electromagnetic field [6], which has the following form for the internal field (inside the transient region) for $t > 0$, $x > 0$:

$$
E_{in}(t,x) = A(t,x) +
$$
$$
-\frac{2\pi}{\varepsilon v}\, \Theta(vt-x) \int_{t-x/v}^{t} dt'\sigma(t') E_{in}\left(t', x-v(t-t')\right) +
$$
$$
-\frac{2\pi}{\varepsilon v}\, \Theta(x-vt) \int_{0}^{t} dt'\sigma(t') E_{in}\left(t', x-v(t-t')\right) +
$$
$$
-\frac{2\pi}{\varepsilon v} \int_{0}^{t} dt'\sigma(t') E_{in}\left(t', x+v(t-t')\right) \tag{1}
$$

where $A(t,x)$ is known because it is determined by the initial field and prehistory of its interaction with the medium:

$$
A(t,x) = E_0(t,x) +
$$
$$
-\Theta(x-vt)\frac{2\pi}{\varepsilon v} \int_{t-x/v}^{0} dt'\sigma(t') E_1\left(t', x-v(t-t')\right) +
$$
$$
-\frac{2\pi}{\varepsilon v} \int_{-\infty}^{0} dt'\sigma(t') E_1\left(t', x+v(t-t')\right)
$$

and for the external field for $t > 0$, $x < 0$:

$$
E_{ex}(t,x) = B(t,x) +
$$
$$
-\frac{2\pi}{\varepsilon v}\, \Theta(vt+x) \int_{0}^{t+x/v} dt'\sigma(t') E_{in}\left(t', v(t-t')+x\right) \tag{2}
$$

where

$$
B(t,x) = E_0(t,x) +
$$
$$
-\frac{2\pi}{\varepsilon v}\, \Theta(vt+x) \int_{-\infty}^{0} dt'\sigma(t') E_1\left(t', v(t-t')+x\right) +
$$
$$
-\frac{2\pi}{\varepsilon v}\, \Theta(x+vt) \int_{-\infty}^{t+x/v} dt'\sigma(t') E_1\left(t', v(t-t')+x\right)
$$

where ε is the dielectric permittivity, $v = c/\sqrt{\varepsilon}$ is the light velocity in considered medium and the conductivity time-dependence (or time-spatial dependence) $E_{ex}(t,x)$ is a function to be found.

Analytical solution of the problem

To obtain an equation for the external field, we firstly solve the equations (1) and (2) jointly to express the initial field after the external one.

As one can see from (2), the external field is determined by the sum of the known function B and a function of one variable $t - x/v$. This fact, which is due to the assumed homogeneity and losslessness of the external half-space, makes impossible to express the internal field through the

external one directly from this expression. However, it allows to obtain a non-integral formula for the external field determined by the internal field on the boundary $x = 0$. For this purpose we introduce a new function F of one variable as:

$$
F(t) = -\frac{2\pi}{\varepsilon v} \int_{0}^{t} dt'\sigma\left(t', v(t-t')\right) E_{in}\left(t', v(t-t')\right), \tag{3}
$$

which determines the external field in the external region $-vt < x < 0$ by the expression

$$
E_{ex}(t,x) - B(t,x) = F(t+x/v).
$$

From (1) we can obtain that the internal field on the boundary is determined by the same function F:

$$
E_{in}(t,0) - A(t,0) = F(t).
$$

Considering this expression for shifted time moment $t + y/v$, $-vt < y < 0$, we have

$$
E_{in}(t+y/v,0) - A(t+y/v,0) = F(t+y/v).
$$

After comparing this formula with (2) we obtain the following expression for the external field:

$$
E_{ex}(t,x) = B(t,x) + E_{in}(t+x/v,0) - A(t+x/v,0),
$$
$$
-vt < x < 0. \tag{4}
$$

Introduce another new function

$$
\Phi(t,x) \equiv E_{in}(t-x/v,x) - A(t-x/v,x) \tag{5}
$$

for $0 < x < vt$, satisfying the following equation obtained from (1):

$$
\Phi'_x(t,x) + \frac{2}{v}\, \Phi'_t(t,x) =
$$
$$
-\frac{4\pi}{\varepsilon v}\frac{\partial}{\partial t} \int_{0}^{t-x/v} dt'\sigma\left(t', v(t-t')\right) E_{in}\left(t', v(t-t')\right) \tag{6}
$$

with the boundary and initial conditions:

$$
\Phi(t,0) = F(t), \text{ and } \Phi(x/v,x) = E_{in}(0,x) - A(0,x) = 0.
$$

Knowing the external field at any point, the field in the whole external region can be determined, including the region close to the boundary:

$$
E_{ex}(t,x) - B(t,x) = E_{ex}(t-x_1/v,x+x_1) +
$$
$$
-B(t-x_1/v,x+x_1) = F(t+x/v) \tag{7}
$$

So it would be enough to obtain the solution for external field close to the boundary at the points where $|x| \ll vt$. Under this approximation, we can solve Eq. (6), hence expressing the internal field through the external one, because the integral at the right-hand part of (6) will be equal to $F(t)$:

$$
\Phi'_x(t,x) + \frac{2}{v}\, \Phi'_t(t,x) \approx 2F'(t). \tag{8}
$$

After substitution of this equation solution into (3) we obtain the conductivity time-dependence in the half-space determined by the scattered field:

$$\sigma(t)\Big(E_{ex}(t-x/v,x)-E_0(t-x/v,x)+E_0(t,0)\Big) =$$
$$= \sigma_0 A(0,0)\,, \qquad (9)$$

where $\sigma_0 = \sigma(0)$ is the known value of initial conductivity, and x means an arbitrary point coordinate (not only $|x| \ll vt$) inside the external region $-vt < x < 0$.

Pulse splitting with amplification by time-harmonic conductivity of the reflecting half-space

For the rectangular pulse $E_0 = \Theta(t-x/v) - \Theta(t-x/v-t_0)$ scattering on the homogeneous half-space with time-harmonic conductivity, computer analysis revealed the scattered pulse features dependence on the conductivity frequency. When it is comparable with reverse incident pulse duration then the pulse of scattered field just changes a little in its shape under the same duration.

When the conductivity frequency is more then four times as much as reverse pulse duration, the scattered pulse has deep valleys (Fig. 2). Their number grows with the frequency increasing. Thus, it becomes a consequence of pulses with joint duration less then that of the initial pulse. These pulses amplitude can be more then ten times as much as that of the initial pulse. The more is the conductivity frequency (Fig. 3(a)), the more is the number of reflected field pulses (Fig. 3(b)).
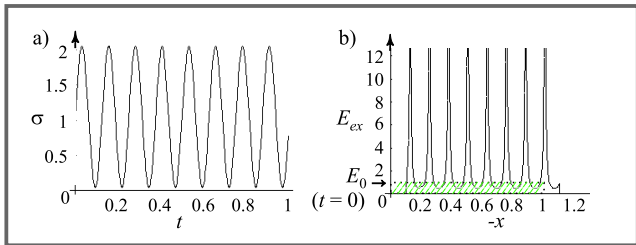

Fig. 3. Time-harmonic conductivity of the reflecting half-space leading to (b) pulse splitting with amplification by

Pulse transformation by reflecting half-space with conductivity changing with time as Bessel function

Bessel-type conductivity time-dependence provides the initial rectangular pulse transformation into a pulse with duration 10^{-3} as much as the initial one, following by reducing oscillating tail (Fig. 4).

Such a pulse collapse can be also followed by the reflected pulse amplification, as Fig. 5 shows.

Consider the same pulse scattering on the half-space with time-splashing conductivity (Fig. 6(a)) with its time dependence described by a difference of reducing exponents.

For the time less then a pulse duration after it began its interaction with the half-space. Figure 6(b) shows the reflected pulse front which then will save its shape and size,
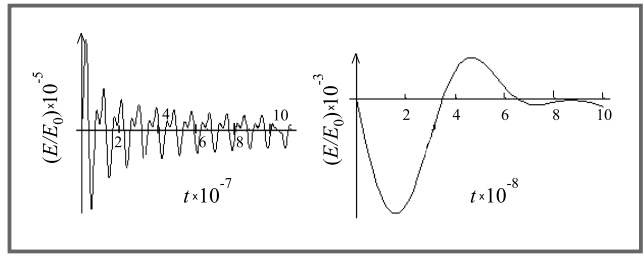

Fig. 4. Reflected pulse amplitude time-dependence for different amplitudes of Bessel-type conductivity change(initial pulse length =1 cm)
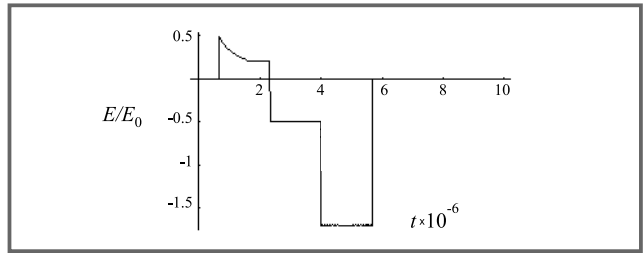

Fig. 5. Reflected pulse amplitude time-dependence for Bessel-type conductivity change (initial pulse length = 0.5 cm)

moving with the correspondent to the medium light velocity (circle incision in Fig. 7). With time this pulse of a small amplitude moving away from the boundary leaves a field trace of a high amplitude (Fig.7). After the end of the conductivity splash the trace amplitude decreases forming so a splash-like pulse. The front of this pulse moves with a velocity lower then that of light for the considered medium. This trace evolution with time leads to its transformation
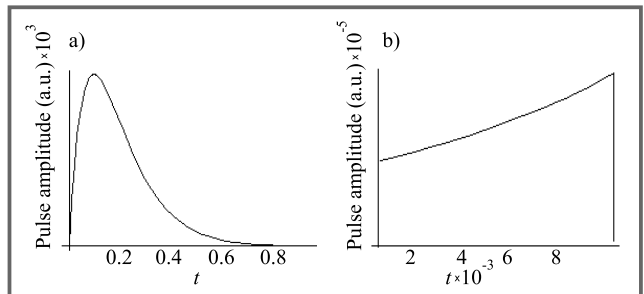

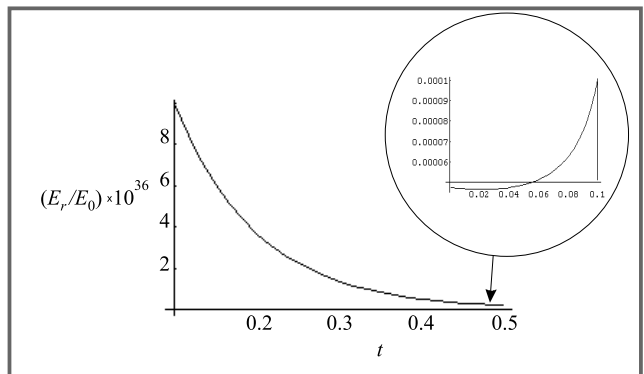**Fig. 6.** Conductivity splash (a) and initial stage of the pulse reflection (b)

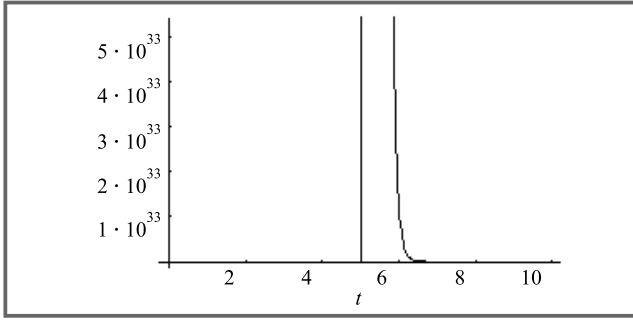**Fig. 7.** Reflected field front and trace

Fig. 8. Short pulse formed from the reflected field trace

into a shot pulse of a very high amplitude which is like to Dirac delta function as Fig. 8 shows.

Obtained solutions enable one to analyse a large number of scattering on the transient conductive half-space problems. Results for the special cases can be useful, for example, for creation short pulses of high amplitude.

The obtained results demonstrate different possibilities of initial pulse splitting or time-compression by time variation of the reflecting medium.

They also show possibilities of the reflected pulse amplification.

For the case of time-harmonic conductivity in the reflecting half-space one can obtain an easy read information when the modulated signal amplitude and frequency are translated into amplitudes and a number of pulses which are the result of the initial pulse subdivision.

2D Problem

In 3D nonstationary media an integral equation for electromagnetic field is [5]:

$$\boldsymbol{E}(t,\boldsymbol{r}) = \boldsymbol{E}_1(t,\boldsymbol{r}) - \frac{2\pi\sigma}{\varepsilon v}\left(\text{graddiv} - \frac{\partial^2}{\partial t^2}\right)\times$$
$$\times \int_0^t dt' \int_{-\infty}^{\infty} d\boldsymbol{r}'\sigma(t',\boldsymbol{r}')\frac{\Theta\left(t-t'-|\boldsymbol{r}-\boldsymbol{r}'|/v\right)}{|\boldsymbol{r}-\boldsymbol{r}'|}\boldsymbol{E}(t',\boldsymbol{r}'), \quad (10)$$

where $\boldsymbol{r} \equiv (x,y,z)$ and
$|r - \boldsymbol{r}'| = \sqrt{(x-x')^2 + (y-y')^2 + (z-z')^2}$.
For the considered 2D problem we assume $\sigma(t,r) \equiv \sigma(t)\Theta(x)$ and $\boldsymbol{E} = E_z\boldsymbol{k}$. In this case we have the following scalar integral equation inside the transient region:
$x \geq 0$

$$E_{in}(t,x,y) = E_1(t,x,y) +$$
$$-\Theta(vt-x)\int_{t-x/v}^{t} dt'\sigma(t')\int_{x-v(t-t')}^{x+v(t-t')} dx' G +$$
$$-\Theta(x-vt)\int_{0}^{\infty} dt'\sigma(t')\int_{x-v(t-t')}^{x+v(t-t')} dx' G +$$
$$-\Theta(vt-x)\int_{0}^{t-x/v} dt'\sigma(t')\int_{0}^{x+v(t-t')} dx' G \quad (11)$$

where

$$G \equiv \frac{2\pi}{\varepsilon v}\int_{y-\sqrt{v^2(t-t')-(x-x')^2}}^{y+\sqrt{v^2(t-t')-(x-x')^2}} dy'$$

$$\ln\frac{v(t-t') + \sqrt{v^2(t-t')^2 - (x-x')^2 - (y-y')^2}}{v(t-t') - \sqrt{v^2(t-t')^2 - (x-x')^2 - (y-y')^2}}E_{in}(t',x',y')$$

and the following formula which expresses the external field after the internal one:
$x < 0$

$$E_{in}(t,x,y) = E_1(t,x,y) +$$
$$-\Theta(vt+x)\int_{0}^{t+x/v} dt'\sigma(t')\int_{0}^{v(t-t')-x} dx' G. \quad (12)$$

We are interested in the external field for which we also can obtain a usual wave equation with constant coefficients directly from Maxwell's equations or from (12):

$$\left(\Delta - \frac{1}{v_0^2}\frac{\partial^2}{\partial t^2}\right)E_{ex}(t,x,y) = 0. \quad (13)$$

However, boundary conditions here will contain the unknown internal field.

Carrying out the procedures analogous with those in 1D problem solution, the following approximate integral equation for the function F determining the field on the boundary as

$$E(t,0,y) = E_1(t,0,y) + F(t,y)$$

can be obtained:

$$F(t,y) = \frac{2\pi}{\varepsilon v}\int_{0}^{t} dt'$$
$$\sigma(t')\int_{y-v(t-t')}^{y+v(t-t')} dy'\frac{F(t',y')(y-y')}{v^2(t-t')^2 - (y-y')^2}. \quad (14)$$

This equation can be solved numerically for concrete types of the conductivity time-dependence using standard procedures. After obtaining the field on the boundary, we can estimate the reflected field by solving the wave equation (13).

Estimating solution of this 2D problem has shown that there will be the same effects of pulse splitting, compression and amplification as in 1D problem.

These effects are not influenced later by multiply re-reflection, because the obtained pulses of short duration already does not feel the conductivity nonstationarity of correspondingly low frequency. It means that for pulse transformation by nonstationarity of the reflecting medium in optical waveguide a homogeneous simultaneous change of the conductivity is not necessary, but it is enough to create local nonstationarity.

References

[1] F. A. Harfoush and A. Taflov, „Scattering of electromagnetic waves by a material half-space with time-varying conductivity", *IEEE Trans. Anten. Propagat.*, vol. 39, no. 7, pp. 898–906, 1991.

[2] A. G. Nerukh and I. Yu. Shavorykina, „Electromagnetic impulse return from a conductive medium which has come into being", *Proc. Int. Symp. Anten. Propagat.*, vol. 2, pp. 585–588, 1992.

[3] M. Marciniak, *Łączność światłowodowa*. Warszawa: WKŁ, 1998.

[4] A. G. Nerukh and I. Yu. Shavorykina, „Transformation of radiation pulse in nonstationary conducting medium", *Radiophys. Quant. Electron.* (Consultants Bureau, New York), vol. 35, no. 3–4, pp. 203–209, 1992.

[5] A. G. Nerukh and N. A. Khizhnjak, „Modern Problems of Transient Macroscopic Electrodynamics". Kharkov, Ukraine: Test-Radio, 1991.

[6] S. Gonda and D. Seko. *Optoelectronics in questions and answers*, Leningrad: „Energoizdat" Publ., 1989 (Russian transl. from Japanees).

[7] I. Vorgul and M. Marciniak, „Electromagnetic pulse scattering on half-space with continuously time-varying conductivity", *Prace IŁ*, no. 110, pp. 29–42, 1998.

Irena Yu. Vorgul
Kharkov State University, 4 Svoboda Sq., Kharkov, 310077, Ukraine

Marian Marciniak
National Institute of Telecommunications, 1 Szachowa Str., 04-894 Warsaw, Poland, e-mail: M.Marciniak@itl.waw.pl

Recent advances
in PBG structures

Irena Yu. Vorgul and Marian Marciniak

Abstract — We propose a review of word science achievements in the extremely extended for the recent few years field of photonic band gap structures. The review concerns both theoretical and experimental investigations on PBG structures toward fabrication of the most optimal ones for different applications. The attention is given to the obtained results as well as to the used and developed methods.

Keywords — photonic band gap, photonic crystals, optical communications.

Introduction

Modelling, development and application of photonic band gap structures is now one of the most actual direction in photonics and optical communication, involving into the research a great number of scientists. A dozen years ago the paper [1] by Yablonovich was published with suggestion that structures with periodical spatial variation of refractive index could for some conditions exhibit a band of frequencies within which electromagnetic wave propagation is forbidden. The band was called a photonic band gap (PBG) by analogy with an electronic gap in semiconductor crystals [2]. We have not the aim to make a historical review but want to stress on the recent investigation to classify its main directions, applications and methods of modelling and development.

By periodically structuring a material in one, two or three dimensions one can fabricate new optical materials with unusual properties. Such PBG crystals materials are of great interest through the word because of their potential applicability to development of new optoelectronic devices. There are obvious such applications of PBG structures as reflectors and narrow-band filters fabrication, for example in a form of photonic crystal waveguide [3, 4].

Photonic band gaps have been both predicted and observed in one, two and three-dimensional photonic crystals. The challenge now is to design functional devices that exploit the new freedom offered by photonic crystal engineering.

Optical fibre band-pass filters based on PBG crystals fulfil a very important role in optical fibre communication systems. Together with the rapidly developing employment of wavelength division multiplexed optical communication systems, a renewed interest in the development of advanced optical fibres for new applications has been seen. The previous years research primarily included the further development of the mature silica fibre technology to handle amplification, dispersion compensation, nonlinearities etc. Completely new fibre concepts have been introduced over the past few years, among which is the photonic crystal fibre (PCF) [5] to be one of the most interesting.

Although it has been possible to fabricate a variety of band-pass filter components, ideal performance is difficult to achieve. For practical applications of PBG structures one needs not only to know the structure parameters and operating characteristics for the chosen model but also to identify quickly the influence of some key parameters because a model could not be perfect for real conditions of its fabrication. All these induce an explosion of different approaches to solving the problems. Theoretical modelling as well as experimental research goes in two directions. The first one is analytical, numerical or experimental investigation of reflection and transmission characteristics for special kinds of the structures and by this way an optimisation of the structures parameters [6]. The second one is an inverse problem approach using different theoretical and measuring techniques to reconstruct the required geometric and material characteristics, which provide the required optical field transformation [7,15].

One of the main principles of the PBG crystals development consists in introduction of microcavities into dielectric. It is now well known [8] that microstructuring of dielectric on the scale of the optical wavelength can strongly alter the photonic density of states, producing what is effectively a new material with optical properties that differ radically from those of the original dielectric [9–12]. It is of particular interest to explore whether this can lead to improved characteristics in devices made from commonly used and well understood optoelectronic materials, where performance limits have already been reached with conventional techniques. For example, work is already underway to improve III-V light emitting devices by incorporating metal-free photonic-crystal-based microcavities that block emission into unwanted modes [13]; and the microstructuring of thin threads of silica glass has been shown to lead to a revolutionary new type of optical fibre which is „endlessly single-mode" irrespective of the wavelength of excitation [5].

An important goal in the microlaser area is high-Q microcavities of volume $(8/2n)^3$ which support only one mode within the gain bandwidth of the lasing medium [11]. A photonic crystal with a true three-dimensional photonic band gap and a single point defect can provide this. The resulting efficient low-threshold lasers could be packed in large numbers onto a single substrate.

We start the review from one-dimensional PBG structures, which are access to consideration of three-dimensional photonic crystals as well as are themselves of a great

interest meaning different coating and other planar applications. Then the consideration will be given to multidimensional. The obtained results and used methods will be reviewed.

One-dimensional photonic crystals

The simplest photonic crystal is one-dimensional one, which possesses the fundamental features of photonic crystals in general [4]. This case corresponds to a periodic multi-layered structure.

This type of PBG structures as well as quasi-periodical ones is attractive for theoretical investigations. Classical periodic layered structures were properly investigated theoretically and experimentally for different wavebands [14]. The conditions of wave propagation in them were defined as well as their reflection characteristics. Detailed description of wave behaviour in them is a fundamental base for all consequent investigations.

However, these structures are not ideal for practical applications and the development there is by increasing complexity of the structures (as, for example, dual periodicity) toward the improved model. The criteria for such an optimization are the gap width and shape (preferably a rectangular-like one) as well as the structure dispersion and simplicity for fabrication.

Some other *special requirement to the structure* can be trying to follow when the investigation is directed to their special application. For example, the antireflection coating with ultra-low reflectivity and broad bandwidth for semiconductor lasers and optoelectronic devices is one of the most desired technologies in the field of modern optoelectronics [15]. For semiconductor laser amplifiers a reflectivity of less than 10^{-4} is required to suppress the Fabry-Perot mode oscillation [16]. For wavelength-tunable external cavity mode-locked semiconductor laser, less than 10^{-5} of ultra-low reflectivity is needed both to eliminate the secondary pulse generation and pulse broadening caused by the residual internal reflectivity [17] and to avoid the axial-mode instability [18]. Specifically, the WDM fiber-optic communication systems can have a bandwidth nearing to 100 nm. The tunable laser sources suitable for testing such systems must have comparable bandwidth and the correspondent coating.

Paper [15] proposes a design procedure of broadband multilayer *antireflection coatings for optical and optoelectronic devices* by numerical mappings on the optimization of the four-layer antireflective coating using TiO_2 and SiO_2. The numerical modelling for the considered inverse problem showed that there are four candidate regions realizing broad bandwidths. Preliminary experiments on the four-layer antireflecting coating on glass and InP substrates showed the broadband performance of the proposed design.

Planar structures could be combined forming so a 2D crystal patterns which offer practical advantages in comparison with classical 2D ones [8]. These advantages are that defects, dislocations and so on are easily incorporated either during or post-fabrication, and it is straightforward to access points on the two-dimensional plane, for example, allowing near-field probing of the modal microstructure. Planar photonic crystals can in fact be used in the design of simpler microcavities, which support only one high-Q resonant mode [30]. While these structures also support many modes that are coupled to the outside world, these unwanted modes have very low Q-factors, reducing the amount of spontaneous emission lost to them. Thus, the vacuum field strength is enhanced in the desired high-Q mode, leading in the case of lasers to a lowering of the threshold for stimulated emission. Of course, unlike in a 3D photonic band gap microcavity, diffractive losses increase as the cavities get smaller, so that a compromise must be struck between small volume and high efficiency.

A microcavity, based on a simple 1D photonic crystal waveguide design, was recently reported with a volume of $0.055\mu m^3$ and a Q-factor of 265 [31,32]. It is important to be clear about what is required of a two-dimensional planar photonic crystal in each particular application. For example, coexistence of waveguiding and strong 2D photonic band gap effects may be desired, as in slow-wave structures (optical delay lines), two-dimensional DFB ring cavity lasers or channel dropping filters [33]. In contrast, large area vertical cavity surface-emitting lasers may be required in which photonic crystal patterning is used to eliminate the in-plane guiding just mentioned, or to stabilize the transverse beam profiles. In the first case, in-plane waveguiding is highly desirable; for the vertical cavity surface-emitting lasers, however, one wants no in-plane guided modes and a one high-Q stationary mode radiating vertically with a designable extraction efficiency [13].

By periodically modulating the refractive index in one and two dimensions it is possible to create a dielectric material that behaves as a quasi-metal, i.e., a material that, within a certain wavelength range, rejects all wavelengths and polarisation states for incidence from a medium of lower index (e.g., air or water) [34]. This can be used to create a full photonic band gap in a low index layer sandwiched between two *1D quasi-metallic dielectric* stacks [35].

So, for successful fabrication of different special devices one should know not only spectral characteristics of the considered structure but also other physical features of the transformed by them field behaviour. Note, that what was mentioned above on the optimization criteria for 1D PBG crystals is also actual for multi-dimensional ones.

Quasi-periodic structures

Many researchers turned now to investigation of photonic quasi-periodic structures [24]. It was noticed that small deviations from periodicity could change sufficiently the structure interaction with incident field. They can perform properties of more sharp frequency filters as well as have wider band gap with a shape more similar to rectangular one in comparison with periodical structures.

In [24] the authors deal with the problem of diffraction of an electromagnetic wave by quasi-periodic multi-

layered structures. They assume three alternating values of the layers permittivity. When studying the reflectance of 1D photonic quasi-crystals numerically they noticed that such structures could exhibit band gap at very large wavelengths. It is necessary still for the global thickness of the structure to be no larger than the wavelength, but the mean thickness of the layers is arbitrary small with respect to the mean wavelength. As a consequence, semi-infinite photonic quasi-crystals cannot be homogenized and can behave as a perfect mirror for arbitrary wavelengths. The stressed result is like to one in diffraction experiments in the domain of x-ray crystals (so called Bragg spectrum consisting of peaks, which reveal the existence of long-range order of solids).

In [25] the gap phenomenon in a common case of aperiodic one-dimensional photonic crystals is investigated analytically. Using a classical characterization of forbidden bands, the authors show that it is possible to define a semi-infinite crystal. They also precise the behaviour of the field in the semi-infinite structure for wavelengths belonging to a forbidden band. The goal of the taking research was to characterize in a simple way the forbidden bands of wavelengths. The used approach is based on detailed explanation of the field behaviour inside the crystal within the gaps. A diffractional approach with introducing the transmission matrix for a period is used.

A general way of specifying the forbidden bands consists in considering periodic medium and in solving for eigensolutions of the introduced wave operator. When the global thickness of the medium is very large with respect to the wavelength, it seems natural to consider that the structure is semi-infinite. The semi-infinite medium has the advantage over the infinite one that it allows at least the formulation of the diffraction problem. In [25] the authors study the limit of the reflection coefficient when the number of periods tends to infinity, but keeping a half-space free. The preceding results is then applied to a structure whose period consists of two layers. The numerical calculations for this case enable one to suppose that the crystal behaves homogeneously within the gap, because of the exponential decrease of the field.

Pulse propagation through one-dimensional photonic band gap structures

Rather a new interesting aspect in considering the 1D PBG crystals is turned to pulse reflection and transmission [35]. An interest in the study of pulse propagation through one-dimensional photonic band gap materials both theoretically and experimentally grows rapidly. In particular, if an optical or microwave pulse is tuned with its carrier frequency well inside the photonic band gap (stop-band), then pulse tunneling takes place with a pseudo-super-luminal group velocity, $v > c$. This curios result has been verified at the single photonic level and reported in [36–38]. On the other hand, if carrier frequency is tuned to one of the photonic band-edge transmission resonances, then the group delay is anomalously large, with a corresponding group velocity

$v << c$. This effect has been used in the development of a new type of optical delay device [39-41].

In [35] the author considers the symmetries associated with the group-velocity delay of pulse transmission and reflection in a one-dimensionally inhomogeneous, planar dielectric structure. From the principles of energy and parity conservation the author derives the generalized Stokes reciprocity relation for such a slab. From these relations, he obtains very general equations relating the group delay and phases of the transmitted and reflected pulses.

Multi-dimensional PBG crystals

Modelling of multi-dimensional PBG structures meets much more difficulties in comparison with 1D case. Actually, the high complexity of three-dimensional nanoprocessing has not allowed the fabrication of three-dimensional photonic band gap structures working in the optical range [43]. Within the microwave and sub-millimetre regime, where fabrication is much simpler than in optical regime, several three-dimensional structures have been suggested [44,45]. An usual way in optics is to use 3D combinations of 2D PBG structures [43,46].

2D PBG crystals (and 3D ones, consequently) are usually made as a set of objects like rods [12] or a lattice with holes [47]. Basically, photonic crystals are derived from periodic structures, which exhibit photonic band gap due to their periodicity. It is well known that the introduction of defects in the periodic lattice generates localized electromagnetic modes. Potential applications in many technological areas, such as the development of efficient semiconductor light emitters, filters, substrates for antennas in microwaves, and lossless mirrors, have generated a growing interest in the study of the properties of multi-dimensional photonic band gap materials.

As there are many difficulties in such structures fabrication in optical waverange to pick up an appropriate solution for them experimentally by creation and testing the different kind of ones. Therefore, many researchers have developed theoretical and numerical techniques to study these periodic or quasi-periodic structures.

Some of the *developed techniques* are converted from those of electromagnetic diffraction theory as ones based on transfer matrix approach [54,55]. They have nevertheless a specific way of application in optical waverange. In the papers mentioned above, problems involving finite-size crystals with defects are solved under the supercell approximation, replacing the nonperiodic structure by a periodic one. These methods are applied in the frequency domain, as well as the methods of the problem solution with variational principle [4,56]. In the latest papers the fields are expanded in a set of harmonic waves and the resulting eigenvalue problem is solved for assumed small variations. In [60] the problem is solved by different approach in time domain.

The paper [12] presents a numerical study of two-dimensional photonic structures of finite extension.

Particularly, the authors consider the photonic crystal as a finite set of parallel rods. A rigorous theory in which each rod is characterized by its scattering matrix, which links the diffracted field to the incoming one, is used. These fields are represented by Fourier-Bessel expansion, which is convenient for the considered cylindrical components of the crystals. From translation properties of Bessel functions the scattering problem is reduced to the resolution of a linear system. The method is able to provide a complete description of all electromagnetic quantities for crystals of finite size, with short computation time and good precession. The authors demonstrate the developed numerical tool on periodic structures with one and two defects. The defects are obtained by removing some cylinders inside the crystal in order to get microcavities. The calculation results from [12] were verified experimentally by other authors [61] showing that the progress of technology makes it possible to design such structures in optical domain.

The concept of band theory to describe the behaviour of electromagnetic waves in 3D PBG structures was presented in [57] proposing to apply the concept of reciprocal space, Brillouin zones, dispersion relations etc. to electromagnetic waves. The nearly free photon model is considered there to solve the problem in the crystallography domain.

A theory on the resolution of the wave propagation equation in the reciprocal lattice domain after decomposing the periodic distribution of the structure permittivity into its Fourier series is presented in [58]. Numerical tools as, for example, FDTD and FDFD are sometimes used [3, 59, 62, 65] when the considered structures are of small size being used with other devices as waveguides or antennas, but they works properly mainly in microwave domain.

Among theoretical techniques used to find resonant frequencies of defect states, the real-space Green function approach turns out to be efficient [63, 64].

For microstructures (periodic ones as well as ones with defects of the periodicity) an effective index model approach is also available. It was used in [68] to investigate two-dimensional honeycomb-rod PBG structure. The carried out analysis showed that a relative in-plane band gap of 10% may be obtained for a structure characterized by a rod dielectric constant of 13, air background, and a filling fraction of 0.13. For this structure, it is found through the application of an effective refractive-index model that propagation for a single frequency may be inhibited over a solid angle covering more than a half of the spontaneous emission from a narrow-linewidth point source. It was found that it is necessary for the considered approach to take into account the effective index dependence on frequency, as the field concentrates in the high-index material for increasing frequency.

Unfortunately, still there are no simple ways to predict the stop-band frequency range. When a 3D structure consists of two-dimensional sublattices it turns out that significant properties of the 3D crystals are determined principally by the characteristics of the 2D sublattices [55], and computation of the latter properties is much less costly than computing those of the 3D crystal directly. The paper [55] considers a class of 3D photonic band gap materials formed by interleaving of a pair of 2D lattices. The lattices uniform directions are assumed mutually orthogonal, that is so called „woodpile" geometry is considered. It was concluded there after numerical calculations that 2D square lattices interleaving can provide the properties of full 3D photonic band gap material.

A possibility of 3D confinement of light in low-dimensional photonic crystals was reported in [67]. The authors show theoretically that strong 3D confinement can be produced in part by a photonic crystal, and in part by index confinement. 2D photonic crystals in 3D optical environment were studied experimentally and theoretically in [43]. Reflection spectra of the crystal as a triangular lattice of cylindrical holes in bulk silicon were measured over a wide range of mid-infrared wavelengths by using a Fourier-transform spectrometer with a convergent incident beam. Very high reflection coefficients are demonstrated for the first-order forbidden bands (reaching 98%). Comparing the results of experimental and numerical investigation, the contributions of different effects that degrade the reflector performances are separated. The authors conclude that fabrication inhomogeneities such as the small roughness of the interface or the hole-radius dispersion are shown to be the prime cause of degradation as long as diffraction effects are weak.

Conclusion

The proposed brief review shows a great interest to PBG materials and the research now is extended widely from microwaves domain into an optical one. The engineering of photonic stop-bands and band gaps is opening up new opportunities in many areas of photonics and optoelectronics. Improved operating characteristics, greater packing density of devices (shrinkage of device dimensions from cm to :m), and multi-functionality are among the benefits. New methods for fabricating photonic crystals are continually emerging.

References

[1] E. Yablonovich, *Phys. Rev. Lett.*, vol. 58, p. 2059, 1987.

[2] S. John, *Phys. Rev. Lett.*, vol. 58, p. 2486, 1987.

[3] A. Mekis, J. C. Chen, I. Kurland, S. H. Fan, P. R. Villeneuve, and J. D. Joannopoulos, „High transmission through sharp bends in photonic crystal waveguides", *Phys. Rev. Lett.*, vol. 77, pp. 3787–3790, 1996.

[4] J. D. Joannopoulos, R. D. Meade, and J. N. Winn, *Photonic Crystals: Molding the Flow of Light*. Princeton, N.J.: Princeton Univ. Press, 1995.

[5] C. Knight, T. A. Birks, P. St. J. Russell, and D. M. Atkin, „All-silica single-mode optical fiber with photonic crystal cladding", *Opt. Lett.*, vol. 21, pp. 1547–1549, 1996. Errata: *Opt. Lett.*, vol. 22, pp. 484–485, 1997.

[6] J. C. Knight, T. A. Birks, P. St. J. Russell, and J. P. de Sandro, „Properties of photonic crystal fiber and the effective index model", *J. Opt. Soc. Amer. A*, vol. 15, no. 3, pp. 748–752, 1998.

[7] F. Caccavale, F. Segato, I. Mansour, and M. Gianesin, „A finite difference method for the reconstruction of refractive index profile from Near-Field Measurements", *J. Lightw. Technol.*, vol. 16, no. 7, pp. 1348–1353, July 1998.

[8] P. St. J. Russell, „Functional Photonic Crystal Devices", in *Proc. ECOC'98*, pp. 439–440, 1998.

[9] C. M. Soukoulis, Ed., *Photonic Band Gap Materials*. Kluwer, 1996.

[10] J. G. Rarity and C. Weisbuch, Eds., *Microcavities and Photonic Bandgaps*. Kluwer, 1996.

[11] E. Burstein and C. Weisbuch, Eds., *Confined Electrons and Photons*. Plenum Press, 1995.

[12] G. Tayeb and D. Maystre, „Rigorous theoretical study of finite-size two-dimensional photonic crystals doped by microcavities", *J. Opt. Soc. Amer. A*, vol. 14, no. 12, pp. 3323–3332, Dec. 1997.

[13] M. Boroditsky *et al.*, „Photonic crystals boost light emission", *Phys. World*, vol. 10, pp. 25–26, 1997.

[14] L. Brillouin and M. Parodi, *Propagation des Ondes dans les Milieux Periodiques*. Paris: Masson, 1956.

[15] J. Lee, T. Tanaka, S. Sasaki, and S. Uchiyama, „Novel design procedure of broadband multilayer antireflection coating for optical and optoelectronic devices", *J. Lightw. Technol.*, vol. 16, no. 5, May 1998.

[16] T. Mukai and Y. Yamamoto, „Gain frequency bandwidth, and saturation output power of AlGaAs DH laser amplifiers", *IEEE J. Quant. Electron.*, vol. QE-17, pp. 1028–1034, Mar. 1981.

[17] M. Schell, A. G. Weber, E. Scholl, and D. Bimberg, „Fundamental limits of sub-ps pulse generation by active mode locking of semiconductor lasers: The spectral gain width and the facet reflectivities", *IEEE J. Quant. Electron.*, vol. 27, pp. 1661–1668, June 1991.

[18] P. Zorabedian, „Axial-mode instability in tunable external-cavity semiconductor lasers", *IEEE J. Quant. Electron.*, vol. 30, pp. 1542–1550, July 1994.

[19] I.-F. Wu, I. Riant, J.-M. Verdiell, and M. Daganais, „Real-time in self-monitoring of antireflection coatings for semiconductor laser amplifier by ellipsometry", *IEEE Photon. Technol. Lett.*, vol. 4, pp. 991–993, Sept. 1992.

[20] E. Marclay, D. J. Webb, P. Buchmann, and P. Vettiger, „Stepwidth-graded-index multilayered broadband low-reflectivity coating for GaAs/GaAs power lasers", *Appl. Phys. Lett.*, vol. 55, pp. 942–945, Sept. 1989.

[21] M. C. Farries, J. Buus, and M. Kearley, „Design and fabrication of two layer antireflection coatings for semiconductor optical amplifiers", *Electron. Opt. Lett.*, vol. 26, pp. 1626–1628, Sept. 1990.

[22] J. Lee, T. Tanaka, S. Uchiyama, M. Tsuchiya, and T. Kamiya, „Broadband double-layer antireflection coatings for semiconductor laser amplifiers", *Japan J. Appl. Phys.*, vol. 36, pp. L52–L54, Jan. 1997.

[23] D. M. Braun and R. L. Jungerman, „Broadband multilayer antireflection coating for semiconductor laser facet", *Opt. Lett.*, vol. 20, pp. 1574–1576, May 1995.

[24] F. Zolla, D. Felbacq, and B.Guizal, „A remarkable diffractive property of photonic quasi-crystals", *Opt. Commun.*, vol. 148, pp. 6–10, 1998.

[25] D. S. Shechtman, I. Blech, D. Gratias, and J. W. Cahn, *Phys. Rev. Lett.*, vol. 53, p. 1951, 1984.

[26] J. Bellissard, B. Iochum, and D. Testard, *Commun. Math. J.*, vol. 141, p. 353, 1991.

[27] M. Kolar, B. Iochum, and L. Raymond, *J. Phys. A*, vol. 26, p. 7343, 1992.

[28] M. Duela, M. Severin, and R. Riklund, *Phys. Rev. B*, vol. 42, 1990.

[29] M. Dumeau and A. Katz, *Phys. Rev. Lett.*, vol. 51, no. 25, 1985.

[30] P. St. J. Russell *et al.*, „Bound modes of photonic crystal waveguides", *Phys. Rev. Lett.*, vol. 58, pp. 203–218, 1987.

[31] J. S. Foresi *et al.*, „Photonic bandgap microcavities in optical waveguides", *Nature*, vol. 390, pp. 143–145, 1997.

[32] B. D'Urso *et al.*, „Modal reflectivity in finite-depth two-dimensional photonic-crystal microcavities", *J. Opt. Soc. Amer. B*, vol. 15, pp. 1155–1159, 1998.

[33] S. H. Fan *et al.*, „Channel drop tunnelling through localized states", *Phys. Rev. Lett.*, vol. 5, pp. 960–963, 1998.

[34] P. J. Roberts *et al.*, „2D photonic band gap structures as quasi-metals", *Opt. Lett.*, vol. 21, pp. 507–509, 1996.

[35] J. P. Dowling, „Parity, time-reversal and group delay for inhomogeneous dielectric slabs: Application to pulse propagation in finite, one-dimensional, photonic band gap structures", *IEE Proc. Optoelectron.*, vol. 145, no. 6, pp. 420–435, Dec. 1998.

[36] A. M. Steinberg, P. G. Kwiat, and R. Y. Chiao, „Measurement of the single-photon tunnelling time", *Phys. Rev. Lett.*, vol. 71, p. 708, 1993.

[37] A. M. Steinberg and R. Y. Chiao, „Subfemtosecond determination of transmittion delay for a dielectric mirror (photonic band gap) as a function of the angle of incidence", *Phys. Rev. A*, vol. 51, p. 3525, 1995.

[38] A. M. Steinberg and R. Y. Chiao, „Tunneling delay times in one-dimension and two-dimensions, *Phys.Rev. A*, vol. 49, p. 3283, 1994.

[39] J. P. Dowling, M. Scalora, M. J. Bloemer, and C. M. Bowden, „The photonic band-edge laser - a new approach to gain enhancement", *J. Appl. Phys.*, vol. 75, p. 1896, 1994.

[40] M. Scalora, R. J. Flynn, S. B. Reinhardt, R. L. Fork, M. D. Tocci, M. J. Bloemer, C. M. Bowden, H. S. Ledbetter, J. M. Bendicksom, J. P. Dowling, and R. P. Leavitt, „Ultrashort pulse propagation at the photonic band edge: Large tunable group delay with minimal distortion and loss", *Phys. Rev. E*, vol. 54, p. 1078, 1996.

[41] J. M. Bendicksom, J. P. Dowling, and M. Scalora, „Analytic expressions for the electromagnetic mode density in finite, one-dimensional, photonic band gap structures", *Phys. Rev. E*, vol. 53, p. 4107, 1996.

[42] T. A. Birks *et al.*, „Endlessly single-mode photonic crystal fibre", *Opt. Lett.*, vol. 22, pp. 961–963, 1997.

[43] C. C. Cheng, V. Arbet-Engels, A. Scherer, and E. Yablonovich, „Nanofabricated three-dimensional photonic crystals operating at optical wavelengths", *Phys. Scripta*, vol. T-68, pp. 17–20, 1996.

[44] E. Ozbay, E. Michel, G. Tuttle, R. Biswas, M. Sigalas, and K.-M. Ho, „Micro-machined millimetre wave photonic band gap crystals", *Appl. Phys. Lett.*, vol. 64, no. 16, pp. 2059–2061, 1994.

[45] E. Ozbay, B. Temelkuran, M. Sigalas, G. Tuttle, C. M. Soukoulis, and K.-M. Ho, „Defect structures in metallic photonic crystals", *Appl. Phys. Lett.*, vol. 69, no. 25, pp. 3797–3799, 1996.

[46] A. L. Reynolds and J. M. Arnold, „Interleaving two-dimensional lattices to create three-dimensional photonic band gap structures", *IEE Proc. Optoelectron.*, vol. 145, no. 6, pp. 436–440, Dec. 1998.

[47] N. Holonyak, Jr., „The semiconductor laser: A thirty-five year perspective", *Proc. IEEE*, vol. 85, no. 11, pp. 1678–1693, Nov. 1997.

[48] T. A. Birks *et al.*, „Full 2-D photonic bandgaps in silica/air structures", *Electron. Lett.*, vol. 31, no. 22, pp. 1941–1942, 1995.

[49] W. F. Liu, P. St. J. Russell, and L. Dong, „Acousto-optic superlattice modulator using fibre Bragg grating", *Opt. Lett.*, vol. 22, pp. 1515–1517, 1997.

[50] J.-L. Archambault *et al.*, „Novel channel-dropping filter by grating-frustrated coupling in single-mode optical fibre", *Opt. Lett.*, vol. 19, pp. 180–182, 1994.

[51] S. Kawakami, „Fabrication of submicrometre 3-D periodic structures composed of Si/SiO$_2$", *Electron. Lett.*, vol. 33, no. 14, pp. 1260–1261, 1997.

[52] M. D. B. Charlton *et al.*, *Mat. Sci. Eng. B*, vol. 49, pp. 155–165, 1997.

[53] T. J. Shepherd *et al.*, „3D microwave photonic crystals: Novel fabrication and structures", *Electron. Lett.*, vol. 34, no. 8, pp. 787–789, 1998.

[54] J. B. Pendry and A. MacKinnon, „Calculation of photon dispersion relations", *Phys. Rev. Lett.*, vol. 69, pp. 2772–2775, 1992.

[55] M. Sigalas, C. M. Soukoulis, E. N. Economou, C. T. Chan, and K.-M. Ho, „Photonic band gap and defects in two dimensions: studies of the transmission coefficient", *Phys. Rev. B*, vol. 48, pp. 14121–14126, 1993.

[56] R. D. Meade, A. M. Rappe, K. D. Brommer, J. Joannopoulos, and O. L. Alerhand, „Accurate theoretical analysis of photonic band gap materials", *Phys. Rev. B*, vol. 48, pp. 8434–8437, 1993.

[57] E. Yablonovich and T. J. Gmitter, „Photonic band structure: The face-centered-cubic case", *J. Opt. Soc. Amer. A*, p. 7, 1990.

[58] D. R. Smith *et al.*, „Photonic band gap structure and defects in one and two dimensions", *J. Opt. Soc. Amer. B*, p. 10, 1990.

[59] M. Thevenot, A. Reineix, and B. Jecko, „FDTD to analyse complex PBG structures in the reciprocal space", *Microw. Opt. Technol. Lett.*, vol. 21, no. 1, pp. 25–28, Apr. 1999.

[60] P. Villeneuve, S. Fan, and J. D. Joannopoulos, „Microcavities in photonic crystals: mode symmetry, tunability, and coupling efficiency", *Phys. Rev. B*, vol. 54, pp. 7837–7842, 1996.

[61] T. Baba and T. Matsuzaki, „GaAs/InP 2-dimensional photonic crystals", in *Microcavities and photonic band gap: Physics and Applications, V. 324 of NATO Advanced Scientific Institute Series E*. J. Rarity and C. Weisbuch, Eds. Dordrecht, The Netherlands: Kluwer Academic, 1996.

[62] S. Fan, J. N. Winn, A. Devenyi, J. C. Chen, R. D. Meade, and J. D. Joannopoulos, „Guided and defect modes in periodic dielectric waveguides", *J. Opt. Soc. Amer. B*, vol. 12, pp. 1267–1272, 1995.

[63] A. A. Maradudin and A. R. McGurn, „Photonic band structures of two-dimensional dielectric media", in *Photonic Band Gap and Lovalisation*. C. M. Soukoulis, Ed. New York: Plenum, pp. 247–628, 1993.

[64] A. R. McGurn, „Green's function theory for row and periodic deffect arrays in photonic band structures", *Phys. Rev. B*, vol. 53, pp. 7059–7064, 1996.

[65] J.-K. Hwang, S.-B. Hyun, H.-R. Ryu, and Y.-H. Lee, „Resonant modes of two-dimensional photonic band gap cavities determined by the finite-element method and by use of the anisotropic perfectly matched layer boundary condition", *J. Opt. Soc. Amer. A*, vol. 15, no. 8, pp. 2316–2324, Aug. 1998.

[66] B. Temelkuran, H. Altug, and E. Ozbay, „Experimental investigation of layer-by layer metallic photonic crystals", *IEE Proc. Optoelectron.*, vol. 145, no. 6, pp. 409–414, Dec. 1998.

[67] P. R. Villeneuve, S. Fan, S. G. Jonson, and J. D. Joannopouls, „Three-dimensional photon confinement in photonic crystals of low-dimensional periodicity", *IEE Proc. Optoelectron.*, vol. 145, no. 6, pp. 384–390, Dec. 1998.

[68] T. Sondergaard, J. Broeng, A. Bjarklev, K. Dridi, and S. E. Barkou, „Supression of spontaneous emission for a two-dimensional honeycomb photonic bandgap structure estimated using a new effective-index model", *IEEE J. Quant. Electron.*, vol. 34, no. 12, pp. 2308–2313, Sept. 1998.

Irena Yu. Vorgul,
Kharkov State University,
4 Svoboda Sq., Kharkov 310077, Ukraine
e-mail: yuts@ira.kharkov.ua

Marian Marciniak,
National Institute of Telecommunications,
1 Szachowa Str., 04-894 Warsaw, Poland,
e-mail: M.Marciniak@itl.waw.pl

Dielectric photonic quasi-crystals with doubled quasi-periodicity

Irena Yu. Vorgul and Marian Marciniak

Abstract — Optical range electromagnetic field interaction with inhomogeneous finite dielectric media is investigated. New method for analysis of this interaction in 1D case based on integral equations for fields in transient media is proposed. Some special cases of quasi-periodical structures with doubled quasi-periodicity are investigated numerically. A possibility to obtain good filtering properties in such structures for small number of quasi-periods is shown.

Keywords — photonic crystals, optical pulse transformation.

Introduction

In the last years research activities on photonic band gap (PBG) structures as artificial periodic and quasi-periodic structures whose transmission properties exhibit frequency bands where the propagation of electromagnetic waves is forbidden [1], becomes one of the most actual direction in photonics and optical communication. It is known also that such structures can display properties of bandpass filters by disruption of the periodicity [2, 3]. Classical periodic layered structures was properly investigated theoretically and experimentally for different wavebands [4, 5]. The conditions of wave propagation in them were defined as well as their reflection characteristics. Detailed description of wave behaviour in them is a fundamental base for all consequent investigations.

However, these structures are not ideal for practical applications and their development by increasing complexity of the structures (as, for example, dual periodicity) is toward the improved model. The criteria for such an optimization are the gap width and shape (preferably a rectangular-like one) as well as the structure dispersion and simplicity of their fabrication.

One of the promising way of the improvement is to use not periodical but quasi-periodical structures. Such structures in a case of small shift of thickness of the layers composing the correspondent periodical structure were considered in [6, 7].

In spite of impressive progress in the new and emerging area of PBG engineering in recent years, their development by increasing complexity of the structures (as, for example, dual periodicity) toward the improved model is still actual. The criteria for such an optimization are the gap width and shape (preferably a rectangular-like one) as well as the structure dispersion and simplicity of their fabrication. There are a lot of works on periodical and quasi-periodical structures with a great number of periods providing for some bands of frequency a full wave reflection. We tried to obtain a high reflection with sharp frequency spectrum from quasi-periodical structures considering a small number of layers, which is much more difficult to obtain but which simplifies sufficiently the structure fabrication.

Previously, we considered mainly semi-infinite structures [8, 9]. In the present paper the investigation of 1D quasi-periodic dielectric structures is carrying out toward finding optimal structures for sharp frequency filter and phase transformer. We consider a planar structure as a dielectric layer with double-quasi-periodical permittivity. An additional complexity of the structure allows to obtain high reflection for a wide band or sharp resonances on defined frequencies as well as a sufficient.

Problem formulation and solution

The considered dielectric layer $0 \leq x \leq a$ has a permittivity mathematically determined by

$$
\begin{aligned}
\varepsilon(x) = {} & \\
= {} & \sum_{n=0}^{N} \left(\alpha - \left(\frac{1}{\beta} \right)^n \right) \left[\theta(x - an) - \theta(x - a(n+1)) \right] + \\
& + \sum_{m=0}^{M} \left(\gamma - \left(\frac{1}{\eta} \right)^m \right) \left[\theta(x - bm) - \theta(x - b(m+1)) \right],
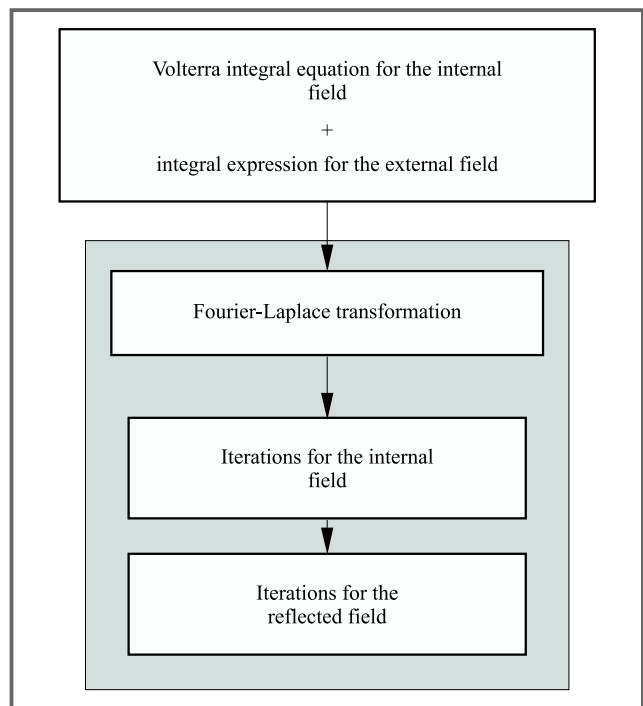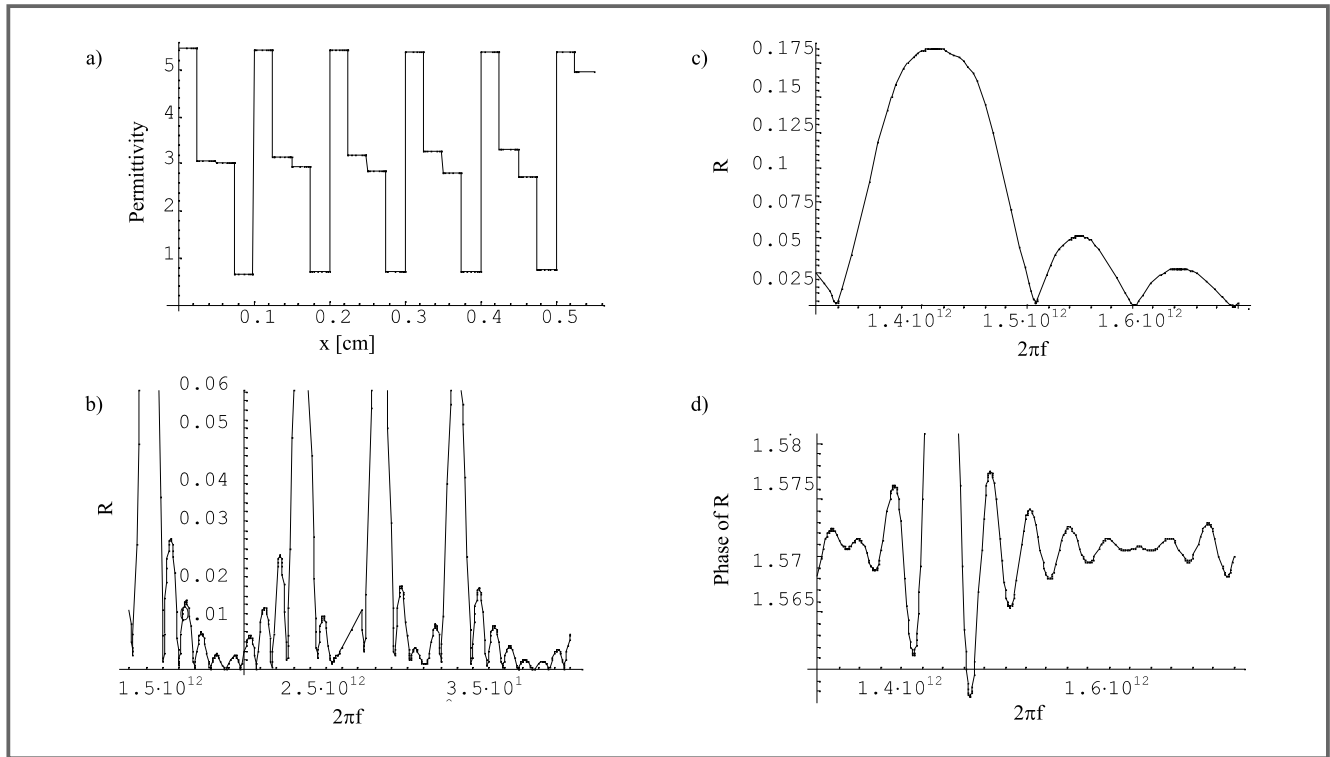\end{aligned} \tag{1}
$$

Fig. 1. Algorithm of analytical solving procedure for the problem

Fig. 2. Permittivity profile in the layer (a); reflection coefficient amplitude in dependence on the incident wave frequency (b), (c); reflection coefficient phase, equal to π at its maximum (d)

being essentially a superposition of two quasi-periodical structures with the composing layers widths equal to a and b, correspondingly, and slight deviation of the layers permittivity from the periodical ones.

The problem is solved based on integral equations for electromagnetic fields in nonstationary media [10]. There are some advantages in using this approach even for stationary structures because the method is based on Volterra integral equation which can be solved by iterations with improved convergence unlike Friedholm and singular equations. So we can easily control the obtained results accuracy. Initial point of the problems solutions are Volterra integral equations [10] which can be obtained from Maxwell equation for the electrical component of electromagnetic field obtained by Green function of corresponding wave equation with all nonstationarities picked up at its right hand part. In the considered 1D case it has the following form: for the internal field ($x > 0$, $t > 0$):

$$E_{in}(t,x) = E_0(t,x) +$$
$$-\theta(vt-x)\int_{t-x/v}^{t} dt' j(t', x-v(t-t')) +$$
$$-\theta(x-vt)\int_{0}^{t} dt' j(t', x-v(t-t')) - \int_{0}^{t} dt' j(t', x+v(t-t'))$$

and for the external field ($x < 0$):

$$E_{ex}(t,x) =$$
$$= B(t,x) - \theta(vt+x)\int_{0}^{t+x/v} dt' j(t', v(t-t') + x), \quad (2)$$

where $\quad j(t,x) = \frac{\partial}{\partial x}\left[\frac{\varepsilon_2(t,x)-\varepsilon_1}{\varepsilon_1} E_{in}(t,x)\right] \quad$ for dielectric

medium, θ is Heaviside step function and $v = c/\sqrt{\varepsilon}$.

Analytical iteration formula for the reflected field determined by the layer permittivity distribution was obtained according to the scheme in Fig. 1. The iteration algorithm was realized as a computer program enabling one to investigate band gap and filtering properties of the considered structures reflection for transient and stationary (as a long-time approximation for the transient one) cases. This approach is worth to be used even in a case of a stationary inhomogeneous layer, because for nonstationary problem we have a Volterra-type integral equation, for which a convergence of the iterative procedure is proved, so we can be sure in the results.

Calculation results

Calculation for different layer parameters showed that for big deviation of the structure permittivity from one of the periodic structure the reflection coefficient oscillates slightly about the value, which is not appropriate neither for anti-reflection coating nor for a good reflector.

We considered big deviations of the structure permittivity from one of periodic structure as well as small ones. In the first case, we found the oscillations of the reflection coefficient seeming not applicable to optical devices.

For small deviations of the structure from the periodical one it is possible to choose such structure parameters which provide good filtering and band gap characteristics of it (Fig. 2).

The reflection coefficient amplitude for the considered structures with doubled quasi-periodicity exceeds its maximal value for simple quasi-periodical structures, as calculated by the same program supposing the existence of only one sum in (1) (Fig. 3).
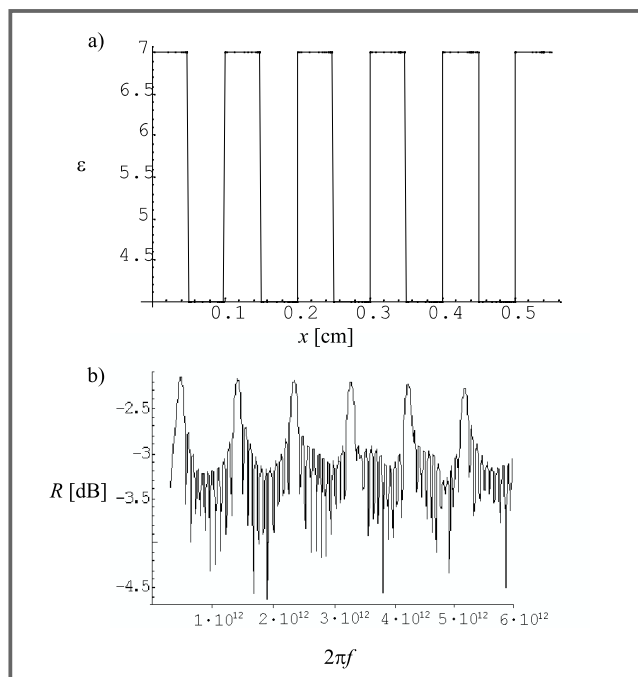
Fig. 3. Permittivity profile in the layer (a); reflection coefficient amplitude in dependence on the incident wave frequency (b)

Conclusion

An additional complexity of the structure allows to obtain high reflection for a wide band or sharp resonances on defined frequencies as well as a sufficient reflected field phase shift for some parameters combinations.

References

[1] E. Yablonovich, *J. Opt. Soc. Amer. B*, no. 10, pp. 283–295, 1993.

[2] H. J. De Los Santos, „On the design of photonic band gap crystal filters", in *Proc. 1998 URSI Symp.*, Atlanta, USA, 1998, p. 121.

[3] N. A. Khizhnyak and K. Yu. Kramarenko, „Propagation of Electromagnetic Waves in Space-Varying Structures with Dual Periodicity", *Ukrain. Phys. J.*, vol. 10, p. 1256–1259, 1997.

[4] L. Brillouin and M. Parodi, *Propagation des Ondes dans les Milieux Periodiques*. Paris: Masson, 1956.

[5] L. M. Brekhovskih, *Waves in Layered Media*. Moscow: USSR Academy of Sciences Publ., 1957.

[6] F. Zolla, D. Felbacq, and B. Guizal, „A remarkable diffractive property of photonic quasi-crystals", *Opt. Commun.*, vol. 148, pp. 6–10, 1998.

[7] D. Felbacq, F. Zolla, and B. Guizal, „Wave propagation in one-dimensional photonic crystal", *Opt. Commun.*, vol. 152, pp. 119–126, 1998.

[8] I. Yu. Vorgul and A. G. Nerukh, „Inverse problems for media with transient conductivity", *Microw. Opt. Technol. Lett.*, vol. 19, no. 3, pp. 148–150, 1998.

[9] I. Yu. Vorgul and M. Marciniak, „Electromagnetic pulse scattering on half-space with continuously time-varying conductivity", *Prace IL*, no. 110, pp. 29–42, 1998.

[10] A. G. Nerukh and N. A. Khizhnyak, *Modern problems of transient macroscopic electrodynamics*. Kharkov: Test-Radio Publ., 1991.

[11] P. J. Roberts *et al.*, „2D photonic band-gap structures as quasi-metals", *Opt. Lett.*, vol. 21, pp. 507–509, 1996.

Irena Yu. Vorgul,
Kharkov State University,
4 Svoboda Sq., Kharkov 310077, Ukraine
e-mail: yuts@ira.kharkov.ua

Marian Marciniak,
National Institute of Telecommunications,
1 Szachowa Str., 04-894 Warsaw, Poland,
e-mail: M.Marciniak@itl.waw.pl

Reflection from layered dielectric structures with combined regular and random inhomogeneities

Michael A. Guzev and Gennadiy V. Popov

Abstract — Optical wave reflection from a layered half-space with regular and random inhomogeneities where the regular perturbations correspond to a linear waveguide near the half-space boundary. Random inhomogeneities are simulated in the frame of the white noise model. The problem is solved analytically in a framework of the embedding method which reduces a boundary problem to the problem with initial values considering the field as a function of the half-space boundary coordinate and obtaining then its solution as a steady-state probability density of the reflection coefficient phase. Numerical calculations revealed some features of the field behaviour under the combined influence of regular and random inhomogeneities such as the reflection coefficient phase increasing inhomogeneity from uniform distribution for small regular inhomogeneities toward a strong peak at the phase equal to $\pi/2$ for increasing ones, and some fine effects which are still greater then the calculation accuracy.

Keywords — optical waveguides, layered structures.

Introduction

Dielectric layered media are widely used as optical field transformers and reflectors. Particularly, artificial layered media can serve as 1D PBG structure whose transmission properties exhibit frequency bands where the propagation is forbidden, or a frequency filter in a case of periodic disturbance of the structure periodicity. Such structures were usually considered as regularly inhomogeneous media. There are two reasons for consideration of random inhomogeneities together with regular ones in such structures. The first one is that on experimental graphical results one can usually see irregular oscillations imposing on theoretically estimated characteristics which suggests the idea of statistical behaviour in addition to the regular one. The second one follows from the well known fact that for 1D half-space with random refraction index is ideal reflector for a wave of any frequency. It allows to assume that consideration of random inhomogeneities together with regular ones can expose new possibilities of creation of structures with properties of PBG crystals.

Random inhomogeneity in high-permittivity media can take place due to interaction processes near the media layers joints as well as the media internal properties appearing in certain external conditions, particularly for nonlinear media one can select a parameters area where its behaviour is chaotic being applicable for a statistic description.

In this work, we consider a model of a stationary problem of wave propagation in a layered half-space with regular and random inhomogeneities with regular perturbations corresponding to a linear waveguide near the half-space boundary. Random inhomogeneities are simulated in the frame of the white noise model. We analyze an influence of regular and random inhomogeneities on probability distribution of the reflection coefficient phase and the wavefield average intensity at the boundary of the half-space.

Mathematical formulation of the problem

We consider a randomly inhomogeneous slab occupying the region $L_0 \leq x \leq L$. An incident field is assumed as a plane harmonic wave $E(t,x) = U_0(x)e^{i\omega t}$, $U_0(x) = e^{ik(l-x)}$, propagating from the region $x > L$ of a homogeneous space. Inside the inhomogeneous slab the field amplitude $U(x)$ is described by Helmholtz equation

$$\frac{\mathrm{d}^2}{\mathrm{d}x^2} U(x) + k^2(x) U(x) = 0, \qquad (1)$$

where function $k(x)$ characterizes regular and statistical inhomogeneities of the medium. Boundary conditions for this equation follows from continuity of $U(x)$ and $\partial U(x)/\partial x$ on the slab boundaries:

$$\frac{i}{k} \frac{\mathrm{d}U(x)}{\mathrm{d}x} + U(x)|_{x=L} = 2$$
$$\frac{i}{k} \frac{\mathrm{d}U(x)}{\mathrm{d}x} - U(x)|_{x=L_0} = 0. \qquad (2)$$

For the problem (1), (2) we are interested in the statistical characteristics of the wavefield when $k(x)$ contains regular and random components.

In previous works [1,2] we had shown that for a spectral parameter comparable with a wave number, a reflection coefficient phase distribution is non-uniform. It can touch the condition for average method applicability leading to false results. So, it is important to investigate the influence of the reflection coefficient phase distribution on field statistical characteristics for determination and expansion of the statistical theory frames.

The problem is solved analytically in a framework of the embedding method which reduces a boundary problem to the problem with initial values considering the field as a

function of the half-space boundary coordinate and obtaining then its solution as a steady-state probability density of the reflection coefficient phase. Numerical calculation is carried out then to reveal some features of the field behaviour.

Dynamical equations solution

Wavefield effects for the considered problem are determined by scattering on inhomogeneities inside the medium and on spatial jumps of $k(L_0)$ and $k(L)$. We exclude the boundaries influence supposing that the medium occupies the half-space $x < L(L_0 \to \infty)$ and that the right boundary is adjusted: $k^2 = k^2(L) = k_L^2$.

Suppose that the wavefield $U(x) = U(x,L)$ is a function of the parameter L. Then in the framework of the embedding method the boundary problem (1), (2) is reduced [3] to the problem with initial values with respect to L, and the equation for the reflection coefficient has the form:

$$\frac{dR_L}{dL} = 2ik_L R_L + \frac{k'_L}{2k_L}\left(1 - R_L^2\right), \ R_{L_0} = 0, \quad (3)$$

where $k'_L/k_L = \partial \ln k_L/\partial L$.

After substitution the representation for the reflection coefficient as $R_L = \rho_L e^{i\phi_L}$ into (3) and taking into account that the quantity $\rho_L = 1$ with probability equal to unit in a case when the wave is incident on a random half-space $(L_0 \to \infty)$, the following differential equation for ϕ_L is obtained:

$$\frac{d\phi_L}{dL} = 2k_L - \frac{k'_L}{k_L}\sin\phi_L. \quad (4)$$

Combined influence of regular and random inhomogeneities on reflection coefficient is considered for the velocity profile as $c(l) = c_0\left(1 + \alpha L + \varepsilon(L)\right)$. It is linked with $k(L)$ by the relation $k(L) = \omega/c(L)$, where ω is a cyclic frequency. Function $\varepsilon(x)$ is supposed to be homogeneous mean zero Gaussian process, that is $\langle\varepsilon(x)\rangle = 0$; correlation function B determined as $B_{\varepsilon\varepsilon}(x,x') = \langle\varepsilon(x)\varepsilon(x')\rangle = \sigma_\varepsilon^2 B\left(|x-x'|/l_0\right)$, parameter σ_ε^2 characterizes the intensity of fluctuations and l_0 denotes a correlation radius. Regular and random inhomogeneities are considered under a condition that $\sigma = |\alpha/p| < 2$, $p = \omega/c_0$. Assuming that the fluctuations are small $\left(\sigma_\varepsilon^2 << 1\right)$ and the regular profile is a slow function of L, Eq. (4) can be written in a shortcut form as follows:

$$\frac{d\phi_L}{dL} = 2p + (\alpha + \xi(L))\sin\phi_L, \ \xi(L) = \frac{\partial\varepsilon(L)}{\partial L}. \quad (5)$$

Function $\xi(x)$ is the Gaussian process with the following parameters:

$$\langle\xi(x)\rangle = 0, \ B_{\xi\xi}(x,x') = \langle\xi(x)\xi(x')\rangle = -\frac{\partial^2}{\partial x^2}B_{\xi\xi}(x-x').$$

Statistical analysis of Eq. (5) is carried out in the framework of the approach of the works [1,2]. Its main ideas are the follows: we introduce the variable $z_L = \tan\phi_L/2$

instead of the phase; to simplify the further solution we assume that $\varepsilon(L)$ is the Gaussian random delta-correlated process (conditions for applicability of this approximation are considered in [3]). Then the steady-state probability density $P(z)$ of this value has the form

$$P(z) = h(z)P_+(z) + h(-z)P_-(z), \quad (6)$$

where

$$P_+(z) = h(z_- - z)P_1(z) + h(z - z_-)h(z_+ - z)P_2(z) + $$
$$+ h(z - z_+)P_3(z), z > 0,$$

$$P_1(z) = CA(z)\int_0^z dz_1 \left(\frac{z_1 - z_-}{z_1 - z_+}\right)^{k\sqrt{d}} z_1^{k\sqrt{d+4}-1},$$

$$P_2(z) = CA(z)\int_z^{z_+} dz_1 \left(\frac{z_1 - z_-}{z_1 - z_+}\right)^{k\sqrt{d}} z_1^{k\sqrt{d+4}-1},$$

$$P_3(z) = CA(z)\int_{z_+}^z dz_1 \left(\frac{z_1 - z_-}{z_1 - z_+}\right)^{k\sqrt{d}} z_1^{k\sqrt{d+4}-1},$$

$$P_-(z) = P_1(z), z < 0,$$

$$A(z) = \frac{1}{\sqrt{d+4}}\frac{(z - z_+)^{k\sqrt{d}-1}}{(z_1 - z_+)^{k\sqrt{d}+1}}z^{k\sqrt{d+4}},$$

h is the Heaviside step-function and parameters are the follows: $d = 16/\sigma^2 - 4$. The constant value $C \equiv C(k,d)$ is defined from the condition with the parameters $k = p/8D$ and $D = p^2\sigma_\varepsilon^2 l_0/2$. The correspondent steady-state probability distribution of the phase ϕ_L defined within the interval $(-\pi, +\pi)$ can be obtained from (6) by the formula

$$P(\phi) = \left(1 + z^2\right)P(z)/2\ |_{z = \tan\phi/2}.$$

Discussion

We had shown that for a spectral parameter comparable with a wave number, a reflection coefficient phase distribution is non-uniform. It can touch the condition for average method applicability leading to false results. So it is important to investigate the influence of the reflection coefficient phase distribution on field statistical characteristics for determination and expansion of the statistical theory frames. Rigorous restriction for applicability of formula (6) is defined by the condition $\alpha/D << 1$. It makes possible to use the shortcut Eq. (5) to describe the wavefield behaviour in a medium with random and regular inhomogeneities. For the limit cases as 1) $k >> 1$ and $|\sigma| << 1$ and 2) $|\sigma| \to 2$ the phase has the uniform distribution or fluctuates near the deterministic solution $\phi_\infty = \pi/2$, correspondingly, which agrees with the known results.

Computer analysis of $P(z)$ behaviour was carried out for three sufficiently different cases: (A) $k = -3.13, \sigma = 0.1$; (B) $k = -3.13, \sigma = 1.0$ and (C) $k = -3.13, \sigma = 1.9$. It is shown that the case A corresponds to the phase uniform distribution. The case C describes the situation when the

phase tends to the deterministic value $\pi/2$. To extract an influence of the regular inhomogeneity on the probability distribution it was calculated in absence of the inhomogeneity for different values of k. $P(\phi)$ maximum occured to be displaced to the right when the parameter σ increases.

Calculation of the wavefield intensity on the boundary as a function of σ for different values of k showed that the results can be approximated by a linear function.

References

[1] M. A. Guzev and V. I. Klyatskin, *Waves in Random Media*, vol. 3, pp. 307–315, 1993.

[2] M. A. Guzev, V. I. Klyatskin, and G. V. Popov, *Waves in Random Media*, vol. 2, pp. 117–123, 1992.

[3] V. I. Klyatskin, *AMS Lectures in Applied Mathematics*, vol. 27, Providence, RI: American Mathematical Society, pp. 447–476, 1991.

Michael A. Guzev
Institute for Automation and Control Processes,
Far East Branch, Russian Academy of Science,
5 Radio Str., Vladivostok 690041, Russia

Gennadiy V. Popov
Pacific Oceanological Inst.,
Far East Branch, Russian Academy of Science,
43 Baltiskaya Str., Vladivostok 690041, Russia

New method of numerical modelling of optical field transformation by inhomogeneous semiconductor layer with time-varying parameters

Irena Yu.Vorgul and Marian Marciniak

Abstract — A time-domain model of a semiconductor layer with time-dependent inhomogeneous permittivity or conductivity is investigated by solving direct and inverse problems using a novel method, revealing a possibility of wavelength shifting and other desirable optical field transformation, as well as a remote diagnostics of fast time-varying inhomogeneous structures.

Keywords — optical field transformation, wavelength conversion, nonlinear phenomena in semiconductor.

Optical field transformation like wavelength conversion and others, being one of the main topics in optical communication, can be achieved with a number of methods. Recent research in this field turns toward all-optical wavelength conversion in semiconductor optical amplifiers using either cross-gain modulation, cross-phase modulation or four-wave mixing.

Media with time-varying parameters can also be used to obtain a desirable field transformation, and combination of temporal and spatial variations here give an extended possibility for it.

In the present paper we consider a model of the transforming structure as a finite 1D layer with arbitrary temporal and spatial (along one coordinate) dependencies of its permittivity or conductivity. Direct and inverse problems are considered, toward such structure synthesis and diagnostics. A novel method, common for solving inverse and direct problems of electromagnetic field scattering on 1D finite structures with arbitrary temporal and spatial dependencies of their parameters (permittivity or conductivity), is proposed. Its schematic algorithm is shown in Fig. 1. It is based on integral equations for electromagnetic field obtained by evolutionary approach assuming that the nonstationarity starts at a certain time moment. Represent a conducting current function as an expansion into series of step-functions on spatial coordinate with transient coefficients like the following:

$$j(t,x) = \sum_{k=0}^{m} S_k(t)\,\theta\,(x-ak),\qquad(1)$$

where $m_{max} = Integer(vt/a)$ (maximum integer number of this ratio). It means that we divide the conducting current function into thin sub-layers in which it is homogeneous being however nonstationary (Fig. 2).
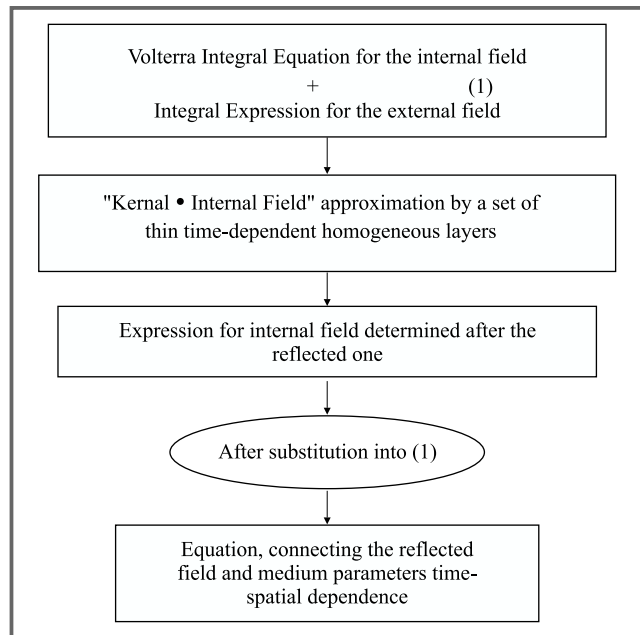

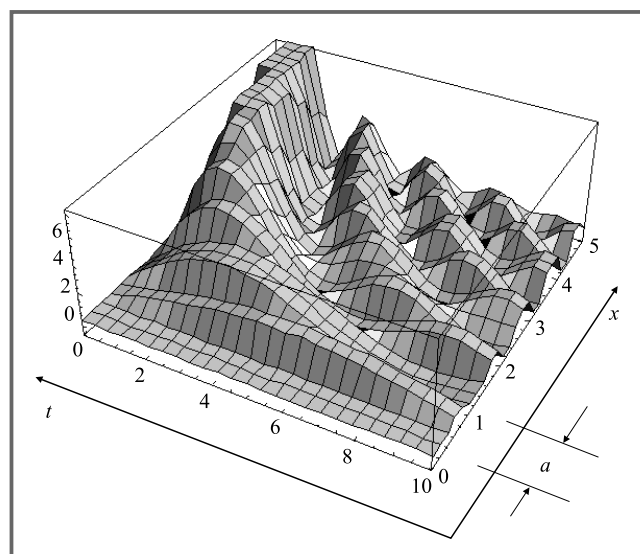**Fig. 1.** Algorithm of the novel method common for solving the inverse and direct problems

Fig. 2. Illustration of the current representation by homogeneous transient sub-layers

Then it is possible to obtain the internal field (that is the field inside the transient inhomogeneous medium) expression after the external one (the external region outside the scattering medium is assumed being stationary and homogeneous). After substitution of this expression into the initial integral equation for the internal field, we have an equation which connect the external field and the scattering medium parameters. This equation can be solved analytically for both inverse and direct problems. That is, one can obtain its exact solutions for the medium parameters temporal and spatial dependencies determined after the external field as well as for the external field determined after these parameters.

The solutions are represented as finite sums. The proposed method was realized in computer programs. Its convergence is rigorously proved due to the extension into the full series of orthogonal functions. Another its advantage is that it enables one to consider scattering of any incident fields on such transient inhomogeneous structures including harmonic waves, pulses and others. The inverse problems technique can be used for solving the problems of the structures synthesis to obtain a required scattered field as well as for diagnostic problems of retrieval of the scatter characteristics by the reflected field (remote sensing). In the latest case calculations showed that the used technique is stable to the input data noises being so a promising one for measurements processing.

Some special cases of the inverse and direct problems were calculated such as layered structures with time-dependent conductivity or permittivity, retrieval of the parameters providing the incident field frequency shift and others. As an example, calculated spectrum of the field reflected from quasi-periodical structure with temporal permittivity is presented in Fig. 3, showing a possibility to obtain high reflection not only at the incident wave frequency (the incident field was assumed as a plane harmonic wave) but also for a wide range of frequencies, forming so by reflection from such a structure not only waves of other frequencies but also optical pulses.

Conclusions

The proposed new method for determination of transient 1D media parameters by the reflected field reveals a possibility of optical field transformation by structures like metal-dielectric-semiconductor diodes and pulse-induced temporal reflectors. Such an induced transient structure can be used as a field transformer for a wide range of medium properties, when considering field interactions with them. Theoretical modelling performed and consequent numerical modelling shows different possibilities of an incident field transformation by reflecting from such structures, like frequency shift, pulse collapse, etc.

Irena Yu. Vorgul,
Kharkov State University,
4 Svoboda Sq., Kharkov 310077, Ukraine
e-mail: yuts@ira.kharkov.ua

Marian Marciniak,
National Institute of Telecommunications,
1 Szachowa Str., 04-894 Warsaw, Poland,
e-mail: M.Marciniak@itl.waw.pl
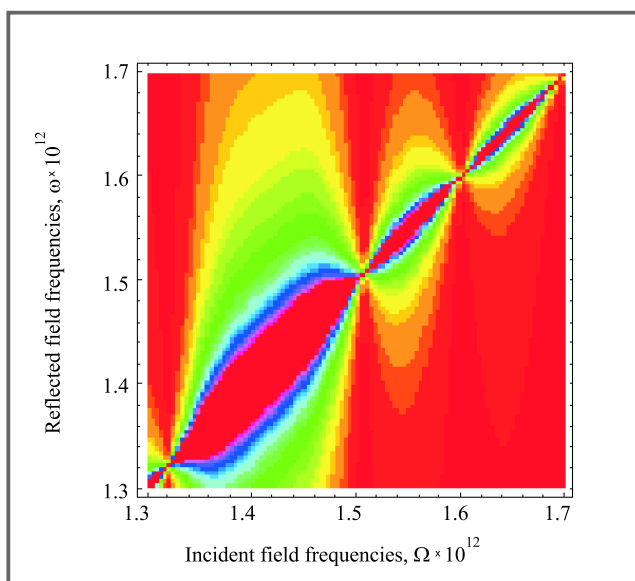
Fig. 3. Reflected field spectrum for transient structure for small t

Side lobes reducing by variation of array apperture edge shape

Nikolay N. Gorobets, Yury N. Gorobets, and Victor I. Kiyko

Abstract — **A possibility of side lobes level reducing in plane antenna array by creation of aperture comb edge in arrays with rectangular and circular aperture shape together with usage of different types of reducing to the array edges amplitude distributions is investigated by computer analysis. It is shown that usage of the comb structure in combination with the reducing amplitude distribution enables one to reach the side lobes level reducing in the array to $-27 \div -29$ dB.**

Keywords — *phone antenna arrays, side lobes level reducing*

For different practical applications a problem of development of plane antenna arrays with low side lobes level (SLL) arises. This problem can be solved forming a reducing amplitude distribution of field sources in the array aperture by reducing of the field amplitude on array elements with approaching to the array edge as well as by reducing the radiators number toward the array edges by using 8-angle, rhombic or circular shape of it.

Another way to realize the reducing amplitude distribution toward the array edges by reducing the radiators number is the radiators thinning out toward the array edge. Such a thinning out can be realized accidentally or periodically.

The presented paper is a sequel of the work started in [1] on computer analysis of a possibility to reduce SLL of plane waveguide-slot antenna arrays.
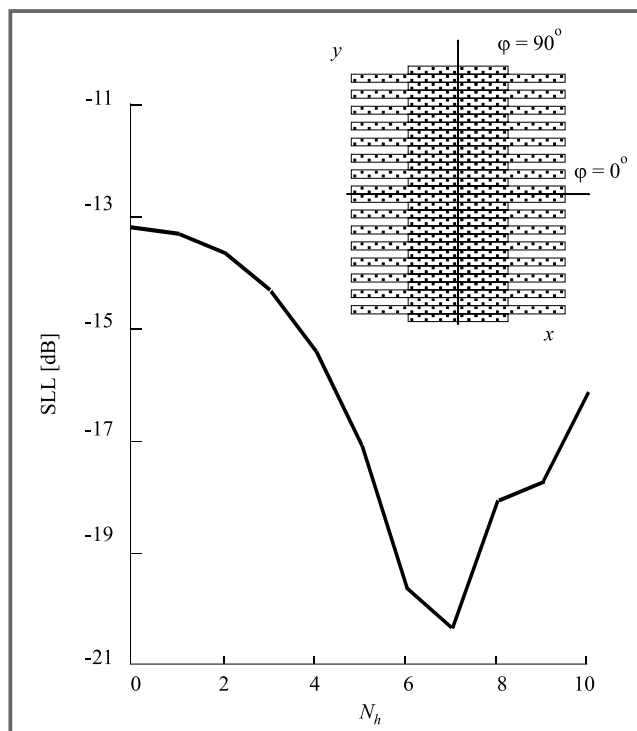
Fig. 1. SLL distribution in rectangular array with comb

Consider a case when the discussed in [1] rectangular array edge which is parallel to y-axis has not a regular shape but is designed as a comb with grooves length equal to N_h, where N_h is an integer number of the radiators excluded from the array alternately starting from its edge (antenna scheme in Fig. 1).

Let us analyse this antenna array characteristics in dependence on the groove length N_h. Firstly, we investigate a case of constant amplitude distribution of the field sources along the array elements. In Fig. 1 the distributions of maximal side lobe level in the plane $\varphi = 0$ are shown.

This is what was to be expected that in the plane $\varphi = 0$ the increase of the groove length leads to fast reducing of the maximal side lobe level from -13.2 dB for the array with regular aperture edge to -20.5 dB for $N_h = 7$. This is a case when the grooves length is equal to a quarter of the array length. Because the second side lobe level increases as a function of the groove length the maximal side lobe level is also enhanced. Moreover, the antenna Radiation Pattern (RP) is enhanced on 16.5%. In the plane $\varphi = 45°$, the side lobes keep up their level lower then -27 dB whereas in the plane $\varphi = 90°$ one can observe a considerable reducing of the side lobe on 0.7 dB. The radiators number in such an array for $N_h = 7$ reduces on 23% in comparison with a square closely filled array.

Let us apply the reducing amplitude distribution to the rectangular antenna array with aregular comb on its edge. We limit our investigation to the directivity characteristics only in the plane $\varphi = 0$, that is in the plane where an influence of the comb structure of the array aperture edge is sufficient. The analysis of side lobes level dependence on the groove length N_h under sine amplitude distribution shows that a maximal comb efficiently here is reached only when the groove length is equal to $5 \div 7$ radiators. The field amplitude on the edge array elements is lower then 0.5. Dependence of the side lobe level on parameter A_0 for the comb grooves length values equal to 0, 6 and 7 radiators is shown in Fig. 2.

One can see that for the antenna array with the comb edge of aperture under the grooves length equal to $6 \div 7$ radiators and for the sine amplitude distribution with $A_0 = 0.1 \div 0.2$ it is possible to obtain the side lobes suppression till the level -26 dB, which is on 2.5 dB more then for the same array without comb [1]. RP width here increases from 2.4° to 3.4° and the radiators number is reduced on $20 \div 23\%$.

For the case of exponential distribution the same calculation shows that minimal side lobe is reached under the grooves length $N_h = 5$ and field amplitude on the edge array elements within the limits $0.2 \div 0.6$. The side lobe level here
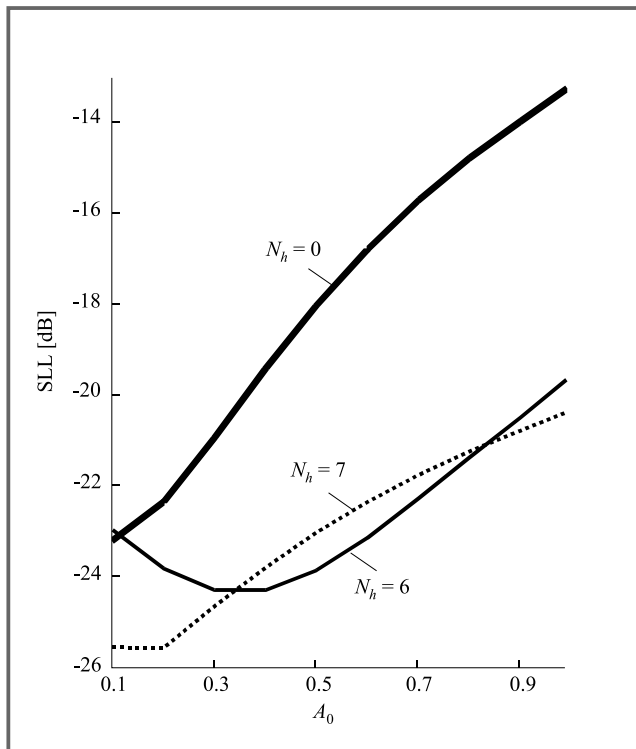
Fig. 2. SLL distribution in array with a comb and a sine amplitude distribution

for $A_0 = 0.4$ is equal to -26.7 dB. This level of maximal side lobe can be reduced more if one can provide a uniform reducing of the amplitude distribution along the columns. On the border between the array regular part and its comb part an amplitude distribution jump takes place. It can be seen in Fig. 3a which is a plot of the field amplitude distribution in the array columns for the comb grooves length $N_h = 5$ and for the exponential amplitude distribution on the array elements (solid curve). To obtain the minimal side lobe the amplitude distribution in the array should be close to linear one. To eliminate the amplitude distribution jump is possible by two ways: to make a transfer from the regular part of the array to the comb one more smooth (for this it is necessary to change periodically the comb grooves length on one radiator) or to use a complex combined amplitude distribution, for example the exponential one on the regular array part and sine one on the comb part. RP in the plane $\varphi = 0$ for the case of the array with a smooth periodic changing of the comb grooves length is shown in Fig. 3b, where the solid curve corresponds to the case of the regular comb with the grooves length $N_h = 5$, whereas the dashed curve corresponds to the irregular comb with alternating grooves $N_h = 5$ and $N_h = 4$.

The correspondent amplitude distribution for the later case is plotted in Fig. 3a by a dashed line. One can see that in the array with irregular comb the maximal side lobe level is reduced to -29 dB. However, in that case the reducing of the maximal side lobe level is due to reducing the level of the third side lobe from -26.7 dB to -30 dB under a simultaneous increase of the first and the second
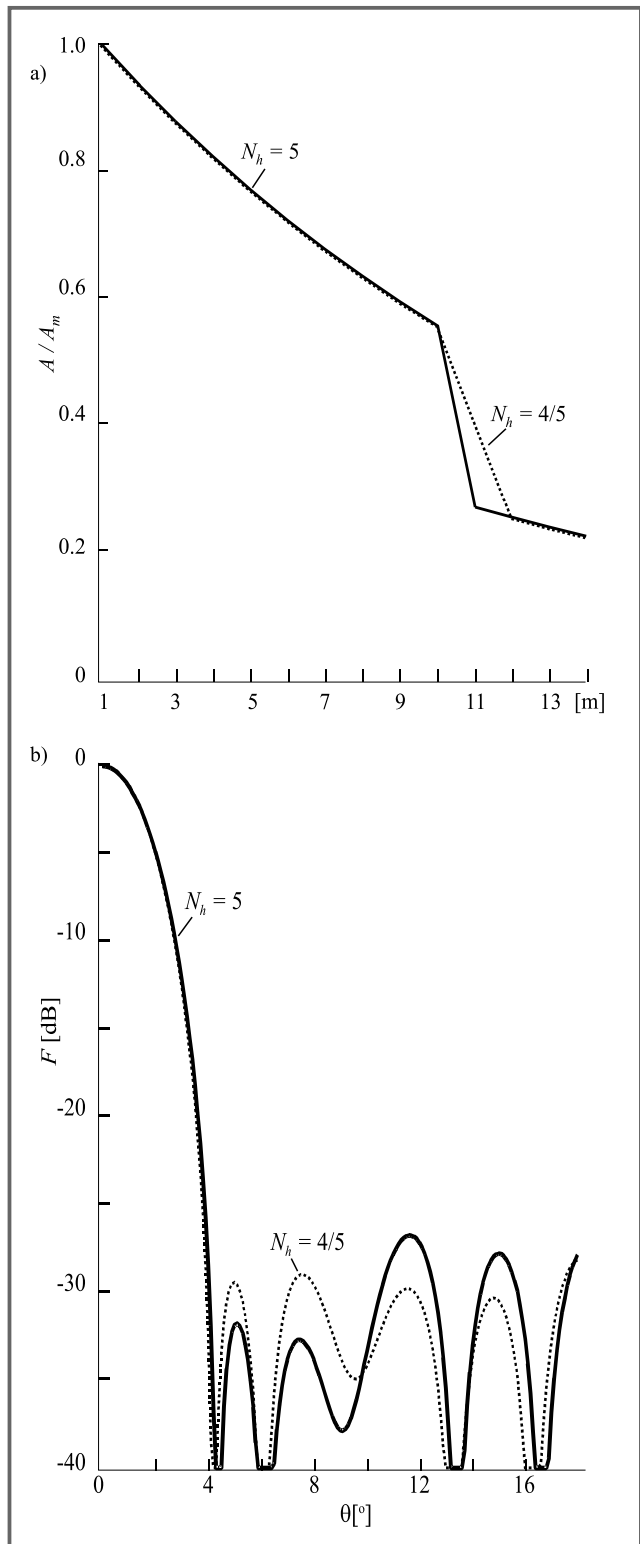
Fig. 3. Amplitude distribution on the columns of the rectangular array with comb under exponential amplitude distribution on the array elements for different grooves length (a) and the correspondent RP (b)

side lobes from -32 dB to -29 dB. Therefor, if one uses sharp-directed isolated radiators in the considered plane, it

is preferable to use the regular comb because far side lobe here suppresses RP of the isolated radiator.

So, for all considered cases of the side lobes reducing in the rectangular antenna array, application of the array with the irregular comb aperture edge and exponential amplitude distribution provides the most suppression of the side lobes. The side lobe here reduces from -13.4 dB to -29 dB under increasing the RP width on 28% when the radiators number reduces on 18%.

Figure 1 shows a scheme of the rectangular array with regular comb on its edge. One can easily see that such a structure provides the side lobes level reducing only in one plane. To provide the side lobe suppression in orthogonal plane for $\varphi = 90°$ it is necessary to obtain a reducing toward the edges amplitude distribution in this plane. Such a distribution can be obtained making the irregular comb with increasing grooves length toward the array edge (see the antenna scheme in Fig. 4).
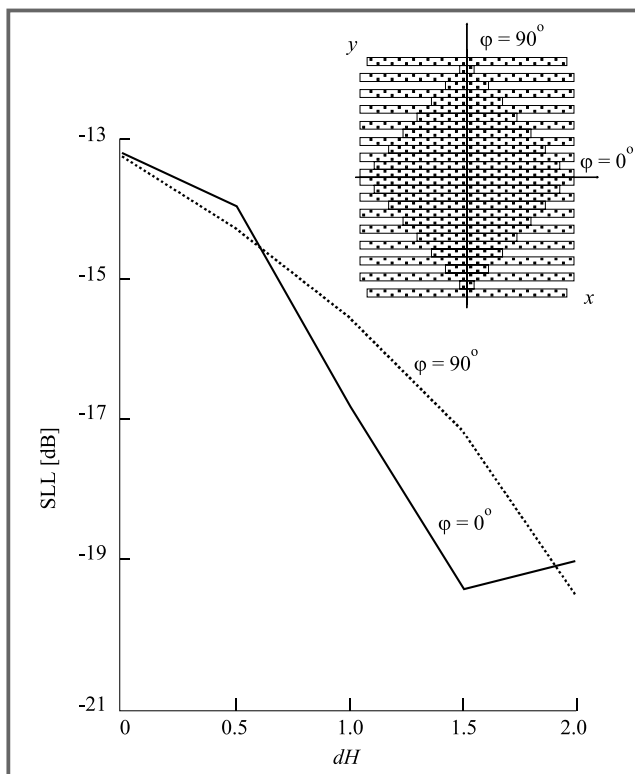
Fig. 4. SLL distribution in rectangular array with uniformly varying comb

Further we analyse the antenna array in which the grooves length of each even line varies from the array centre toward its edge on the value dH. Figure 4 shows the maximal side lobes level as a function of the parameter dH in the plane $\varphi = 0$ (solid lines) and in the plane $\varphi = 90°$ (dashed lines). In the plane $\varphi = 45°$ the side lobes level does not exceed -24 dB. As one can see from the figure, in the square array with irregular comb under maximal length of the edge grooves reaching a half of the array length ($dH = 2$), and for constant amplitude distribution on all radiators one managed to obtain RP symmetrical on all angles (with

the side lobes level not higher then -19 dB. RP width here is maximal in the plane $\varphi = 0$ being equal to $2.7°$. The radiators number in this case reduces on 30%.

Use the reducing toward the array edges amplitude distribution of the array on its elements. For sine amplitude distribution in the main planes $\varphi = 0$ and $\varphi = 90°$ the more the comb grooves length, the less the side lobes level reducing to $-20 \div -30$ dB in dependence on the parameter A_0, whereas in the diagonal plane $\varphi = 45°$ situation is quite the opposite: the more dH the more the side lobe level. Maximal side lobe suppression in all these three cross-sections can be observed for $dH = 2.0$. The same for all these three cross-sections level of the side lobes, being equal to -25.5 dB, takes place for $A_0 = 0.5$, whereas maximal side lobes suppression up to -32 dB in the main planes can be obtained for $A_0 = 0.2$.

For exponential amplitude distribution a dependence of the side lobes level on dH for different A_0 has more complicated character. In this case minimal (equal to -22 dB) side lobes in the main cross-sections can be obtained for $dH = 2.0$ and $A_0 = 0.3 \div 0.6$, whereas in the diagonal cross-section the side lobes level for the same conditions is equal to $-25 \div -27$ dB.

Let us investigate a circular antenna array with a comb aperture edge and a constant field amplitude on all radiators. Firstly, consider the case when the comb grooves length is the same for all grooves. Such an array scheme is shown in Fig. 5b for $N_h = 7$. Figure 5a shows the maximal side lobes level as a function of the grooves length N_h in the cross-section $\varphi = 0, 45°, 90°$. One can see that RP with axis-symmetrical side lobes is obtained for the grooves length equal to $8 \div 9$ radiators. The value of the maximal side lobe level here is equal to $-22 \div -23$ dB and RP width is within the limits $2.89 \div 3.3°$. The number of radiating elements in this array is equal to 49% in comparison with the initial square closely filled array. Figure 5b shows RP of this antenna array in three cross-sections $\varphi = 0, 45°, 90°$.

In the case when the comb grooves length in the circular antenna array is uniformly increased on the value dH by approaching to the array edge, the minimal side lobe level is more then in the former case on $3 \div 4$ dB, but RP width in the later case is less then that in the former case on about 20%.

Apply the amplitude distribution reducing toward the edges to the circular antenna array. Firstly, we consider the case of the array with equal length of all comb groves N_h and sine amplitude distribution on the array elements. Calculation results show that axial symmetry for the side lobes under their minimal values takes place in the antenna array with the grooves length N_h being within the limits $8 \div 9$ radiators. In Fig. 6, the side lobes levels as a function of A_0 for three planes $\varphi = 0, 45°, 90°$ under N_h equal to 8 (solid lines) and to 9 (dashed lines) elements are plotted. These figures analysis leads to a conclusion that axis-symmetrical RP with the same level of the side lobes in all three cross-sections cannot be designed in this case. The main cross-sections $\varphi = 0$ and $90°$ are determining here
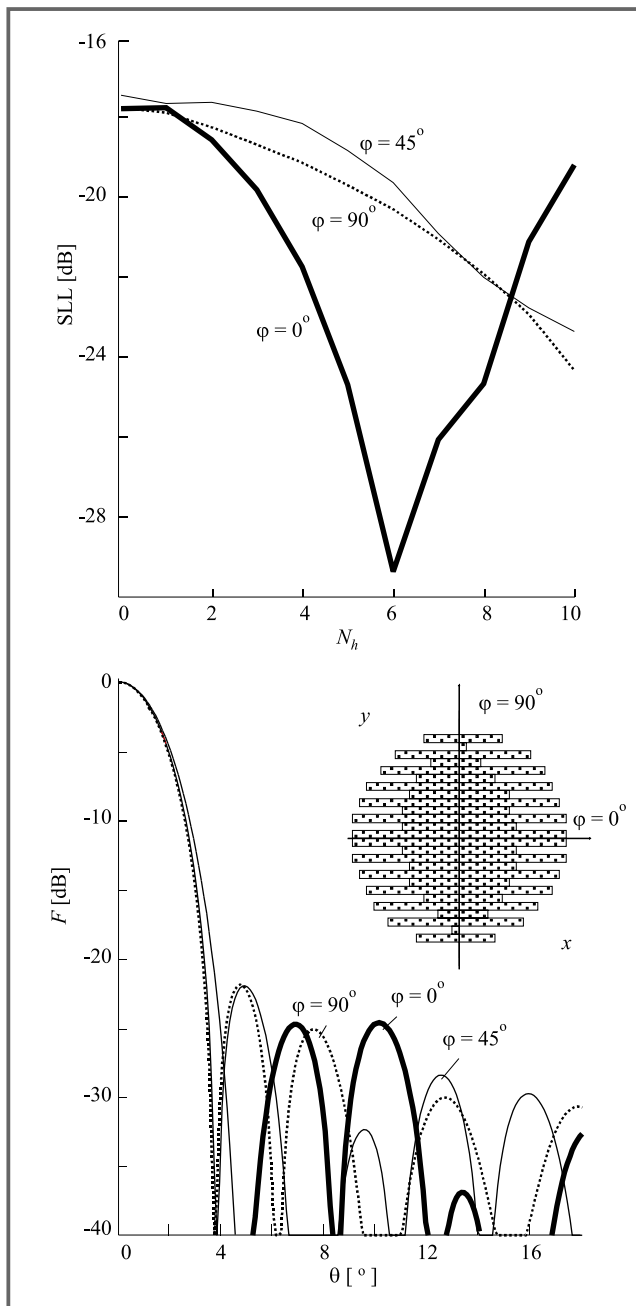
Fig. 5. SLL in circular array with comb under a constant amplitude distribution on the array elements for three observation planes (a) and the correspondent RP for $N_h = 8$ (b)
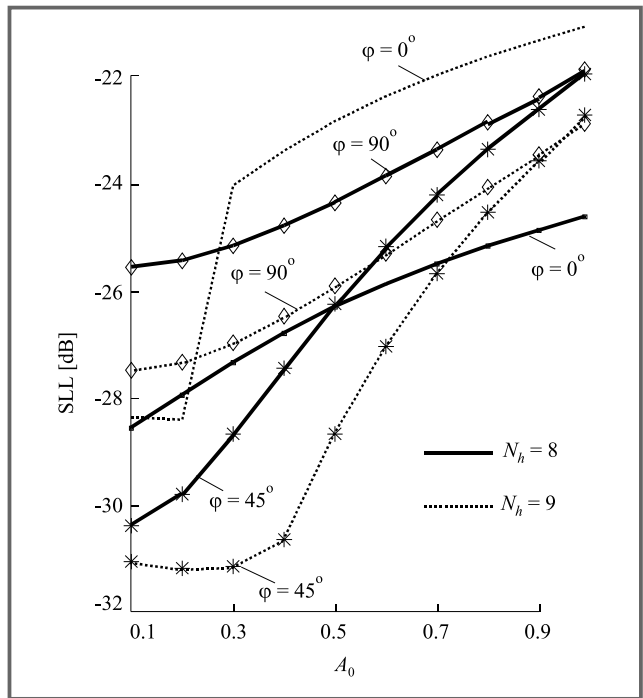

Fig. 6. SLL distribution in circular array with the comb for sine amplitude distribution

In the case of exponential amplitude distribution the minimal side lobe level in all these three cross-sections for $dH = 0.5$ and $A_0 = 0.35$ is also equal to -23 dB, $\varphi = 90°$.

The main results of the analysis of various shapes and filling densities of the array aperture calculated in order to obtain optimal side lobes level are shown in Table 1. In these cases the optimal antenna array is which provides (wherever it is possible) the axis – symmetrical (for the side lobes) radiation pattern. So, for the different planes determined by φ (for each case of the considered antenna arrays) the parameters which enable one to obtain the limit reached side lobes level much less then those in the optimal case exist.

If the axi-symmetrical (for the side lobes) radiation pattern is needed then the minimal possible side lobes equal to -27 dB can be obtained by means of the circular antenna array with regular comb on its edge and sine amplitude distribution. RP width in this case increases on about 50% whereas the radiators number reduces on 54% in comparison with the square regularly filled array. The same array with the exponential amplitude distribution provide approximately the same side lobes level but more narrow RP (on 4%) and radiating elements number increases on 5% in comparison with the previous case.

If we need to obtain the minimal possible side lobes level only in one plane then it is preferable to use the square array with irregular comb and exponential amplitude distribution. In this case the side lobes level is equal to -29 dB under RP width equal to $3.2°$. The elements number here is 85% in comparison with that of the initial array.

and minimal possible side lobe level is determined by its value in the plane $\varphi = 90°$ being equal to -27.3 dB for $N_h = 9$ and $A_0 = 0.1 \div 0.2$. RP width in this case is equal to $3.72 \div 3.29°$ for the angle $\varphi = 90°$.

In the case of exponential amplitude distribution, the side lobes level is equal to -24.8 dB which is more then the same in the case of sine amplitude distribution.

The analysis of circular antenna array for the irregular comb and reducing sine amplitude distribution shows that the minimal side lobe in three cross-sections can be obtained when $dH = 1.5$ and $A_0 = 0.1 \div 1.15$ and is equal to -23 dB.

Table 1
Parameters and characteristics of the array

Parameters and characteristics of the array		Shape of antenna array aperture							
		Without comb			Regular comb		Comb with uniformly increasing length of grooves		Irregular comb
		Square	8-angle	Circular	Square	Circular	Square	Circular	Square
Uniform	SLL [dB]	-13.2	-17.5	-17.8	-20.3	-23.5	-19.0	-19.0	
	$2\Delta\theta$, [°]	2.34	2.73	2.8	2.82	3.0	2.7	2.5	
	A_0	1.0	1.0	1.0	1.0	1.0	1.0	1.0	
	N	960	820	634	736	440	672	528	
	N/N_0 [%]		85	66	77	46	70	55	
	M, N_h, dH		13		7	7	2	2	
SIN	SLL [dB]	-23.3		-24.4	-25.5	-27.3	-25.5	-23.0	
	$2\Delta\theta$, [°]	3.2		3.39	3.48	3.5	3.0	3.35	
	A_0	0.1		0.1	0.2	0.2	0.5	0.12	
	N	960		634	736	440	672	578	
	N/N_0 [%]			66	77	46	70	60	
	M, N_h, dH				7	8	2	1.5	
EXP	SLL [dB]	-20.2		-23.8	-26.7	-24.8	-22.0	-23.0	-29.0
	$2\Delta\theta$, [°]	2.95		3.04	3.24	3.3	2.9	3.3	3.2
	A_0	0.3		0.5	0.4	0.5	0.45	0.35	0.4
	N	960		634	800	462	672	632	816
	N/N_0 [%]			66	83	48	70	66	85
	M, N_h, dH				5	7	2	0.5	4-5

References

[1] N. N. Gorobets, Yu. N. Gorobets, and V. I. Kiyko, „Side lobes reducing for plane antenna arrays", *Vestnik Kharkov. Univ.*, no. 405, pp. 3–10, 1998.

———————

Nikolay N. Gorobets, Yury N. Gorobets, Victor I. Kiyko
Kharkov State University,
4 Svoboda Sq., Kharkov, 310077, Ukraine
e-mail: Nikolay.N.Gorobets@univer.kharkov.ua